Nanocrystal-Molecule Energy Transfer Conjugates for Chemical and Biological Sensing

Rebecca C. Somers

B.A. Chemistry
Northwestern University, 2003

Submitted to the Department of Chemistry
In Partial Fulfillment of the Requirements
For the Degree of

DOCTOR OF PHILOSOPHY IN INORGANIC CHEMISTRY

at the

MASSACHUSETTS INSTITUTE OF TECHNOLOGY

September 2008

Signature of Author: _____
Department of Chemistry
July 2, 2008

Certified by: _____
Daniel G. Nocera
The Henry Dreyfus Professor of Energy and Professor of Chemistry
Thesis Supervisor

Accepted by: _____
Robert W. Field
Haslam and Dewey Professor of Chemistry
Chairman, Departmental Committee on Graduate Studies

This doctoral thesis has been examined by a Committee of the Department of Chemistry as follows:

Professor Stephen J. Lippard _____
Arthur Amos Noyes Professor of Chemistry
Chairman

Professor Daniel G. Nocera _____
The Henry Dreyfus Professor of Energy and Professor of Chemistry
Thesis Supervisor

Professor Moungi G. Bawendi _____
Lester Wolfe Professor in Chemistry

To my parents, David and Kiyomi,
and to my best buddy Holly,
for their love and encouragement

Abstract

NANOCRYSTAL-MOLECULE ENERGY TRANSFER CONJUGATES FOR CHEMICAL AND BIOLOGICAL SENSING

by Rebecca C. Somers

Submitted to the Department of Chemistry on
July 2, 2008
in partial fulfillment of the requirements for the degree of
Doctor of Philosophy in Inorganic Chemistry

Abstract

New tools and probes are constantly being developed for chemical and biological sensing. As novel materials emerge, growing demand for sensing in specific applications can be addressed. One such class of materials is fluorescent inorganic semiconductor nanocrystals (NCs), popularly known as quantum dots. The unique, size-dependent properties of NCs are promising for biological microscopy applications in cancer research; however, obstacles such as biocompatibility and sensitivity must be overcome (Chapter I). This Thesis work addresses the challenge of converting the chemically inert NCs into a dynamic equilibrium-based sensor. A strategy of implementing fluorescence resonance energy transfer (FRET) as the signal transduction mechanism of a CdSe/ZnS NC-molecule donor-acceptor pair with a rhodamine-based acceptor dye is investigated. Energy transfer in NC-dye pairs is found to be efficient, with k_{FRET} rates approaching 10^8 s^{-1} (Chapter II). A reversible and ratiometric NC pH sensor is synthesized by tethering NCs to a squaraine-based pH dye. The presence of an isosbestic point between the two emission maxima from the NC and the dye allows the sensor to be self-calibrating (Chapter III). The ratiometric nature of the NC-based sensor signifies potential for emission-based sensing in biological environments. Various NC surface modifications and coupling strategies using a physiologically relevant pH dye are compared to determine the characteristics needed to introduce NC based sensors into a biological environment (Chapter IV). NCs functionalized with poly(ethylene glycol) ligands (PEG) were deemed best suited to impart biocompatibility, and first generation PEGylated bio-applicable NC pH sensors were photophysically characterized under single and two-photon excitation and its stability evaluated (Chapter V). The PEGylated NC pH sensors were introduced into an *in vivo* tumor environment, and using multiphoton laser scanning microscopy (MPLSM), the sensors are able to ratiometrically report a change in pH induced by an external stimulus. Challenges such as calibration in *in vivo* experiments are currently being addressed (Chapter VI). New conjugation techniques with NCs are further explored with Click Chemistry (Chapter VII). The NC-molecule sensing developed during this Thesis work is general and may be applied towards sensing of other analytes in other applications, using a variety of NC materials (Chapter VIII).

Thesis Supervisor: Daniel G. Nocera
The Henry Dreyfus Professor of Energy and Professor of Chemistry

Contents

Table of Contents

List of Figures

Chapter I

Contents

List of Schemes

List of Tables

Chapter II

Chapter IV

Chapter VII

List of Abbreviations

A	acceptor
Å	Ångstrom (1 Å = 10^{-10} m)
BAOEC	bovine aortal endothelial cell
BCECF	2',7'-bis(2-carboxyethyl)-5(6)-carboxyfluorescein
BOP	(benzotriazol-1-yloxy)tris(dimethylamino)phosphonium hexafluorophosphate
br	broad
BSA	bovine serum albumin
CCD	charge-coupled device
$CdMe_2$	dimethylcadmium
CdSe	cadmium selenide
CdTe	cadmium telluride
CdZnS	cadmium zinc sulfide
cm^{-1}	wavenumber
Cy	cyanine
D	donor
DCC	dicyclohexylcarbodiimide
DHLA	dihydrolipoic acid
DIC	differential interference contrast
DIEA	diisopropylethylamine
DLS	dynamic light scattering
DMAP	4,4'-dimethylaminopyridine
DMF	dimethylformamide
DMSO	dimethylsulfoxide
DNA	deoxyribonucleic acid
dNTP, N=A,C,G,U	deoxy(nucleotide)triphosphate, nucleotide = adenine, cytosine, guanine, uracil
DTT	dithiothreitol
E	efficiency
FBS	fetal bovine serum
EDC	1-ethyl-3-(3-dimethylaminopropyl)carbodiimide

eq.	equation
equiv.	equivalent
ESI	electrospray ionization
FRET	fluorescence resonance energy transfer
FWHM	full-width at half-maximum
GFC	gel filtration chromatography
GM	Goeppert Meyer
GPC	gel permeation chromatography
HDA	hexadecylamine
HOBt	1-hydroxybenzotriazole
HPA	hexylphosphonic acid
ip	intraperitoneal
IR	infrared
iv	intraveneous
J	spectral overlap integral
k_{FRET}	rate constant for fluorescence resonance energy transfer
λ	wavelength
L, mL, μL	liter, milliliter, microliter
NC	nanocrystal
NHS	*N*-hydroxysuccinimide
NIR	near infrared
NMR	nuclear magnetic resonance
m, mm, nm	meter or multiplet, millimeter, nanometer
MALDI	matrix-assisted laser desorption by ionization
MBP	maltose binding protein
MPLSM	multi-photon laser scanning microscopy
min	minute
mol	mole (1 mol = 6.022×10^{23} units)
MS	mass spectrometry
MW, MWCO	molecular weight, molecular weight cut-off
PAMAM	poly(amido amine)
PBS	phosphate buffered saline

PEG	poly(ethylene glycol)
PLE	photoluminescence excitation
PMT	photomultiplier tube
ppm	parts per million
r	distance
R_0	critical transfer distance
RITC	rhodamine B isothiocyanate
RNA, mRNA, siRNA	ribonucleic acid, messenger ribonucleic acid, small interfering ribonucleic acid
s, ns, ps, fs	singlet or second, nanosecond, picosecond, femtosecond
SNARF	seminaphthorhodafluor
t	triplet
TA	thioctic acid
TBP	tributylphosphine
TDPA	tetradecylphosphonic acid
TFA, pfp-TFA	trifluoroacetic acid, pentafluorophenyl trifluoroacetate
THF	tetrahydrofuran
$(TMS)_2S$	bis(trimethylsilyl)sulfide
TNT	trinitrotoluene
TOF	time-of-flight
TOP	trioctylphosphine
TOPO	trioctylphosphine oxide
UV	ultraviolet
vis	visible
xs	excess
$ZnEt_2$	diethylzinc
ZnS	zinc sulfide
ZnSe	zinc selenide

Chapter I

Introduction: Optical Sensing Strategies and Progress of Nanocrystal-based Sensors for Biological Applications

Parts of this Chapter have been published:
Somers, R. C.; Bawendi, M. G. and Nocera D. G.
Chem. Soc. Rev. **2007**, *36*, 579-591.

Chapter I

I.1 Introduction

The need for sensing and continuous monitoring of chemical and biological analytes is ubiquitous, spanning areas of environmental sciences,[1-3] fundamental bioprocesses,[4-11] critical care medicine,[12-17] and national defense.[18-20] The growing demand for chemical and biological sensing has been accompanied by an increased activity devoted to the development of chemosensors for the fields of chemistry, biology, and materials science. Chemosensors recognize, by chemical or physical means, and signal the presence of analytes on a molecular scale.[21-31] A chemosensor consists of an analyte binding site and a reporter site. Signal transduction is established upon analyte binding. The overall architecture leads to the "3R scheme" of recognize, relay, and report. The recognition event between the analyte and the binding site must be reversible for continuous monitoring of analyte concentrations. A rapid equilibrium between the analyte and receptor site permits continuous measurements of dynamic optical response to changes in analyte concentration. The selectivity and the sensitivity of the sensor are determined by the specificity and strength of association of the analyte to the recognition site, as well as the efficiency of the relay signal transduction mechanism to the reporter and the response of the reporter itself.

Whereas sensing can operate by numerous transduction mechanisms, including oxidation-reduction, electron transfer, and colorimetric changes, the largest group of chemical sensors produce a signal by fluorescence.[32] Sensors that operate by detection of emission are distinguished by numerous advantages over other signal transduction mechanisms. Emission based sensors may:

1) provide a signal against a low background in comparison to other types of sensing[33]
2) be non- or minimally invasive in biological applications[34,35]
3) report on nanometer length-scales with nanosecond time responses[36-38]
4) permit analytes to be monitored continuously in real time[39,40]
5) achieve sensitivity down to the single molecule limit[41-46]
6) be incorporated into a variety of imaging technologies, such as optical fibers and waveguides[47-50]

7) typically be low-cost[33]

In addition, by fully understanding the excited state mechanisms that govern a luminescent event, a signal transduction mechanism may be tailored through manipulation of the photophysical properties of the lumiphore for the creation of new and specific detection schemes.

I.1.a Photophysics of Optical Chemosensing Pathways

Once a molecule is excited to an electronic excited state, M*, numerous intramolecular pathways exist for its decay back to its ground state, as illustrated by the Jablonski Diagram in Figure I.1a. Figure I.1b depicts the photophysical pathways should the molecule undergo a photochemical reaction upon excitation. A new product, P, is formed upon relaxation. The pathways are described by the radiative (k_r), and non-

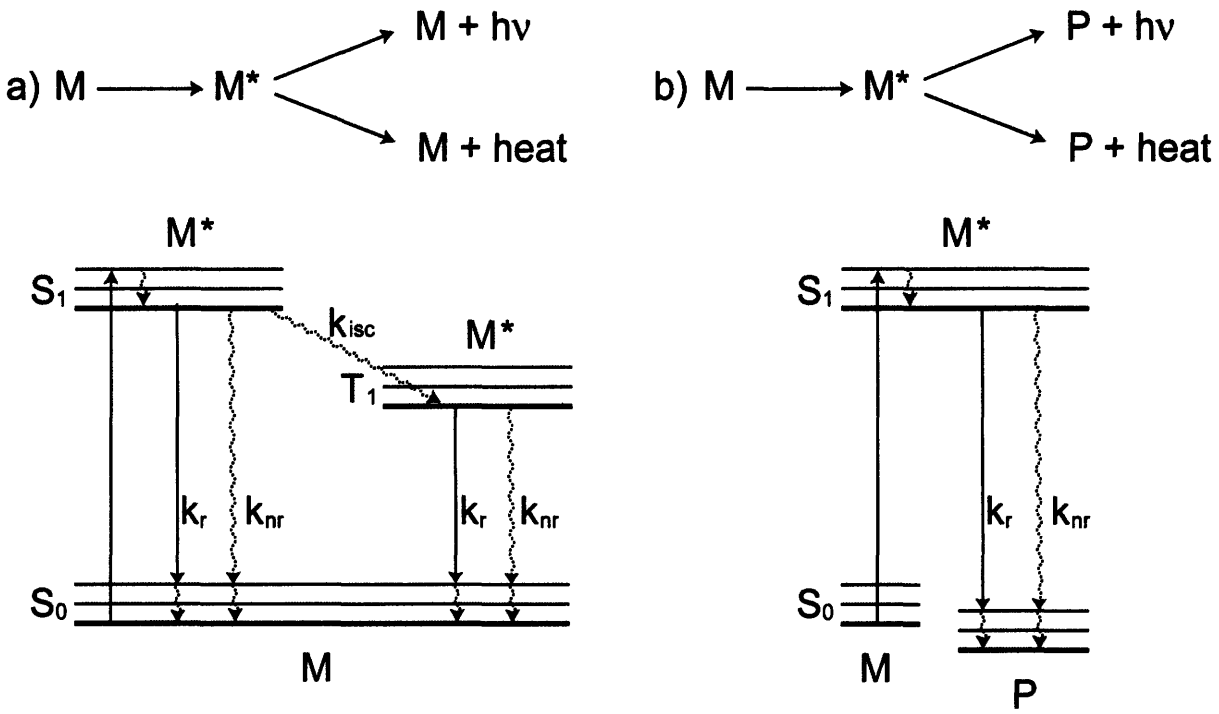

Figure I.1 Jablonski diagram for molecule M in its excited state M*. Fluorescence is represented by the radiative decay rate, k_r. Non-radiative decay pathways are represented by k_{nr}. a) A molecule excited to its singlet excited state (S_1) may return back to its ground state through k_r and k_{nr}, or undergo an intersystem crossing (k_{isc}) to the first excited triplet state (T_1) to either phosphoresce or non-radiatively decay back to its ground state. b) In a case where photochemical processes occur, an excited molecule may radiatively or non-radiatively decay to form a distinct product.

radiative (k_{nr}) rate constants as well as the rate for intersystem crossing (k_{isc}). The radiative decay constant, k_r, which is the rate of fluorescence or phosphorescence depending on whether the decay originates from the singlet excited state or the triplet excited state, is an intrinsic property of the molecule and reflects the probability for emission of a photon of a given frequency.[51-53] The non-radiative decay constant, k_{nr}, includes all other intramolecular decay pathways that do not lead to emission of light, and typically is rooted in the conversion of electronic energy from the excited state into higher-energy vibrations of the ground state molecule; as vibrational relaxations occur, heat (thermal energy) is released.[54-56] Alternatively, non-radiative decay pathways can originate from electronic trap states.[57-59] The competition between the two decay pathways of k_r and k_{nr} is evident in the resulting luminescence intensity, (I_0) and is directly proportional to the quantum yield (ϕ_{em}), as shown in eq. I.1:

$$I_0 \propto \phi_{em} = \frac{k_r}{k_r + k_{nr}} = k_r \tau_0 \qquad (I.1)$$

The natural lifetime of the electronic excited state is $\tau_0 = (k_r+k_{nr})^{-1}$.[33] Generally, non-radiative relaxation pathways dominate ($k_{nr} >> k_r$), leaving the molecule non-luminescent. Only when $k_r >> k_{nr}$ will an excited molecule emit. Based on this analysis of excited state decay pathways, it is evident that manipulation of k_r vs. k_{nr} or an introduction of a new decay pathway is essential for design of chemosensing strategies.

I.1.b Sensing via Collisional Quenching

The simplest method of perturbing the relation between k_r and k_{nr} is to introduce another pathway that competes with the radiative pathway, k_r, resulting in decrease of emission intensity. A bimolecular collision of M* with an analyte (*Q*, for quencher) will further modify emission intensity and lifetime of M*, by introducing a pathway that is non-radiative. The equation I.1 can simply be modified by adding $k_Q[Q]$ to the denominator to give eq. I.2,[60]

$$I_0 \propto \phi_{em} = \frac{k_r}{k_r + k_{nr} + k_Q[Q]} = k_r \tau \qquad (I.2)$$

where $k_Q[Q]$ is the quenching rate in the presence of quencher at concentration [Q]. By taking the ratio of emission intensities (I_0, I) and lifetimes (τ_0, τ) in the (absence,

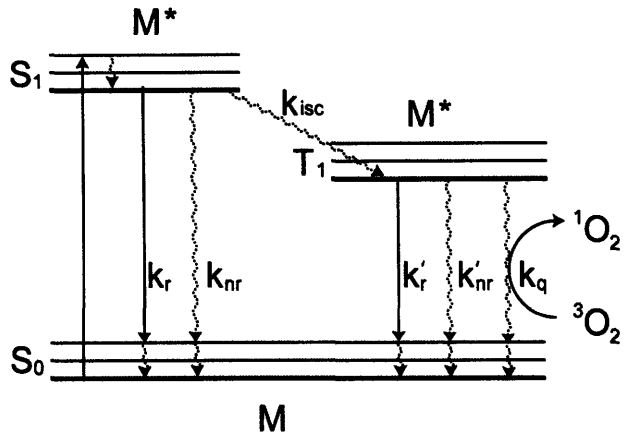

Figure I.2 Jablonski diagram depicting phosphorescent quenching of an excited state molecule (M*) by oxygen.

presence) of *Q*, collisional quenching can be expressed by the Stern-Volmer equation I.3, given as follows:

$$\frac{I_0}{I} = \frac{\tau_0}{\tau} = 1 + k_Q \tau_0 [Q] = 1 + K[Q] \qquad (I.3)$$

In this equation, *K* is the Stern-Volmer quenching constant.[33] Despite the ease of implementing detection schemes in which the quencher is the analyte, the sensitivity and selectivity of collisional quenching based mechanism are limited. In the case of fluorescence, where the molecule decays from the first excited singlet-state, the ratio of k_r to $k_Q[Q]$ is large. Thus the excited state is little affected by oxygen. In the case of phosphorescence, where the molecule decays from the first excited triplet-state, high reactivity towards oxygen circumvents collisional quenching with an analyte. Oxygen, which has a low energy singlet state that readily accepts energy, and thus it acts as an interferent of the collisional quenching sensing mechanism.[61] Accordingly, the most utilized application of collisional quenching is oxygen sensing itself. Because phosphors tend to have a longer lifetime (due to the spin-forbidden transition to the triplet state), phosphorescence quenching is the primary mechanism in which oxygen is quantified,[33] as shown in Figure I.2.

I.1.c Two-State Fluorescent Sensors

A second mechanism for sensing is available when the emissive response of the sensor changes upon analyte binding. The equilibrium between the free fluorophore and

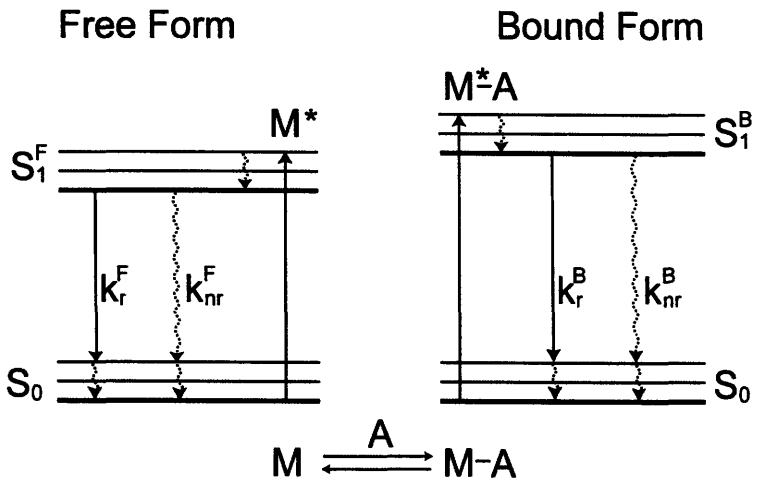

Figure I.3 Jablonski diagram for the free (F) and bound (B) forms of a two-state probe of a molecule (M), when interacting with an analyte (A).

the bound fluorophore will reflect the analyte concentration. If a fluorophore can exist in two emissive states, then the sensor may be emission wavelength-ratiometric, where the ratio of emission intensities of the two forms may be used to determine analyte concentration. A sensor may be excitation wavelength-ratiometric as well, where ratios of emission intensities at two different excitation wavelengths (due to different absorptions with respect to analyte binding) are taken to determine analyte concentration. Ratiometric sensing is powerful, as it allows the sensor to be self-calibrating. As long as there are different photophysics of the bound versus unbound forms of the probe that are resolvable, ratios of emission can be taken. Alternatively, if one form is fluorescent while the other form is not, emission will only be seen in the absence or presence of an analyte. Many pH indicators are examples of two-state fluorescent sensors.[62,63] Figure I.3 depicts the excited state energetics of the two-state fluorescent sensor.

I.1.d Sensing by Fluorescence Resonance Energy Transfer

Fluorescence Resonance Energy Transfer (FRET) is a phenomenon in which photo-excitation energy is non-radiatively transferred from a donor fluorophore to an acceptor molecule.[33] Collisional quenching mechanisms or two-state sensors must be uniquely sensitive to the analyte while possessing attractive fluorescence spectral properties, two qualities that are often difficult to find in the same molecule. However,

with FRET, the donor and acceptor are separate molecules, so the donor may be selected for use with simple light sources and desired lifetimes while the acceptor can be chosen for analyte sensitivity (Scheme I.1). Thus, incorporation of FRET into a sensing scheme simplifies the design of the fluorescent sensor. Figure I.4 depicts the Jablonski diagram for FRET processes. Förster theory models the rate for this energy transfer according to the spectral overlap between donor emission and acceptor absorption, J, the donor-acceptor distance, r, and a constant B, as shown in eq. I.4.[33]

$$k_{FRET} = \frac{B \times J}{r^6} k_r \tag{I.4}$$

The FRET rate is dependent on the inverse 6th power of the donor-acceptor distance. The radiative rate of the donor is obtained from the donor lifetime and the quantum yield, as described in eq. I.5, where k_{nr} is the non-radiative decay rate:

$$\phi_D = \frac{k_r}{k_r + k_{nr}} = k_r \tau_D \tag{I.5}$$

With substitution of eq. I.5 to I.4, one obtains:

$$k_{FRET} = \frac{(B \times J \times \phi_D)}{\tau_D r^6} \tag{I.6}$$

A characteristic distance, R_0, can then be defined such that at $r = R_0$, the rate of energy transfer, k_{FRET}, is equal to the rate of the donor radiative decay, τ_D^{-1}, as described by eq. I.7.

$$k_{FRET} = \frac{1}{\tau_D}\left(\frac{R_0}{r}\right)^6 \quad \text{with} \quad R_0 = (B \times J \times \phi)^{1/6} \tag{I.7}$$

Expanding the constant B gives eq. 1.8, where n is the refractive index of the medium, N is Avogadro's number, and κ^2 is a constant reflecting the relative orientation of donor and acceptor dipoles.

Scheme I.1 The signal transduction mechanism for a sensor based on FRET between a donor (green) and acceptor (blue) pair. Upon analyte binding, the acceptor changes its absorptive and/or emissive properties to modulate the emissive signal from the construct through FRET.

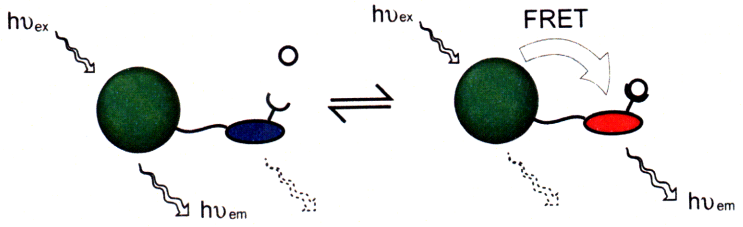

$$D^* + A \longrightarrow D + A^*$$

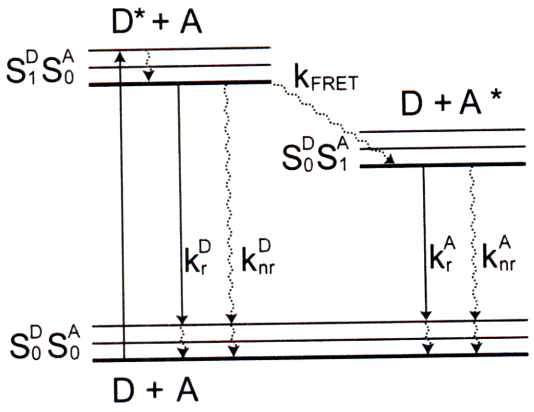

Figure I.4 Jablonski diagram depicting FRET processes between a donor (D) and acceptor (A).

$$R_0 = \left(\frac{9000 \ln(10) \kappa^2 \phi_D J}{128 \pi^5 n^4 N} \right)^{1/6} \quad \text{where} \quad J = \int_0^\infty d\nu \frac{f_D(\nu) e_A(\nu)}{\nu^4} \tag{I.8}$$

The overlap integral, J, is comprised of $f_D(\nu)$, the normalized fluorescence intensity of the donor in wavenumbers (cm^{-1}), and $\varepsilon_A(\nu)$, the extinction coefficient of the acceptor. The Förster analysis is best calculated in units of cm, as the extinction coefficient of the acceptor is described in units of M^{-1} cm^{-1}. As shown in eq. I.8, the transfer distance is determined by the spectral overlap between the emission of the donor and the absorbance of the acceptor.

The efficiency (E) of FRET, or the fraction of photons absorbed by the donor that are transferred to the acceptor, is the ratio of the transfer rate to the total decay rate of

the donor and is described by eq. I.9:

$$E = 1 - \frac{\tau_{D-A}}{\tau_D} = \frac{k_{D-A}}{k_{D-A} + \tau_D^{-1}} = \frac{R_0^6}{R_0^6 + r^6} \quad \text{(I.9)}$$

Eq. I.9 can be modified when more than one acceptor can interact equally with the donor as shown in eq. I.10:

$$E = \frac{mR_0^6}{mR_0^6 + r^6} \quad \text{(I.10)}$$

Eq. I.10 shows that the efficiency of energy transfer is generally enhanced by increasing the number of acceptor molecules, *m*. It is important to note in a study that utilizes one donor and multiple acceptors, any distance measurement will represent a statistical average distance in a given solution of donor-acceptor pairs unless every pair has an identical fixed distance between the donor and acceptor and an identical number of acceptors per donor.[64] Critical transfer length scales are often found to lie between 20 to 90 Å; the study of FRET is useful for distances comparable to biological macromolecules and is often applied for sensing changes in protein conformation and analyte binding events.[33]

Sections I.1.b - I.1.d described three common techniques to manipulate the excited state dynamics for luminescence based sensing. The sensing strategies developed and discussed in this Thesis are based on FRET.

I.2 The Necessity of New Sensing Tools for the Discovery of New Cancer Therapies

Fluorescent tracers and sensors are popular in biological applications due to their non-invasive nature, their ability to report continuously in real-time, and their sensitivity.[65] Tracers that emit different colors may be used and detected simultaneously for multiplexing analyses.[5] In addition, fluorescent sensors and probes that can be wavelength-ratiometric or can be used as an analyte-dependent lifetime-based sensor allows for accurate and reproducible measurement in the highly scattering and absorptive biological environments.[3,33] Fluorescent probes can be synthetically modified

and tailored for specificity in labeling and sensing purposes, and new tools and probes for biological applications are constantly being developed.[32]

One area where the necessity of new sensing tools and probes is evident is in the field of tumor biology. In order to understand how cancer progresses and in order to develop selective therapies, probing the intricacies of the tumor environment is essential. Normal tissues consist of vessels that are well-organized and regulated with dichotomous branching. In contrast, tumor environments are characterized by dilated, tortuous and heterogeneous blood vessels that are leaky.[66-68] Formation of new blood vessels, or angiogenesis, is governed by a strict balance of pro- and anti-angiogenic factors occurring only when needed, for example during wound healing and embryonic development. This careful control of angiogenesis is askew in tumor tissues.[66-68] The chemical environment of the tumors is also markedly different. pH and oxygen (O_2) are the two main parameters that define metabolic environment in tumors. Because the tumor vasculature is so leaky, which makes for inadequate delivery, the environment is hypoxic, lacking in oxygen.[66,67] Low extracellular pH also characterizes the tumor environment. Lactic acid, the product of anaerobic glycolysis, and carbonic acid, formed from dissolved CO_2 as a product of aerobic respiration, are the two principal sources of H^+ ions in tumors. They may also accumulate due to their reduced removal pathways.[69] The hypoxic and acidic metabolic tumor environment incapacitates immune cells, renders tumor cells invasive and metastatic, and induces expression of angiogenic factors, all of which can continue to trigger tumor growth.[66,67,70-72]

Since tumors require blood vessels for growth and metastasis, targeting angiogenesis in tumors is one strategy that has been pursued for treatment.[73-75] However, anti-angiogenic therapy has only produced short-term beneficial responses, and long-term studies have shown that tumors tend to grow back aggressively.[74-76] In combination with chemotherapy, anti-angiogenic therapy has been shown to be effective in the long term.[77] While combinatorial therapy is promising, there exists a paradox: chemotherapy and radiation therapy are methods that attack cancerous tissues directly. Anti-angiogenic therapy deprives the tumors of nutrients and waste-removal mechanisms by attacking the tumor vasculature, which is the exact vasculature that is needed to deliver the chemotherapeutic drugs and oxygen for radiative therapy.

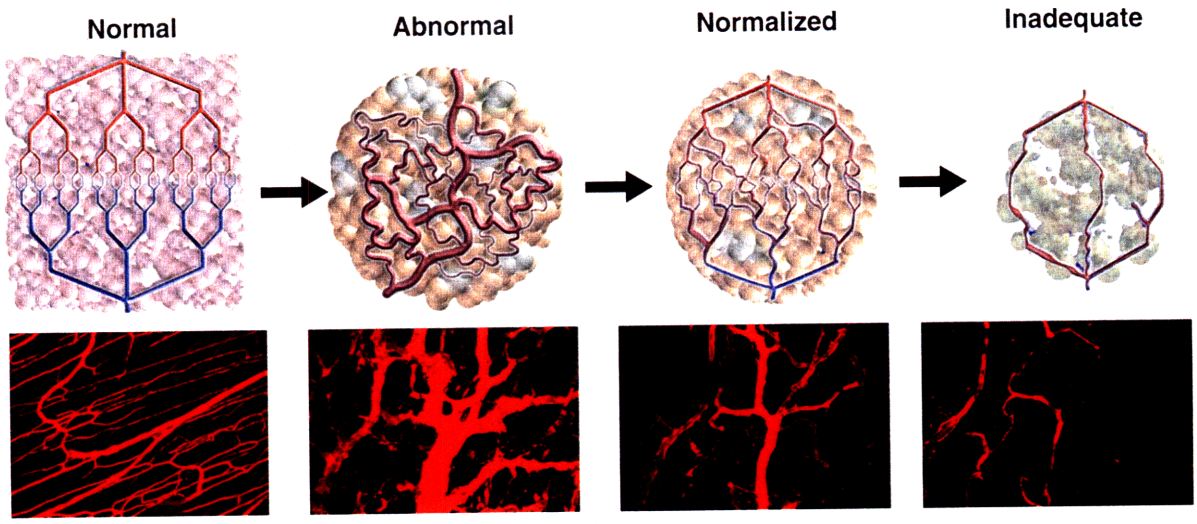

Figure I.5 Schematic (Above) and two-photon image (Below) of tissue vasculature within 1) normal tissues, 2) Abnormal (tumor) tissues, 3) 'Normalized' or abnormal tissues treated with anti-angiogenic therapy, 4) 'Inadequate' or starved tissues treated with aggressive anti-angiogenic therapy. Figure adapted from ref. 68.

The effect of anti-angiogenic therapy might be expected to hinder the effectiveness of chemotherapy and radiation.[78-80]

Jain has proposed the "Normalization Hypothesis" in order to guide the development of more efficient methods to deliver combinatorial treatment.[68] They hypothesize that there exists a window of time, after the application of anti-angiogenic agents, that the abnormal tumor tissue becomes "normalized", resembling and functioning as normal tissue (Figure I.5). As shown in Figure I.5, the changes in *morphological parameters* during the normalization window can be characterized by multiphoton laser scanning microscopy (MPLSM), a photoluminescence imaging technique with significant depth penetration with high three-dimension resolution.[81,82] The normalized tissue has a less leaky and less dilated vasculature. The transport of nutrients, wastes, and drugs is thus enhanced, similar to that of normalized tissues. Too much dosage of anti-angiogenic drugs will result in tissues with inadequate vasculature to deliver chemotherapeutic drugs.

Anti-angiogenic agents improve tumor tissue oxygenation for brief periods of time,[83,84] thus suggesting a window of normalization. However, the changes in *functional parameters* of pH and O_2 have not been characterized in detail. The local pH and O_2 concentrations have a significant impact on tumor treatment. Radiation therapy

depends on the oxygen content for production and propagation of free radicals to kill tumor cells.[85] As tumors becomes more hypoxic, they become less sensitive to radiaton.[66] Chemotherapeutics are affected by pH. Many drugs, such as paclitaxel, doxorubicin, and mitoxantrone are weak bases, the cellular uptake of which are prevented by the acidic extracellular pH environment.[86] As the *functional parameters* of the tumor environment affects the efficacy of chemotherapy and radiation, the knowledge of how anti-angiogenic treatment impacts pH and O_2 is essential for combinatorial treatment.

I.3 Limitations of Conventional Sensors and Dyes for Biological Applications

Measurements of pH and oxygen in biological environments are often performed under single-photon excitation conditions.[87-92] Briefly, one photon of high energy light (typically UV) is used to excite a fluorophore, which in turn emits a lower-energy photon. In the case of two-photon excitation, two simultaneous photons (within ~0.5 fs) of lower-energy (typically red to NIR) are used to excite a fluorophore through a virtual state, eliciting a response as if it were excited by a single-photon (Figure I.6). Using single-photon microscopy, pH indicators, such as 2',7'-bis-(2-carboxyethyl)-5-(and-6)-carboxyfluorescein (BCECF) and seminaphthorhodafluor-5F 5-(and-6)-carboxylic acid

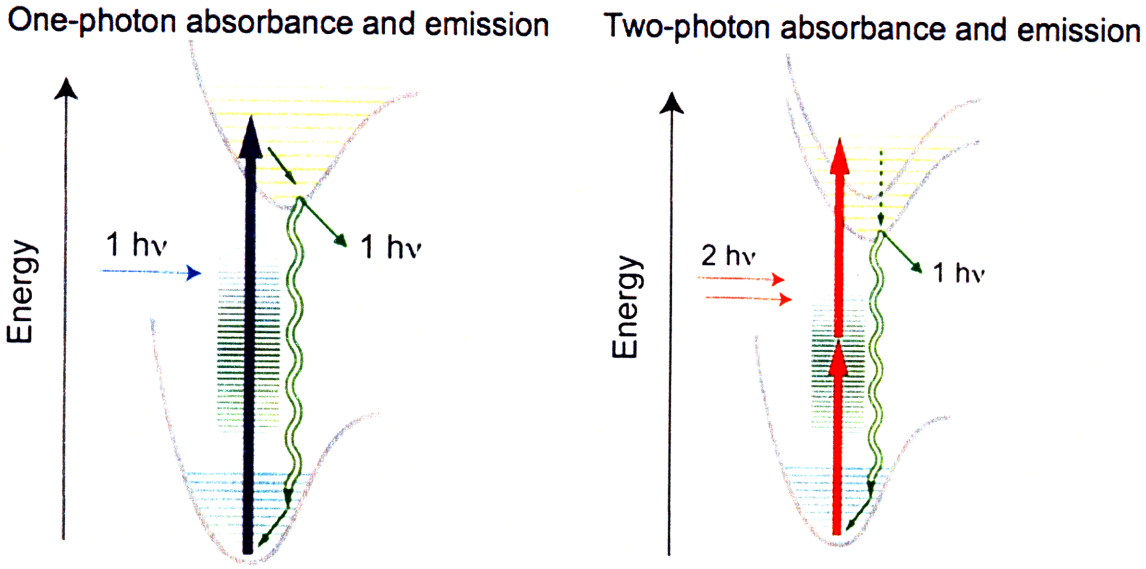

Figure I.6 Schematic diagram of one- and two- photon excitation events.

(SNARF-5F) allow for calibration in a biological environment via ratiometric sensing, because the absorption or emission lineshapes of the compounds exhibit a change with respect to pH. Photoluminescence measurements of O_2 are generally determined through lifetime quenching, with quantification through the Stern-Volmer relation,[33,93] although a few examples of wavelength ratiometric emissive probes for O_2 exist.[94,95]

The challenge arises when moving into the multi-photon excitation regime. Multi-photon Laser Scanning Microscopy (MPLSM) is a powerful technique that allows for a three-dimensional resolution of 1 micron up to depths of 600 microns.[81,96] The two-photon excitation event is rare and scales with the square of the excitation intensity. Such techniques thus depend on ultrafast (fs) laser excitation of small excitation volumes. Because of the narrow focal point, excitation scattering is minimized and photodamage is limited. NIR excitation falls within the biological window and its use minimizes extraneous absorption by tissues, globins, and water, thus decreasing autofluorescence of tissues (Figure I.7).[97] MPLSM can also image tissues non-invasively in real-time.[81,98,99] Unfortunately, in the case of pH sensors, the excitation lineshape dramatically changes when the transition is changed from single-photon excitation to two-photon excitation, and it becomes more difficult to spectrally resolve the acid and base forms of the excitation cross section, which is the measure for the probability of an absorption process by the molecule. Either the acid or base form of the cross section dominates under two-photon excitation, causing the emission spectrum to be overwhelmed with fluorescence of one form, and a two-state emissive sensor is obviated.[100] One pH indicator, 2,3-dicyanohydroquinone has been reported as a two-photon active ratiometric sensor at one single excitation wavelength; however, the dye is toxic, limiting its use in biological studies. Common O_2 sensors, such as porphyrins, exhibit very low two-photon absorption cross-sections, which is challenging to MPLSM applications.[101]

In view of the limitations posed by traditional analyte-sensitive dyes for MPLSM applications, new fluorophores must be explored for biological sensing applications. Semiconductor nanocrystals (NCs) are attractive candidates for use as biological probes under multi-photon excitation. They have a high two-photon absorption cross section, around ~10^5 Goeppert-Mayer (GM) units (1 GM = 10^{-50}cm^{4}s photon^{-1}

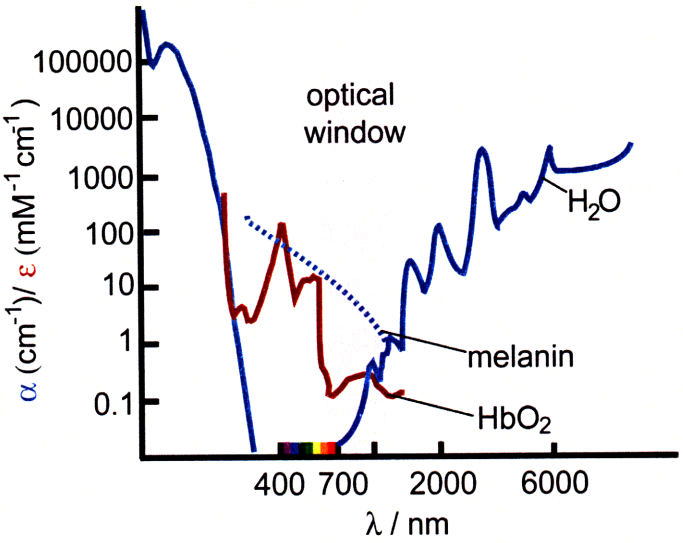

Figure I.7 The optical 'window' shows the optimal excitation wavelengths of biological species to be between 700 – 1100 nm.

molecules^{-1}) as opposed to ~10^1 - 10^2 GM units of traditional organic dyes. The NCs additionally exhibit a high quantum yield and photostability when two-photon excited.[102] Finally, they have also been used as imaging agents within the tumor milieu.[103,104] A more detailed discussion on NCs and the potential advantages of incorporating NCs into sensing schemes that are ratiometric under multi-photon excitation follows.

I.4 Semiconductor Nanocrystals as Fluorophores and Imaging Agents

Inorganic semiconductor NCs (also known as quantum dots) are a class of fluorophores that have attracted considerable interest owing to their unique photophysical characteristics.[105-119] In semiconductors, photophysics are determined by excitons, which are excited electrons bound through Coulombic interactions to the holes left behind in the valence band.[120] Quantum confinement in semiconductors occurs when the dimensions of the semiconductor approaches that of the exciton.[120] In such a regime, energy associated with the confinement in a crystal exceeds the Coulomb energy; as such, molecule-like states become resolvable, and we describe the nanocrystalline semiconductor as quantum dots. The effective bandgap of the NC widens with decreasing size, giving rise to unique, size-dependent optical and spectroscopic properties.[105] Broad absorption profiles and high extinction coefficients

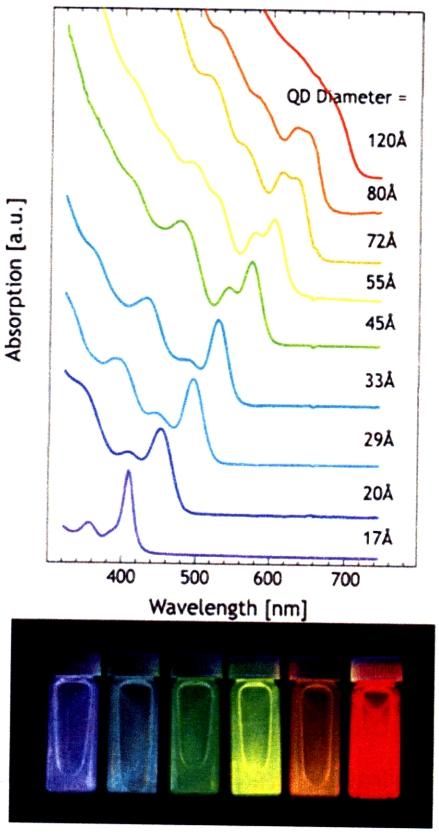

Figure I.8 (Top) Size dependent absorption of CdSe NCs, from ref. 105. (Bottom) Size dependent emission of CdSe NCs. Photography by Felice Frankel.

are complemented by a narrow (FWHM ~30 nm) and spectrally tunable emission profile. Figure I.8 shows the size-dependent optical properties of CdSe NCs. For example, small (2.3 nm diameter) CdSe NCs emit blue light under optical excitation whereas their larger counterparts (5.5 nm diameter) emit red light. The NCs exhibit appreciable quantum efficiencies for emission, though coating the outer surface of NCs with higher band gap inorganic materials further improves the photoluminescence quantum yield.[121,122] The coating presumably passivates sites associated with surface states that promote non-radiative recombination.[121,122] Along with higher quantum yields, "overcoated" core-shell CdSe/ZnS NCs are more chemically robust and possess high photobleaching thresholds.[121,122] These properties of NCs contrast with organic dyes, which tend to possess low resistance to photobleaching, narrow absorption profiles, and emission spectra that tail to the red; the spectral congestion that results from the tailing emission profiles can complicate multi-color imaging applications.[123]

Despite the apparent advantages of NCs as compared to organic dyes, the

implementation of NCs for fluorescence imaging was initially hampered by their insolubility in aqueous media as a result of the long-chained organic solvents needed for their high-temperature synthesis. This obstacle was overcome by further modifying the surface of the CdSe NCs. Alivisatos and co-workers prepared bio-compatible CdSe/CdS or CdSe/ZnS NCs by adding an additional layer of silica to the core-shell.[124] Nie and co-workers reported the use of mercaptoacetic acid to cap the surface of CdSe/ZnS NCs to impart water solubility.[125] The synthesis of water-soluble NCs now includes modifications with phospholipids,[126] amphiphilic polymers,[127] dendrimers,[128-133] oligomeric phosphines[134] and cap-exchanging the hydrophobic surface of NCs with multidentate hydrophilic ligands.[135,136] These ligands have greatly facilitated the use of NCs as bio-imaging agents and probes because they can be conjugated to proteins and peptides, such as streptavidin for cell-labeling studies.[123] The stability and quantum yields of such water-soluble NCs greatly vary among the different solubilization methods. For example, mono-thiol caps are photochemically unstable,[137] whereas multidentate ligands are reported to yield an aggregate free construct and to be stable in solutions of pH 5-12 over a course of one year with quantum yields around 25-30%.[138] Toxicity of NCs is a concern for biological *in vivo* experiments; however, most studies report no toxicity in live animals, even up to after 4 months after injection under standard conditions.[139] Oxidation of CdSe by air or UV light can cause Cd^{2+} to be released, which is toxic to cells.[140] Overcoating CdSe with a ZnS layer has also been reported to mitigate cell death significantly in embryos.[141] Therefore, protection of NCs from oxidation reduces toxicity, but long term cadmium leaching from NCs has not been studied.

More recently, the utility of NCs has been expanded by their use as optical sensors.[50] Initial applications centered on physical sensing. Previous work in our research group, reported by Walker *et al.* exploited the temperature-dependent photoluminescence properties of CdSe/ZnS NCs embedded in poly(lauryl methacrylate) to develop a temperature probe.[142] These initial studies have subsequently been elaborated for the measurement of temperature[143] and fluid flow near walls and in confined channels[144] opening the way for tandem flow measurements of temperature and velocimetry.

The water-solubility of overcoated NCs has rapidly led to their use as fluorescent *chemical* sensors. For this application, NC luminescence must be perturbed by the presence of a target analyte in the NC's environment. In some cases, the fluorescence is suppressed by morphological changes to the lattice. For example, Ag^{+}, Pb^{2+}, and Cu^{2+} ions quench NC luminescence by replacing the Cd^{2+} ions in the NC lattice.[145] Only by overwhelming the NC with excess Cd^{2+} can luminescence be partially recovered. However, permanent quenching of NC luminescence is not practical as a sensing strategy, as it is usually not analyte specific, nor is it easily reversible. Recently, detection of specific chem- / bio- (CB) target analytes has been achieved reversibly using overcoated CdSe NCs that have been modified with a conjugate attached to the overcoated layer. Work has also been performed with NCs composed of materials other than CdSe, most notably CdTe.[146-149] The NC sensors described in the following Chapters of this Thesis are primarily CdSe based. CdSe was chosen as a starting point for sensor design as it is the most studied and well-understood of the semiconductor inorganic NCs. CdSe NC constructs, together with the excited state mechanisms that underpin their sensing function, constitute the scope of the discussion that follows.

I.5 NC Sensing by Fluorescence Resonance Energy Transfer

Fluorescence Resonance Energy Transfer (FRET) has been the primary photophysical mechanism by which NCs report the presence of a target analyte. Although the NC is a fairly large object (nanometer scale) in proximity to the dye, the NC excited state is typically approximated as an oscillating point dipole (with $\kappa^2 = 2/3$ for a random orientation). This approximation works well for the FRET experiments described in this Thesis.

I.5.a NC Energy Transfer

Energy transfer among CdSe NCs was observed by Kagan *et al.* when they prepared thin films comprised of a mixture of closely-packed 555-nm emitting (smaller) and 620-nm emitting (larger) NCs.[150] Steady-state emission from the smaller NCs decreased concomitantly with an increase in emission from the larger NCs. Correspondingly, the lifetime of the smaller NCs shortened whereas that of the larger

NC lengthened. Analysis of the lifetime data by Förster theory supported the occurrence of energy transfer. This study established that CdSe NCs can act as both FRET donors and acceptors.

FRET involving CdSe NCs in aqueous media has been observed to occur between oppositely charged CdSe/ZnS NCs. Wargnier *et al.* prepared negatively charged CdSe/ZnS by treating the NCs with a mixture of mercaptosuccinic and mercaptosulfonic acids.[151] Positively charged ZnCdSe/ZnS NCs were synthesized by treating the NC surface with cystinamine. Upon mixing with larger NCs (which naturally carry a negative charge), emission from the positively-charged and smaller NCs was found to be quenched. On the basis of the diameters of the NC donor and acceptors, a Förster critical distance and efficiency were calculated to be 7.3 nm and 91%, respectively. These values were found to be in reasonable agreement to the Förster critical distance and efficiency determined from the quenching of the PL decay times.

I.5.b NCs as FRET Donors

Energy transfer from a NC donor to an organic acceptor in aqueous solution was demonstrated by Willard *et al.*[152,153] Water-soluble CdSe/ZnS NCs were conjugated to a thiolated biotinilated bovine serum albumin (bBSA, 9:1 biotin:BSA ratio). Calculations revealed that 11 bBSA molecules were bound to the surface of the NC. The acceptor complex was prepared separately by conjugating streptavidin to tetramethylrhodamine (TMR). Upon titrating the dye-modified streptavidin to the NC-bBSA complex in PBS buffer, NC luminescence was quenched and TMR fluorescence was enhanced.

A penetrating study of energy transfer between donor NCs and acceptor dye molecules has been performed by Mattoussi and co-workers.[64,154] Water-soluble CdSe/ZnS NCs were prepared by exchanging ligands on the NC surface with dihydrolipoic acid, which possesses bidentate thiol groups. A maltose binding protein (MBP) from an engineered *Escherichia coli* containing site-specific labeled dye acceptors was assembled onto the surface of the NC by either: (1) electrostatic self-assembly of the negatively charged dihydrolipoic acid to a basic leucine zipper on the MBP or (2) metal-affinity coordination between the NC surface and a C-terminal oligohistidine chain on the MBP (Figure I.9).[64,154] In synthesizing these constructs, the

emission wavelength of the NC and the number of dye-labeled MBPs bound to the NC were systematically varied. The total number of MBPs per NC was maintained for the different-sized NCs in order to keep the average distance between the NC and the acceptor dyes as well as the NC quantum yield constant. As the fraction of dye-labeled MBPs was increased, emission from the dye increased while that from the NCs decreased. Time-resolved fluorescence experiments confirmed that the NC lifetime shortened as more dye-labeled MBPs surrounded the NCs.[64,154] Additionally, experiments varying the spectral overlap (by changing the NC donor emission wavelengths) revealed that the efficiency of energy transfer varied as expected from a Förster model. As expected from eq. I.8, efficiency improved with increasing numbers of dye-labeled MBPs around the NC. All of these studies support an energy transfer mechanism between a CdSe NC donor and an organic acceptor dye.

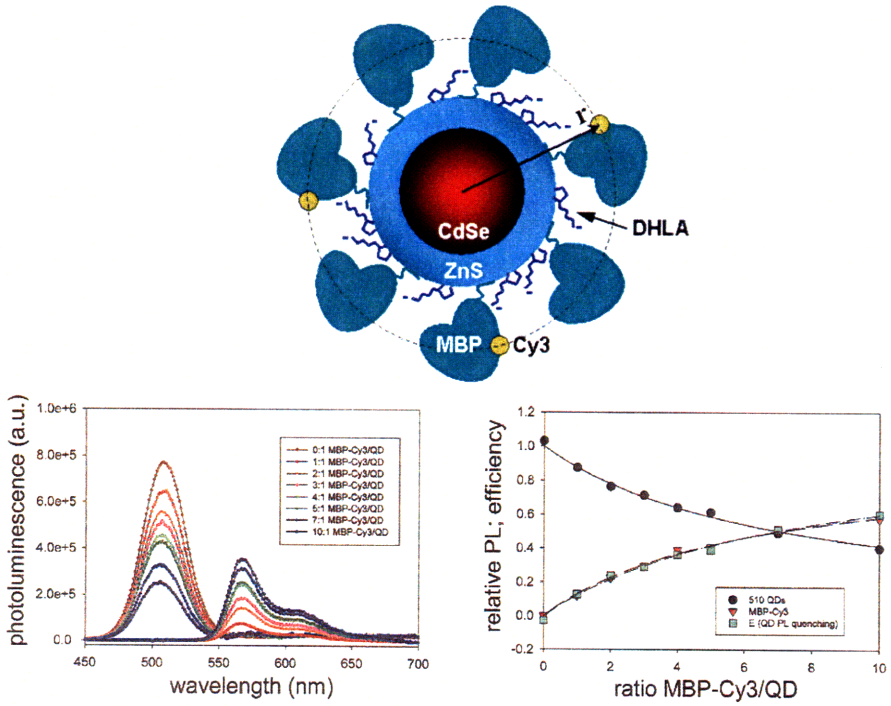

Figure I.9 (Top) A schematic representation of the NC-MBP assembly developed by Mattoussi and co-workers. The dihydrolipoic acid (DHLA) caps the NC and allows the MBP to self-assemble onto the NC. A Cy3 dye is attached to the MBP. (Bottom left) Photoluminescence spectra from 510 nm emitting NC and Cy3 dyes in the NC-MBP-Cy3 construct with increasing dye to NC ratio. (Bottom right) Experimental values for the NC emission decay percentage versus dye to NC ratio (circle ●), the rate of FRET extracted for the NC emission loss (triangle ▼), and the rate of FRET deduced from acceptor gain (square ■). Figure adapted from ref. 64.

Energy transfer between a NC donor and a dye acceptor has also been observed at the single molecule level.[155] Hohng *et al.* used a commercially available streptavidin-coated NC to immobilize the NC on a quartz surface coated with bBSA. A cyanine dye, Cy5, was positioned near the NC surface by placing it with biotin on the same end of a duplex DNA. Energy transfer was monitored with the steady-state emission of the NC and Cy5. Conformational change in the DNA should, in principle, lead to a change in FRET efficiency. However, very low signal intensity complicated such an interpretation. The low signal was ascribed, in part, to the very large energy transfer distance between the streptavidin coated NC and biotinylated dye, emphasizing the need for simple conjugates in which the energy transfer distance can be short.

Zhou *et al.* directly coupled an Alexa 594-labeled DNA acceptor to a NC donor through a thiol linker.[156] Commercially obtained CdSe/ZnS NCs were treated with 3-mercaptopropionic acid (MPA) to produce a water-soluble NC. Coupling to Alexa 594-labeled DNA was achieved using a C_6 thiol linker. The ability to couple without protein linkers minimized the distance between the NC and the dye. Owing to the short donor-acceptor distance, the FRET efficiency in these constructs was found to be as high as 88% in ensemble and single-molecule constructs. A Förster critical transfer distance of 4.2 nm was calculated from the quenched luminescence.

I.5.c NCs as FRET Acceptors

Whereas there have been numerous studies on CdSe NCs as FRET donors, very few studies have reported CdSe NCs as FRET acceptors.[157-160] To summarize briefly, studies have indicated that NCs are able to behave as FRET acceptors, especially when coupled to a donor with a longer lifetime, such as metal complexes[159,160] and polymers.[158] However, because NCs are easily excited (due to the broad continuous absorption) and there exists a possibility for different donor molecules to transfer energy into an NC acceptor, sensing mechanisms using NCs are best implemented when NC is given the role of a FRET donor.

I.6 FRET Schemes for Sensing with NCs

The ability of NCs to participate in FRET provides a mechanism for signal

transduction in optical sensing schemes. Figure I.10 summarizes the different sensing strategies that have been employed with NCs. Of the five signal transduction mechanisms, four rely on the NC as the FRET donor. The broad excitation spectrum of the NCs complicates their utilization as FRET acceptors since it is difficult to excite a dye selectively without also exciting the NC acceptor. In Figure I.10 A-D, sensing is accomplished by modulating the FRET donor-acceptor distance. For Figure I.10 E, the FRET distance is preserved but the analyte causes the spectral overlap function to change, thus modulating the efficiency of FRET upon analyte recognition.

I.6.a Sensing by Nucleic Acid Recognition

Figure I.10A has been exploited to probe biological activity via FRET. Telomerization and DNA replication can be monitored with CdSe/ZnS NCs.[161] Patolsky *et al.* conjugated NCs to thiolated oligonucleotides with approximately 25 oligonucleotides per NC. Incubation with a dNTP (deoxy(nucleotide)triphosphate) mixture (dATP, dCTP, and dGTP) and Texas-Red labeled dUTP, in the presence of telomerase, initiated a change in the emission spectra of the NC and the dye over time. As telomerization proceeded, NC emission decreased and Texas Red emission increased due to FRET. DNA replication was probed by labeling CdSe/ZnS NCs with a DNA primer, followed by incubation with the complementary DNA sequence to allow for hybridization. Replication was initiated by adding polymerase mixed with dNTPs and Texas-Red labeled dUTPs. As replication progressed, the Texas-Red dUTP was brought in proximity to the NC, resulting in FRET from the NCs to the dye. These results suggested the application of NCs for the detection of cancer cells or for amplified detection of DNA on chip arrays.

Gill *et al.* have used FRET interactions of DNA to probe hybridization and cleavage.[162] In a similar manner to that discussed above, NCs were modified with a DNA strand and hybridized with a Texas-Red labeled nucleic acid. As hybridization proceeded, energy transfer occurred, and the NC emission progressively became weaker while the dye emission increased. The resulting CdSe NC-dye DNA duplex was cleaved with a hydrolytic enzyme DNase I. Cleavage of the DNA strand resulted in a partial restoration of the NC emission and a loss of dye emission. The incomplete

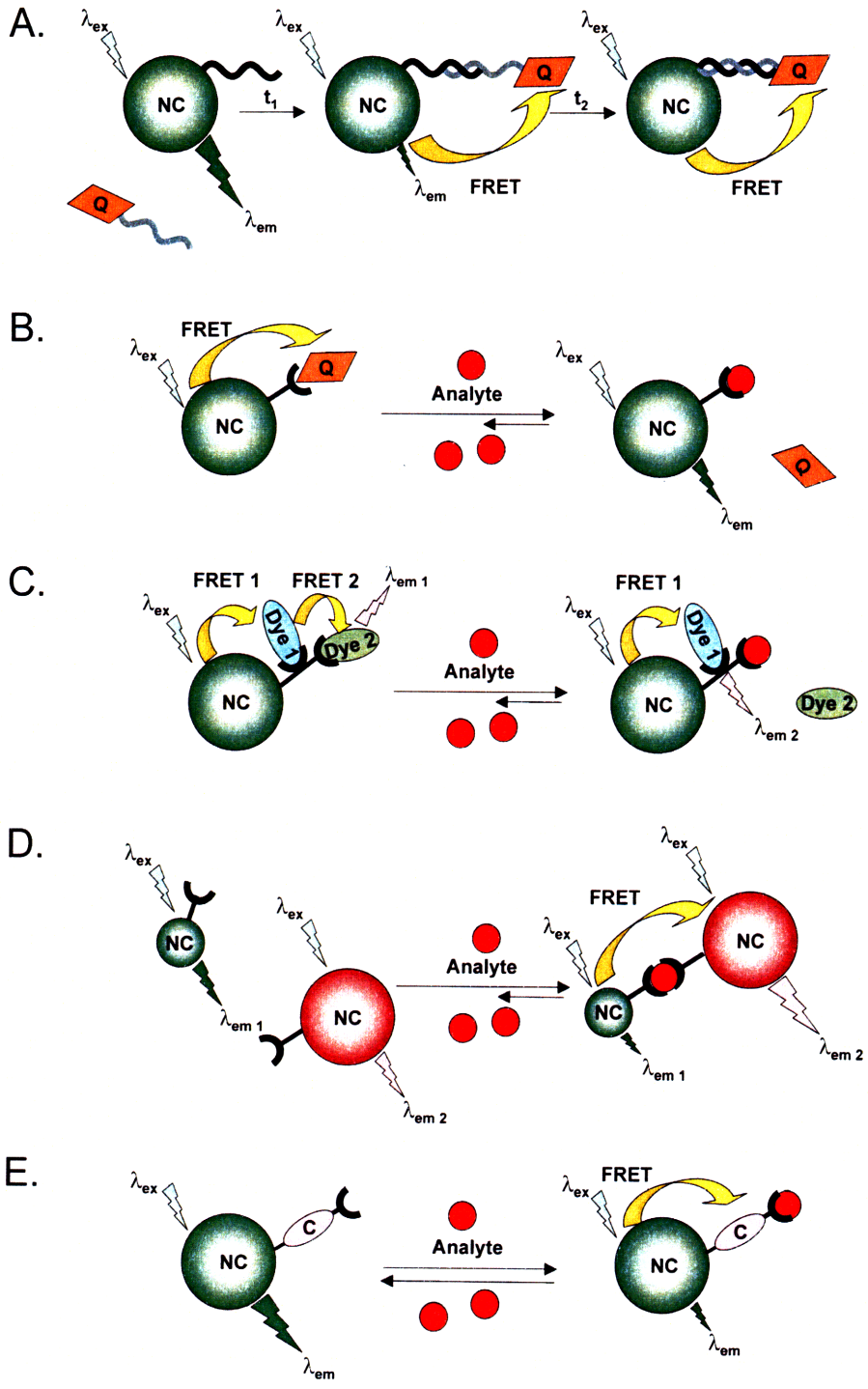

Figure I.10 Schematic diagram of the five different sensing strategies using FRET that are the focus of section I.6. A) is a biological probe sensing by nucleic acid recognition, B) and C) are sensors with two different strategies incorporating quencher displacement, D) is a construct relying on FRET between two different NCs, and E) is a single emission sensor relying on a FRET between NC and a colorimetric sensor.

recovery of the NC emission was attributed to the adsorption of dye molecules to the NC surface. Adsorption by the NCs presents a hurdle for their implementation as bioanalytical tools.

FRET from NCs can be used as a screen for small interfering RNAs (siRNA).[163] Bakalova *et al.* conjugated a single stranded siRNA to a NC to yield a hybridization probe while amplifying the target mRNA in the presence of Cy5 labeled nucleotides. The Cy5-mRNA was used as the hybridization template. A short hybridization time for siRNA/mRNA duplexes ensured for the selection of efficient, target-selective siRNA sequences. The affinity of the siRNA to the mRNA was detected by FRET from the NC to the Cy5. The Cy5 emission was only detected when there was good accessibility and high affinity between the two RNA strands.

The interaction of a HIV-1 regulatory protein, REV with its responsive element (designated RRE), has also been assayed by NC-dye FRET.[164] The 5′ end of the RRE RNA was biotinylated while a Cy5 dye was attached to the N-terminus of a model REV peptide sequence. A RRE-NC conjugate was synthesized by using a streptavidin-coated NC. The Cy5 modified REV was slowly titrated to the RRE-NC solution. Excitation at 488 nm, where the Cy5 does not absorb, yielded emission from both NC and Cy5 upon complexation of the REV to the RRE-NC. The ratio of the dye intensity to NC intensity increased with the addition of REV.

Per Figure I.10 A, the foregoing bioassays rely on modulating the FRET distance between the NC and an acceptor dye upon biological recognition of different macromolecules. A change in emission lifetime and intensity may be detected. Applications based on this model assume that the NCs do not interfere with macromolecule binding as a result of either size or charge perturbations. This assumption must be assessed for the development of reliable bioassays.

I.6.b Sensing by Analyte-induced Displacement

FRET coupled to quenching, as schematically represented in Figure I.10 B and C, provides alternative strategies for sensing. Here, luminescence due to FRET is turned on by the appearance of analyte, which displaces a quencher (Figure I.10 B) or a terminal energy acceptor (Figure I.10 C).

Mattoussi and co-workers have developed a sensor for maltose by adapting their CdSe-MBP conjugates for both analyte-displacement strategies depicted by Figure I.10 B and Figure I.10 C.[165,166] In the first construct, a β-cyclodextrin (β-CD) conjugated to a non-fluorescent QSY9 quencher dye was docked to the MBP saccharide binding site of the CdSe/ZnS-MBP. Maltose displaces the β-CD-QSY9 conjugate to restore NC emission. In their second strategy, defined by Figure I.10 C, the CdSe/ZnS-MBP construct is labeled with two different cyanine dyes: Cy3, which is bound directly to the MBP, and a β-CD conjugated to a Cy3.5, docked to the MBP binding site. Prior to maltose binding, Cy3.5 emission prevails by a two-step energy transfer from Cy3, which in turn accepts energy from CdSe. Upon binding to maltose, the β-CD-Cy3.5 conjugate is displaced and, in the absence of the terminal acceptor, Cy3 is the predominant emitting species.

A hybrid NC-antibody senses TNT operates by the mechanism shown in Figure I.10 B.[166] In place of MBP, an anti-TNT specific antibody fragment is appended with an

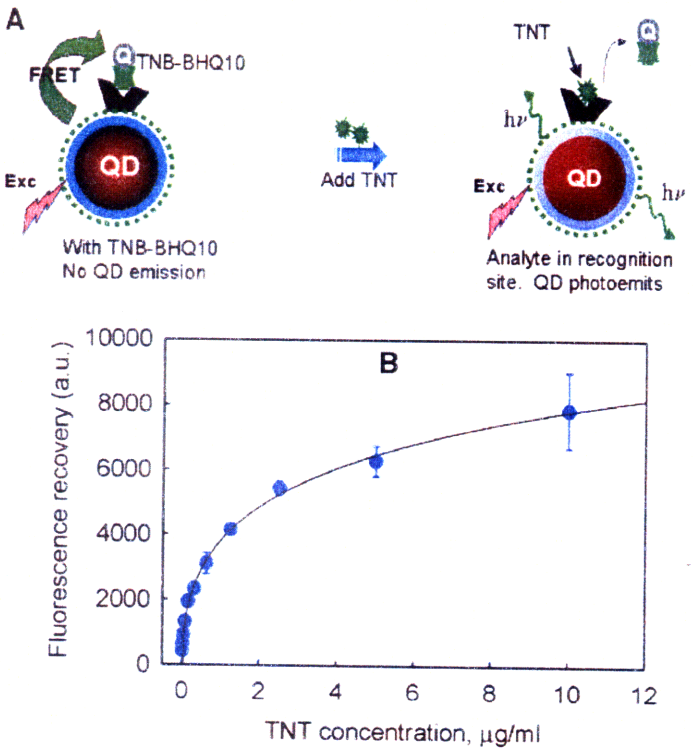

Figure I.11 (A) A schematic diagram of the quencher-displacement mechanism to sense TNT. (B) Increase in the NC photoluminescence versus concentration of TNT. Figure adapted from ref. 166.

oligohistidine sequence, which is bound to the surface of a CdSe/ZnS NC. A TNT analogue pre-labeled with a quencher dye (Black Hole Quencher-10, BHQ-10) was pre-docked in the recognition site of the antibody. The docked dye quenches NC emission. The NC emission is "turned-on" when TNT displaces the quencher from the sensor, as shown in Figure I.11. The specificity of the TNT sensor was tested by comparing the effectiveness of FRET from the NC to the quencher dye for three different TNT analogues. The analyte specificity of the original antibody fragment was conserved after being bound to the NC. This approach is general and constructs involving an antibody fragment bound to a NC surface through noncovalent self-assembly should find wider use as a target of other analytes of interest.

I.6.c Sensing by NC to NC FRET

The NC-dye constructs incorporating analyte-displacement strategies are excellent single-response sensors. To realize maximum sensitivity and utility, however, a more ideal sensor would be reversible and /or self-referencing (ratiometric). One such scheme is shown by Figure I.10 D. FRET between small (green) and large (red) CdSe/ ZnS NCs has been implemented to sense potassium ions.[167] 15-crown-5 ethers were adsorbed onto the surface of the NCs through the bidentate thiol of dihydrolipoic acid. Prior to adding K^+ ions, both green and red NC emissions are present; the NC solutions were dilute enough to prevent energy transfer between the two NCs. Upon adding $KClO_4$, the green emission of the smaller NCs gradually decreased, while the red emission of the larger NCs increased. This synchronous change in emission intensities was ascribed to an energy transfer mechanism caused by aggregation of the NCs. The aggregate formed by the recognition of K^+ ions by the 15-crown-5 ethers to furnish a 15-crown-5/K^+/15-crown-5 sandwich complex. It was unclear whether the sandwich complex was formed from the coordination of two ether molecules from the neighboring arms of the same NC (intraparticle association) or from the two ether molecules of different NCs (interparticle association). A response was observed over a 10^{-6} - 10^{-4} M concentration of $KClO_4$; the NCs were observed to precipitate from solution at higher $KClO_4$ concentrations. The construct showed excellent sensitivity; however, high

association between the K^+ ion and the crown ether as well as aggregation between the NCs at high concentrations makes reversible sensing difficult.

I.6.d Sensing by NC Conjugation to Analyte-sensitive Chromophores

A reversible CdSe/ZnS NC sensor of pH operates according to Figure I.10 E.[168,169] A pH-sensitive chromophore was conjugated to NC with a lipoic acid derivatized with a [1,3]-oxazine ring. The [1,3]-oxazine ring may be opened by hydroxide anion to generate a 4-nitrophenylazophenolate chromophore. The absorption spectrum of this chromophore overlaps with the emission spectrum of the NC. This spectral overlap activates FRET, leading to a diminution of NC luminescence. Specifically, the NC emission intensity decreases by 35% over the pH from 7.1 to 8.5. The sole emission from the NC results in a detection signal that is not referenced, making calibration difficult.

I.7 Goals and Scope of This Thesis

The concentration of any analyte is generally difficult to quantify with a simple change in emission intensity of a single emitting species. An accurate measurement of analyte concentration is unattainable if the overall background intensity changes, emission from species in the environment is present, or if the dye emission is sensitive to an interferent. In order to develop new tools to probe analyte changes in a biological environment, the construct must be ratiometric, reversible, and stable. This Thesis attempts to address the development of such sensors for applications in biology, focusing on the following considerations:

1) Explorations of new surface modifications of NCs, including size, stability, and biocompatibility
2) Development of covalent conjugation strategies of receptors to NCs
3) Investigations into energy transfer efficiencies with new ligand scaffolds
4) Design of ratiometric and reversible sensing mechanisms using NCs
5) Preliminary studies of NC constructs in an *in vivo* environment

Chapter II explores new coatings for NCs that allow for efficient FRET and facile

conjugation in aqueous environments. A full photophysical characterization was performed to determine the efficiency and applicability of energy transfer using the new surface coating. In Chapter III, the synthesis and characterization of a proof-of-concept pH sensor that displays ratiometric emission is described. Chapter IV is devoted towards making bio-applicable and efficient NC-based pH sensors by exploring more NC surface modifications and by varying NC-dye coupling strategies. Chapter V describes the full synthetic and photophysical characteristics of a PEGylated biocompatible pH sensor. In Chapter VI, preliminary investigations with a biocompatible NC pH sensor in an *in vivo* tumor environment using mouse models are discussed. FRET-based sensing under two-photon excitation is shown to behave in a similar manner to that of one-photon excitation. Chapter VII describes another bio-stable coupling strategy using Click chemistry to couple NCs to dyes. Finally, this Thesis concludes with Chapter VIII, which discusses future directions and preliminary results for development of additional NC based chemosensors.

I.8 References

1. Niessner, R. *Trends Anal. Chem.* **1991**, *10*, 310-316.

2. Scully, P.; Chandy, R.; Edwards, R.; Merchant, D.; Morgan, R. *Environ. Sci. Res.* **2001**, *56*, 175-199.

3. Szmacinski, H.; Lakowicz, J. R. *Sens. Actuators, B* **1995**, *B29*, 16-24.

4. Stark, E.; Hitzmann, B.; Schugerl, K.; Scheper, T.; Fuchs, C.; Koster, D.; Markl, H. *Adv. Biochem. Eng. Biotechnol.* **2002**, *74*, 21-38.

5. Ulber, R.; Frerichs, J.-G.; Beutel, S. *Anal. Bioanal. Chem.* **2003**, *376*, 342-348.

6. Blagoi, G.; Rosenzweig, N.; Rosenzweig, Z. in *Fluorescence Sensors and Biosensors,* Thompson, R. B., Ed.; CRC Taylor & Francis: Boca Raton, 2006, p. 93-105.

7. Borisov, S. M.; Wolfbeis, O. S. *Chem. Rev.* **2008**, *108*, 423-461.

8. Bosch, M. E.; Sanchez, A. J. R.; Rojas, F. S.; Ojeda, C. B. *Comb. Chem. High T. Screen.* **2007**, *10*, 413-432.

9. Cullum, B. M. *Opt. Sci. Eng.* **2007**, *118*, 109-131.

10. Dacres, H.; Narayanaswamy, R. *Recent Research Developments in Analytical Biochemistry* **2005**, *4*, 35-79.

11. Wang, X.; Massey, M.; Piunno, P. A. E.; Krull, U. J. *Opt. Sci. Eng.* **2007**, *118*, 83-108.

12. Arnold, M. A.; Small, G. W. *Anal. Chem.* **2005**, *77*, 5429-5439.

13. Aslan, K.; Zhang, J.; Lakowicz, J. R.; Geddes, C. D. *J. Fluoresc.* **2004**, *14*, 391-400.

14. Ballerstadt, R.; Evans, C.; McNichols, R.; Gowda, A. *Biosens. Bioelectron.* **2006**, *22*, 275-284.

15. Kondepati, V. R.; Heise, H. M. *Anal. Bioanal. Chem.* **2007**, *388*, 545-563.

16. Pickup, J. C.; Hussain, F.; Evans, N. D.; Rolinski, O. J.; Birch, D. J. S. *Biosens. Bioelectron.* **2005**, *20*, 2555-2565.

17. Wang, J. *Chem. Rev.* **2008**, *108*, 814-825.

18. Cable, M. L.; Kirby, J. P.; Sorasaenee, K.; Gray, H. B.; Ponce, A. *J. Am. Chem. Soc.* **2007**, *129*, 1474-1475.

19. Yung, P. T.; Lester, E. D.; Bearman, G.; Ponce, A. *Biotechnol. Bioeng.* **2007**, *98*, 864-871.

20. Royo, S.; Martinez-Manez, R.; Sancenon, F.; Costero, A. M.; Parra, M.; Gil, S. *Chem. Commun.* **2007**, 4839-4847.

21. Bell, T. W.; Hext, N. M. *Chem. Soc. Rev.* **2004**, *33*, 589-598.

22. de Silva, A. P.; Gunaratne, H. Q. N.; Gunnlaugsson, T.; Huxley, A. J. M.; McCoy, C. P.; Rademacher, J. T.; Rice, T. E. *Chem. Rev.* **1997**, *97*, 1515-1566.

23. *Chemosensors of Ion and Molecular Recognition*; Kluwer Academic Publishers: Dordrecht, The Netherlands, 1997; Vol. 492.

24. *Fluorescent Chemosensors for Ion and Molecule Recognition*; American Chemical Society: Washington, D. C., 1993.

25. Czarnik, A. W. *Acc. Chem. Res.* **1994**, *27*, 302-308.

26. Rudzinski, C. M.; Hartmann, W. K.; Nocera, D. G. *Coord. Chem. Rev.* **1998**, *171*, 115-123.

27. Rudzinski, C. M.; Nocera, D. G. in *Optical Sensors and Switches*, Ramamurthy, V.; Schanze, K.S., Eds.; Marcel Dekker: New York, 2001, p. 1-91.

28. Rudzinski, C. M.; Young, A. M.; Nocera, D. G. *J. Am. Chem. Soc.* **2002,** 124, 1723-1727.

29. Swager, T. M. *Acc. Chem. Res.* **1998**, *31*, 201-207.

30. Mohr, G. J. *Chem.- Eur. J.* **2004**, *10*, 1082-1090.

31. de Silva, A. P.; Fox, D. B.; Moody, T. S.; Weir, S. M. *Trends Biotechnol.* **2001**, *19*, 29-34.

32. Wolfbeis, O. S. *J. Mater. Chem.* **2005**, *15*, 2657-2669.

33. Lakowicz, J. R. *Principles of Fluorescence Spectroscopy, 2nd ed.*; Kluwar Academic/ Plenium Publishing: New York, 1999.

34. Buck, S. M.; Xu, H.; Brasuel, M.; Philbert, M. A.; Kopelman, R. *Talanta* **2004**, *63*, 41-59.

35. Peng, J.; He, X.; Wang, K.; Tan, W.; Wang, Y.; Liu, Y. *Anal. Bioanal. Chem.* **2007**, *388*, 645-654.

36. Verhey, H. J.; Gebben, B.; Hofstraat, J. W.; Verhoeven, J. W. *J. Polym. Sci., Part A: Polym. Chem.* **1995**, *33*, 399-405.

37. Tan, W.; Shi, Z. Y.; Smith, S.; Birnbaum, D.; Kopelman, R. *Science* **1992**, *258*, 778-781.

38. Sharp, S. L.; Warmack, R. J.; Goudonnet, J. P.; Lee, I.; Ferrell, T. L. *Acc. Chem. Res.* **1993**, *26*, 377-382.

39. Campbell, C. G.; Ghodrati, M.; Garrido, F. *Soil Sci.* **1999**, *164*, 156-170.

40. O'Connell, K. P.; Valdes, J. J.; Azer, N. L.; Schwartz, R. P.; Wright, J.; Eldefrawi, M. E. *J. Immunol. Methods* **1999**, *225*, 157-169.

41. Dahan, M.; Levi, S.; Luccardini, C.; Rostaing, P.; Riveau, B.; Triller, A. *Science* **2003**, *302*, 442-445.

42. Shimizu, K. T.; Neuhauser, R. G.; Leatherdale, C. A.; Empedocles, S. A.; Woo, W. K.; Bawendi, M. G. *Phys. Rev. B* **2001**, *63*, 205316.

43. Xie, X. S.; Lu, H. P. *Springer Ser. Chem. Phys.* **2001**, *67*, 227-240.

44. Deniz, A. A.; Dahan, M.; Grunwell, J. R.; Ha, T.; Faulhaber, A. E.; Chemla, D. S.; Weiss, S.; Schultz, P. G. *Proc. Natl. Acad. Sci. U.S.A.* **1999**, *96*, 3670-3675.

45. Weiss, S. *Science* **1999**, *283*, 1676-1683.

46. Ha, T.; Ting, A. Y.; Liang, J.; Caldwell, W. B.; Deniz, A. A.; Chemla, D. S.; Schultz, P. G.; Weiss, S. *Proc. Natl. Acad. Sci. U.S.A.* **1999**, *96*, 893-898.

47. Chan, Y.; Snee, P. T.; Caruge, J.-M.; Yen, B. K.; Nair, G. P.; Nocera, D. G.; Bawendi, M. G. *J. Am. Chem. Soc.* **2006**, *128*, 3146-3147.

48. Sundar, V. C.; Eisler, H.-J.; Deng, T.; Chan, Y.; Thomas, E. L.; Bawendi, M. G. *Adv. Mater.* **2004**, *16*, 2137-2141.

49. Vezenov, D. V.; Mayers, B. T.; Conroy, R. S.; Whitesides, G. M.; Snee, P. T.; Chan, Y.; Nocera, D. G.; Bawendi, M. G. *J. Am. Chem. Soc.* **2005**, *127*, 8952-8953.

50. Wun, A. W.; Snee, P. T.; Chan, Y.; Bawendi, M. G.; Nocera, D. G. *J. Mater. Chem.* **2005**, *15*, 2697-2706.

51. Balzani, V.; Carassiti, V. *Photochemistry of Coordination Compounds*; Academic Press: London, 1970.

52. Forster, L. S. *Concepts of Inorganic Photochemistry*; Wiley-Interscience: New York, 1975.

53. Wayne, R. P. *Principles and Applications of Photochemistry*; Oxford University Press: Oxford, 1980.

54. Jortner, J.; Rice, S. A.; Hochstrasser, R. M. *Adv. Photochem.* **1969**, *7*, 149-309.

55. Freed, K. F. *Acc. Chem. Res.* **1978**, *11*, 74-80.

56. Lin, S. H. *Radiationless Transitions*; Academic Press: New York, 1980.

57. Califano, M.; Franceschetti, A.; Zunger, A. *Nano Lett.* **2005**, *5*, 2360-2364.

58. Kippeny, T. C.; Bowers, M. J., II; Dukes, A. D., III; McBride, J. R.; Orndorff, R. L.; Garrett, M. D.; Rosenthal, S. J. *J. Chem. Phys.* **2008**, *128*, 084713/1-084713/7.

59. Petrov, E. P.; Cichos, F.; von Borczyskowski, C. *J. Lumin.* **2006**, *119-120*, 412-417.

60. Balzani, V.; Moggi, L.; Manfrin, M. F.; Bolletta, F.; Laurence, G. S. *Coord. Chem. Rev.* **1975**, *15*, 321-433.

61. Turro, N. J. *Modern Molecular Photochemistry*; Benjamin, Cummings: Menlo Park, 1978.

62. Baeyer, A. *Justus Liebigs Ann. Chem.* **1876**, 1-74.

63. Liu, J.; Diwu, Z.; Leung, W.-Y. *Bioorg. Med. Chem. Lett.* **2001**, *11*, 2903-2905.

64. Clapp, A. R.; Medintz, I. L.; Mauro, J. M.; Fisher, B. R.; Bawendi, M. G.; Mattoussi, H. *J. Am. Chem. Soc.* **2004**, *126*, 301-310.

65. Wouters, F. S.; Verveer, P. J.; Bastiaens, P. I. H. *Trends Cell Biol.* **2001**, *11*, 203-211.

66. Fukumura, D.; Jain, R. K. *Microvasc. Res.* **2007**, *74*, 72-84.

67. Fukumura, D.; Jain, R. K. *J. Cell. Biochem.* **2007**, *101*, 937-949.

68. Jain, R. K. *Science* **2005**, *307*, 58-62.

69. Helmlinger, G.; Sckell, A.; Dellian, M.; Forbes, N. S.; Jain, R. K. *Clin. Cancer Res.* **2002**, *8*, 1284-1291.

70. Erler, J. T.; Bennewith, K. L.; Nicolau, M.; Dornhoefer, N.; Kong, C.; Le, Q.-T.; Chi, J.-T. A.; Jeffrey, S. S.; Giaccia, A. J. *Nature* **2006**, *440*, 1222-1226.

71. Pennacchietti, S.; Michieli, P.; Galluzzo, M.; Mazzone, M.; Giordano, S.; Comoglio Paolo, M. *Cancer Cell* **2003**, *3*, 347-361.

72. Rofstad, E. K.; Mathiesen, B.; Kindem, K.; Galappathi, K. *Cancer Res.* **2006**, *66*, 6699-6707.

73. Folkman, J. *N. Engl. J. Med.* **1971**, *285*, 1182-1186.

74. Yang, J. C.; Haworth, L.; Sherry, R. M.; Hwu, P.; Schwartzentruber, D. J.; Topalian, S. L.; Steinberg, S. M.; Chen, H. X.; Rosenberg, S. A. *N. Engl. J. Med.* **2003**, *349*, 427-434.

75. Cobleigh, M. A.; Langmuir, V. K.; Sledge, G. W.; Miller, K. D.; Haney, L.; Novotny, W. F.; Reimann, J. D.; Vassel, A. *Semin. Oncol.* **2003**, *30*, 117-124.

76. Mayer, R. J. *N. Engl. J. Med.* **2004**, *350*, 2406-2408.

77. Hurwitz, H.; Fehrenbacher, L.; Novotny, W.; Cartwright, T.; Hainsworth, J.; Heim, W.; Berlin, J.; Baron, A.; Griffing, S.; Holmgren, E.; Ferrara, N.; Fyfe, G.; Rogers, B.; Ross, R.; Kabbinavar, F. *N. Engl. J. Med.* **2004**, *350*, 2335-2342.

78. Ma, J.; Pulfer, S.; Li, S.; Chu, J.; Reed, K.; Gallo, J. M. *Cancer Res.* **2001**, *61*, 5491-5498.

79. Murata, R.; Nishimura, Y.; Hiraoka, M. *Int. J. Radiat. Oncol.* **1997**, *37*, 1107-1113.

80. Fenton, B. M.; Paoni, S. F.; Ding, I. *Radiother. Oncol.* **2004**, *72*, 221-230.

81. Denk, W.; Strickler, J. H.; Webb, W. W. *Science* **1990**, *248*, 73-76.

82. Brown, E. B.; Campbell, R. B.; Tsuzuki, Y.; Xu, L.; Carmeliet, P.; Fukumura, D.; Jain, R. K. *Nat. Med.* **2001**, *7*, 864-868.

83. Lee, C.-G.; Heijn, M.; Di Tomaso, E.; Griffon-Etienne, G.; Ancukiewicz, M.; Koike, C.; Park, K. R.; Ferrara, N.; Jain, R. K.; Suit, H. D.; Boucher, Y. *Cancer Res.* **2000**, *60*, 5565-5570.

84. Hansen-Algenstaedt, N.; Stoll, B. R.; Padera, T. P.; Dolmans, D. E. J. G. J.; Hicklin, D. J.; Fukumura, D.; Jain, R. K. *Cancer Res.* **2000**, *60*, 4556-4560.

85. Brown, J. M. *Cancer Res.* **1999**, *59*, 5863-5870.

86. Vukovic, V.; Tannock, I. F. *Brit. J. Cancer* **1997**, *75*, 1167-1172.

87. Helmlinger, G.; Yuan, F.; Dellian, M.; Jain, R. K. *Nat. Med.* **1997**, *3*, 177-182.

88. Clark, H. A.; Kopelman, R.; Tjalkens, R.; Philbert, M. A. *Anal. Chem.* **1999**, *71*, 4837-4843.

89. Kreft, O.; Javier, A. M.; Sukhorukov, G. B.; Parak, W. J. *J. Mater. Chem.* **2007**, *17*, 4471-4476.

90. Bussink, J.; Kaanders, J. H. A. M.; Strik, A. M.; Vojnovic, B.; Van der Kogel, A. J. *Radiat. Res.* **2000**, *154*, 547-555.

91. Kellner, K.; Liebsch, G.; Klimant, I.; Wolfbeis, O. S.; Blunk, T.; Schulz, M. B.; Gopferich, A. *Biotechnol. Bioeng.* **2002**, *80*, 73-83.

92. Liebsch, G.; Klimant, I.; Frank, B.; Holst, G.; Wolfbeis, O. S. *Appl. Spectrosc.* **2000**, *54*, 548-559.

93. Vanderkooi, J. M.; Maniara, G.; Green, T. J.; Wilson, D. F. *J. Biol. Chem.* **1987**, *262*, 5476-5482.

94. Hochreiner, H.; Sanchez-Barragan, I.; Costa-Fernandez, J. M.; Sanz-Medel, A. *Talanta* **2005**, *66*, 611-618.

95. Park, E. J.; Reid, K. R.; Tang, W.; Kennedy, R. T.; Kopelman, R. *J. Mater. Chem.* **2005**, *15*, 2913-2919.

96. Xu, C.; Zipfel, W.; Shear, J. B.; Williams, R. M.; Webb, W. W. *Proc. Natl. Acad. Sci. U.S.A.* **1996**, *93*, 10763-10768.

97. Konig, K. *J. Microsc.-Oxford* **2000**, *200*, 83-104.

98. Brown, E. B.; Campbell, R. B.; Tsuzuki, Y.; Fukumura, D.; Jain, R. K. *Proc. SPIE-Int. Soc. Opt. Eng.* **2001**, *4262*, 134-145.

99. Brown, E. B.; Campbell, R. B.; Tsuzuki, Y.; Xu, L.; Carmeliet, P.; Fukiumura, D.; Jain, R. K. *Nat. Med.* **2001**, *7*, 864-868.

100. Baker, G. A.; Munson, C. A.; Bukowski, E. J.; Baker, S. N.; Bright, F. V. *Appl. Spectrosc.* **2002**, *56*, 455-463.

101. Kruk, M.; Karotki, A.; Drobizhev, M.; Kuzmitsky, V.; Gael, V.; Rebane, A. *J. Lumin.* **2003**, *105*, 45-55.

102. Larson, D. R.; Zipfel, W. R.; Williams, R. M.; Clark, S. W.; Bruchez, M. P.; Wise, F. W.; Webb, W. W. *Science* **2003**, *300*, 1434-1437.

103. Chan, Y.; Zimmer, J. P.; Stroh, M.; Steckel, J. S.; Jain, R. K.; Bawendi, M. G. *Adv. Mater.* **2004**, *16*, 2092-2097.

104. Stroh, M.; Zimmer, J. P.; Duda, D. G.; Levchenko, T. S.; Cohen, K. S.; Brown, E. B.; Scadden, D. T.; Torchilin, V. P.; Bawendi, M. G.; Fukumura, D.; Jain, R. K. *Nat. Med.* **2005**, *11*, 678-682.

105. Murray, C. B.; Norris, D. J.; Bawendi, M. G. *J. Am. Chem. Soc.* **1993**, *115*, 8706-8715.

106. Bawendi, M. C.; Steigerwald, M. L.; Brus, L. E. *Annu. Rev. Phys. Chem.* **1990**, *41*, 477-496.

107. Kastner, M. A. *Phys. Today* **1993**, *46*, 24-31.

108. Anscombe, N. *Nat. Photonics* **2007**, *1*, 360-361.

109. Azzazy, H. M. E.; Mansour, M. M. H.; Kazmierczak, S. C. *Clin. Biochem.* **2007**, *40*, 917-927.

110. Hammer, N. I.; Emrick, T.; Barnes, M. D. *Nanosc. Res. Lett.* **2007**, *2*, 282-290.

111. Coe-Sullivan, S. *Mater. Matters* **2007**, *2*, 13-14.

112. Corbin, J. G.; Haydar, T. F. *Nanomedicine* **2007**, *2*, 579-581.

113. Guyot-Sionnest, P. *Mater. Matters* **2007**, *2*, 10-12.

114. Pinaud, F.; Michalet, X.; Bentolila, L. A.; Tsay, J. M.; Doose, S.; Li, J. J.; Iyer, G.; Weiss, S. *Biomaterials* **2006**, *27*, 1679-1687.

115. Reithmaier, J. P.; Somers, A.; Kaiser, W.; Deubert, S.; Gerschuetz, F.; Forchel, A.; Parillaud, O.; Krakowski, M.; Alizon, R.; Hadass, D.; Bilenca, A.; Dery, H.; Mikhelashvili, V.; Eisenstein, G.; Gioannini, M.; Montrosset, I.; Berg, T. W.; van der Poel, M.; Mork, J.; Tromborg, B. *Phys. Status Solidi B* **2006**, *243*, 3981-3987.

116. Samia, A. C. S.; Dayal, S.; Burda, C. *Photochem. Photobiol.* **2006**, *82*, 617-625.

117. Scholz, M.; Aichele, T.; Benson, O. *Adv. Solid State Phys.* **2008**, *46*, 3-14.

118. Wu, M. H.; Ueda, A.; Mu, R. *Opt. Sci. Eng.* **2005**, *99*, 331-350.

119. Somers, R. C.; Bawendi, M. G.; Nocera, D. G. *Chem. Soc. Rev.* **2007**, *36*, 579-591.

120. Brus, L. E. *J. Chem. Phys.* **1983**, *79*, 5566-5571.

121. Hines, M. A.; Guyot-Sionnest, P. *J. Phys. Chem.* **1996**, *100*, 468-471.

122. Dabbousi, B. O.; RodriguezViejo, J.; Mikulec, F. V.; Heine, J. R.; Mattoussi, H.; Ober, R.; Jensen, K. F.; Bawendi, M. G. *J. Phys. Chem. B* **1997**, *101*, 9463-9475.

123. Jaiswal, J. K.; Simon, S. M. *Trends Cell. Biol.* **2004**, *14*, 497-504.

124. Bruchez, M., Jr.; Moronne, M.; Gin, P.; Weiss, S.; Alivisatos, A. P. *Science* **1998**, *281*, 2013-2016.

125. Chan, W. C.; Nie, S. *Science* **1998**, *281*, 2016-2018.

126. Dubertret, B.; Skourides, P.; Norris, D. J.; Noireaux, V.; Brivanlou, A. H.; Libchaber, A. *Science* **2002**, *298*, 1759-1762.

127. Wu, X.; Liu, H.; Liu, J.; Haley Kari, N.; Treadway Joseph, A.; Larson, J. P.; Ge, N.; Peale, F.; Bruchez Marcel, P. *Nat. Biotechnol.* **2003**, *21*, 41-46.

128. Guo, W.; Li, J. J.; Wang, Y. A.; Peng, X. *Chem. Mater.* **2003**, *15*, 3125-3133.

129. Guo, W.; Li, J. J.; Wang, Y. A.; Peng, X. *J. Am. Chem. Soc.* **2003**, *125*, 3901-3909.

130. Huang, B.; Tomalia, D. A. *Inorg. Chim. Acta* **2006**, *359*, 1961-1966.

131. Liu, Y.; Kim, M.; Wang, Y.; Wang, Y. A.; Peng, X. *Langmuir* **2006**, *22*, 6341-6345.

132. Wang, Y. A.; Li, J. J.; Chen, H.; Peng, X. *J. Am. Chem. Soc.* **2002**, *124*, 2293-2298.

133. Wisher, A. C.; Bronstein, I.; Chechik, V. *Chem. Commun.* **2006**, 1637-1639.

134. Kim, S.; Bawendi, M. G. *J. Am. Chem. Soc.* **2003**, *125*, 14652-14653.

135. Uyeda, H. T.; Medintz, I. L.; Jaiswal, J. K.; Simon, S. M.; Mattoussi, H. *J. Am. Chem. Soc.* **2005**, *127*, 3870-3878.

136. Liu, W.; Howarth, M.; Greytak, A. B.; Zheng, Y.; Nocera, D. G.; Ting, A. Y.; Bawendi, M. G. *J. Am. Chem. Soc.* **2008**, *130*, 1274-1284.

137. Aldana, J.; Wang, Y. A.; Peng, X. *J. Am. Chem. Soc.* **2001**, *123*, 8844-8850.

138. Medintz, I. L.; Uyeda, H. T.; Goldman, E. R.; Mattoussi, H. *Nat. Mater.* **2005**, *4*, 435-446.

139. Ballou, B.; Lagerholm, B. C.; Ernst, L. A.; Bruchez, M. P.; Waggoner, A. S. *Bioconj. Chem.* **2004**, *15*, 79-86.

140. Derfus, A. M.; Chan, W. C. W.; Bhatia, S. N. *Nano Lett.* **2004**, *4*, 11-18.

141. Chan, W.-h.; Shiao, N.-h. *Acta Pharm. Sinic.* **2008**, *29*, 259-266.

142. Walker, G. W.; Sundar, V. C.; Rudzinski, C. M.; Wun, A. W.; Bawendi, M. G.; Nocera, D. G. *Appl. Phys. Lett.* **2003**, *83*, 3555-3557.

143. Koochesfahani, M. M.; Pouya, S; Snee, P. T.; Bawendi, M. G.; Nocera, D. G. *Proc. 6th Int. Symp. PIV* **2005**, KN03, Pasadena, CA.

144. Pouya, S.; Koochesfahani, M. M.; Snee, P. T.; Bawendi, M. G.; Nocera, D. G. *Exp. Fluids* **2005**, *39*, 784-786.

145. Son, D. H.; Hughes, S. M.; Yin, Y.; Alivisatos, A. P. *Science* **2004**, *306*, 1009-1012.

146. Mamedova, N. N.; Kotov, N. A.; Rogach, A. L.; Studer, J. *Nano Lett.* **2001**, *1*, 281-286.

147. Wang, S.; Mamedova, N.; Kotov, N. A.; Chen, W.; Studer, J. *Nano Lett.* **2002**, *2*, 817-822.

148. Lee, J.; Govorov, A. O.; Kotov, N. A. *Nano Lett.* **2005**, *5*, 2063-2069.

149. Ramadurai, D.; Geerpuram, D.; Alexson, D.; Dutta, M.; Kotov, N. A.; Tang, Z.; Stroscio, M. A. *Superlattices Microstruct.* **2006**, *40*, 38-44.

150. Kagan, C.R.; Murray, C.B.; Nirmal, M. Bawendi, M. G. *Phys. Rev. Lett.* **1996**, *76*, 1517-1520.

151. Wargnier, R.; Baranov, A. V.; Maslov, V. G.; Stsiapura, V.; Artemyev, M.; Pluot, M.; Sukhanova, A.; Nabiev, I. *Nano Lett.* **2004**, *4*, 451-457.

152. Willard, D. M.; Carillo, L. L.; Jung, J.; van Orden, A. *Nano Lett.* **2001**, *1*, 469-474.

153. Willard, D. M.; Carillo, L. L.; Jung, J.; van Orden, A. *Nano Lett.* **2001**, *1*, 581.

154. Tran, P. T.; Goldman, E. R.; Anderson, G. P.; Mauro, J. M.; Mattoussi, H. *Phys. Status Solidi B* **2002**, *229*, 427-432.

155. Hohng, S.; Ha, T. *Chem. Phys. Chem.* **2005**, *6*, 956-960.

156. Zhou, D.; Piper, J. D.; Abell, C.; Klenerman, D.; Kang, D.-J.; Ying, L. *Chem. Commun.* **2005**, 4807-4809.

157. Clapp, A. R.; Medintz, I. L.; Fisher, B. R.; Anderson, G. P.; Mattoussi, H. *J. Am. Chem. Soc.* **2005**, *127*, 1242-1250.

158. Anni, M.; Manna, L.; Cingolani, R.; Valerini, D.; Creti, A.; Lomascolo, M. *Appl. Phys. Lett.* **2004**, *85*, 4169-4171.

159. Anikeeva, P. O.; Madigan, C. F.; Coe-Sullivan, S. A.; Steckel, J. S.; Bawendi, M. G.; Bulovic, V. *Chem. Phys. Lett.* **2006**, *424*, 120-125.

160. Hildebrandt, N.; Charbonniere, L. J.; Beck, M.; Ziessel, R. F.; Loehmannsroeben, H.-G. *Angew. Chem., Int. Ed. Engl.* **2005**, *44*, 7612-7615.

161. Patolsky, F.; Gill, R.; Weizmann, Y.; Mokari, T.; Banin, U.; Willner, I. *J. Am. Chem. Soc.* **2003**, *125*, 13918-13919.

162. Gill, R.; Willner, I.; Shweky, I.; Banin, U. *J. Phys. Chem. B* **2005**, *109*, 23715-23719.

163. Bakalova, R.; Zhelev, Z.; Ohba, H.; Baba, Y. *J. Am. Chem. Soc.* **2005**, *127*, 11328-11335.

164. Zhang, C.-Y.; Johnson, L. W. *J. Am. Chem. Soc.* **2006**, *128*, 5324-5325.

165. Medintz, I. L.; Clapp, A. R.; Mattoussi, H.; Goldman, E. R.; Fisher, B.; Mauro, J. M. *Nat. Mater.* **2003**, *2*, 630-638.

166. Goldman, E. R.; Medintz, I. L.; Whitley, J. L.; Hayhurst, A.; Clapp, A. R.; Uyeda, H. T.; Deschamps, J. R.; Lassman, M. E.; Mattoussi, H. *J. Am. Chem. Soc.* **2005**, *127*, 6744-6751.

167. Chen, C.-Y.; Cheng, C.-T.; Lai, C.-W.; Wu, P.-W.; Wu, K.-C.; Chou, P.-T.; Chou, Y.-H.; Chiu, H.-T. *Chem. Commun.* **2006**, 263-265.

168. Tomasulo, M.; Yildiz, I.; Kaanumalle, S. L.; Raymo, F. M. *Langmuir* **2006**, *22*, 10284-10290.

169. Tomasulo, M.; Yildiz, I.; Raymo, F. M. *J. Phys. Chem. B* **2006**, *110*, 3853-3855.

Chapter II

Investigation of CdSe/ZnS Nanocrystals for FRET-based Applications in Optical Chemosensing

Parts of this Chapter will be published:
Somers, R. C.; Snee, P. T.; Bawendi, M.G. and Nocera, D. G.
Manuscript in Preparation

II.1 Introduction

Traditionally, sensing by fluorescence involves the use of organic chromophores that are limited by narrow absorptions, significant overlap between absorbance and emission profiles (narrow Stokes shift), broad red tailing emissions, and photochemical instabilities.[1-3] Colloidal inorganic nanocrystals (NCs) have generated considerable interest as fluorophores due to their size-dependent physical properties caused by quantum confinement, such as broad absorption, narrow and tunable emission, high quantum yields, and improved photostability relative to organic fluorophores.[1-3] Numerous studies have been undertaken to exploit the photoluminescence properties of NCs for bioimaging purposes[4-10] in addition to their use in devices such as LEDs.[11-13]

NC-acceptor conjugates have not been extensively investigated. Mattoussi and co-workers have exploited NC fluorescence properties to achieve fluorescence resonance energy transfer (FRET) for sensing purposes as described in Chapter I.6.b, studying NCs as both energy donors and energy acceptors.[3,14-23] Although sensing through FRET was established, their system presents several disadvantages, including a difficult and tedious synthesis that requires custom re-engineered and recombinant proteins and a dependence on an electrostatic interaction between the CdSe NC and the acceptor molecule. A simpler approach to creating a NC-dye conjugate is desirable. Moreover, due to the relatively few examples of energy transfer between NCs and molecules, a complete investigation of the fundamental photophysics of a simpler system is imperative in order to practically implement inorganic NCs in FRET-based sensing schemes. This Chapter discusses the synthesis and thorough photophysical investigation of a model energy transfer system: a rhodamine B isothiocyanate (RITC) dye (acceptor) coupled to water-solubilized NCs (donor). The photophysics of RITC-NC conjugates were investigated by steady-state and time-resolved spectroscopic methods. The goal of this study is to design and characterize a NC-dye platform that is suitable for FRET-based sensing purposes.

II.2 Results and Discussion

II.2.a Synthetic Design

The most challenging issue to overcome when designing a NC-based donor-acceptor FRET pair is the appropriate modification of the NC surface. Synthesized in high-boiling, coordinating solvents of trioctylphosphine oxide (TOPO) and hexadecylamine (HDA), the NCs are covered in long alkyl chains that permit them to be natively soluble in nonpolar solvents, such as hexanes and chloroform. In order to reach the goal of incorporating NCs for optical sensing, especially in biological environments, it is essential for the NCs to be soluble in water; therefore, the ligand coating of the NCs must be altered to present a hydrophilic interface. Many methods for water-soluble NCs exist, either by encapsulating a NC via modifications with a layer of silica shell[4] or amphiphilic polymers,[9] or by directly exchanging the native oily ligands with monodentate thiols,[5,24] phospholipids,[25] dendrimers,[26] oligomeric phosphines,[27] or multidentate thiols.[28-31] An ideal NC scaffold should have the following properties:

(1) impart water solubility

(2) preserve the high quantum yields of the NCs

(3) provide a functional handle for covalent conjugation of acceptor molecules

(4) offer long-term stability in aqueous solutions

(5) allow for facile and large scale synthesis

Based on these requirements, a method of encapsulating NCs using an amphiphilic polymer was chosen. Micellular encapsulated NCs are attractive, because instead of displacing the original TOPO capping, which can drastically reduce the quantum yield, the hydrophobic portion of the amphiphilic polymer interdigitates within the long alkyl chains of the cap to coat the NC. When placed in a polar solvent, the hydrophilic segment of the polymer presumably situates itself on the surface of the QD to be miscible with aqueous solutions. Bruchez and co-workers have reported micellular encapsulated semiconductor quantum dots using *N*-octylamine modified poly(acrylic acid) for labeling markers in cells.[9] However, the amphiphilic polymer only presents carboxylic acid functionality, limiting the scope of the methods able to conjugate acceptor dyes. In order to access a wider variety of coupling strategies to NCs, we

modified poly(acrylic acid) with 5-amino-1-pentanol, which adds hydroxyl functionality to NCs as shown in Scheme II.1. In the design presented here, 40% of the acid groups in 1800 MW poly(acrylic acid) were targeted for functionalization with *N*-octylamine, as previously reported;[9] an additional 40% of the acid group were functionalized with 5-amino-1-pentanol and the remainder (20%) was left as free carboxylic acid. Water-soluble CdSe/ZnS NCs were prepared with this polymer as shown in Scheme II.2. The quantum yield depends on the quality of the NC used. We achieved quantum yields in water as high as 50% for NCs with suitable inorganic overcoating.

Rhodamine B isothiocyanate (RITC) was chosen to be the acceptor dye for the study of energy transfer from polymer coated NCs. The dye exhibits a high extinction coefficient and a $\lambda_{max,abs}$ = 556 nm.[32] CdSe NCs can be easily synthesized so that their emission matches this wavelength thereby engendering RITC as an ideal FRET acceptor for NCs. In addition, the isothiocyanate functionality is readily susceptible to nucleophilic attack by the hydroxyl group of the amphiphilic polymer to yield a covalently-bonded thiocarbamate conjugate, as depicted in Scheme II.3. The average

Scheme II.1 (Top) Synthesis of *N*-octylamine-modified poly(acrylic acid) reported by Wu,[9] and (bottom) the additional 5-amino-1-pentanol modification incorporated for coupling acceptor dyes to NCs through the hydroxyl functionality.

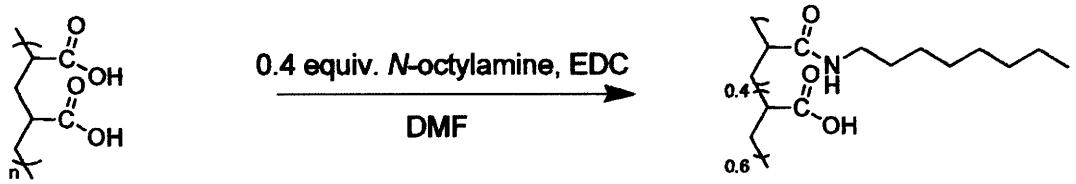

1800 MW poly(acrylic acid) — **octylamine-modified poly(acrylic acid)**

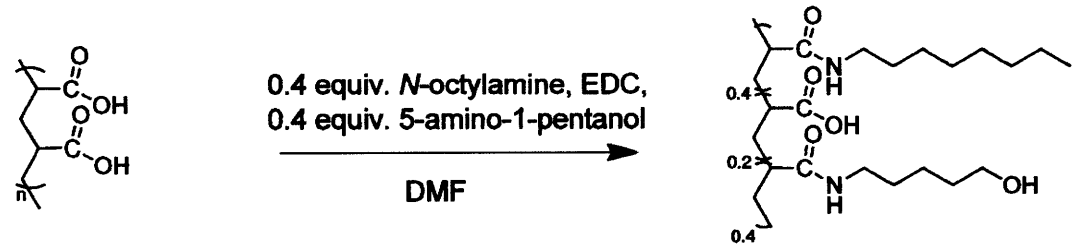

1800 MW poly(acrylic acid) — **octylamine and aminopentanol-modified poly(acrylic acid)**

number of dyes conjugated to each NC was controlled through stoichiometry, and the constructs were separated from excess uncoupled dye and starting material through dialysis with 50,000 molecular weight cutoff centrifugal filters until the filtrate was optically transparent.

Scheme II.2 A simple mixture of the amphiphilic polymer with NCs (precipitated from its growth solution with methanol) imparts water solubility in a facile manner.

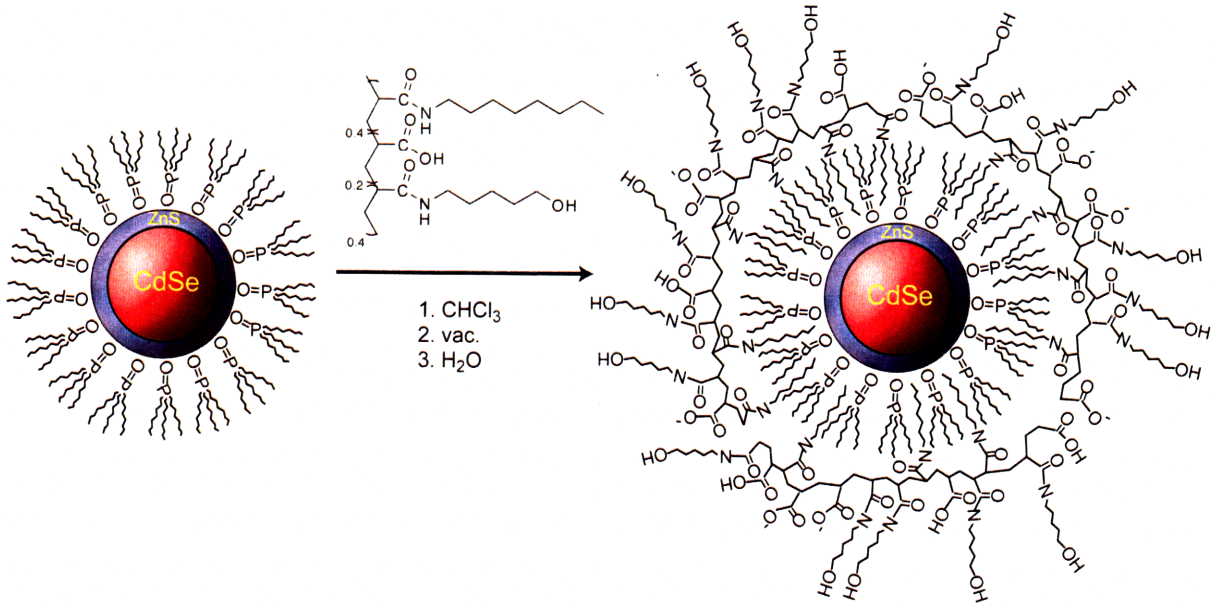

Scheme II.3 Conjugation of the acceptor dye to the water-solubilized NCs proceeds in a one-step process.

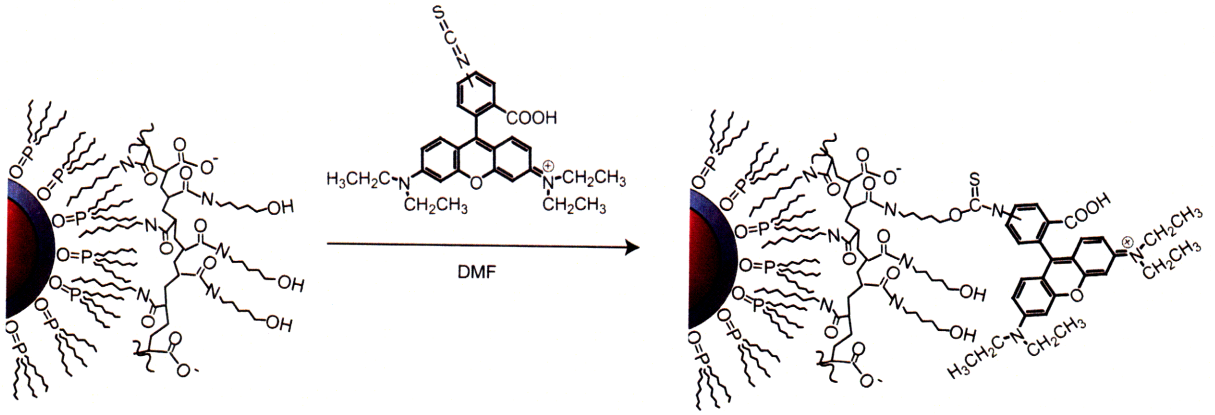

II.2.b Characterization of the Amphiphilic Polymer

The efficacy of energy transfer has been the chief (or sole) means of characterization of NC FRET constructs. Poor materials characterization of modified NCs seems to be the rule rather than the exception.[4,8,9] We wished to undertake a more extensive analysis of the RITC-NC conjugates. Therefore, an emphasis on characterization was a major objective of this work. The characterization of the *N*-octylamine and 5-amino-1-pentanol modified poly(acrylic) acid can be described as challenging at best. This section discusses the characterization attempts for the amphiphilic polymer used in this study.

Proton NMR of the *N*-octylamine and 5-amino-1-pentanol modified poly(acrylic acid) revealed very broad peaks presumably due to the amphiphilic nature of the polymer.[33,34] The peaks were too broad to accurately integrate or reference in order to probe the degree of side-chain coupling to the polymer backbone. Qualitative information could be obtained through IR spectroscopy (Figure II.1), as amide peaks can be distinguished at 1653 cm^{-1} and 1551 cm^{-1} and the carbonyl peak can be distinguished at 1718 cm^{-1}. Unfortunately, an amide bond of *N*-octylamine conjugated to the poly(acrylic acid) backbone is hardly distinguishable from an amide bond of 5-

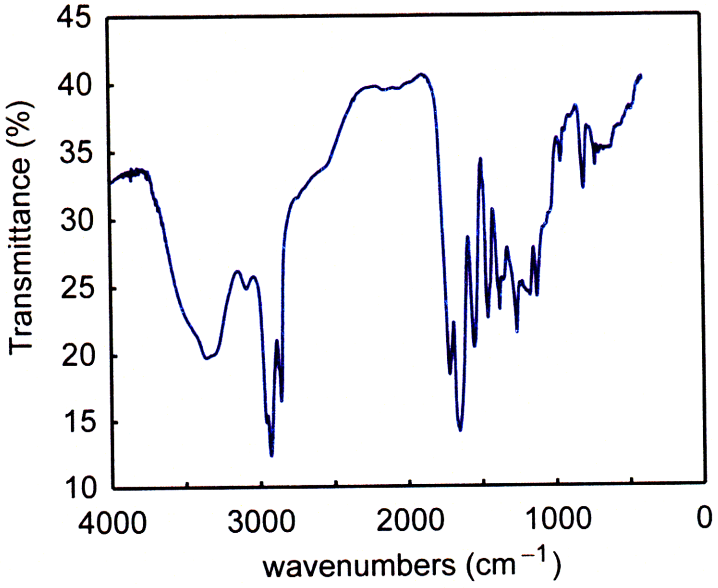

Figure II.1 IR spectrum of 5-amino-1-pentanol and *N*-octylamine modified poly(acrylic acid).

amino-1-pentanol conjugated to the backbone, and indeed, only one amide environment is present in the IR spectrum. Attempts were made to determine exact molecular weights with MALDI-TOF (matrix assisted laser desorption by ionization with time-of-flight detector) and ESI (electrospray ionization) mass spectrometry; however, the polymer did not fly, even with attempts to dope with sodium ions, change matrices, and vary concentrations.

Gel Permeation Chromatography (GPC) gave qualitative insight to the degree of coupling. Figure II.2 shows a calibration curve of five polystyrene molecular weight standards that was used to extrapolate the molecular weights of the polymer samples. By comparing the retention times of 1800 MW poly(acrylic acid), 40% octylamine-modified poly(acrylic acid), and 40% octylamine / 40% 5-amino-1-pentanol modified poly(acrylic acid) against the retention times of polystyrene standards, approximate masses were found. The molecular weights estimated by GPC are given in Table II.1. The increasing trend in molecular weights from poly(acrylic acid) to the *N*-octylamine-modified polymer to the *N*-octylamine/ 5-amino-1-pentanol-modified polymer confirmed that the degree of coupling increased. The molecular weight obtained by GPC

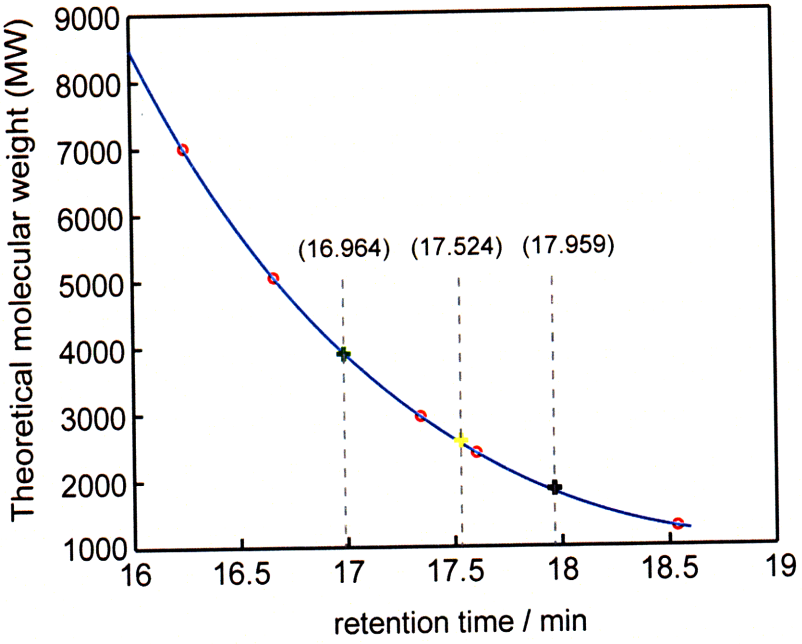

Figure II.2 GPC calibration curve of molecular weights vs. retention time. Polystyrene standards of 5 molecular weights (O), poly(acrylic acid) (+), *N*-octylamine modified poly(acrylic acid) (+), and *N*-octylamine and 5-amino-1-pentanol-modified poly(acrylic acid) (+) are shown.

Table II.1 Samples studied by gel permeation chromatography. Expected molecular weight assumes 100% coupling efficiency, and molecular weight calculated from GPC is given vs. polystyrene.

Sample	Expected Molecular Weight	Molecular Weight GPC
Poly(acrylic acid)	1800	1824
N-octylamine-modified poly(acrylic acid)	2910	2555
N-octylamine / 5-amino-1-pentanol modified poly(acrylic acid)	3760	3978

correlates well to the weights that were expected for a coupling efficiency of 100%. However, two aspects prevent us from assigning absolute molecular weight. First, the molecular weights are calibrated against a poly(styrene) standard, which has a very different structure compared to poly(acrylic acid). Second, the structures of the three polymers listed in Table II.1 are varied enough that their viscosities are likely to be different. Viscosities affect the flow rate of a polymer through a gel, which affects the retention time. Therefore, the three samples cannot be directly compared to allow for a direct calculation of the degree of coupling of the side chains. However, enough information was obtained through this technique to qualitatively state that *N*-octylamine and 5-amino-1-pentanol are both contained as side chain groups as part of the polymer to provide a method to water-solubilize NCs and to provide the hydroxyl group functionality.

II.2.c Photophysical Properties

The UV-vis absorption spectra of RITC, water-solubilized unconjugated CdSe/ZnS NCs, and RITC-NC conjugates are presented in Figure II.3. The spectra of the RITC-NC conjugates clearly exhibit the absorption characteristics of both the NC (with the broad absorption feature extending to the bluer wavelengths) and RITC (with the dye first absorption feature at λ_{max} = 556 nm). The UV-vis spectrum of each conjugate can therefore be deconstructed into the two components, and since the extinction coefficients of each chromophore at a specific wavelength can be calculated,

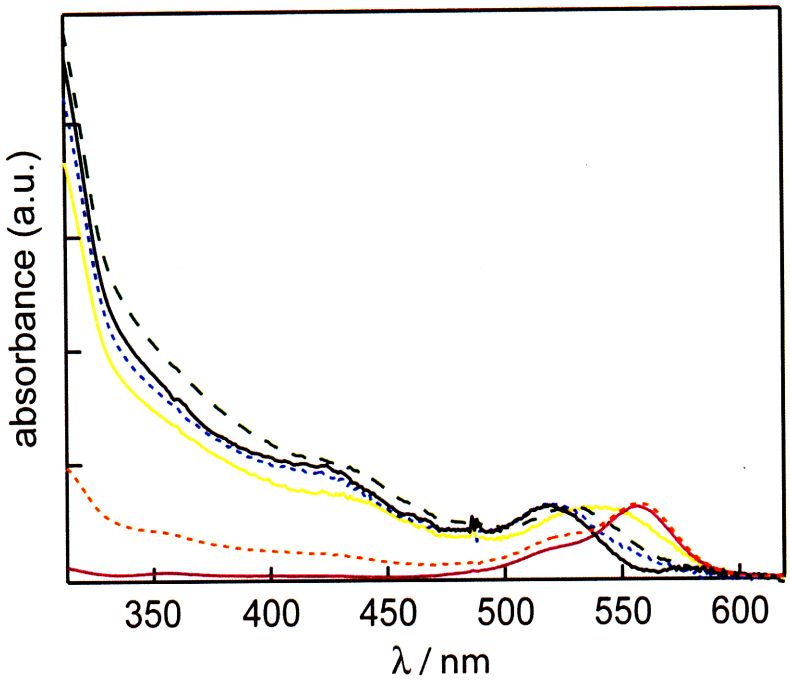

Figure II.3 UV-vis spectra of RITC (red solid line —), NC (black solid line —), and RITC-NC conjugates with RITC:NC ratio of 12:1 (orange dashed line - - -), 2.5:1 (yellow solid line —), 0.8:1 (green dashed line – –), and 0.3:1 (blue dashed line - - -).

an estimate of the RITC to NC ratio can be ascertained. Four different samples with dye to NC ratios of 12:1, 2.5:1, 0.8:1 and 0.3:1 were obtained.

The emission spectra of the RITC, NC, and the RITC-NC conjugates are shown in Figure II.4. The samples were excited at λ_{ex} = 350 nm, where the NC absorption is large and the RITC absorption is minimized. Accordingly, the choice of this excitation wavelength minimized direct excitation of the acceptor dye. As illustrated in Figure II.4, the sample with the most dye conjugated (12:1) exhibits features nearly identical to the dye; only a minor CdSe emission is observed. Conversely, the emission spectrum of the sample with the least conjugation (0.3:1) resembles that of the CdSe NC. These comparative results are indicative of energy transfer, as the FRET efficiency is greater for the more conjugated sample where the spectral overlap is greatest.

As discussed in Chapter I, Förster theory correlates the rate and efficiency of energy transfer to the spectral overlap of donor and acceptor molecules (which is the predominant factor for the critical transfer distance, R_0), their spatial arrangement, and the number of acceptor molecules per donor.[35] The R_0 between 540 nm emitting NCs

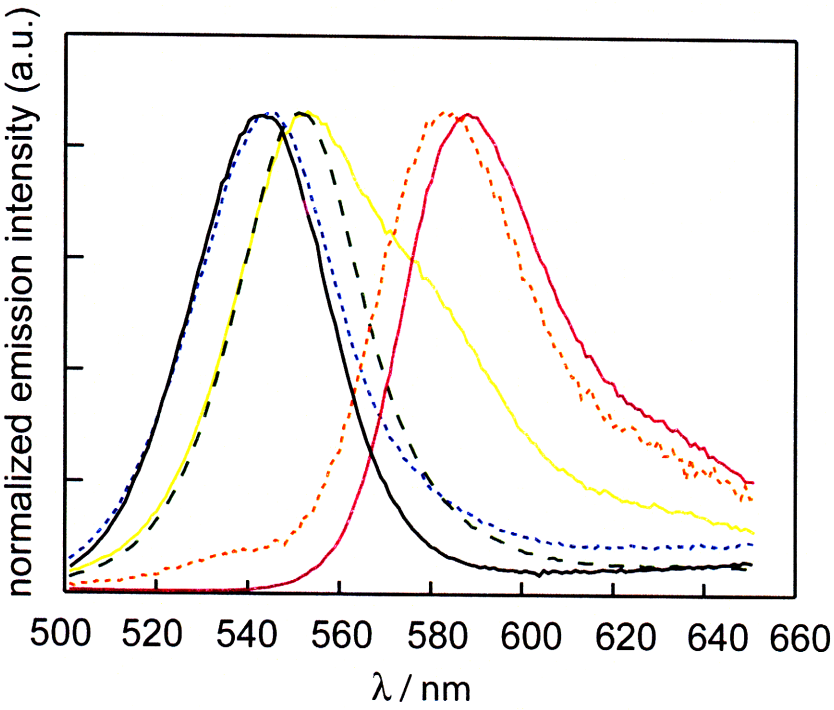

Figure II.4 Emission (λ_{ex} = 350 nm) of RITC (red solid line —), NC (black solid line —), and RITC-NC conjugates with RITC:NC ratio of 12:1 (orange dashed line - - -), 2.5:1 (yellow solid line —), 0.8:1 (green dashed line – –), and 0.3:1 (blue dashed line - - -). Where there is sufficient concentration of RITC conjugated to NC, the emission resembles RITC.

with 3% QY and RITC acceptor in water, assuming random dipole orientation, was calculated as 36 Å using eq. I.8. This R_o falls within the typical Förster distance range of 20 – 90 Å.[35] As shown by the data in Figure II.2, increasing the number of acceptor molecules, *m*, enhances the FRET efficiency. This result is consistent with the prediction of eq. I.10. The sample with the most dye conjugated to the NC (12:1) exhibits almost no NC emission owing to efficient FRET from NC to dye.

In order to ensure that the emission spectra obtained reflected FRET instead of trivial re-absorption of the NC emission by the dye-acceptor, uncoupled mixtures of RITC and CdSe/ZnS were prepared. The isothiocyanate on the RITC was allowed to hydrolyze in water and then the solution was mixed with the NCs. The re-absorption efficiency depends on the total concentration of dye in solution, whereas the FRET efficiency requires the dye to be proximate to the NC. The absorbances of each component were matched to that of a control RITC-NC conjugate to ensure that the relative concentrations would be comparable. The RITC:NC ratio for the conjugate was

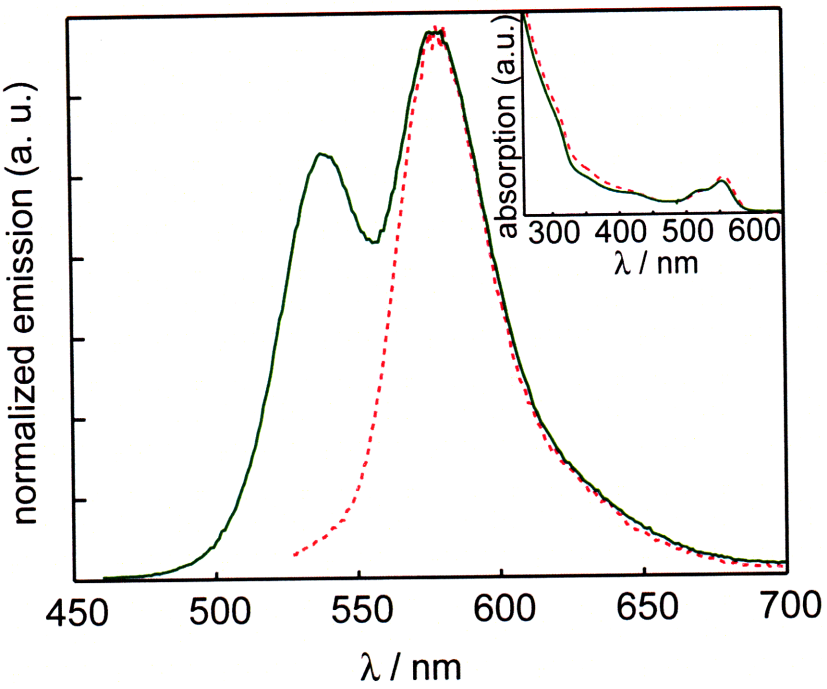

Figure II.5 Emission spectra of the mixture of NC and RITC (solid green line —) vs. the Förster Pair of the conjugated NC-RITC (red dashed line - - -), normalized by the maximum intensity of the dye emission. (Inset) The concentrations are matched by absorbance.

calculated as 11:1 for this control experiment. Figure II.5 clearly shows substantial residual NC emission in the unconjugated mixture, in contrast to the nearly exclusive emission from the dye in the conjugate. From this result, it can be concluded that trivial re-absorption of NC emission by the dye cannot account for the enhanced dye emission when tethered to the NC surface. In addition, dialysis of the mixture yielded the uncoupled NCs, confirming that there are no additional interactions between the rhodamine dye and NCs.

In order to gain insight into the origin of the excited energy that is emitted by the acceptor dye, the NC-RITC constructs were studied by photoluminescence excitation spectroscopy (PLE). By monitoring the emission at one single wavelength and scanning a range of excitation wavelengths, the intensity of emission for each excitation wavelength gives information on which species is excited and which is responsible for the emission of the acceptor molecule. Figure II.6 shows the PLE spectra collected for RITC, NC and the RITC-NC conjugates. The emission intensity was monitored at λ_{em} = 620 nm, where only the dye emits, and excitation wavelengths were scanned from 350

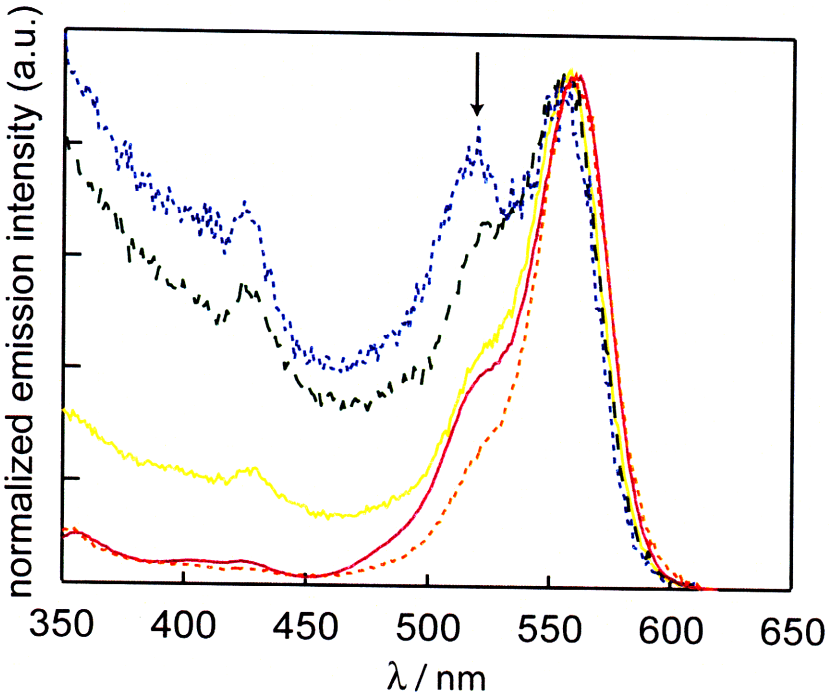

Figure II.6 PLE spectra of RITC (red solid line —) and RITC-NC conjugates with RITC:NC ratio of 12:1 (orange dashed line - - -), 2.5:1 (yellow solid line —), 0.8:1 (green dashed line – –), and 0.3:1 (blue dashed line - - -). The emission of each sample is scaled to the λ_{max} of dye at 583 nm to highlight the differences of each sample in the bluer wavelengths. The arrow points to the NC 1st absorption feature.

nm to 620 nm. If energy transfer is occurring from the NC, high emission intensity is expected when the excitation wavelength falls in the UV, due to the broad NC absorption band; however, if there is no energy transfer, the excitation spectrum is expected to mirror the RITC absorbance spectrum, as only the excitation of the dye should be responsible for the observed emission. The absorption spectra of the conjugates indicate minimal change in the absorption spectrum of the dye upon binding to NCs. Figure II.6 reveals that there is a NC component to each PLE spectrum of the conjugates, except for the sample with the greatest concentration of dye (12:1). The lack of the NC contribution to the observed emission can be explained by the fact that the spectrum is overwhelmed by the dye absorption, which presumably indicates that the emission spectra of the 12:1 RITC:NC conjugate is most likely due to direct excitation of the dye. However, the PLEs for the rest of the conjugates exhibit emission intensity in the blue excitation wavelengths (between 350 – 500 nm) that can only be attributed to the NC. As the ratio of dye to NC increases, the emission intensity from the

NC component decreases, which can be explained by the fact that the energy from one excited NC is distributed among multiple dyes upon FRET.

FRET was further characterized by time-resolved fluorescence spectroscopy. The lifetime is useful for obtaining FRET rates and structural information of the donor-acceptor pair. Note that issues such as direct dye excitation and trivial re-absorption are not a problem in time-resolved measurements, which focus on decay rates rather than emission intensities. Time-resolved fluorescence decay curves were fit by convolving a bi-exponential decay curve with the signal obtained from the instrument response. CdSe exciton recombination has been reported to be bi-exponential due to an existence of two different kinds of excitonic states,[36] with which our results are consistent.

The donor (NC) lifetimes of the RITC-NC conjugates and the NC were extracted from the photoluminescence decay spectra of the NC emission and are presented in Figure II.7. Because the NC emission of the conjugate with the highest dye coupling (12:1) was completely quenched, lifetime data on the donor of this particular conjugate could not be obtained. The decay curves show that the lifetimes of the NC emission in

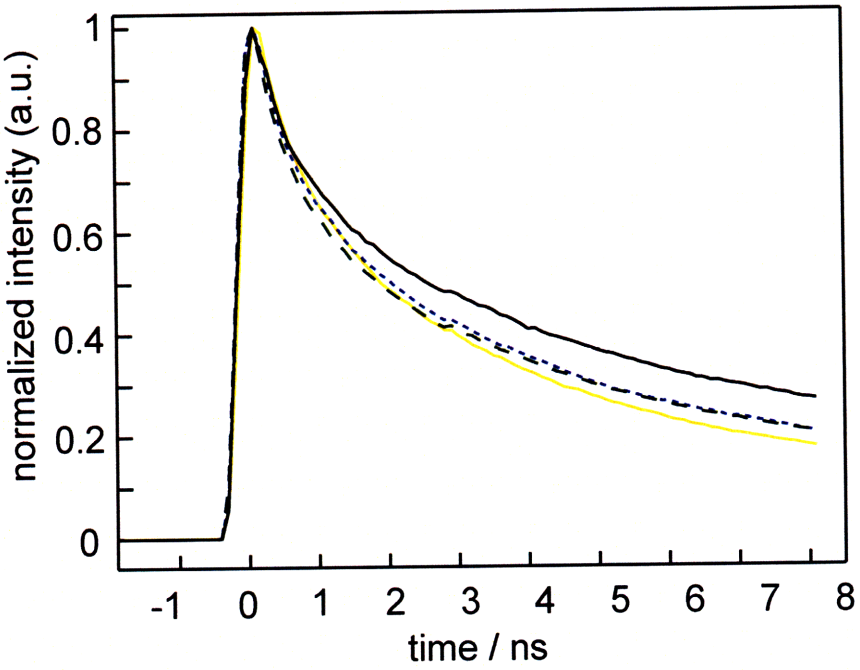

Figure II.7 Time-resolved fluorescence decay curves of NC (black solid line —) and RITC-NC conjugates with RITC:NC ratio of 2.5:1 (yellow solid line —), 0.8:1 (green dashed line – –), and 0.3:1 (blue dashed line - - -). The lifetimes of NCs in the conjugates are quenched.

Table II.2 FRET parameters obtained from time-resolved fluorescence measurements.

Sample	RITC:NC Ratio	Long τ_D / ns	Short τ_D / ns	r / Å	E / %	k_{FRET} / s^{-1}
CdSe/ ZnS NC		14.11	2.01			
RITC-NC	2.5:1	6.12	0.87	40	57	3.8×10^7
RITC-NC	0.8:1	6.20	0.53	33	56	1.2×10^8
RITC-NC	0.3:1	9.18	0.12	33	35	1.2×10^8

the RITC-NC conjugates are shorter than the lifetime of the emission of the unconjugated NC itself. The degree of quenching is also proportional to the number of acceptor dyes per NC, which is indicative of enhanced efficiency of energy transfer.

By examining the decay in the region where NC emission is dominant, lifetimes (τ_D), rate of energy transfer (k_{FRET}) and efficiency of energy transfer (E) were calculated and are listed in Table II.2. The longer lifetime component is assigned to the band edge excitonic recombination[16] and was used to calculate the E, r, and k_{FRET} using eqs. I.7 – I.10. The construct with more dyes conjugated (2.5:1) shows the highest energy transfer efficiency of 57%. Even with minimal amounts of acceptor dye attached (0.3:1), the efficiency is still high, on average approximately 40%. The rate of energy transfer was found to be on the order of 10^8 s^{-1}. One possible explanation for the discrepancy between the donor-acceptor distances, r, may be the potential inhomogeneity arising from the way the amphiphilic polymer forms a micelle around the NC. Consequently the donor-acceptor distance would be changed. The conjugate with the shorter distance exhibits a dramatic increase in the efficiency of energy transfer, emphasizing that the distance between the donor and acceptor is crucial for the rate and efficiency of FRET. Another explanation is potential aggregation of the NCs in some samples. The NC maximum emission wavelengths appeared to drift, as shown in Figure II.4. If the NCs themselves undergo FRET to emit a lower-energy photon, the spectral overlap between the donor and acceptor would increase, which in turn will increase k_{FRET}. However, given that the efficiency of a RITC-NC conjugate with only one dye per NC is high, the utility of the amphiphilic polymer scaffold for NC FRET studies is evident.

II.3 Concluding Remarks

There are many advantages offered by the NC-dye conjugates as they combine the positive features of NC with the emissive properties of the dye. The photophysical properties of a water-soluble NC covalently conjugated to a dye through the use of a new amphiphilic polymer was investigated. Fluorescent resonance energy transfer (FRET) was found to be present and efficient even with a single dye acceptor. This result is consistent with the observations of Mattoussi and co-workers who have investigated the energy transfer from a NC to various acceptor dyes (cyanines and rhodamines).[14] The ease of synthesizing the NC-RITC construct underscores the significance of this work. Unlike other reports, a distinguishing feature of the construct studied in this Chapter is the ability to solubilize and the functionalize NCs at once. The synthesis of the polymer and the coupling of the dye to the NC are both facile. The functionalization of the polymer allows for multiple energy acceptor molecules to be coupled easily and permits an increased efficiency in energy transfer.

An immediate application of energy transfer between CdSe/ZnS NC and an energy acceptor is chemical and biological sensing. By providing a straightforward method of coupling a receptor molecule onto the NC, a plethora of new NC-acceptor constructs may be synthesized. As developed by Mattoussi and co-workers, adding a quencher molecule onto the NC, which subsequently becomes displaced when the appropriate analyte comes along permits a turn-on sensor to be constructed.[20,37] Alternatively, any acceptor molecule that changes its absorbance properties upon binding an analyte will in turn modulate the emission of the NC through FRET, thus leading to yet another sensing strategy based on harnessing the energy transfer properties in such constructs. As the analyte interaction with the NC-construct is in equilibrium, this sensing strategy is reversible. This latter approach to sensing using NCs will be discussed in Chapters III, IV, and V.

II.4 Experimental Procedures

II.4.a Materials and Methods

Rhodamine B isothiocyanate (RITC), decylamine, anhydrous *N,N'*-

dimethylformamide (DMF), trioctylphosphine oxide (90%, TOPO), cadmium 2,4-pentanedionate, dodecanal, 1800 MW poly(acrylic acid), 5-amino-1-pentanol, *N*-octylamine, 0.1 M tetrabutylammonium hydroxide in methanol and Sephadex LH-20 were purchased from Sigma-Aldrich, Inc. 1-Ethyl-3,3′-dimethylaminopropylcarbodiimide (EDC), hexadecylamine (HDA), bis-(trimethylsilyl)sulfide [$(TMS)_2S$], and diethylzinc ($ZnEt_2$) were purchased from Fluka. Selenium shot and hexylphosphonic acid (HPA) were obtained from Alfa Aesar. Trioctylphosphine (TOP) was purchased from Strem Chemicals. All air sensitive materials were handled in an Omni-Lab VAC glove box under dry nitrogen atmosphere with oxygen levels < 0.2 ppm. All materials were used as purchased, except for TOPO and 5-amino-1-pentanol, which were purified through vacuum distillation, and diethylzinc which was passed through a 0.2 μm syringe filter before use. Centrifugal filters equipped with a 50,000 Da molecular weight cutoff (MWCO) dialysis membrane were purchased through Millipore Corporation.

II.4.b Spectroscopic Characterization

UV-vis spectroscopy of RITC-coupled CdSe/ZnS was measured on a Hewlett-Packard 8453 UV-vis spectrophotometer with the Chemstation software version A.06.03. Steady-state fluorescence measurements were obtained in a 1 cm pathlength cuvette from a custom-built Photon Technology Instruments fluorometer installed with a Hamamatsu R928 photomultiplier tube and a 150 W Xe excitation lamp.

Quantum yield (Φ) measurements were calculated using eq. II.1, where *A* is the measured absorbance at the excitation wavelength, *I* is the integrated emission intensity, and η is the refractive index of the solvent.

$$\Phi_{sample} = \Phi_{ref}\left(\frac{A_{ref}}{A_{sample}}\right)\left(\frac{I_{sample}}{I_{ref}}\right)\left(\frac{\eta_{sample}}{\eta_{ref}}\right) \qquad \text{(II.1)}$$

The quantum yield of the reference, Φ_{ref}, was taken to be 0.95 for rhodamine 590 in ethanol. [38]

A 400 nm emitting Ti:Sapphire laser equipped with a gated intensified CCD camera was used to obtain time-resolved fluorescence spectra. Data were collected at room temperature using a 1 cm optical path fluorescence cuvette. Matlab was used to fit

the lifetime decay curve as a bi-exponential decay.

All NMR spectra were collected at the MIT Department of Chemistry Instrumentation Facility (DCIF) on a Varian Inova 500 MHz NMR Spectrometer at room temperature. Chemical shifts are reported using the standard δ notation in ppm and are referenced to tetramethylsilane (TMS) using the residual ^1H signal of the deuterated solvent, CD_3OD, as an internal standard. IR Spectra of samples were collected on a Perkin-Elmer 2000 FTIR Spectrometer. Gel permeation chromatography was performed on a Hewlett-Packard series 1100 HPLC instrument equipped with a PLgel 5 μm (300 x 7.5 mm) column and a diode-array detector at 254 nm using THF as the eluent at a flow rate of 1.0 mL/ min.

II.4.c Synthesis of CdSe/ZnS Nanocrystals

CdSe NCs overcoated with ZnS were prepared using a modified literature method.[39-41] A vial containing cadmium 2,4-pentanedionate (0.317 g, 0.00100 mol), dodecanal (0.50 mL, 0.0023 mol) in trioctylphosphine (6.0 mL, 0.014 mol) was degassed at 180 °C for an hour, then cooled to yield a homogenous bright yellow solution. 1.5 M trioctylphosphine selenide (TOPSe, 4 mL, prepared from dissolving 5.92 g Se shot into 50 mL TOP) was subsequently added to the vial being cooled to room temperature. The contents of the vial were subsequently injected rapidly at 360 °C into a three-necked flask (equipped with an air condenser, temperature controller, and a stirbar) containing degassed solvent of trioctylphosphine oxide (6.25 g, 0.0162 mol), hexadecylamine (5.75 g, 0.0238 mol), and trioctylphosphine (3.4 mL, 0.0076mol). The temperature of the reaction was lowered immediately by removing the heating mantle to obtain NCs with emission wavelength of 520 nm.

The bare CdSe NCs were precipitated out of the growth solution with butanol and methanol twice and brought up in 4 mL hexanes. The NCs were overcoated by injecting the hexane solution of core CdSe into a degassed solvent of distilled trioctylphosphine oxide (10.0 g, 0.0259 mol) and n-hexylphosphonic acid (0.40 g, 0.0024 mol). The hexane was removed *in vacuo* at 80 °C, and decylamine (0.50 mL, 0.0020 mol) was added. After stirring for 1 hr, the solution temperature was raised to 140 °C. A precursor solution of bis(trimethylsilyl)sulfide and diethylzinc in 5.0 mL trioctylphosphine was

slowly dripped at approximately 1 drop per second using an addition funnel. Exact amounts were chosen to yield a ~3 monolayer coating of ZnS on the bare CdSe NCs. The final emission wavelength was 540 nm with a FWHM of 30 nm. The quantum yield of NCs prepared in this manner was generally on the order of 20 - 30% against a rhodamine 590 standard which is taken to be $\Phi = 0.95$ in ethanol.[38]

II.4.d Synthesis of *N*-Octylamine-modified Poly(acrylic acid)

A functionalized polymer was synthesized by derivatizing a fraction (40%) of the carboxylic acid groups of a 1800 MW poly(acrylic acid) (2.0 g, 0.0011 mol) with *N*-octylamine (1.44 g, 0.0110 mol) using 1-ethyl-3-(3-dimethylaminopropyl)carbodiimide (EDC) (2.12 g, 0.0110 mol) in *N,N'*-dimethylformamide according to a previous report.[9] The functionalized polymer was purified by size-exclusion chromatography using Sephadex LH-20 with methanol as the mobile phase. ^{1}H NMR (500MHz, CD_3OD, δ): 3.15 (br s), 2.25 (br, s), 1.98 (s), 1.60 (br s), 1.46 (br s), 1.28 (s), 0.866 (s). IR (KBr, cm^{-1}): 3289 (OH, br), 2930-2853 (CH, aliphatic), 1712 (C=O), 1641 (CO-NH-R), 1564 (CO-NH-R).

II.4.e Synthesis of *N*-Octylamine and 5-amino-1-pentanol-modified Poly(acrylic acid)

A functionalized polymer was synthesized by coupling a fraction (40%) of the carboxylic acid groups of a 1800 MW poly(acrylic acid) (2.0 g, 0.0011 mol) with *N*-octylamine (1.44 g, 0.0110 mol) using 1-ethyl-3-(3-dimethylaminopropyl)carbodiimide (EDC) (2.12 g, 0.0110 mol) in *N,N'*-dimethylformamide according to a previous report.[9] An additional 40% of the acid groups were coupled to vacuum-distilled 5-amino-1-pentanol (1.13 g, 0.0110 mol) using EDC (2.12 g, 0.0110 mol) in DMF, while the remaining 20% was left as free carboxylic acid. The functionalized polymer was purified by size-exclusion chromatography using Sephadex LH-20 with methanol as the mobile phase. ^{1}H NMR (500MHz, CD_3OD, δ): 3.66 (br s), 3.53 (br s) 3.11 (br s), 1.50 (br s), 1.42 (br s), 1.28 (s), 0.89 (s). IR (KBr, cm^{-1}): 3365 (OH, br), 2928 - 2857 (CH, aliphatic), 1718 (C=O), 1653 (CO-NH-R), 1531 (CO-NH-R).

II.4.f Preparation of Polymer Micelle Encapsulated NCs

Water-soluble CdSe/CdZnS NCs were prepared by precipitating 0.50 mL of the NC stock solution. The resulting dried CdSe/ ZnS (5 mgs) was added to octylamine and 5-amino-1-pentanol modified poly(acrylic acid) (30 mgs) in a vial and dissolved in chloroform. The chloroform solution was sonicated and stirred vigorously for 1 hour, after which the solvent was removed *in vacuo.*

II.4.g Preparation of NC-RITC Conjugates

Four individual samples of the polymer coated NCs were dissolved in 2 mL DMF, to which controlled amounts of RITC ((3.0 mg, 5.6 μmol), (0.30 mg, 0.56 μmol), (0.060 mg, 0.11 μmol), (0.030 mg, 56 nmol)) in 1 mL DMF were added and stirred overnight. Evaporation of DMF and addition of H_2O and 0.1 mL 0.1 M tetrabutylammonium hydroxide in methanol yielded water-solubilized CdSe/ZnS NCs conjugated to RITC. The conjugates were purified by dialysis through Millipore centrifuge tubes equipped with 50000 MWCO filters. After multiple washings, the free dye was completely removed from the NC-dye construct as verified by the absence of the parent dye absorption features in the UV-vis absorption spectrum of the filtrate.

II.5 References

1. Jaiswal, J. K.; Simon, S. M. *Trends Cell. Biol.* **2004**, *14*, 497-504.

2. Somers, R. C.; Bawendi, M. G.; Nocera, D. G. *Chem. Soc. Rev.* **2007**, *36*, 579-591.

3. Clapp, A. R.; Medintz, I. L.; Mattoussi, H. *Chem. Phys. Chem.* **2006**, *7*, 47-57.

4. Bruchez, M., Jr.; Moronne, M.; Gin, P.; Weiss, S.; Alivisatos, A. P. *Science* **1998**, *281*, 2013-2016.

5. Chan, W. C.; Nie, S. *Science* **1998**, *281*, 2016-2018.

6. Michalet, X.; Pinaud, F. F.; Bentolila, L. A.; Tsay, J. M.; Doose, S.; Li, J. J.; Sundaresan, G.; Wu, A. M.; Gambhir, S. S.; Weiss, S. *Science* **2005**, *307*, 538-544.

7. Kim, S.; Lim, Y. T.; Soltesz, E. G.; De Grand, A. M.; Lee, J.; Nakayama, A.; Parker, J. A.; Mihaljevic, T.; Laurence, R. G.; Dor, D. M.; Cohn, L. H.; Bawendi, M. G.; Frangioni, J. V. *Nat. Biotechnol.* **2004**, *22*, 93-97.

8. Gao, X.; Cui, Y.; Levenson, R. M.; Chung, L. W. K.; Nie, S. *Nat. Biotechnol.* **2004**, *22*, 969-976.

9. Wu, X.; Liu, H.; Liu, J.; Haley Kari, N.; Treadway Joseph, A.; Larson, J. P.; Ge, N.; Peale, F.; Bruchez Marcel, P. *Nat. Biotechnol.* **2003**, *21*, 41-46.

10. Alivisatos, P. *Nat. Biotechnol.* **2004**, *22*, 47-52.

11. Colvin, V. L.; Schlamp, M. C.; Alivisatos, A. P. *Nature* **1994**, *370*, 354-357.

12. Coe-Sullivan, S.; Woo, W. K.; Steckel, J. S.; Bawendi, M.; Bulovic, V. *Org. Electron.* **2003**, *4*, 123-130.

13. Steckel, J. S.; Zimmer, J. P.; Coe-Sullivan, S.; Stott, N. E.; Bulovic, V.; Bawendi, M. G. *Angew. Chem., Int. Ed. Engl.* **2004**, *43*, 2154-2158.

14. Clapp, A. R.; Medintz, I. L.; Mauro, J. M.; Fisher, B. R.; Bawendi, M. G.; Mattoussi, H. *J. Am. Chem. Soc.* **2004**, *126*, 301-310.

15. Clapp, A. R.; Medintz, I. L.; Fisher, B. R.; Anderson, G. P.; Mattoussi, H. *J. Am. Chem. Soc.* **2005**, *127*, 1242-1250.

16. Mattoussi, H.; Mauro, J. M.; Goldman, E. R.; Green, T. M.; Anderson, G. P.; Sundar, V. C.; Bawendi, M. G. *Phys. Status Solidi B* **2001**, *224*, 277-283.

17. Sapsford, K. E.; Medintz, I. L.; Golden, J. P.; Deschamps, J. R.; Uyeda, H. T.; Mattoussi, H. *Langmuir* **2004**, *20*, 7720-7728.

18. Pons, T.; Medintz, I. L.; Wang, X.; English, D. S.; Mattoussi, H. *J. Am. Chem. Soc.* **2006**, *128*, 15324-15331.

19. Medintz, I. L.; Clapp, A. R.; Mattoussi, H.; Goldman, E. R.; Fisher, B.; Mauro, J. M. *Nat. Mater.* **2003**, *2*, 630-638.

20. Tran, P. T.; Goldman, E. R.; Anderson, G. P.; Mauro, J. M.; Mattoussi, H. *Phys. Status Solidi B* **2002**, *229*, 427-432.

21. Medintz, I. L.; Uyeda, H. T.; Goldman, E. R.; Mattoussi, H. *Nat. Mater.* **2005**, *4*, 435-446.

22. Goldman, E. R.; Medintz, I. L.; Hayhurst, A.; Anderson, G. P.; Mauro, J. M.; Iverson, B. L.; Georgiou, G.; Mattoussi, H. *Anal. Chim. Acta* **2005**, *534*, 63-67.

23. Medintz, I. L.; Clapp, A. R.; Melinger, J. S.; Deschamps, J. R.; Mattoussi, H. *Adv. Mater.* **2005**, *17*, 2450-2455.

24. Liu, W.; Choi, H. S.; Zimmer, J. P.; Tanaka, E.; Frangioni, J. V.; Bawendi, M. *J. Am. Chem. Soc.* **2007**, *129*, 14530-14531.

25. Dubertret, B.; Skourides, P.; Norris, D. J.; Noireaux, V.; Brivanlou, A. H.; Libchaber, A. *Science* **2002**, *298*, 1759-1762.

26. Guo, W.; Li, J. J.; Wang, Y. A.; Peng, X. *Chem. Mater.* **2003**, *15*, 3125-3133.

27. Kim, S.; Bawendi, M. G. *J. Am. Chem. Soc.* **2003**, *125*, 14652-14653.

28. Uyeda, H. T.; Medintz, I. L.; Jaiswal, J. K.; Simon, S. M.; Mattoussi, H. *J. Am. Chem. Soc.* **2005**, *127*, 3870-3878.

29. Susumu, K.; Uyeda, H. T.; Medintz, I. L.; Pons, T.; Delehanty, J. B.; Mattoussi, H. *J. Am. Chem. Soc.* **2007**, *129*, 13987-13996.

30. Clapp, A. R.; Goldman, E. R.; Mattoussi, H. *Nat. Protoc.* **2006**, *1*, 1258-1267.

31. Liu, W.; Howarth, M.; Greytak, A. B.; Zheng, Y.; Nocera, D. G.; Ting, A. Y.; Bawendi, M. G. *J. Am. Chem. Soc.* **2008**, *130*, 1274-1284.

32. McHedlov-Petrosyan, N. O.; Kholin, Y. V. *Russ. J. Appl. Chem. (Engl. Trans.)* **2004**, *77*, 414-422.

33. Chen, M.-H.; Kumar, R.; Parmar, V. S.; Kumar, J.; Samuelson, L. A.; Watterson, A. C. *J. Macromol. Sci., Pure Appl. Chem.* **2004**, *A41*, 1489-1496.

34. Liu, X.-M.; Yang, Y.-Y.; Leong, K. W. *J. Colloid Interf. Sci.* **2003**, *266*, 295-303.

35. Lakowicz, J. R. *Principles of Fluorescence Spectroscopy, 2nd ed.*; Kluwar Academic/ Plenium Publishing: New York, 1999.

36. Javier, A.; Magana, D.; Jennings, T.; Strouse, G. F. *Appl. Phys. Lett.* **2003**, *83*, 1423-1425.

37. Goldman, E. R.; Medintz, I. L.; Whitley, J. L.; Hayhurst, A.; Clapp, A. R.; Uyeda, H. T.; Deschamps, J. R.; Lassman, M. E.; Mattoussi, H. *J. Am. Chem. Soc.* **2005**, *127*, 6744-6751.

38. Kubin, R. F. F., A. N. *J. Lumin.* **1982**, *27*, 455-462.

39. Murray, C. B.; Norris, D. J.; Bawendi, M. G. *J. Am. Chem. Soc.* **1993**, *115*, 8706-8715.

40. Hines, M. A.; Guyot-Sionnest, P. *J. Phys. Chem.* **1996**, *100*, 468-71.

41. Dabbousi, B. O.; Rodriguez-Viejo, J.; Mikulec, F. V.; Heine, J. R.; Mattoussi, H.; Ober, R.; Jensen, K. F.; Bawendi, M. G. *J. Phys. Chem. B* **1997**, *101*, 9463-9475.

Chapter III

Proof-of-Concept Sensing Studies: A Ratiometric CdSe/ CdZnS Nanocrystal pH Sensor

Parts of this Chapter have been published:
Snee, P. T.; Somers, R. C.; Nair, G.; Zimmer, J. P.; Bawendi, M.G. and Nocera, D. G.
J. Am. Chem. Soc. **2006**, *128,* 13320-13321.

III.1 Introduction

Semiconductor nanocrystals (NCs) serve as useful fluorescent labels owing to their photostability, continuous absorption spectra, and efficient, narrow and tunable emission, as introduced in Chapter I.[1-6] Whereas NCs are useful in identifying position in a microenvironment, their intrinsic insensitivity to the presence of most biological or chemical agents renders them of limited utility as sensing probes of that microenvironment. An important step in this direction has been the recent development of water soluble CdSe NCs with the ability to sense target analytes through the use of a quencher displacement strategy using Fluorescence Resonance Energy Transfer (FRET) as a signal transduction mechanism, as was discussed in Chapter I.6.b.[7-11] These previous studies, however, do not demonstrate reversible chemical sensing using fluorescent NCs. In addition, previous sensing constructs rely on self-assembled recombinant fusion protein to coat the NCs and to provide a functional handle for the attachment of dyes, which makes the synthesis tedious.

A new surface encapsulation of CdSe NCs was explored in Chapter II. The *N*-octylamine and 5-amino-1-pentanol modified poly(acrylic acid) serves to impart water solubility as well as to provide a hydroxyl functional group for isothiocyanate or ester coupling. CdSe nanocrystal energy transfer studies with an acceptor dye, rhodamine isothiocyanate (RITC), revealed a high transfer efficiency even with a donor:acceptor ratio of 1:1. This Chapter describes efforts to take advantage of the information obtained from Chapter II in order to synthesize a reversible and ratiometric CdSe nanocrystal sensor. As a proof-of-concept, pH, or H^+ concentration, was targeted as the analyte of interest. We show that a reversible NC-based fluorescent sensor can be designed by conjugating a dye with an equilibrium response to an analyte to the surface of a CdSe/CdZnS NC, and that such a sensor can be synthesized easily using the polymer coating described in Chapter II. The dual emissive nature of the NC-dye conjugate naturally lends itself to ratiometric sensing. By properly controlling the energy transfer between the NC and dye, a general method for ratiometric NC sensors can be developed, thus providing a mean for detecting analytes with high precision, irrespective

of changes in excitation intensity, excitation wavelength, probe concentration, or collection efficiency.

III.2 Results and Discussion

III.2.a Synthetic Design

Our synthetic strategy focused on a method that would allow for reversible and ratiometric sensing using fluorescent NCs. By tethering a dye with an equilibrium response to an analyte to the surface of a CdSe/ZnS NC, a FRET-based reversible sensor could be designed. The choice of the analyte-sensitive FRET acceptor centered on four basic requirements:

(1) The acceptor must be absorptive where the FRET donor (CdSe NCs) emits, between λ = 525-660 nm

(2) The acceptor should possess functional groups (*i.e.* -OH, -COOH, $-NH_2$) that would be amenable to covalent conjugation to the donor NC

(3) The acceptor must exhibit a change in its optical absorptive properties with respect to analyte concentration

(4) The acceptor must have no absorption where the donor NC is excited, in order to minimize direct excitation

The first two points are necessary for efficient FRET for a NC-acceptor pair. While the third and fourth requirements are not necessarily required for a NC based FRET sensor, these features allow for the modulation of FRET efficiency through changes in the spectral overlap, *J*, (as opposed to donor-acceptor distance, *r*) as the signal

Scheme III.1 Synthetic steps for the pH-sensitive squaraine dye, **4**.

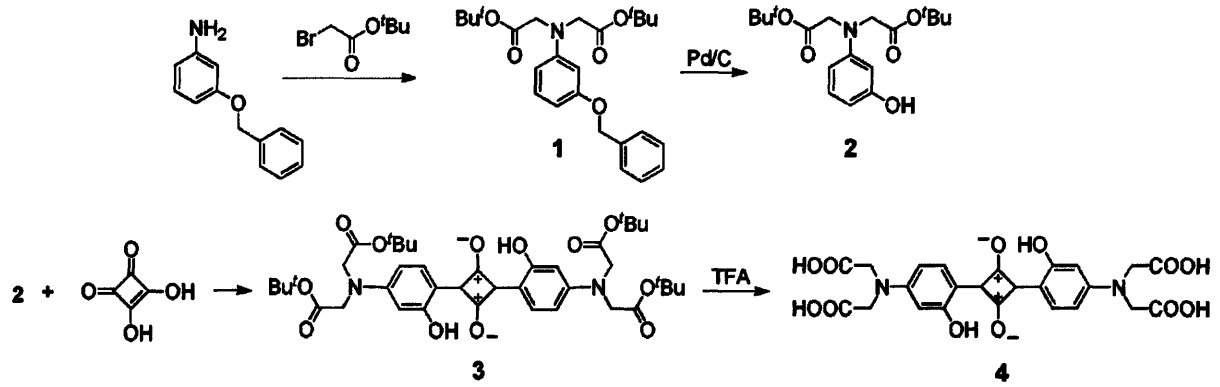

Scheme III.2 A sensor constructed from a colloidal CdSe NC that is overcoated with an outer layer of ZnS. The native phosphine oxide ligands are encapsulated with an amphiphilic polymer upon which a pH sensitive squaraine dye is conjugated.

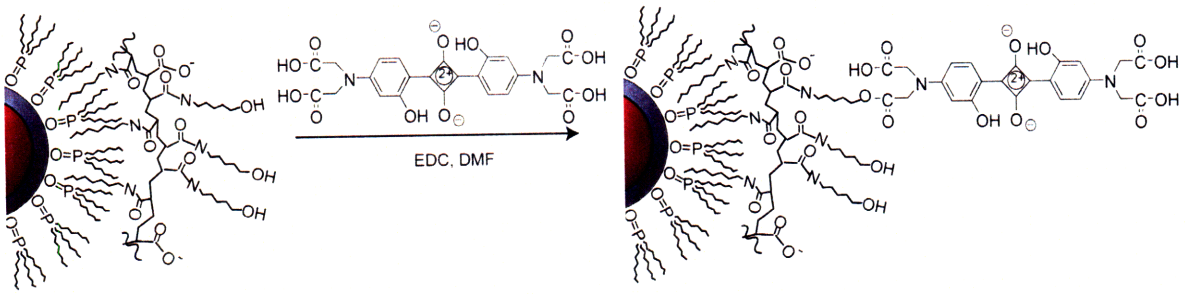

transduction mechanism. The modulation of spectral overlap is particularly convenient and advantageous for pH sensing, as most pH sensors are colorimetric sensors by nature. Based on the above four requirements, a squaraine-based pH sensitive dye that exhibits both pH-sensitive absorption and emission[12] was chosen as the FRET acceptor in this proof-of-concept reversible NC sensor. The squaraine pH dye was synthesized in four simple steps, as illustrated by Scheme III.1. The overall yield for the four-step synthesis was 21%, and the final product contained four carboxylic acid groups that allow for facile covalent coupling to the NCs.

CdSe NCs overcoated with ZnS and capped with trioctylphosphine oxide ligands were encapsulated by a hydrophobically modified poly(acrylic acid) in order to impart water solubility.[13] In addition to modifying with octylamine, 5-amino-1-pentanol was also used to modify the poly(acrylic acid) in order to add hydroxyl moieties on the polymer scaffold. The squaraine dye was linked to the polymer backbone via ester linkages using 1-ethyl-3-(3-dimethylaminopropyl)carbodiimide (EDC) as the coupling agent to make the NC sensor as shown in Scheme III.2. We have also found that the same dye conjugation method may be applied to NCs that have been cap exchanged with dihydrolipoic acid-functionalized polyethylene glycols, a water-solubilization method developed by Mattoussi and co-workers, which is discussed in more detail in Chapters IV and V.[14] The samples were easily purified with dialysis filters to ensure that unreacted dyes were removed from the sample. The following photophysical discussion pertains to the polymer-encapsulated NC-squaraine constructs.

III.2.b Photophysical Properties

The sensing action of the NC-squaraine conjugate is imparted by modulation of the FRET efficiency arising from the engineered overlap of the pH-sensitive dye absorption spectrum with the (pH-insensitive) quantum dot emission (Figure III.1). Owing to the pH dependence of the dye absorption spectrum, the spectral overlap between the dye absorption and the NC emission increases as the pH is lowered. The spectral overlap integral, J, is directly related to the critical FRET distance, R_o, which in turn affects the energy transfer efficiency, E, according to eqs. I.8 and I.9. The inset of Figure III.1 shows a calculation of R_o as a function of pH, with the assumption of a dipole orientation factor being random at $\kappa^2 = 2/3$, and the NC possessing a Gaussian emission centered at 620 nm with a 30 nm FWHM and a 30% quantum yield. At high pH, FRET should be inefficient as the spectral overlap is small. Hence, the emission spectrum should be dominated by luminescence from the NC. As the pH is lowered, R_o grows larger and the FRET efficiency increases owing to a strengthening of the dye absorption cross-section $\varepsilon_{pH}(\lambda)$. The NC emission should then be quenched as a result of energy transfer to the dye, which will in turn become more emissive. While the

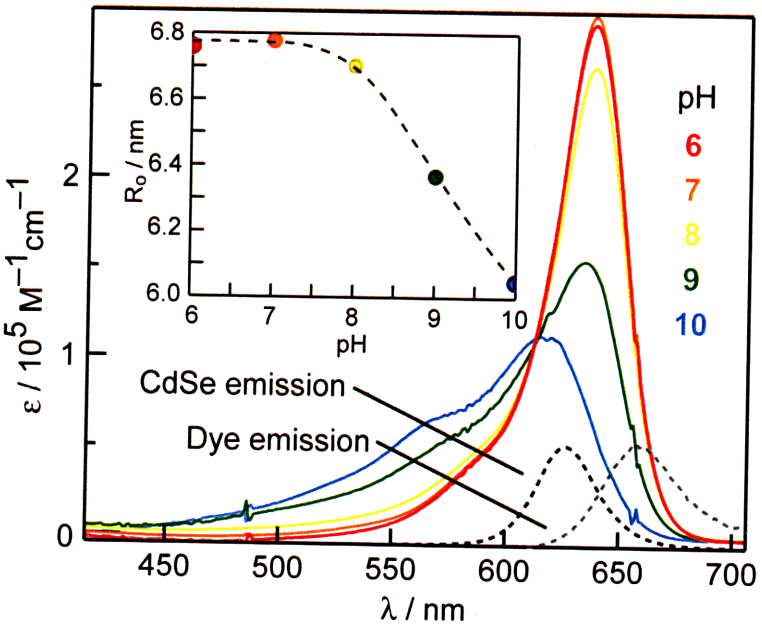

Figure III.1 The pH dependent absorption profile of the squaraine dye. Also shown in gray and black dashed line are the emissions of the dye and NC, respectively, at pH 6.0. The inset shows the critical transfer distance (R_0) for FRET.

squaraine dye has a pH-sensitive absorbance, consisting of both acidic and basic form, it only has a single emissive state; the change in emission is due to the planarity of the squaraine pH dye, **4**, being broken when the phenolic protons are deprotonated, causing changes in the electronic structure of the molecule.[12] At neutral pH, hydrogen bonding interactions between the oxygen atoms on the squaraine backbone and the hydroxyl groups on the phenol forces the molecule to be planar and rigid, allowing for the confirmation with the maximum fluorescence. Owing to the single-emissive nature of the squaraine dye, the quenching of NC emission can be directly correlated to the rise in dye emission, and the construct itself may be seen as a two-state dual emission sensor. The modulation between the two emissions is directly related to the pH-dependent FRET rate and efficiency.

The results shown in Figure III. and Figure III.3 are consistent with the calculated trend in R_o and expected FRET efficiency. Figure III. shows the response of the absorption profile of the NC-dye conjugate. The NC to dye ratio, which was 3.4:1, was determined by decomposing the absorption spectra and using the known optical cross-sections for the NC and dye.[15] As observed for the free dye in homogeneous solution (Figure III.1) the dye absorption band is suppressed under basic conditions. Consequently, energy transfer from the NC to the dye is inefficient and the emission spectrum shown in Figure III.3 is dominated by the NC at 613 nm. As pH is lowered, the absorption cross-section of the dye is increased and FRET from the NC to the dye becomes more efficient; emission from the NC-dye conjugate is now dominated by that of the dye at 650 nm. The largest changes occur near the dye pK_a of 8.8. The steady-state emission results are confirmed by time-resolved emission studies of the NC-dye conjugate. As shown in Figure III.4, NC emission of a conjugated sensor has a reduced lifetime with τ = 19 ns as compared to that of the unconjugated NC with τ = 31 ns. Förster analysis of the quenching according to eq. I.9 suggests that the overall efficiency of energy transfer for this construct is 40%. These results establish that the emission from the NC donor is quenched by the presence of the organic dye acceptor, as has been previously observed in other constructs.[7,9,16]

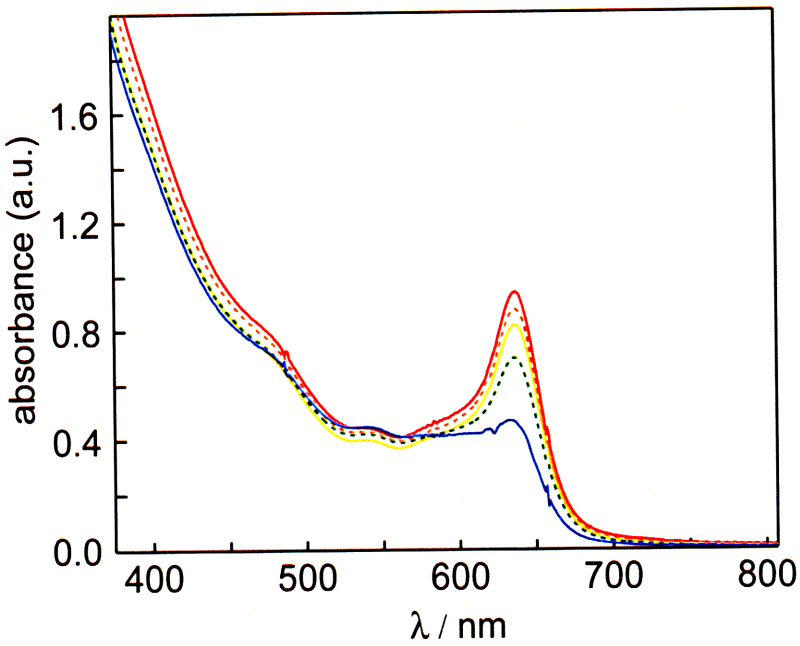

Figure III.2 The UV-visible absorption profile of a water-soluble (3.2 nm radius) NC-squaraine dye conjugate changes as a function of pH (— 6.0, - - - 7.0, — 8.0, - - - 9.0 and — 10). Both the highly absorptive NC features in the blue, as well as the pH dependent nature of the dye are preserved in the conjugate.

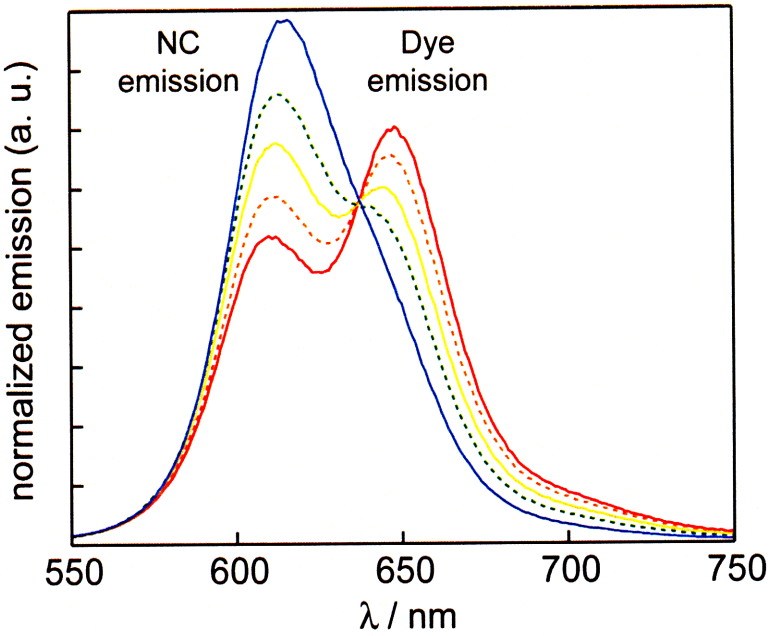

Figure III.3 The emission profile of a water-soluble (3.2 nm radius) NC-squaraine dye conjugate changes as a function of pH (— 6.0, - - - 7.0, — 8.0, - - - 9.0 and — 10) with λ_{ex} = 380 nm. The normalized spectra show pH dependence with an isosbestic point appearing at 640 nm. The overall quantum yield of this construct is 7 ±1%.

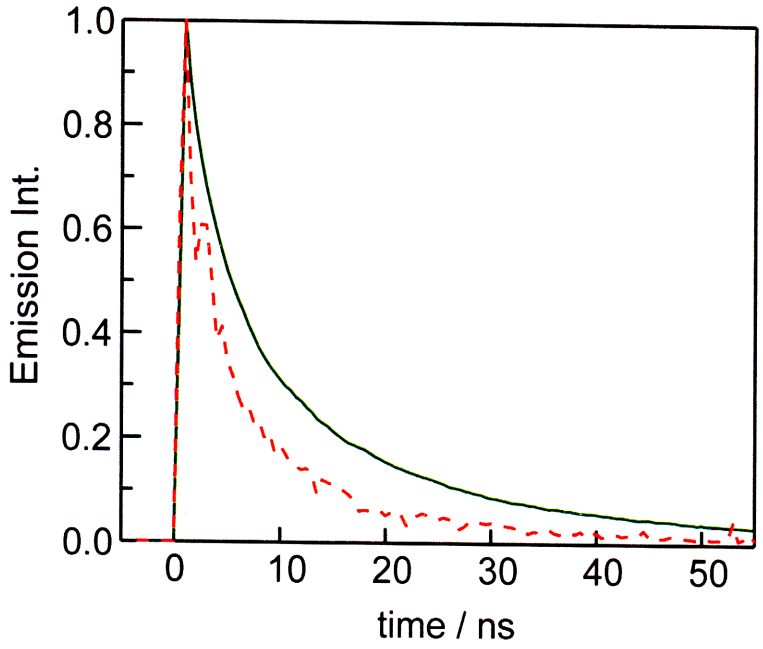

Figure III.4 The time-resolved NC emission decay of a control NC blank (— green solid line) versus the NC-dye conjugate at pH = 6 (- - - red dashed line).

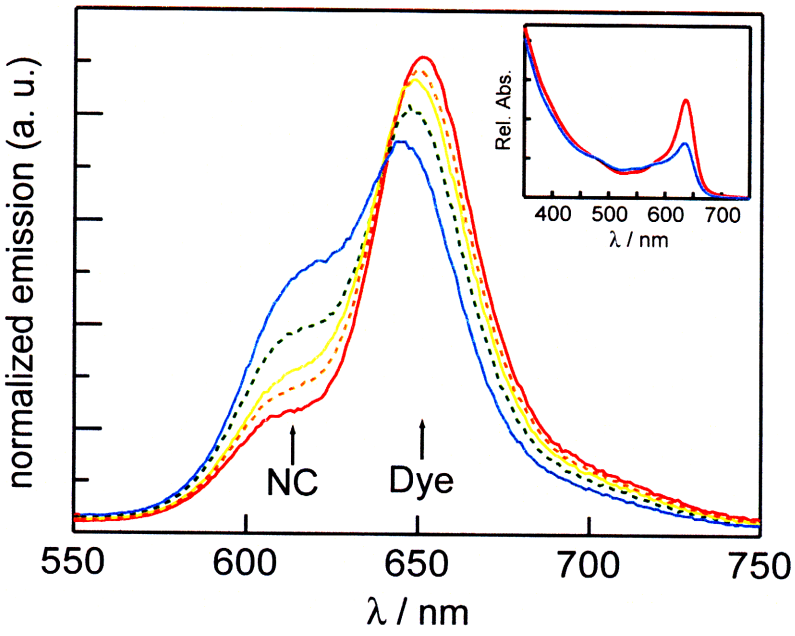

Figure III.5 The pH dependent emission (— 6.0, - - - 7.0, — 8.0, - - - 9.0 and — 10) of a NC-squaraine conjugate with a 7.5 : 1 dye to NC ratio, as calculated by decomposing the absorption spectra, shown in the inset.

Emission of a construct with a different dye to NC ratio is shown in Figure III.5. Note that the overall emission profile differs from that shown in Figure III.3 owing to different dye loading. However, in both cases, the modulation of the FRET efficiency by pH results in an emission between the NC and dye that is naturally ratiometric. The change in the NC-dye emission occurs about an isosbestic point at 640 nm. The important point drawn from these results is that the isosbestic point is maintained regardless of loading, and thus, sensing may be performed without the need for precise control of the loading ratio. As long as a point that remains independent of pH exists, a simple calibration curve may be constructed by plotting the ratio of dye or NC emission intensity to the isosbestic point as a function of pH.

In order to prove that the dye emission of our constructs (when excited at λ_{ex} = 380 nm) is indeed due to FRET instead of direct excitation, the pH dependence on the emission of the squaraine dye, the NC alone, as well as that of a NC-dye mixture, were investigated. Figure III.6 shows the emission spectra of the squaraine alone at various pH. The emission is highest at neutral pH and is minimized at basic pH. Compared to the squaraine dye, the response of the NC to pH is minimal, as shown in Figure III.7. The UV-visible and steady-state emission spectra of a mixture of NCs and squaraine dye in different pH environments are shown in Figure III.8 and Figure III.9. The pH dependent nature of the dye, when mixed in a solution of NCs, is still conserved as seen in Figure III.8 and looks very similar to the absorption of the tethered construct (Figure III.). However, in Figure III.9, the squaraine emission is hardly present when excited at 380 nm, where only the NC absorbs. This is in stark contrast to Figure III.3 and Figure III.5 where dye emission is present in the tethered construct. The lack of FRET in the mixture case indicates that the NC and the dye do not associate without the covalent tether, confirming the importance of the linking chemistry in the sensor. The distance dependent nature of FRET underscores the necessity of a covalent bond between the NC and the acceptor dye.

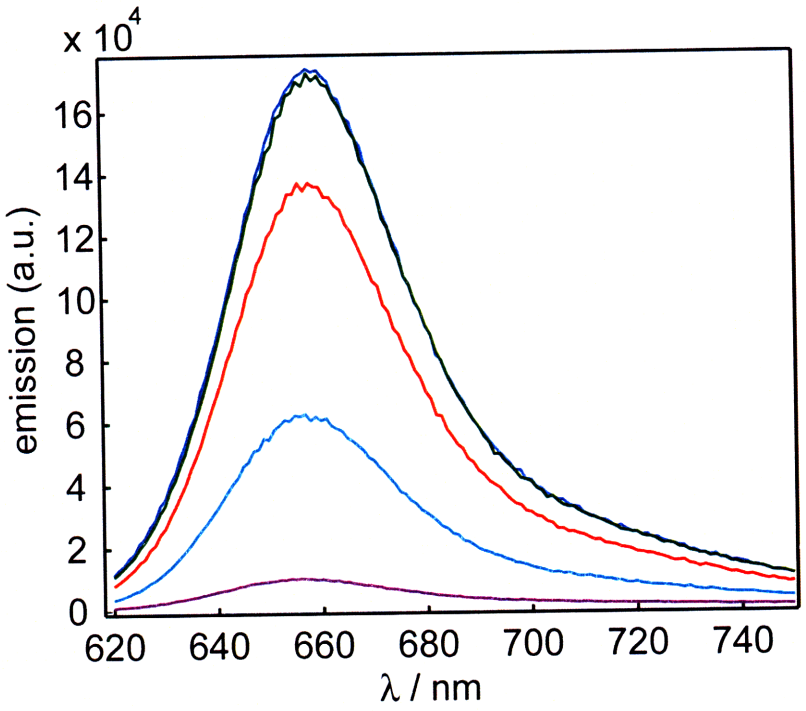

Figure III.6 The pH-dependent emission spectra (— 6.0, —7.0, — 8.0, — 9.0 and — 10) of the squaraine dye at λ_{ex} = 615 nm.

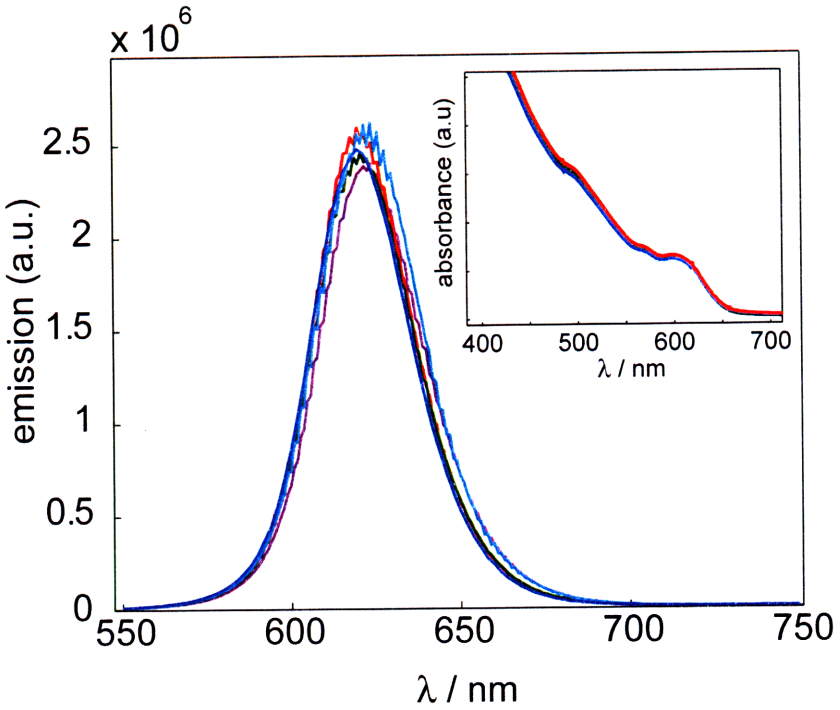

Figure III.7 The emission spectra of NCs at different pH (— 6.0, —7.0, — 8.0, — 9.0 and — 10) at λ_{ex} = 380 nm is similar to each other. The inset shows the pH-independent absorption profile of the NCs.

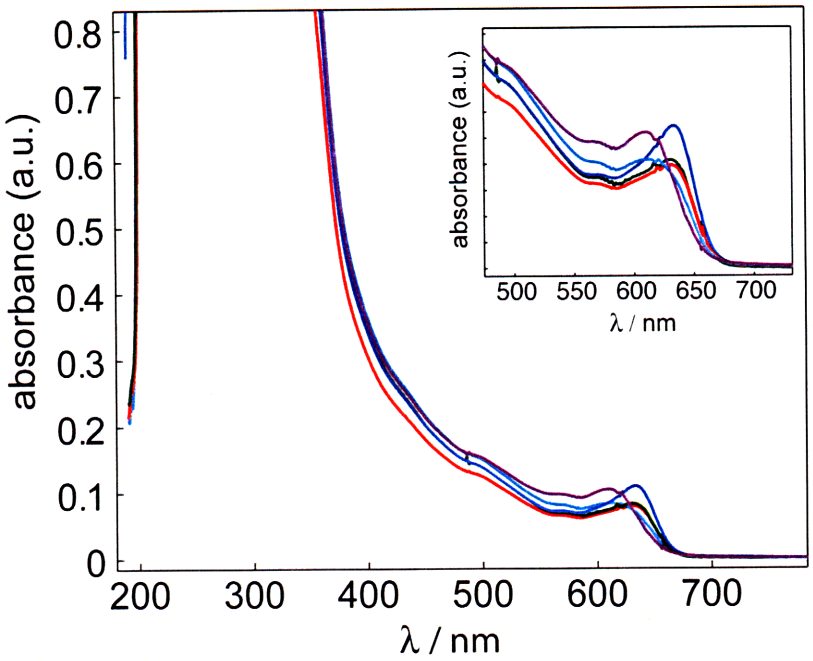

Figure III.8 UV-visible profile of NC and dye mixture, with the inset showing the close-up of the first absorption feature of the NC and the pH dependent absorption of the dye (pH= — 6.0, —7.0, — 8.0, — 9.0 and — 10).

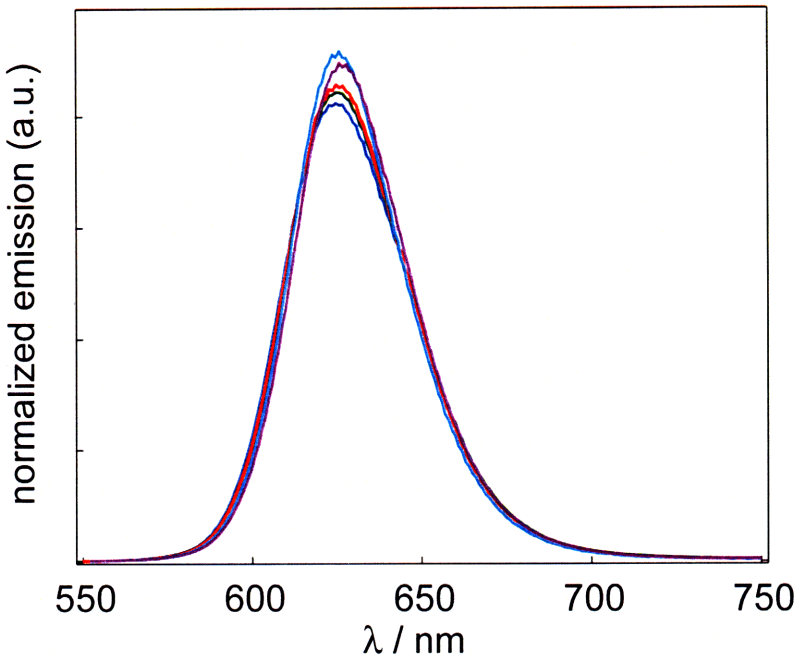

Figure III.9 Normalized emission spectra of the NC and dye mixture (λ_{ex} = 380 nm). Note the lack of dye emission.

III.2.c Ratiometric Sensing

The NC-squaraine sensor functions by the modulation of the FRET efficiency by analyte concentration, in this case, protons. The resulting optical emission is ratiometric, due to the existence of an isosbestic point at 640 nm. The solution pH can be read out precisely by taking the ratio of each emission peak intensity or area (NC and dye) to the intensity at the isosbestic point, which functions as an internal reference. This ratiometric approach is powerful when compared to typical chem- and bio-sensors that display a single intensity-based response to analytes (i.e. either brightening or darkening) because the ratiometric construct is not sensitive to fluctuations of light excitation or collection efficiency as sensing is self-referencing.[17,18]

To highlight the importance of the self-referencing capability of our constructs compared to other organic sensing nanomaterials, we have examined the effect of modulating the excitation intensity and wavelength on the normalized fluorescent spectra of the sensor in pH 6 and pH 10 buffered solutions. In separate experiments, ~130 nm silica microspheres were added to the solutions to produce a highly scattering medium. Figure III.10 shows the resulting emission spectra, normalized by area. Using the ratio of NC to dye emission in clear solutions as a calibration, we are able to reproduce the emission ratio to within 5% when altering the excitation intensity over ~1 decade and varying the composition of the environment. Such precision is impossible to be achieved by the dye alone.

In addition, the continuous absorption manifold of the CdSe NCs results in a bandshape independent of excitation-wavelength, a feature that is not present in single molecular ratiometric sensors.[19] When excited at λ_{ex} = 380 nm, 450 nm, and 520 nm, the emission profile remained constant between pH 6 and 10, as shown in Figure III.11 Thus, the NC-dye conjugate does not need to use two independent excitation sources (or alternatively a single excitation specifically at an absorptive isosbestic point) for proper function.

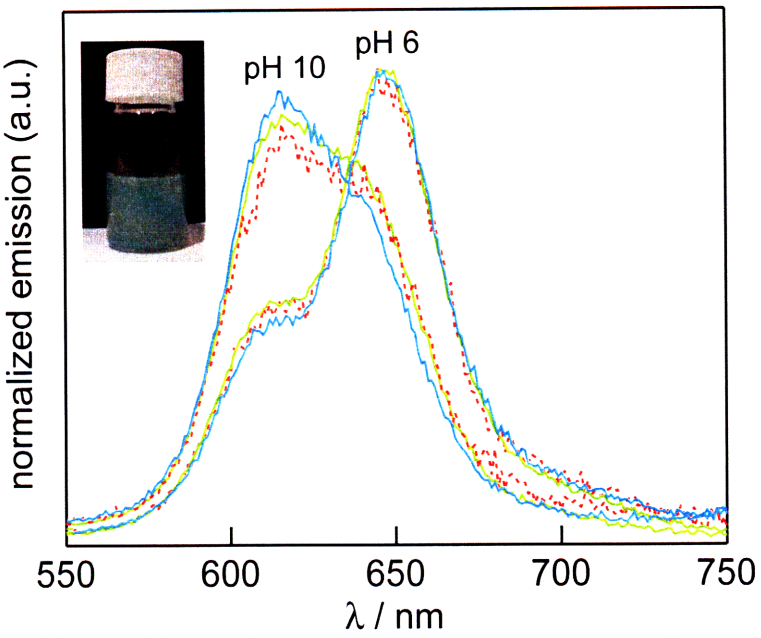

Figure III.10 The ratio of NC to dye emission varies such that the pH is determined within 5% when altering the slit entrance of the Xe lamp excitation of the fluorometer (- - - 0.5 mm; — 2.00 mm) and when examining the construct within a highly scattering media (—) shown by the picture of the vial.

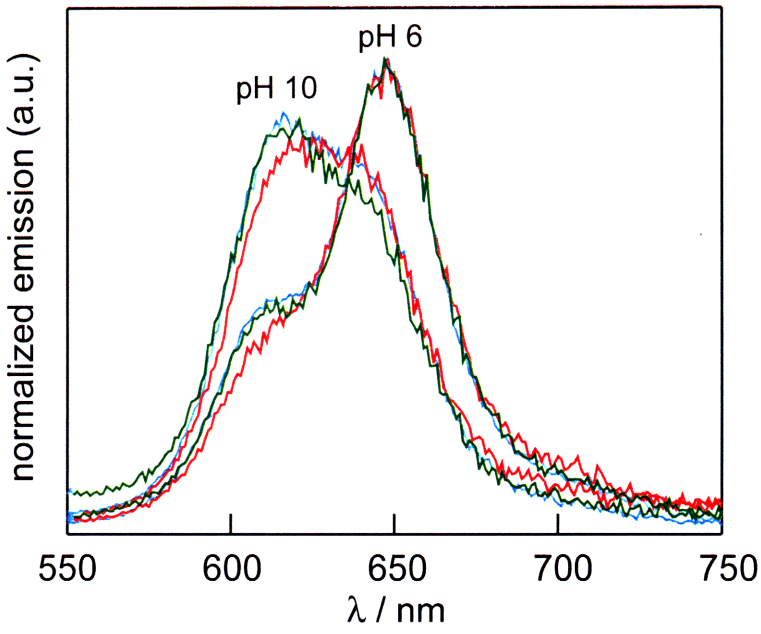

Figure III.11 Emission of the NC-dye construct is independent of excitation wavelength (λ_{ex} = — 380 nm; — 450 nm; — 520 nm).

III.3 Concluding Remarks

In summary, a new strategy for chemical and biological sensing was developed by tethering emissive water solubilized NCs to environmentally sensitive dye molecules. The sensitivity of our sensors can be tuned to other pH regimes by altering the pK_a of the dye. In addition, other pH dyes may be used for which we match the nanocrystal emission to overlap the new dyes's absorption. We have observed a ratiometric response to pH owing to the modulation of FRET efficiency between the emissive NC and dyes conjugated to the NC surface. The approach can be generalized to other sensing targets because the narrow, size-tunable emission spectrum of NCs enables them to be FRET donors that may be easily custom-engineered to match the acceptor absorption features of a dye conjugated to the surface of the NC. Taken together with the broad excitation spectrum and photostability conferred by NCs, the reversible and ratiometric approach presented here makes NCs versatile agents for chemical and biological sensing.

III.4 Experimental Procedures

III.4.a Materials and Methods

3-Benzyloxyaniline, t-butylbromoacetate, 1,8-bis(dimethylamino)naphthalene (proton sponge), 10% palladium on carbon, 3,4-dihydroxy-3-cyclobutene-1,2-dione (squaric acid), decylamine, *N*-octylamine, anhydrous *N,N'*-dimethylformamide (DMF), trioctylphosphine oxide (90%, TOPO), cadmium 2,4-pentanedionate, dodecanal, 1800 MW poly(acrylic acid), 5-amino-1-pentanol and Sephadex LH-20 were purchased from Sigma-Aldrich, Inc. 1-Ethyl-3,3'-dimethylaminopropylcarbodiimide (EDC), hexadecylamine (HDA), Bis(trimethylsilyl)sulfide [$(TMS)_2S$], and diethylzinc ($ZnEt_2$) were purchased from Fluka. Selenium shot, dimethylcadmium ($CdMe_2$), and n-hexylphosphonic acid (HPA) were obtained from Alfa Aesar. Trioctylphosphine (TOP) was purchased from Strem Chemicals. Silica microspheres (0.13 μm mean diameter) were obtained from Bangs Laboratories, Inc. All air-sensitive materials were handled in an Omni-Lab VAC glove box under dry nitrogen atmosphere with oxygen levels < 0.2 ppm. All materials were used as purchased, except for TOPO and 5-amino-1-pentanol,

which were purified through vacuum distillation, and diethylzinc and dimethylcadmium, which were passed through a 0.2 μm syringe filter before use. Centrifugal filters equipped with a 50,000 Da molecular weight cutoff (MWCO) dialysis membrane were purchased through Millipore corporation.

III.4.b Spectroscopic Characterization

UV-visible spectroscopy of squaraine-coupled CdSe/ ZnS was measured on a Hewlett-Packard 8453 UV-vis spectrophotometer with the Chemstation software version A.06.03. The samples were diluted in appropriate standard pH phosphate buffers for pH 6-8 and borate buffers for pH 9 and 10. Steady-state fluorescence measurements were obtained in a 1 cm pathlength cuvette from a custom-built Photon Technology Instruments fluorometer installed with a Hamamatsu R928 photomultiplier tube and a 150 W Xe excitation lamp. Quantum yield (Φ) measurements were calculated using eq. II.1. The quantum yield of the reference, Φ_{ref}, was taken to be 1.00 for rhodamine 640 in ethanol.[20]

A 400 nm emitting Ti:Sapphire laser equipped with a gated intensified CCD camera was used to obtain time-resolved fluorescence spectra. Data were collected at room temperature using a 1 cm optical path fluorescence cuvette. Matlab was used to fit the lifetime decay curve as a bi-exponential decay.

All NMR spectra were collected at the MIT Department of Chemistry Instrumentation Facility (DCIF) on a Varian Mercury 300 MHz or Varian Inova 500 MHz NMR spectrometer at room temperature. Chemical shifts are reported using the standard δ notation in ppm and are referenced to tetramethylsilane (TMS) using the residual ^1H signal of the deuterated solvent, $CDCl_3$, CD_3OD, or DMSO-d_6, as an internal standard. IR Spectra of samples were collected on a Perkin-Elmer 2000 FTIR spectrometer.

III.4.c Synthesis of Squaraine pH Dye

The squaraine dye was synthesized by a modified literature procedure and is described below.[12]

III.4.c.1 *N*-[2-(1,1-dimethylethoxy)-2-oxoethyl]-*N*-[3-(phenylmethoxy) phenyl]glycine, 1,1-dimethylethyl ester (1)

In a 50 mL aluminum foil covered round bottom flask, 3-benzyloxyaniline (1.99 g, 0.0100 mol) was allowed to react for 12 hours with excess butylbromoacetate (5.91 mL, 0.0400 mol) in the presence of a proton sponge (1,8-bis(dimethylamino) naphthalene) in 35 mL refluxing dry acetonitrile under nitrogen. Precipitated salts were removed through filtration, and solvent was removed through rotary evaporation to isolate a crude yellow oil. Purification by flash chromatography (CH_2Cl_2) gave the bis-alkylated benxyloxyaniline product, **1**, in 63% yield. ^{1}H NMR (300MHz, $CDCl_3$, δ): 7.44-7.31 (m, 5H, -$OCH_2C_6H_5$), 7.10 (dd, *J* = 8.1 Hz, 1H, meta Ar *H*), 6.39 (dd, *J* = 8.4 and 2.4, 1H, Ar *H*), 6.25-6.19 (m, 2H, Ar *H*), 5.02 (s, 2H, -$OCH_2C_6H_5$), 3.99 (s, 4H, -NCH_2COOtBu), 1.46 (s, 18H, -$C(CH_3)_3$).

III.4.c.2 *N*-[2-(1,1-dimethylethoxy)-2-oxoethyl]-*N*-(3-hydroxyphenyl) glycine, 1,1-dimethylethyl ester (2)

Compound **1** (3.32 g, 0.00630 mol) dissolved in 25 mL ethanol was placed in a 50 mL round bottom flask to which 10% mol Pd/ C (0.075 g) was added. The flask was subsequently equipped with a balloon filled with H_2 gas and flushed with H_2 twice. The balloon was refilled with H_2, sealed, and the solution was stirred vigorously for 6 hours. Ethanol was removed through rotary evaporation. Purification by flash chromatography (1:1 pentane: ether) gave the deprotected aniline, compound **2** in 40% yield as a pale yellow oil. ^{1}H NMR (300MHz, $CDCl_3$, δ): 7.02 (dd, *J* = 8.1 Hz, 1H, meta Ar *H*), 6.21 (dd, *J* = 8.1 and 2.4, 1H, Ar *H*), 6.12 (dd, *J* = 7.8 and 2.4, 1H, Ar *H*), 6.06 (t, *J* = 2.4, 1H, Ar *H*), 5.46 (s, 1H, -O*H*), 3.97 (s, 4H, -NCH_2COOtBu), 1.46 (s, 18H, -$C(CH_3)_3$).

III.4.c.3 1,3-bis[4-[bis(tert-butoxymethyl)amino]-2-hydroxyphenyl]-2,4-dihydroxy-cyclobutenediylium (3)

Compound **2** (0.885 g, 0.00240 mol) was allowed to react with 3,4-dihydroxy-3-cyclobutene-1,2-dione (squaric acid, 0.142 g, 0.00120 mol) in a refluxing 1:1 solvent mixture of toluene and *n*-butanol (50 mL) to form a dark green solution with red fluorescence. Water, formed during the reaction, was removed through azeotropic

distillation. Upon cooling, the product, compound **3**, precipitated as green needles in 84% yield. ^{1}H NMR (300MHz, $CDCl_3$, δ): 6.27 (d, *J* = 2.1 Hz, 2H, Ar *H*), 6.24 (d, *J* = 2.1, 2H, Ar *H*), 6.08 (d, *J* = 2.7, 2H, Ar *H*), 4.11 (s, 8H, -C*H*$_2$COOtBu), 1.49 (s, 36H, -C(C*H*$_3$)$_3$).

III.4.c.4 1,3-bis[4-[bis(carboxymethyl)amino]-2-hydroxyphenyl]-2,4-dihydroxycyclobutenediylium (4)

To an ethanolic solution of compound **3** (0.509 g, 0.000647 mol) was added trifluoroacetic acid, and the mixture was stirred for five hours. All solvent was removed *in vacuo* to yield a shiny green powder, compound **4**, in quantitative yield. ^{1}H NMR (500MHz, DMSO-d_6, δ): 13.03 (br s, 4H, -COO*H*), 11.86 (br s, 2H, -O*H*), 7.74 (d, *J* = 8.5, 2H, Ar *H*), 6.52 (d, *J* = 9.5, 2H, Ar *H*), 6.07 (s, 2H, Ar *H*), 4.35 (s, 8H, C*H*$_2$COOH). UV-vis (pH 6 phosphate buffer) λ_{max}, nm (ε): 635 (280,000). UV-vis (pH 10 borate buffer) λ_{max}, nm (ε): 616 (115,000).

III.4.d Synthesis of CdSe/CdZnS Nanocrystals

CdSe NCs overcoated with alloyed CdZnS were prepared using a modified literature method.[21,22] A vial containing cadmium 2,4-pentanedionate (0.317 g, 0.00100 mol), dodecanal (0.50 mL, 0.0023 mol) in trioctylphosphine (6.0 mL, 0.014 mol) was degassed at 180 °C for an hour, then cooled to yield a homogenous bright yellow solution. 1.5 M trioctylphosphine selenide (TOPSe, 4 mL, prepared from dissolving 5.92 g Se shot into 50 mL TOP) was subsequently added to the vial being cooled to room temperature. The contents of the vial were subsequently injected rapidly at 360 °C into a three-necked flask (equipped with an air condenser, temperature controller, and a stir bar) containing degassed solvent of trioctylphosphine oxide (6.25 g, 0.0162 mol), hexadecylamine (5.75 g, 0.0238 mol), and trioctylphosphine (3.4 mL, 0.0076 mol). The growing CdSe NCs were then maintained at 240 °C until the desired emission wavelength of 600 nm was reached.

The bare CdSe NCs were precipitated out of the gross solution with butanol and methanol twice and brought up in 4.0 mL hexanes. The NCs were overcoated by injecting the hexane solution of core CdSe into a degassed solvent of distilled

trioctylphosphine oxide (10.0 g, 0.0259 mol) and n-hexylphosphonic acid (0.40 g, 0.0024 mol). The hexane was removed *in vacuo* at 80 °C, and decylamine (0.50 mL, 0.0020 mol) was added. After stirring for one hour, the solution temperature was raised to 160 °C. Two separate precursor solutions of (1) bis(trimethylsilyl)sulfide in 5.0 mL trioctylphosphine and (2) a 80:20 molar ratio of diethylzinc and dimethylcadmium in 5.0 mL trioctylphosphine were slowly dripped in over the course of two hours using a syringe pump. Exact amounts were chosen to yield a ~5 monolayer coating of ZnS on the bare CdSe NCs. The final emission wavelength was 613 nm with a FWHM of 30 nm. The quantum yield of NCs prepared in this manner was generally on the order of 70% against a rhodamine 640 standard which is taken to be $\Phi = 1.00$ in ethanol.[20]

III.4.e Synthesis of *N*-octylamine and 5-amino-1-pentanol-modified Poly(acrylic acid)

A functionalized polymer was synthesized by coupling a fraction (40%) of the carboxylic acid groups of a 1800 MW poly(acrylic acid) (2.0 g, 0.0011 mol) with octylamine (1.44 g, 0.0110 mol) using 1-ethyl-3-(3-dimethylaminopropyl)carbodiimide (EDC) (2.12 g, 0.0110 mol) in DMF according to a previous report.[13] An additional 40% of the acid groups were coupled with vacuum-distilled 5-amino-1-pentanol (1.13 g, 0.0110 mol) using EDC (2.12 g, 0.0110 mol) in DMF, while the remaining 20% was left as free carboxylic acid. The functionalized polymer was purified by size-exclusion chromatography using Sephadex LH-20 with methanol as the mobile phase. ^{1}H NMR (500MHz, CD_3OD, δ): 3.66 (br s), 3.53 (br s) 3.11 (br s), 1.50 (br s), 1.42 (br s), 1.28 (s), 0.89 (s). IR (KBr, cm^{-1}): 3365 (OH, br), 2928-2857 (CH, aliphatic), 1718 (C=O), 16583(CO-NH-R), 1531 (CO-NH-R).

III.4.f Preparation of Polymer Micelle Encapsulated NCs

Water-soluble CdSe/CdZnS nanocrystals were prepared by precipitating 0.50 mL of the NC stock solution. The resulting dried CdSe/ CdZnS (5 mgs) was added to octylamine and 5-amino-1-pentanol modified poly(acrylic acid) (30 mgs) in a vial and dissolved in chloroform. The chloroform solution was sonicated and stirred vigorously for 1 hour, after which the solvent was removed *in vacuo.*

III.4.g Preparation of NC-squaraine Conjugates

A vial with squaraine pH dye **4** (2.0 mg, 0.0038 mmol) and EDC (4.0 mg, 0.021 mmol) was dissolved in 1 mL of DMF and stirred for 10 minutes. The polymer-coated nanocrystals were solubilized in 5 mL DMF, to which the squaraine pH dye solution was added and stirred overnight. Removal of DMF *in vacuo* and addition of H_2O and 0.1 mL 0.1 M tetrabutylammonium hydroxide in methanol yielded water-solubilized CdSe/CdZnS NC conjugated with the squaraine dye. The pH dye-nanocrystal conjugates were purified by dialysis using centrifugal filters equipped with 50,000 Da MWCO filters to remove any unreacted dye and other side-products. After multiple washings, the free dye was completely removed from the conjugates, as verified by the absence of the parent dye absorption features in the UV-visible absorption spectrum of the filtrate.

III.5 References

1. Dahan, M.; Levi, S.; Luccardini, C.; Rostaing, P.; Riveau, B.; Triller, A. *Science* **2003**, *302*, 442-445.

2. Dubertret, B.; Skourides, P.; Norris, D. J.; Noireaux, V.; Brivanlou, A. H.; Libchaber, A. *Science* **2002**, *298*, 1759-1762.

3. Jaiswal, J. K.; Mattoussi, H.; Mauro, J. M.; Simon, S. M. *Nat. Biotechnol.* **2003**, *21*, 47-51.

4. Michalet, X.; Pinaud, F. F.; Bentolila, L. A.; Tsay, J. M.; Doose, S.; Li, J. J.; Sundaresan, G.; Wu, A. M.; Gambhir, S. S.; Weiss, S. *Science* **2005**, *307*, 538-544.

5. Pinaud, F.; Michalet, X.; Bentolila, L. A.; Tsay, J. M.; Doose, S.; Li, J. J.; Iyer, G.; Weiss, S. *Biomaterials* **2006**, *27*, 1679-1687.

6. Somers, R. C.; Bawendi, M. G.; Nocera, D. G. *Chem. Soc. Rev.* **2007**, *36*, 579-591.

7. Goldman, E. R.; Medintz, I. L.; Whitley, J. L.; Hayhurst, A.; Clapp, A. R.; Uyeda, H. T.; Deschamps, J. R.; Lassman, M. E.; Mattoussi, H. *J. Am. Chem. Soc.* **2005**, *127*, 6744-6751.

8. Medintz, I. L.; Clapp, A. R.; Melinger, J. S.; Deschamps, J. R.; Mattoussi, H. *Adv. Mater.* **2005**, *17*, 2450-2455.

9. Clapp, A. R.; Medintz, I. L.; Mauro, J. M.; Fisher, B. R.; Bawendi, M. G.; Mattoussi, H. *J. Am. Chem. Soc.* **2004**, *126*, 301-310.

10. Medintz, I. L.; Clapp, A. R.; Mattoussi, H.; Goldman, E. R.; Fisher, B.; Mauro, J. M. *Nat. Mater.* **2003**, *2*, 630-638.

11. Medintz, I. L.; Uyeda, H. T.; Goldman, E. R.; Mattoussi, H. *Nat. Mater.* **2005**, *4*, 435-446.

12. Isgor, Y. G.; Akkaya, E. U. *Tet. Lett.* **1997**, *38*, 7417-7420.

13. Wu, X.; Liu, H.; Liu, J.; Haley Kari, N.; Treadway Joseph, A.; Larson, J. P.; Ge, N.; Peale, F.; Bruchez Marcel, P. *Nat. Biotechnol.* **2003**, *21*, 41-46.

14. Uyeda, H. T.; Medintz, I. L.; Jaiswal, J. K.; Simon, S. M.; Mattoussi, H. *J. Am. Chem. Soc.* **2005**, *127*, 3870-3878.

15. Leatherdale, C. A.; Woo, W. K.; Mikulec, F. V.; Bawendi, M. G. *J. Phys. Chem. B* **2002**, *106*, 7619-7622.

16. Clapp, A. R.; Medintz, I. L.; Uyeda, H. T.; Fisher, B. R.; Goldman, E. R.; Bawendi, M. G.; Mattoussi, H. *J. Am. Chem. Soc.* **2005**, *127*, 18212-18221.

17. Liu, J.; Diwu, Z.; Leung, W.-Y. *Bioorg. Med. Chem. Lett.* **2001**, *11*, 2903-2905.

18. Rink, T. J.; Tsien, R. Y.; Pozzan, T. *J. Cell Biol.* **1982**, *95*, 189-196.

19. Grynkiewicz, G.; Poenie, M.; Tsien, R. Y. *J. Biol. Chem.* **1985**, *260*, 3440-3450.

20. Karstens, T.; Kobs, K. *J. Phys. Chem.* **1980**, *84*, 1871-1872.

21. Dabbousi, B. O.; Rodriguez-Viejo, J.; Mikulec, F. V.; Heine, J. R.; Mattoussi, H.; Ober, R.; Jensen, K. F.; Bawendi, M. G. *J. Phys. Chem. B* **1997**, *101*, 9463-9475.

22. Fisher, B. R.; Eisler, H.-J.; Stott, N. E.; Bawendi, M. G. *J. Phys. Chem. B* **2004**, *108*, 143-148.

Chapter IV

Explorations of NC Surface Chemistry Towards Biological Sensing

Parts of this Chapter will be published:
Somers, R. C.; Snee, P. T.; Bawendi, M. G.; and Nocera, D. G.
Manuscript in Preparation

IV.1 Introduction

Chapter III introduced the first *reversible* and *ratiometric* nanocrystal (NC) based FRET sensor, with the squaraine dye acting as the pH sensitive energy acceptor. By engineering the construct so that the emission of the NC overlaps with the pH-dependent absorption of the squaraine dye, FRET from the NC donor to the dye acceptor was modulated by pH. An isosbestic point was observed in the emission spectrum from the NC construct which permits the sensor to be self-calibrating when taking the ratio of either dye or NC emission intensity to the emission intensity at the isosbestic point. Although this work represents an important proof-of-concept for the general method in developing ratiometric NC sensors, the biological utility of the construct is limited due to the high pK_a of the sensor (pK_a ~ 8.8) and the potential lability of the ester bond linking the dye to the NC. Ester bonds are often susceptible to cleavage by extracellular esterases,[1] and any type of NC-receptor conjugate probing the biological milieu must be robust to such degradations. In addition, the squaraine dye in aqueous solution was revealed to have limited stability when exposed to light at room temperature.[2]

An ideal pH sensor for biological applications would include the following design features:

(1) An acceptor dye with physiological pH sensitivity (pK_a ~ 7.3)
(2) A NC-dye conjugation strategy that features more robust bonds, e.g. amides
(3) Stability against photobleaching of the construct
(4) An acceptor dye that exhibit pH-sensitive absorbance and/or quantum yield which can be exploited to construct a ratiometric emission spectrum when paired with a NC donor that emits between 520 nm and 660 nm

Whereas most requirements are determined by the properties of the acceptor dye itself, an NC scaffold that would readily lead to a formation of an amide bond depends on the water solubilization method of the NCs. Two general methods were explored in this Chapter to impart water solubility to the NCs (Scheme IV.1). First, as shown in Chapters II and III, an amphiphilic polymer may be used.[3,4] Second, a direct 'cap exchange', or the displacement of the native trioctylphosphine oxide ligands with new ligands, provides an alternative strategy to modify the surface chemistry and solubility of NCs.[5-7] The two different methods have varying advantages and disadvantages. Polymer encapsulated NCs tend to be bright, robust, and stable in water because the native ligands are conserved, which minimizes any additional oxidative damage or introduction of surface defects. However, the NCs tend to be quite large (20-

Scheme IV.1 Two general methods of imparting water solubility to a NC have distinct advantages and disadvantages. An example of micellular encapsulation shown in this scheme utilized *N*-octylamine-modified poly(acrylic acid), and dihydrolipoic acid is the ligand used to displace TOPO in the second example.

Characteristics of Micellular Encapsulation:

High Quantum Yield
Stable
Large Diameter
Characterization of NC Surface Challenging

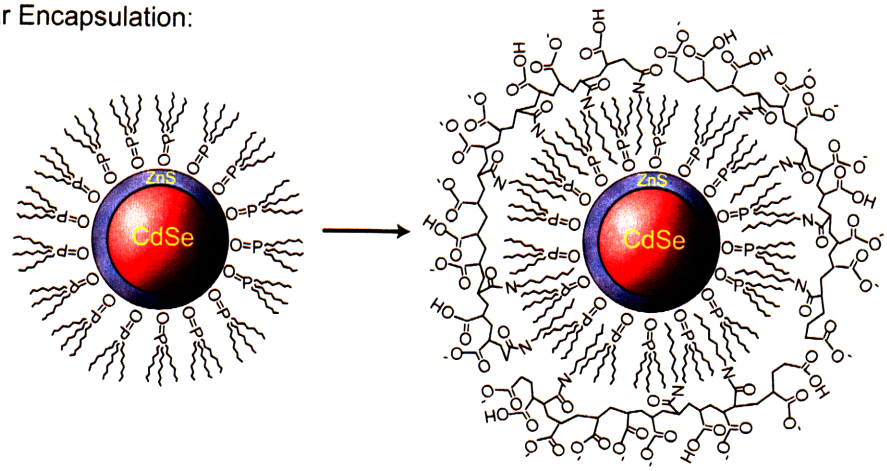

Characteristics of Direct Cap Exchange:

Small Diameter
Characterization of NC Surface Facile
Lower Quantum Yield
Limited Stability

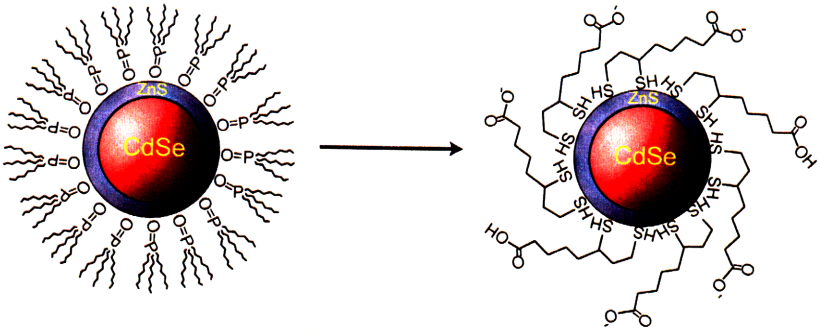

30 nm diameter) and the exact nature of the polymer interaction with the NCs is difficult to characterize. On the other hand, water-soluble NCs prepared through a cap exchange have the potential to be more compact (less than 10 nm diameter), since the original ligand layer is not retained. They may be readily characterized through conventional spectroscopic methods such as NMR because they are small molecule surfactants[8]; however, they are less stable due to ligand dissociation and exhibit lower quantum yields, possibly as a result of additional chemistry taking place directly on the surface of the NCs.

Another important criterion for sensing in a biological environment is the use of excitation within the 'optical window' between 700 nm – 1100 nm so that background absorption is minimized.[9,10] Most probes and dyes generally are excited by visible blue to UV-light. In addition, excitation with a high energy photon leads to tissue damage and autofluorescence in biological specimens. Multiphoton microscopy allows for the excitation of probes using two (or more) simultaneous photons of lower energy light, allowing for minimal scattering of excitation, diminished photodamage, and excitation of probes confined to a small excitation volume.[9-11] In addition, this technique is popular in biological imaging because it is non-invasive and significant depth penetration may be achieved, thus providing a high three-dimensional resolution due to the small excitation volume.[11,12] NCs possess a distinct advantage for multiphoton excitation schemes since they have very high two-photon absorption cross-sections, two-to-three orders of magnitude higher than those of conventional organic dyes.[13]

This Chapter explores and describes the differences in the properties of various NC scaffolds so as to achieve the best candidates for biological sensing applications. Three main coupling strategies are discussed and compared. The investigation of our sensors using two-photon microscopy is also introduced as we apply the NC-dye sensors towards biological applications.

IV.2 Results and Discussion

IV.2.a Choice of the pH Sensitive Acceptor

Fluorescent pH indicators used extensively in biological applications include

CypHer 5E[14,15], fluorescein[16], 2',7'-bis-(2-carboxyethyl)-5-(and-6)-carboxyfluorescein (BCECF)[17], 5-(and-6)-carboxynaphthofluorescein[18], and SNARF-5F.[19] With the exception of cyanine based dyes, most common pH indicators are fluorescein derivatives, the pH response of which can be modified by following general trends. Starting with fluorescein, longer emission wavelengths are accessed by appending phenyl groups to the xanthene backbone. pK_a is lowered by installing electron-withdrawing functionalities on the xanthene backbone, and in the case of the SNARF sensors, a dual-emissive response is engendered by the rhodamine-like half. Fluorescein and BCECF absorbed at wavelengths that are too high in energy to match CdSe emission. Cyanine based dyes such as CypHer 5E tend to be susceptible to photobleaching.[20,21] 5-(and-6)-Carboxynaphthofluorescein has a pK_a of 7.6, which is too high for our targeted applications in a tumor environment. Conversely, a very similar dye, 1,2,7,8-dibenzofluorescein exhibits an ideal pK_a of 6.00[22] for such applications.

Accordingly, a sample of 1,2,7,8-dibenzofluorescein was prepared via a condensation of phthaloyl dichloride with 1,3-dihydroxynaphthalene under heat. The hydrophobic nature of the dye, however, caused NC-dye sensing constructs to precipitate at lower pH. Also the dye exhibited poor photostability when conjugated to the NC.[2] Consequently, subsequent work was undertaken using SNARF-5F 5-(and-6) carboxylic acid as the dye. SNARF-5F was chosen owing to its broad pH-sensitive absorbance (from 450 nm – 650 nm, λ_{max} of 579 nm, see Figure IV.1), its pH dependent absorbance and emission, a pK_a of 7.2 (which is slightly lower than the physiological pK_a of 7.3), and the presence of carboxylic acid functional groups that can be useful for amide coupling.

IV.2.b Strategies of Amide Bond Formation between NC and SNARF

The condensation of a carboxylic acid and an amine to form an amide bond is straightforward and well-documented.[23] An amide linkage can in principle be established between a carboxylic acid-bearing NC and an amine-presenting dye substituent, or vice versa. The polymer-coated NCs described previously in Chapters II and III naturally incorporate carboxylic acids and therefore, our initial strategy focused on modifying SNARF-5F with an amine for its subsequent coupling to the NC (Section

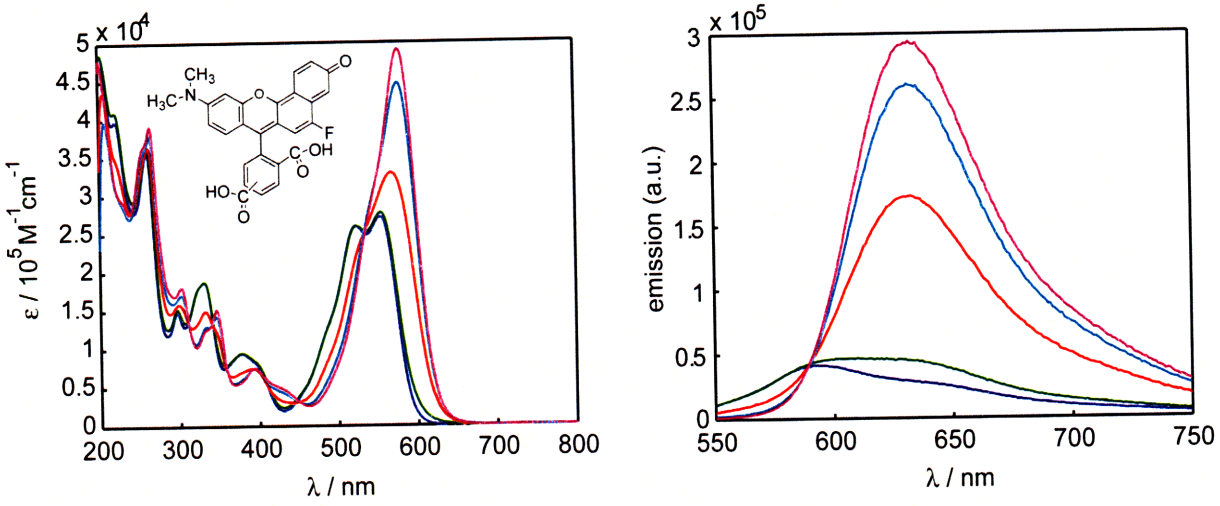

Figure IV.1 pH-dependent absorption and emission of SNARF-5F (blue line — pH 5, green line — pH 6, red line — pH 7, teal line — pH 8, purple line — pH 9). The structure of the SNARF-5F is shown in the upper left.

IV.2.d). As SNARF-5F already contains carboxylic acid groups, methods to install amines on the NC were also explored. The acid terminated micellular encapsulated NCs were further modified with bis-amines to enable subsequent coupling with SNARF-5F (Section IV.2.f). Finally, a poly(amido amine) dendrimer ligand was synthesized for a cap exchange to incorporate amines on the surface of quantum dots (Section IV.2.h).

IV.2.c NC-NHS Ester as a Synthon

The tactic to modify SNARF-5F with an amine for coupling NCs was a natural choice since *N*-octylamine modified poly(acrylic acid) NCs have a surface rife with carboxylic acids. 1-Ethyl-3-(3-dimethylaminopropyl)-carbodiimide (EDC) is a water soluble peptide coupling agent that is used to effect the formation of amide bonds by activating the carboxyl group to form an unstable *O*-acylisourea intermediate. Addition of *N*-hydroxysuccinimide (NHS) to an EDC-activated acid forms a NHS ester that is selectively reactive towards amines.[24] When an overwhelming excess of EDC and NHS were added to the micelle coated NCs in distilled water, the NCs immediately precipitated, leaving a clear solution behind. The determination of the NC-NHS ester was based on its solubility properties, although the FTIR spectrum confirmed the presence of multiple C=O stretches (Section IV.4.h). The polymer coating imparts solubility because it is ionized at neutral pH. Conversion to the NHS ester yields a

neutrally charged and less hydrophilic NC, which is problematic due to its propensity to precipitate out of solution. Replacing the NHS with a sulfonated derivative, *N*-hydroxysulfosuccinimide (S-NHS) mitigates precipitation of the NCs, since the ester maintains its ionized form. Nevertheless, over the course of several hours, precipitation of the NCs does occur.

After decanting the supernatant and isolating the NC-NHS as a precipitate, NC-NHS was shown to completely re-dissolve in DMF, chloroform, or neat liquid amines. The formation of the NC-NHS ester is an example of how an NC can be prepared in a similar fashion to a molecular compound. The NC-NHS ester may be prepared and stored for chemical transformations at a later time.

IV.2.d NC-SNARF Construct with Micelle Encapsulated NCs and Amine-terminated SNARF-5F

The carboxylic acid of SNARF-5F was modified with ethylenediamine by using (benzotriazol-1-yloxy)tris(dimethylamino)phosphonium hexafluorophosphate (BOP) and 1-hydroxybenzotriazole (HOBt) as ester intermediate stabilizers as shown in Scheme IV.2. The reaction of amine-modified SNARF-5F with 580 nm emitting NCs was attempted in water using sulfo-NHS. However, the reaction proceeds with low coupling efficiency. Therefore, the SNARF-5F was coupled to the NC-NHS ester (Scheme IV.3), which was prepared as discussed in Section IV.2.c. The NC-NHS ester was dissolved in DMF, to which the aminated SNARF was added. A small catalytic amount of a tertiary amine, diisopropylethylamine (DIEA), was added in order to ensure that the amine was deprotonated and nucleophilic. After stirring overnight, the DMF was removed *in vacuo* and 0.2 M NaOH was added to guarantee the complete hydrolysis of NHS esters on the

Scheme IV.2 Modification of SNARF-5F with ethylenediamine

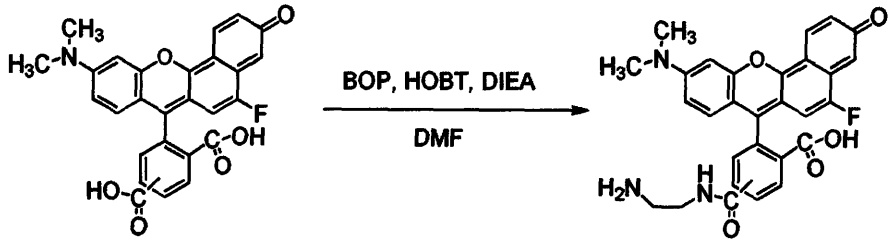

Scheme IV.3 Conjugation of amine-modified SNARF-5F to NC-NHS ester

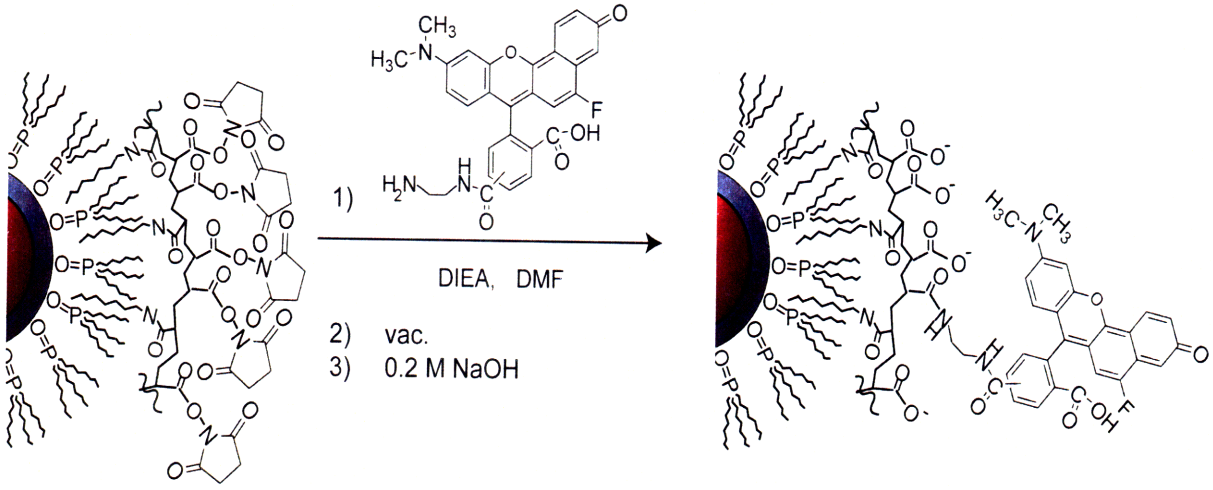

NC surface. As the esters were hydrolyzed, the NC-SNARF construct slowly dissolved in aqueous solution, which was subsequently neutralized and purified through dialysis with deionized water.

The photophysical properties of the NC-SNARF construct with an ethylenediamine linker is shown in Figure IV.2 and Figure IV.3. When the spectra from Figure IV.2 is deconstructed into the dye and NC components and their concentrations estimated, the dye:NC ratio was found to be approximately 15. Figure IV.3 shows that the NC emission decreases and the SNARF emission increases as the pH increases, which is indicative of energy transfer. The NC donor emission is increasingly quenched as the spectral overlap increases with increased pH. The construct remains responsive to pH; however, the pK_a appears to shift as evidenced by the maximal change in the emission intensity between pH 8-10, which does not provide sensitivity in the physiological range. As shown in Figure IV.1, 580 nm excitation of the NC-dye construct is predominately captured by the basic form of the SNARF-5F. The maximal change in pH for the basic form of the SNARF absorbance occurs between pH 8-10. Therefore, it is possible that the pK_a of the SNARF emission is higher because energy transfer from the NC putatively occurs to the basic form of SNARF.

In order to probe whether the NC emission wavelength affected the pK_a of the dye sensitivity profoundly, 550 nm emitting ZnSe/ CdSe/ ZnS NCs were coupled to the

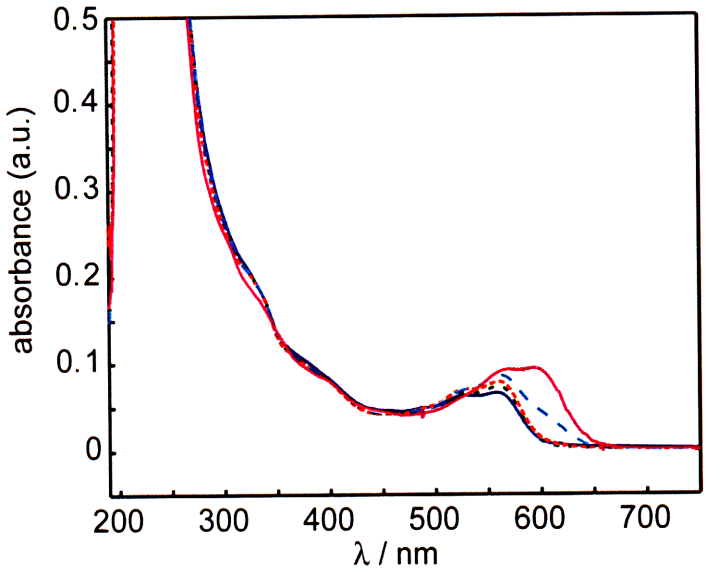

Figure IV.2 UV-vis absorbance spectra of ethylenediamine linked 580 nm emitting NC-SNARF construct at pH 6 (blue solid line —), pH 7 (green dashed line – –), pH 8 (red dashed line --), pH 9 (teal dashed line — —), and pH 10 (purple solid line —).

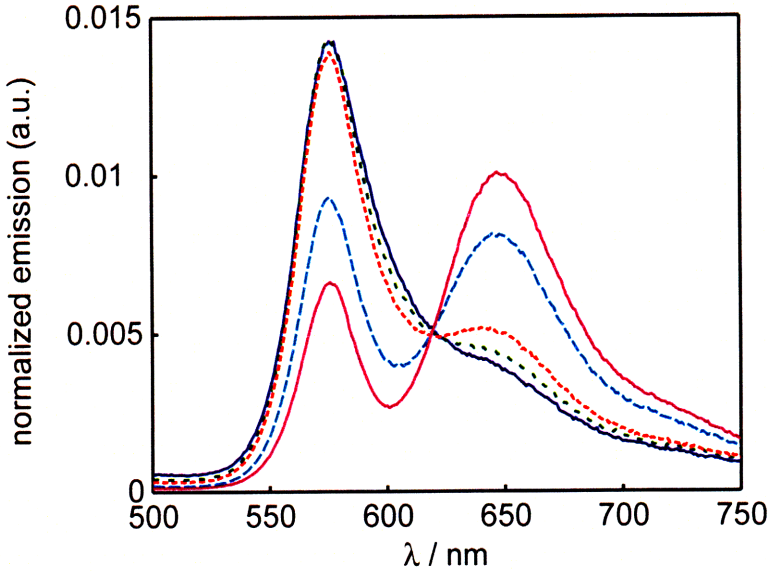

Figure IV.3 Normalized emission spectra (λ_{ex} = 365 nm) of ethylenediamine linked 580 nm emitting NC-SNARF construct at pH 6 (blue solid line —), pH 7 (green dashed line – –), pH 8 (red dashed line --), pH 9 (teal dashed line — —), and pH 10 (purple solid line —).

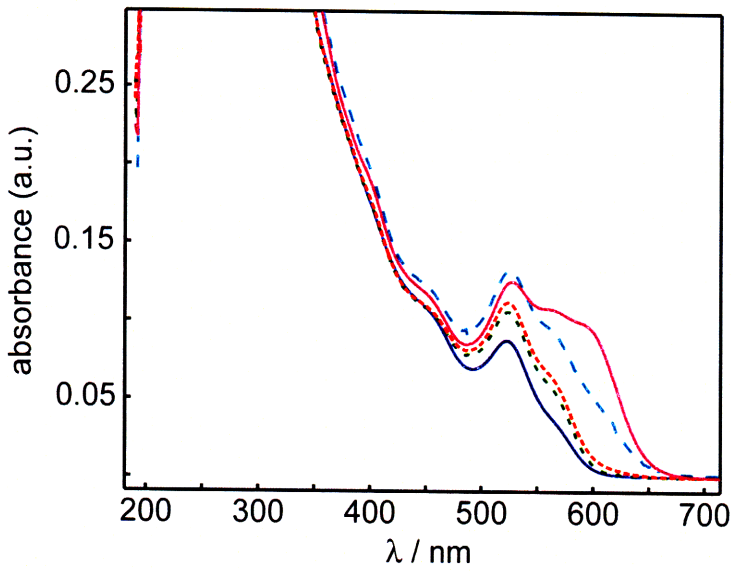

Figure IV.4 UV-vis absorbance spectra of ethylenediamine linked 550 nm emitting NC-SNARF construct at pH 6 (blue solid line —), pH 7 (green dashed line – –), pH 8 (red dashed line --), pH 9 (teal dashed line — —), and pH 10 (purple solid line —).

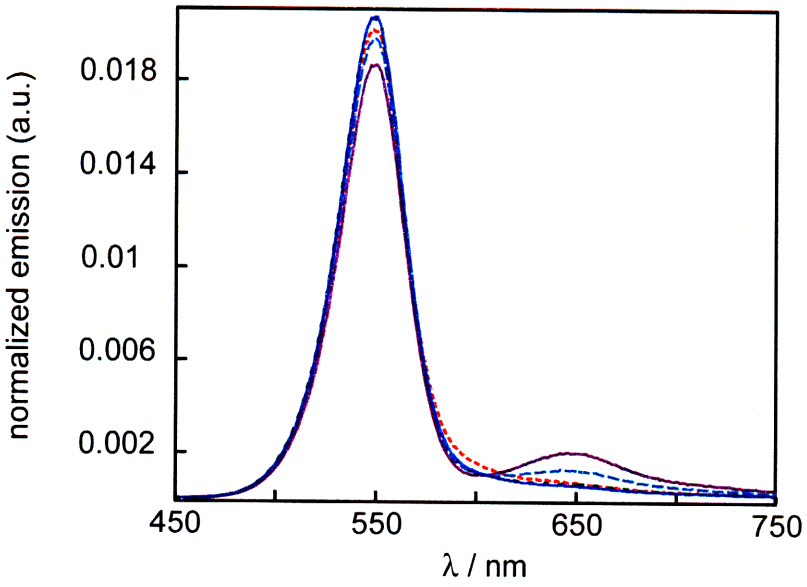

Figure IV.5 Normalized emission spectra (λ_{ex} = 365 nm) of ethylenediamine linked 550 nm emitting NC-SNARF construct at pH 6 (blue solid line —), pH 7 (green dashed line – –), pH 8 (red dashed line --), pH 9 (teal dashed line — —), and pH 10 (purple solid line —).

aminated SNARF-5F. The photophysical properties are shown in Figure IV.4 and Figure IV.5. Although a higher energy emitting NC was used, the apparent pK_a of the sensor did not change from the construct shown in Figure IV.2 and Figure IV.3.

IV.2.e pH Dependence Studies on Modified SNARF-5F

Two main concerns arise from the apparent higher pK_a shift in the sensor response. First, the emission spectrum is different when the acid or the base form is excited. Second, there exists a possibility that, upon conjugating SNARF-5F, changes in the pK_a will occur that determine the relative population of acid and base forms as a function of pH. Based on the studies from Section IV.2.d, the emission spectra seen when acid or base form of SNARF-5F is excited are similar to each other. The pH dependence on aminated SNARF was investigated to see whether the electronic structure of the dye itself was modified when an amide bond was introduced to the molecule. Specifically, the emission of ethylenediamine-modified SNARF and the *N*-octylamine modified poly(acrylic acid)-coupled SNARF (prepared through BOP and HOBt coupling) were compared to that of unmodified SNARF-5F (Figure IV.6). As shown, the SNARF-5F emission is not substantially perturbed when ethylenediamine is coupled to the carboxylic acid group; a slight increase in the emission of the basic form is observed at pH 6. In contrast, conjugation of the dye to the *N*-octylamine modified poly(acrylic acid) through an ethylenediamine linker shows a difference at pH 6. The

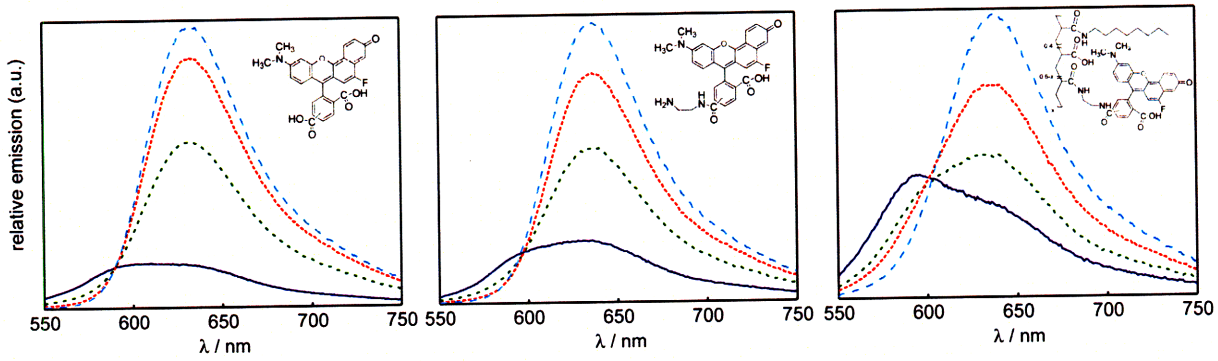

Figure IV.6 Comparison of the pH dependent SNARF-5F emission to modified SNARF-5F emissions: pH 6 (blue solid line —), pH 7 (green dashed line – –), pH 8 (red dashed line --), and pH 9 (teal dashed line — —). Emissions are corrected by absorbance at the excitation wavelength (λ_{ex} = 543 nm).

emission intensity at pH 6 is enhanced relative to those at other pH values, and the acid form of the dye at pH 6 predominates. One possible explanation for the change in spectral shape can be the environment that the amphiphilic polymer provides; the proximity of the ionized carboxylate groups may alter the pK_a of the dye due to Coulombic interactions, enhancing its acidic form as shown in Figure IV.6. In addition, the amphiphilic polymer may provide a more hydrophobic environment to the dye as well, which can in turn modulate the electronic properties of the dye. However, the contrast shown in the emission of the SNARF-5F tethered to the polymer is not significant enough to explain the change in the apparent pK_a of the NC-sensor. The structure and polarity of the free polymer in the solution may be different than those on the NC. The SNARF-5F's proximity to the NC may change the emissive properties of the dye owing to the different dielectric environment that the NC bestow upon the dye or the different polarity of the environment, both of which could alter the emission spectra.

IV.2.f Micellular NC Scaffold with Bis(amino)PEG Linker

A second strategy that we pursued for conjugating SNARF to NCs was to modify the polymer coated NCs with amine functionality afforded by a bis(amino) PEG linker. The amine surface permitted the use of unmodified SNARF-5F conjugation. Moreover, poly(ethylene glycol) derivatives are biocompatible.[6,25,26] In addition to being the source of amine functionality, the aminoPEG ligand increases the distance between the dye and NC. If, as suggested above, the proximity of the NC to dye causes the apparent shift in the pK_a of the SNARF-5F dye, then the use of a linker that is approximately 4.8 nm long and with a different environment from the modified poly(acrylic acid) should mitigate the changes seen in the dye response.

A NC-NHS synthon was prepared, dried and reacted with neat *O,O'*-bis-(2-aminopropyl)polypropylene glycol-block-polyethylene glycol-block polypropylene glycol 500, which effectively is a poly(ethylene glycol) that is terminated at both ends with a 2-aminopropyl group. The NC-NHS ester dissolved readily in the bis-aminoPEG liquid to give a clear solution. Subsequent addition of water resulted in the formation of a slight precipitate, which was removed with a 0.2 μm syringe filter. Dialysis of the aqueous solution of NCs removed the excess aminoPEG starting material to yield

Scheme IV.4 Coupling of SNARF-5F to an aminoPEGylated NC

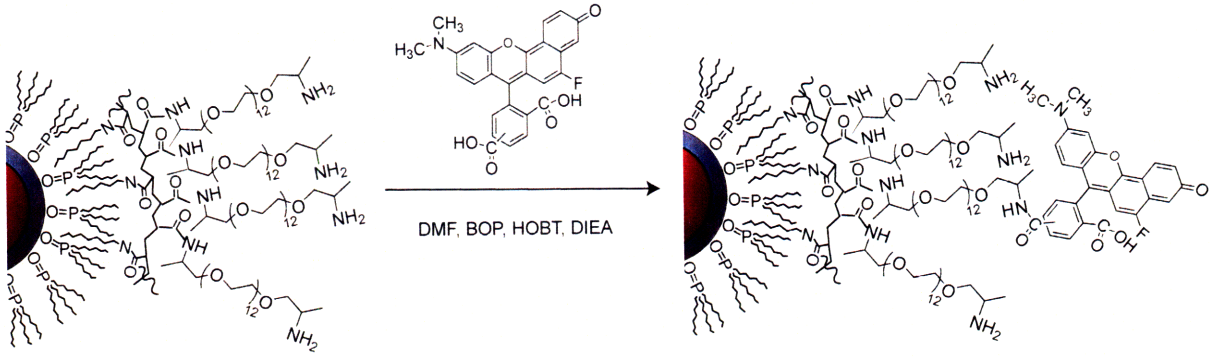

aminoPEGylated polymer encapsulated NCs. Removal of water and addition of DMF and DIEA completed the preparation of aminoPEGylated NCs for peptide coupling under organic conditions. SNARF-5F was activated with BOP and HOBT and added to the NC solution to make the NC-dye conjugate shown in Scheme IV..

Figure IV. and Figure IV.8 illustrates the photophysical properties of the aminoPEGylated NC-SNARF sensor. Figure IV. shows that a high dye to NC ratio was obtained by the large absorbance intensity of the SNARF dye; we estimate 16 dyes per NC by deconstructing the spectra in Figure IV. into the dye and NC components,

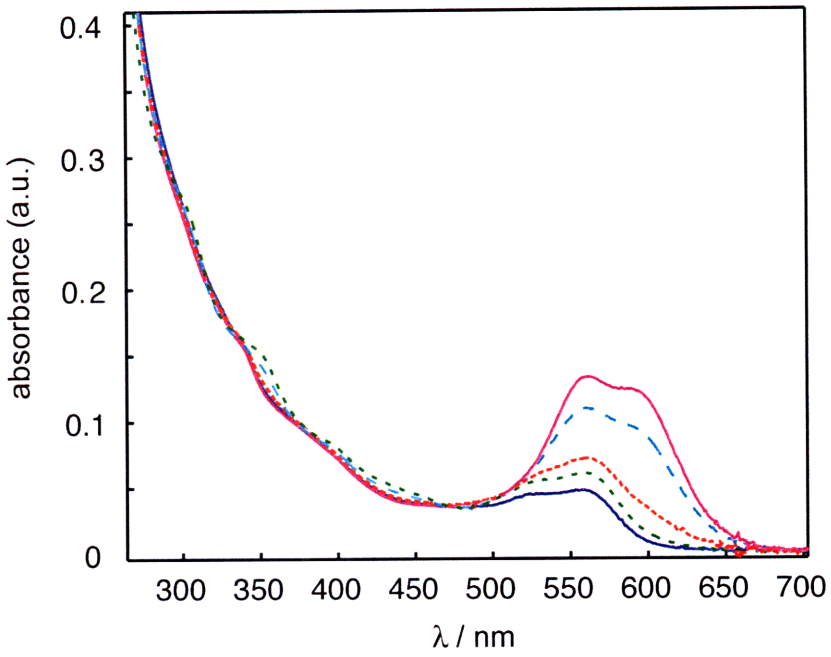

Figure IV.7 UV-vis absorbance spectra of bis(aminoPEG) linked 570 nm emitting NC-SNARF construct at pH 6 (blue solid line —), pH 7 (green dashed line – –), pH 8 (red dashed line --), pH 9 (teal dashed line — —), and pH 10 (purple solid line —).

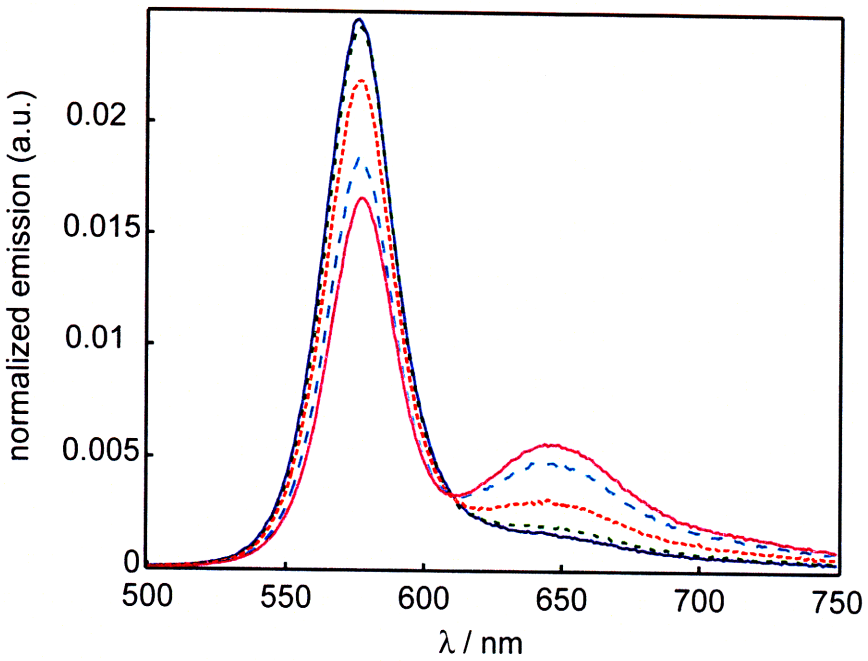

Figure IV.8 Steady-state emission spectra (λ_{ex}= 365 nm) of bis(aminoPEG) linked 570 nm emitting NC-SNARF construct at pH 6 (blue solid line —), pH 7 (green dashed line – –), pH 8 (red dashed line --), pH 9 (teal dashed line — —), and pH 10 (purple solid line —).

obtaining their relative concentrations. Figure IV.8 indicates that the greatest change in the NC-dye emission intensities occur between pH 8 and 10. Unfortunately, increasing the distance between the NC and dye did not circumvent the problems seen in the micellular NC sensing constructs that were discussed in Section IV.2.d of this Chapter.

IV.2.g The Switch from Micellular NC-SNARF to Cap-exchanged SNARF Sensors

Sections IV.2.d and IV.2.f described two methods by which SNARF-5F pH-sensitive acceptor was coupled to a micelle encapsulated NC. In most cases, the dye emission is not intense compared to the NC emission, decreasing sensitivity of the sensor. In addition, coupling through the use of an NC-NHS ester resulted in some precipitation of the NCs, presumably due to aggregate formation, which also decreased the overall yield for the synthesis. Donor emission wavelength and the NC-acceptor distance were varied to see whether the cause of the apparent pK_a could be determined; however, neither of these two factors could explain the shift in the apparent

pK_a of the sensor. Coupling of the SNARF-5F to the *N*-octylamine modified poly(acrylic acid) changes the pH response of the SNARF emission somewhat, but does not explain the significant change shown in the emission of the sensing construct. Two additional factors could be considered for the lack of pH sensitivity in the desired physiological pH range. First, the NC emission is bright relative to the SNARF emission, which may cause the acid form of the SNARF-5F emission to be overwhelmed. The use of NCs that emit to the blue of 550 nm may potentially be helpful in regaining the sensitivity of the SNARF-5F by allowing the acid form of the emission to be more easily detected. More importantly, sensitivity can be obtained if dye emission was more intense in the spectra of the conjugate. The distance between the NC and the SNARF is large when using micellular encapsulated NCs. Micelle encapsulated NCs are ~15 nm in diameter. Addition of bis(aminoPEG) will add approximately 4.8 nm to the radius (with 12 PEG units, at approximately 4 Å per unit, and completely elongated), as approximated by a model (Chem 3D Ultra software package). Efficiency of energy transfer depends strongly upon the donor-acceptor distance and the number of acceptor molecules per donor. The construct in Section IV.2.f exemplified a construct with a high (16:1) dye to NC ratio, with the dye emission nonetheless significantly weaker than the NC emission. Therefore, the donor-acceptor distance must be responsible for the lack of efficient energy transfer. The longer donor-acceptor distance imposed by the bis(aminoPEG) as compared to the micellular constructs, in addition to the slight precipitation problems encountered during amide bond formations between the dye and the NC, compelled us to consider cap-exchanged water-soluble NCs as a mean to covalently coupled conjugates.

IV.2.h Dendrimer-capped NC-SNARF Sensors

The use of poly(amido amine) (PAMAM) dendrimer ligands as caps for the NCs was explored for the construction of a bio-compatible sensor. The advantage of using PAMAM is two-fold: (1) The "starburst" structure provides a high degree of valency for coupling of multiple dye substituents per NC, and (2) the amines allowed for the formation of a robust amide bond. Dendrimer-capped NCs have been previously reported by Wisher *et al.* to water-solubilize NCs through a cap-exchange with a

thiolated PAMAM dendrimer. [27] These dendrimer-coated NCs were then shown to permeate through the cell membrane and act as good transfection agents for other proteins and molecules, when they were incubated together in the cells.[27] However, in Wisher's work, the dendrimers were modified with mercaptopropionic acid, which only coordinates to the NCs in a monodentate fashion. Other reports have shown that the stability of water-soluble NCs relying on a monodentate thiol ligand coordination is short-lived.[6,28]

In order to prepare dendrimer coated NCs with greater stability, our dendritic ligand was prepared as shown in Scheme IV.5. Instead of modifying PAMAM with mercaptopropionic acid, dihydrolipoic acid, a bidentate thiol, was chosen to enhance the stability of the NCs. The cap-exchange of the NCs was accomplished by a facile phase-exchange method, as shown in Scheme IV.6, where the distilled water was layered on top of a vigorously stirred chloroform/methanol (3:2 by volume) solution of NCs and excess dendrimer ligand (10-fold excess by mass). Over the course of few hours, the colorful NCs phase transfer to the top aqueous layer, leaving excess ligands in the organic phase. After water-solubilization, NCs possessing appreciable quantum yield (26%) were obtained, which was greater than NCs capped with other thiolated or DHLA-based molecules. The DHLA-PAMAM NCs were also found to be stable for months when stored at 4 °C.

The EDC-mediated coupling of the SNARF-5F to the surface of the NCs was

Scheme IV.5 Synthetic scheme of the DHLA-PAMAM adduct for ligand exchange of NCs.

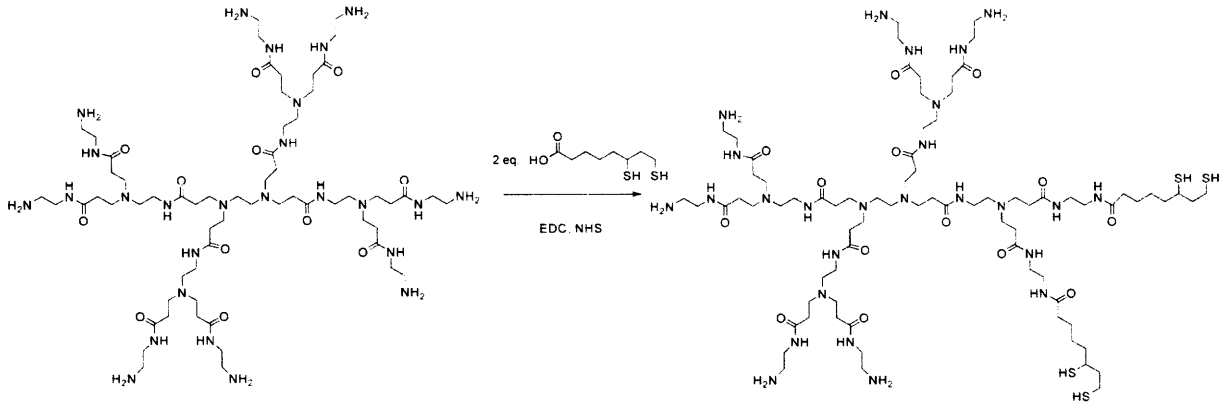

PAMAM G(1) PAMAM-DHLA

Scheme IV.6 Schematic description of ligand exchange of NCs. Note: The structure of the PAMAM ligand is abbreviated for clarity.

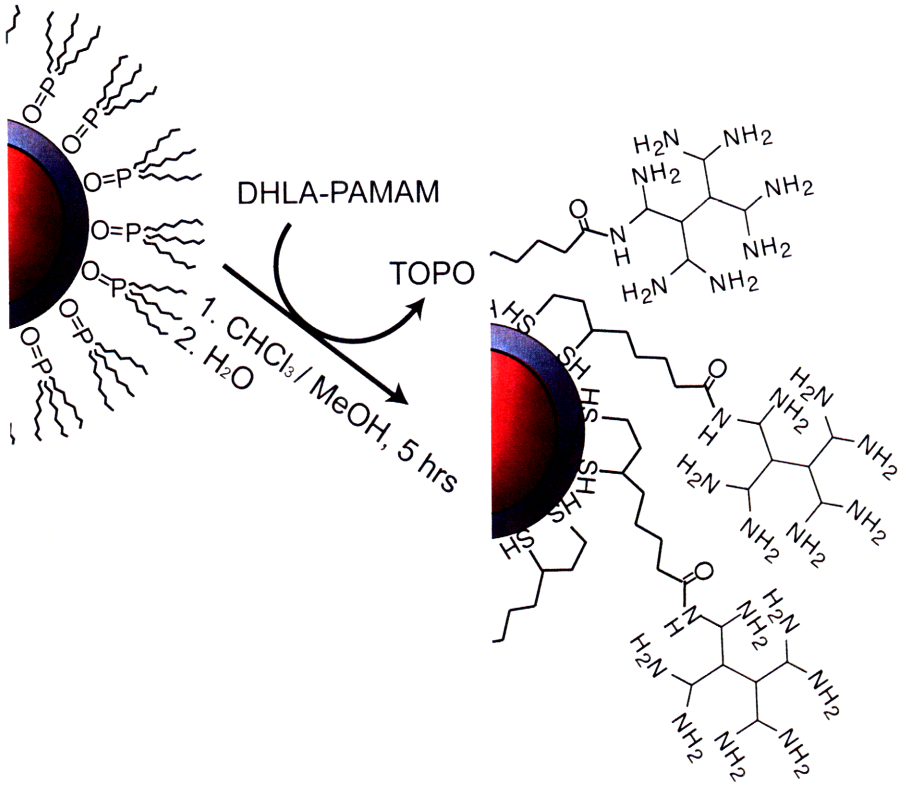

performed in distilled water. The use of the bicarbonate buffer system, conventional in peptide coupling chemistry, resulted in poor coupling yields and precipitation of the amine-terminated NCs. However, a high coupling efficiency was achieved in distilled water owing to the high valency of the amines on the NCs. The yield of the reaction was as high as 86%, which was measured by determining the amount of unreacted dye that was filtered by dialysis.

The hydrodynamic radius of the dendrimer capped NCs was determined by dynamic light scattering measurements and was observed to be 16 ± 1 nm. The large size, as well as the stability, of the construct is most likely explained by the cross coupling of the dendrimers, through dithiol ring formation, to give multiple PAMAM layers on the NC. The pK_a of a primary amine on a generation 1 PAMAM dendrimer is 9.00.[29] The dendrimer-NC scaffold that is comprised of branched amines may be prone to slight size changes based on the pH due to protonation of the scaffold, which adds another dimension to Förster analysis. Unlike in our previous work[4], the FRET efficiency

may reflect changes in the donor-acceptor distance (r) in addition to the changes in the spectral overlap. However, because the pK_a of the PAMAM amine is relatively high, the changes encountered in biological environments (pH 5 – 7.2) will be minimal.

The UV-vis spectrum at each pH value (Figure IV.9) is a composite sum of the continuous NC absorption in the higher energies and of the pH dependent SNARF-5F absorption between 470 – 620 nm. By separating the NC and the dye contributions to the overall conjugate spectrum, the large dye to NC ratio of 26 to 1 was estimated for this construct (Figure IV.10). Steady-state emission (Figure IV.11) exhibits spectra that are indicative of FRET that is pH dependent. When the construct was excited at λ_{ex}= 365 nm, where the SNARF-5F has little absorption, dye emission is clearly evident. In addition, the SNARF-5F becomes more absorptive as the pH is increased, thus augmenting the spectral overlap between the donor-acceptor pair. As such, the donor NC emission is decreased, which is also consistent with the occurrence of energy transfer.

The critical transfer distances at pH 6 and 9 were calculated using eq. I.8. The value of n =1.333 was used for index of refraction, the constant reflecting dipole orientation was taken to be κ^2 = 2/3, and the quantum yield of the donor was ϕ_D = 0.26.

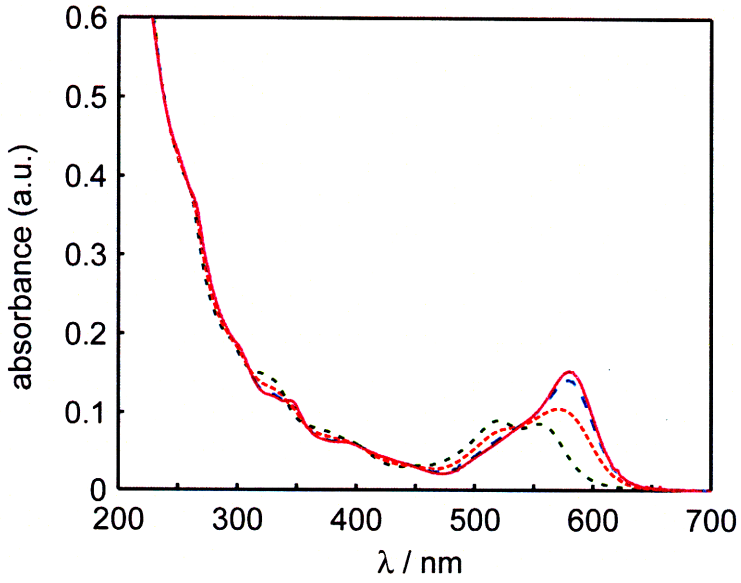

Figure IV.9 UV-vis absorbance spectra of dendrimer NC-SNARF construct at pH 6 (green dashed line – –), pH 7 (red dashed line --), pH 8 (blue dashed line — —), and pH 9 (purple solid line —).

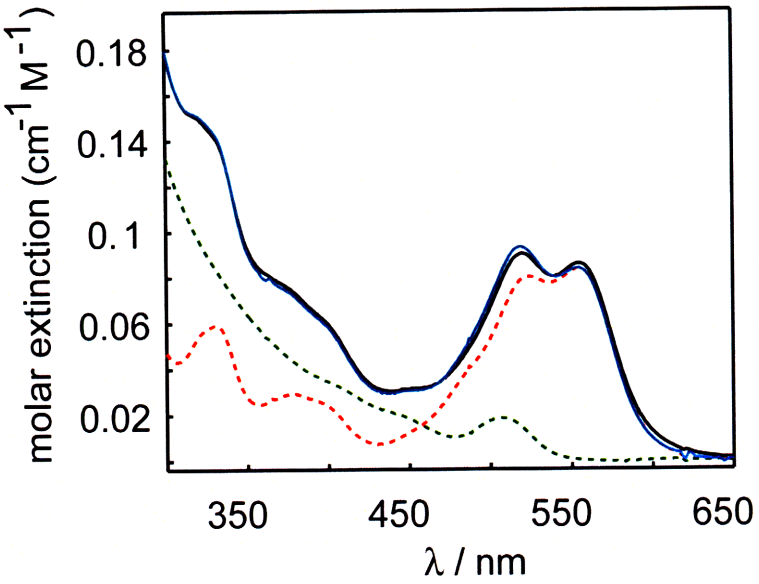

Figure IV.10 An example of a fit of a UV-vis spectrum of the NC-SNARF conjugate at pH 6 (black solid line —). A NC component spectrum (green dashed line – –) and a dye component spectrum (red dashed line - -) are extracted from the data, and combination of the two components generates a fit (blue solid line—) that agrees well with the original spectrum. Using extinction coefficients and the component spectra, the NC and the dye concentration was found to be 3.370 and 0.130 μM respectively, leading to a final dye to NC ratio to be approximately 26.

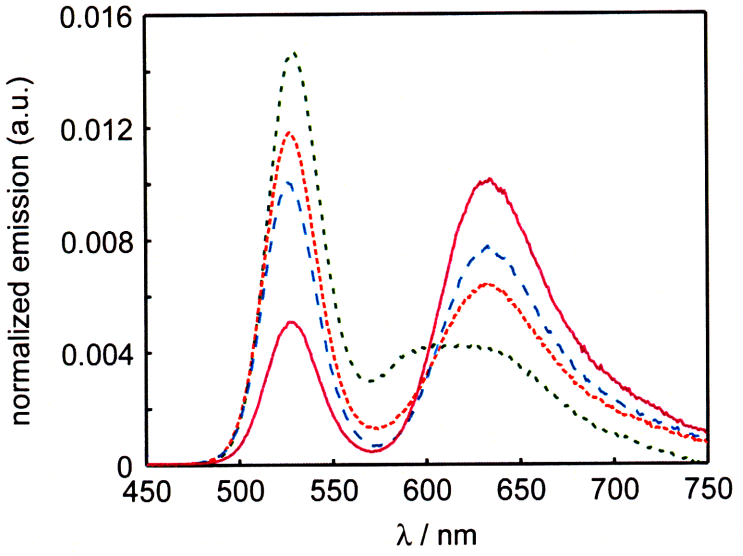

Figure IV.11 Normalized emission spectra (λ_{ex} = 365 nm) of NC-SNARF construct in phosphate buffers at pH 6 (green dashed line – –), pH 7 (red dashed line --), pH 8 (blue dashed line — —), and in borate buffer at pH 9 (purple solid line —).

Depending on the degree of spectral overlap, which is modulated by the pH, the critical transfer distance (R_0) was found to be between 4.46 nm (at pH 6) and 4.68 nm (at pH 9).

Additionally, FRET was confirmed by time-resolved emission spectroscopy. Figure IV.12 shows the lifetime decays fit to a bi-exponential, consistent to prior literature,[4,30] and the time constants are listed in Table IV.1. As in Chapters II and III, the longer lifetime component was used to compare the degree of lifetime quenching. The lifetime of the unconjugated NC was 16 ns at pH = 6. The lifetime of the donor NC is pH dependent; owing to enhanced energy transfer, the donor NC lifetime shortens as the pH increases. At pH 6, the lifetime was decreased to 12 ns, and at pH 9, the lifetime was further shortened to 10 ns.

With lifetime quenching rate constants in hand, the energy transfer efficiency can be extracted using eq. I.9. FRET is most efficient (37.5%) under the highest basic conditions, since the spectral overlap is greatest. The FRET efficiency decreases to 25% at pH 6, consistent with decreased spectral overlap between the donor and acceptor. Using eq. I.10 the actual donor-acceptor distance, *r*, can be evaluated and compared to the size of the construct. Assuming a dye to NC ratio of 26:1, the distance

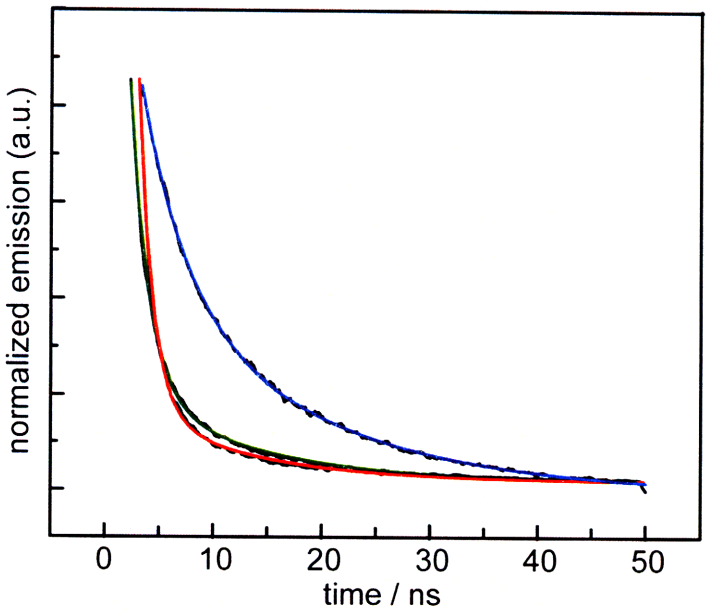

Figure IV.12 Lifetime decay curves of NC donor at pH 6 (blue line —), NC-SNARF at pH 6 (green line —), and NC-SNARF at pH 9 (red line —).

Table IV.1 Experimental and calculated FRET parameters for the dendritic NC-SNARF system

Sample	τ / ns	R_0 / nm[a]	r / nm[b]	E / %[c]	m[d]
NC-SNARF pH 6	12	4.46	9.6	25	25
NC-SNARF pH 9	10	4.68	8.7	37.5	25

[a] Determined from eq. I.8, [b] Determined from eq. I.10, [c] Determined from eq. I.9, [d]determined from deconstructing the UV-visible spectra

between the SNARF and NC was 8.7 nm at pH 9 compared to 9.6 nm at pH 6. This is significantly smaller than the hydrodynamic radius measured by DLS. One possible explanation for this behavior is that the conjugation sites are presumably distributed throughout the dendrimer ligand coating, whose thickness is 2 nm per dendrimer ligand, and at least 4 nm if cross coupling of the dendrimers occurred. The difference in the radius between the pH 6 and 9 values may also be explained by the protonation state of the dendrimers. Despite the large hydrodynamic size of the NC-SNARF dendrimer construct, which is disadvantageous for donor-acceptor proximity, the FRET efficiency was sufficiently large due to a high number of acceptor molecules that was conjugated to the NC. The emission profiles of the construct (Figure IV.11) are clearly ratiometric and unique over a range of pH values.

In order to determine the effectiveness of the NC-SNARF sensor in a biological environment, the sensor was placed in 4% bovine serum albumin (BSA) in phosphate solutions buffered between pH 6.0 and pH 8.0 at 0.2 pH increments. Albumin was chosen as a blood mimic as it is generally the most abundant plasma protein in mammals;[31] in addition, BSA naturally introduces a highly scattering environment and thus captures a challenge in biological sensing. Figure IV.13 shows the pH dependence of the emission from the construct in BSA buffers. It is interesting to note that the ratio of the integrated dye to NC area decreases with BSA versus neat phosphate buffer (Figure IV.11).

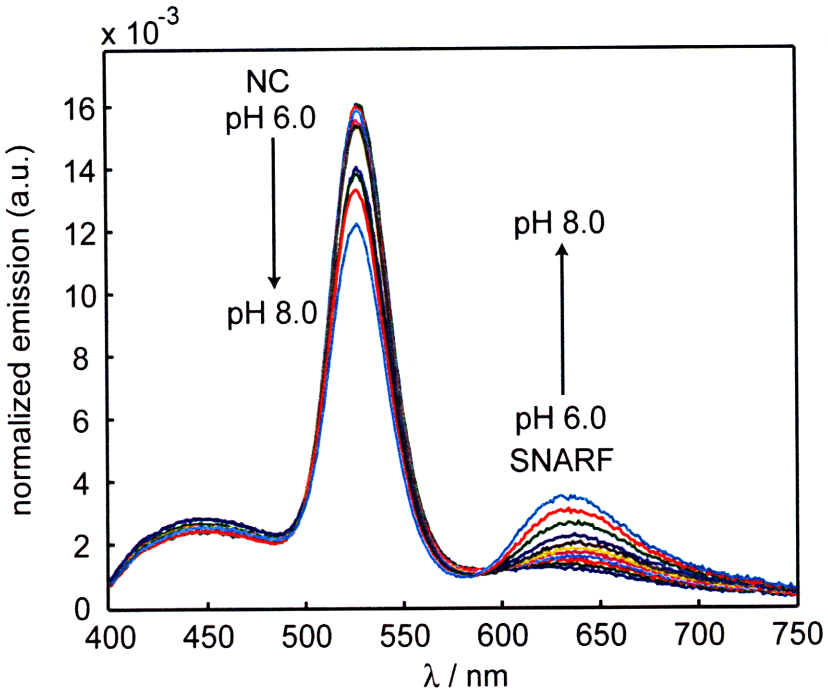

Figure IV.13 Normalized emission spectra of NC-SNARF construct in phosphate buffers containing 4% BSA. Spectra taken at 0.2 pH increments between pH 6.0 and 8.0.

The SNARF to NC integrated emission ratio decreased in the presence of BSA; therefore, the NC emission is enhanced and/or the SNARF emission is quenched. NCs have previously been shown to exhibit increased quantum yields when directly conjugated to BSA.[32,33] It has been suggested that BSA passivates the surface of the NCs by acting as a physical barrier of O_2 for surface oxidation.[33] Although our construct was only placed in a solution of BSA and not directly coupled, it is quite possible that the electrostatic attraction between the dendrimer coated NCs and BSA was strong enough to further passivate the NCs to increase their quantum yields. A second possibility involves quenching of the dye, where the electrostatic interactions between the dendritic NC and BSA may have propelled the tethered SNARF dyes into proximity, causing them to self-quench through re-absorption.

Matched concentrations of dendrimer coated NCs and SNARF-5F were individually placed in regular phosphate buffer and BSA buffer to see whether any differences existed in emission intensity. Figure IV.14 shows that while dendrimer coated NCs exhibit approximately the same intensity, the intensity of SNARF-5F is diminished by approximately 90%. As albumin provides a hydrophobic environment, the

diminished intensity of SNARF-5F may be due to solvent effects, phenomena commonly exhibited by xanthene-based dyes.[34-36] It is also possible that the dye may be forming a complex with the albumin, which has also been reported for fluorescein.[37,38] In this case, the covalent attachment of SNARF to the NC is beneficial, as the large NC scaffold will mitigate SNARF interactions with outside moieties. The significant change in the dye emission between different kinds of buffers underscores the importance of a ratiometric readout. An intensity-based sensor is not sufficient to accurately determine the change in pH as the surrounding environment may affect the intensity. The tethered NC does allow for a ratiometric output, and a change in the ratio of the NC sensing construct in the BSA buffers further emphasizes the importance of calibration in a buffer closely resembling the intended application environment as a technique to maximize precision. Given the degree of quenching of SNARF-5F alone vs. SNARF-5F on the NC surface, the large NC scaffold also seems to provide protection to the dye from outside environments.

A calibration curve can easily be constructed either by calculation of the ratio of the maximum emission intensities of the NC and dye or by the ratio of the total integrated areas of the individual peaks. Figure IV.15 illustrates an example calibration constructed using the different methods, constructed from emission spectra that were averaged over three times. As shown in Figure IV.15.A and Figure IV.15.B, the ratio

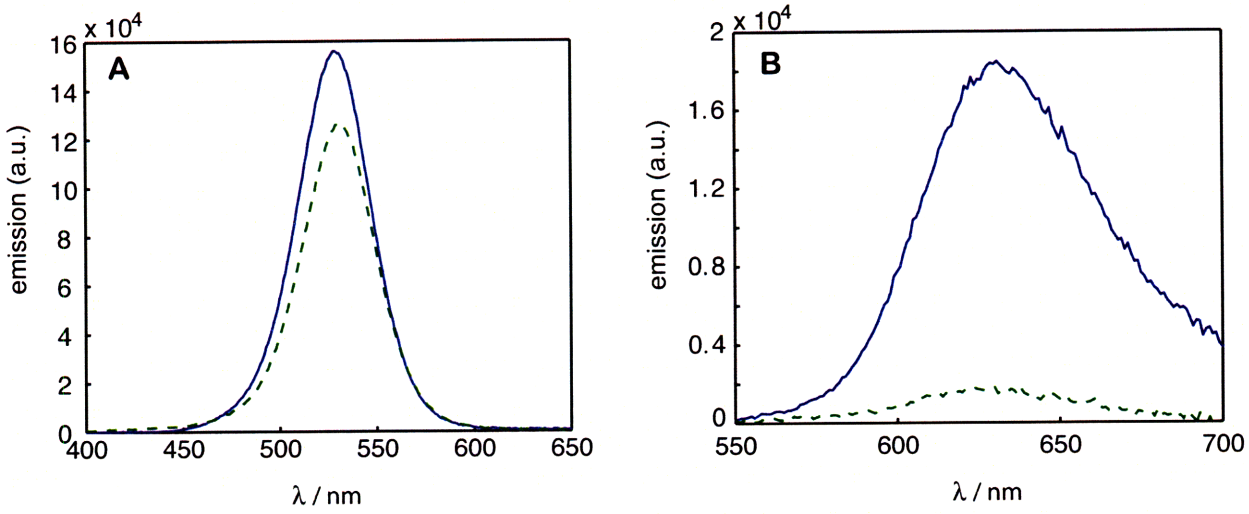

Figure IV.14 Change in emission of (A) NC and (B) SNARF-5F when equal concentrations are placed in pH 7.4 phosphate buffered solution (— solid blue line) vs. pH 7.4 4% BSA phosphate buffered solution (- - green dashed line).

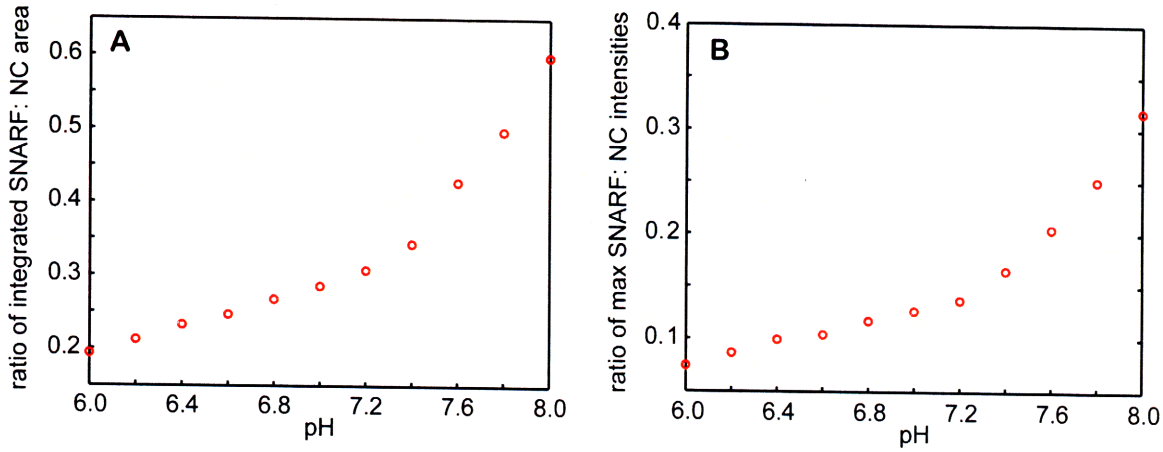

Figure IV.15 Two methods for constructing a calibration curve. A plot of the ratio of (A) integrated SNARF emission to NC emission and (B) maximum SNARF to NC emission intensities. Note the monotonic increase in the ratio as pH is increased.

monotonically increases from pH 6.0 to pH 8.0, and in this case, the signal is sufficiently strong that both methods produce smoothly varying ratios. In general, integration over a range will give lower noise and thus, is the preferred method. All calibrations described henceforth will be based on the ratio of the integrated areas of the two emissions, as exemplified in Figure IV.15.A. Integration of the emission minimizes errors arising from fluctuations and spikes in emission intensities at one single wavelength only.

With our construct well characterized under one-photon excitation, its response under two-photon excitation (λ_{ex} = 800 nm) was examined, under collaboration with the Jain lab. Infrared excitation permits the biological environment to be probed against minimal background emission and leads to less damage to the tissues. Two methods of data collection were used. First, an emission spectrum at a single point in the sample is collected and an integrated dye to NC ratio is calculated from the spectrum. Figure IV.16 shows the spectra of a set of samples at various pHs. Using the data from Figure IV.16, a similar plot of the integrated SNARF to NC emission was constructed (Figure IV.17). The large error associated with the pH 7.8 or 8.0 values may be explained by the high signal to noise of the emission spectrum collected at a single point. The second method used is an image calibration. A fluorescence image was taken from an area of the sample, and two filters were used to collect individual emissions from the NC and the SNARF, respectively. Then, a ratio of the images can be taken to produce a calibration curve.

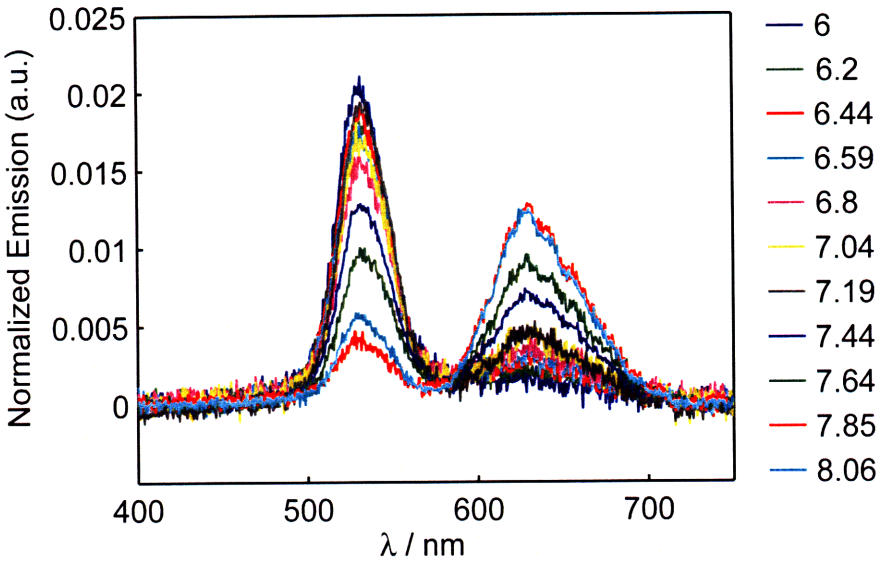

Figure IV.16 Emission profiles of NC-SNARF under two-photon excitation.

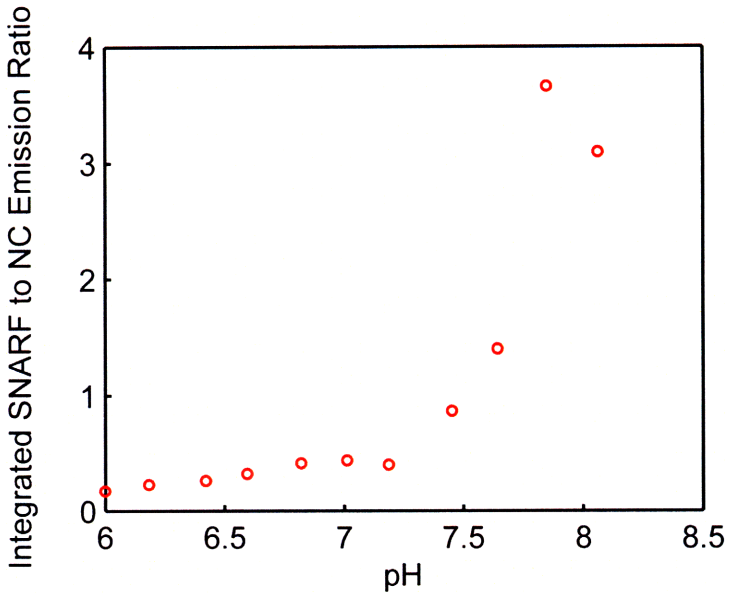

Figure IV.17 A plot of the ratio of integrated SNARF to NC emission from Figure IV.16 under two-photon excitation. pH 7.8 or pH 8.0 is an outlier from the curve.

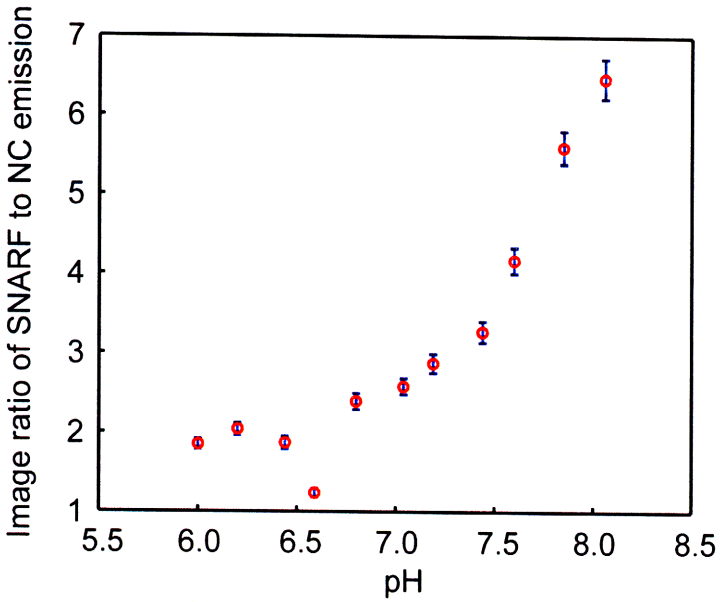

Figure IV.18 Calibration curve constructed for the NC-SNARF pH sensor, under two-photon excitation, by taking the ratio of the two PMT channels that collected NC and SNARF emissions respectively.

A dichroic filter centered at λ = 565 nm allowed for the green (NC) and the red (SNARF) intensities to be collected separately and to be resolved. A calibration is shown in Figure IV.18 and reflects the monotonic increase of the ratio of the two emissions as the pH increases. Error in calibration (with the exception of pH 6.6) suggests that in the relevant physiological range (6.4-7.8), pH may be accurately (error within 4%) and ratiometrically determined using the NC-SNARF construct. The dynamic range of the sensor decreases rapidly below pH 6.4. Thus, alternative dyes are needed to accurately probe this pH range. The emission spectra of the sensor in various phosphate buffers closely match the profiles obtained with one-photon excitation, which suggests that FRET-based sensing responds similarly under both one and multi-photon absorption. Hence we expect that a sensing scheme based on the modulation of the spectral overlap between the donor and acceptor may be established under the conditions of two-photon excitation.

IV.2.i Introduction of Dendrimer NCs into an *in vivo* Environment

With a two-photon excitable pH sensor active in physiological ranges of pH in

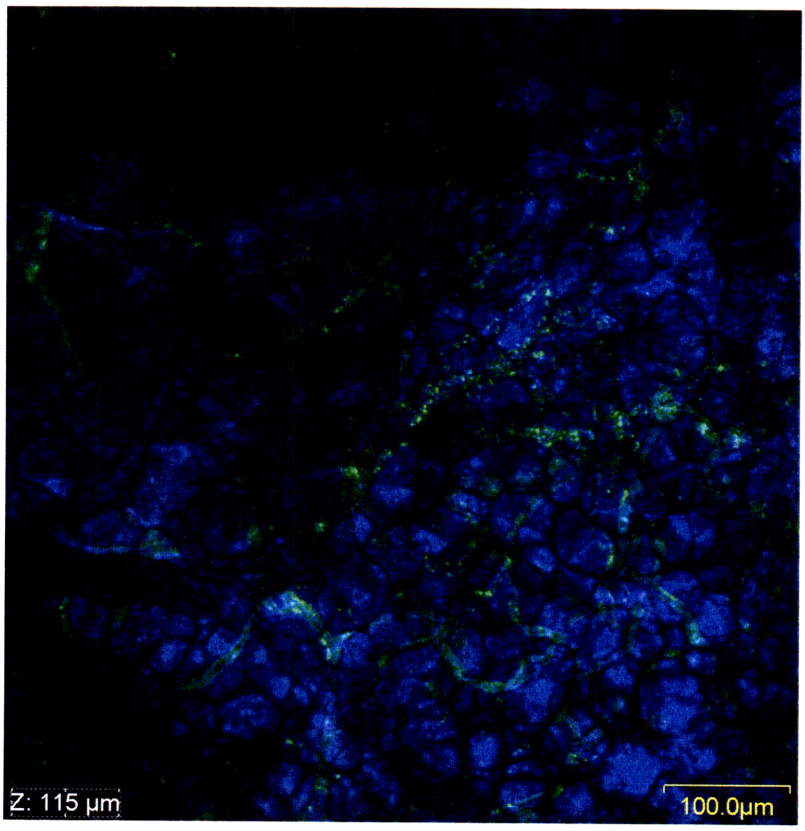

Figure IV.19 Two-photon excited image of the tumor. The vasculature is highlighted by the dendrimer NCs (green) which clump in the blood vessels.

hand, we proceeded to test its application in a biological tumor environment. The imaging capability of the dendrimer NCs was studied. In collaboration with the Jain lab, dendrimer coated NCs were tail-vein injected into a mouse implanted with a HT1089 human fibrosarcoma cell line. Figure IV.19 depicts a two-photon excited image of the tumor. The NCs image the vasculature as a bright green. The observation of speckled clumps of intense green light within the vessels indicates aggregation of the sensors, most likely exacerbated by the dendritic surface coating. Whereas the dendrimer-coated NCs provide a high amine ligand density allowing for 86% coupling efficiency, the resulting system is highly positively charged. Given that albumin possesses a highly negative charge, pI ~ 5,[31] it is not surprising that the positively charged NCs are likely aggregating with albumin or other biological moieties in the blood. Thus, the aggregation of the NC conjugates *in vivo* makes the construct unsuitable for biological sensing.

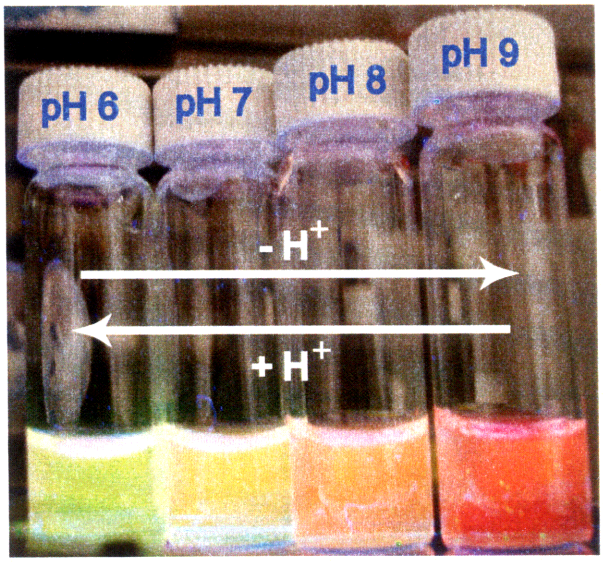

Figure IV.20 The change in emission of the NC-SNARF sensor with respect to pH is visible by eye.

IV.3 Conclusions

Methods of constructing a biocompatible NC pH sensor were explored in this Chapter. A NC-NHS ester was synthesized and isolated for coupling chemistry, although some aggregation could not be avoided. We found sensors made with micellular NC constructs to be bright, but energy transfer to the dye to be inefficient. The size of the scaffold increased the donor-acceptor FRET distance to sufficiently long distances that FRET was inefficient.

A cap-exchange strategy was then explored with the goal of minimizing the FRET distance. Though the poly(amido amine) dendrimer yielded large NC constructs, around 20 – 30 nm in diameter, due to the high number of amine functional groups on the scaffold, extensive coupling (86%) was observed and FRET-based sensing was achieved. The construct demonstrated sensitivity between pH 6.0 and 8.0 in buffers made with 4% bovine serum albumin. FRET-based sensing was also demonstrated under two-photon microscopy, and a calibration curve was constructed with minimal error. Although the dendrimer based NC sensors performed well in solution, with bright emission change visible to the eye (Figure IV.20), introduction of the dendrimer NCs into the tumor environment of a mouse resulted in aggregation of the NC-dye construct. As the highly charged scaffold is the likely cause of NCs clumping within blood vessels,

a new cap-exchanged water-soluble NC that is not so highly charged must be developed. One such near-neutral cap-exchanged scaffold will be presented in Chapter V.

IV.4 Experimental Procedures

IV.4.a Materials and Methods

Trioctylphosphine oxide (90%, TOPO), cadmium oxide (CdO), cadmium 2,4-pentanedionate, dodecanal, 1800 MW poly(acrylic acid), Sephadex LH-20, (benzotriazol-1-yloxy)tris(dimethylamino) phosphonium hexafluorophosphate (BOP), 1-hydroxybenzotriazole (HOBt), diisopropylethylamine (DIEA), *N*-octylamine, *N*-hydroxysuccinimide (NHS), decylamine, phthaloyl dichloride, 1,3-dihydroxynaphthalene, ethylenediamine and *N,N'*-dimethylformamide (DMF) were purchased from Sigma-Aldrich. 1-Tetradecylphosphonic acid (98%, TDPA), n-hexylphosphonic acid (HPA), and selenium shot were purchased from Alfa Aesar. Trioctylphosphine (TOP) was obtained from Strem Chemicals. 1-Ethyl-3,3'-dimethylaminopropylcarbodiimide (EDC), hexadecylamine (HDA), *O,O'*-bis-(2-aminopropyl)polypropylene glycol-block-polyethylene glycol-block polypropylene glycol 500, Bis(trimethylsilyl)sulfide [$(TMS)_2S$] and diethylzinc ($ZnEt_2$) were obtained from Fluka. SNARF-5F 5-(and 6-) carboxylic acid was purchased from Molecular Probes Inc., a division of Invitrogen. Poly(amido amine) generation 1 amine terminated dendrimer, with 8 terminal amines, was purchased from Dendritech. All materials were used as purchased, except for TOPO, which was purified through vacuum distillation, and diethylzinc, which was passed through a 0.2 μm syringe filter before use. All air sensitive materials were handled in an Omni-Lab VAC glove box under dry nitrogen atmosphere with oxygen levels < 0.2 ppm. Centrifugal filters equipped with a 50,000 Da molecular weight cutoff (MWCO) dialysis membrane were purchased through Millipore Corporation. Glass microslides were obtained from VitroCom. Broadband filters and dichroics were obtained through Chroma Technologies.

IV.4.b Spectroscopic Characterization

UV-visible spectra of SNARF coupled CdSe/ZnS were obtained on a Hewlett-Packard 8453 UV-vis Spectrophotometer with the Chemstation software. The samples were diluted in appropriate standard pH phosphate buffers for pH 6-8 and borate buffers for pH 9-10. Potassium phosphate buffered solution with 4% BSA were used for BSA calibration studies. Steady-state fluorescence measurements were obtained in a 1 cm pathlength cuvette from a custom-built Photon Technology Instruments fluorometer installed with a Hamamatsu R928 photomultiplier tube and a 150 W Xe excitation lamp. Size measurements were obtained by using ProteinSolutions DynaPro Titan Dynamic Light Scatterer equipped with Dynamics version 6.7.7.9 instrument control software. Samples were filtered through a 0.2 μm syringe filter and microcentrifuged to remove large particulates (such as dust) before measurements were taken at 25 °C. A 400 nm emitting Ti:Sapphire laser equipped with a gated intensified CCD camera was used to obtain time-resolved fluorescence spectra. Data were collected at room temperature using a 1 cm optical path fluorescence cuvette. Origin 6.0 was used to fit the lifetime decay curve as a bi-exponential decay. All NMR spectra were collected at the MIT Department of Chemistry Instrumentation Facility (DCIF) on a Varian Inova 500 MHz NMR Spectrometer at room temperature. Chemical shifts are reported using the standard δ notation in ppm. ^{1}H NMR spectra were referenced to the residual solvent peak of 3.31 ppm for CD_3OD and 7.26 ppm for $CDCl_3$. IR Spectra of samples were collected on a Perkin-Elmer 2000 FTIR Spectrometer.

Two photon-excited emission spectra were taken in collaboration with Rakesh Jain's group in the Edwin L. Steele Laboratories for Tumor Biology, Department of Radiation Oncology at the Massachusetts General Hospital and Harvard Medical School. NC-SNARF solutions were prepared in potassium phosphate buffers with 4% bovine serum albumin. Buffered sample solutions were placed in 0.1 × 1 mm^2 inner diameter glass microslides attached to a standard microscope slide. All spectral measurements were taken on a custom-built multiphoton laser scanning microscope (MPLSM) with the emission output fiber-coupled to a spectrometer. Multiphoton excitation was performed by a Broadband MaiTai diode pumped Ti:Sapphire laser

(Spectra-Physics) using 800 - 920 nm light at sample powers ranging from 10 - 60 mW. All measurements were made with the MRC 600 Bio-Rad MPLSM scan-head parked versus scanning on a Zeiss Axioskop20 microscopy using a Zeiss X20/0.5NA water objective. Fluorescence emission was coupled into a 100-micron core fiber bundle after passing through a 720 nm short-pass filter. Spectra of the fiber-coupled emission were collected on a Shamrock 303 spectrograph with Newton DU-420 CCD detector system (Andor Technology) using a 100 micron slit opening and 1-second detector integration. Emission spectra were analyzed in MATLAB.

Two-photon laser scanning microscopy (MPLSM) imaging was performed on an Olympus Fluoview 300 Laser Scanning Microscope modified with a MaiTai laser (Spectra-Physics). All images were taken at either 800 or 850 nm with excitation powers of 42 or 35 mW, respectively. Non-descanned fluorescence emission was detected by Hamamatsu HC125-02 PMTs. Nanocrystal and dye fluorescence was directed to separate PMTs using a 565nm-shortpass dichroic. The NC and dye channels were further selected using 660/50 nm and 535/40 nm AR-coated broadband filters, respectively. Image stacks (512 × 512 pixels and 5-micron z-step) were collected throughout the 100 micron pathlength of the microslide for each calibration sample using an Olympus ×20/0.95NA/water objective. Image analysis was performed using NIH ImageJ. Briefly, average intensity projections for each stack were created and converted to 32-bit. Then the dye channel was divided by the NC channel. The pixel average and standard deviation of the ratiometric image were used to create a calibration curve.

A dorsal skinfold window chamber model was prepared on 8-10 week old male SCID mice as previously described.[39] After recovery a small piece of HT1089 human fibrosarcoma tumor (~1 mm diameter) from a serially passaged subcutaneous in vivo source from the same murine background is implanted in the center of the chamber. At 1-2 weeks time the tumor in the chamber is of appropriate size for experiments (~4 mm diameter). All mice are bred and maintained in a defined-flora animal colony located at the Steele Laboratory.

IV.4.c Synthesis of CdSe/CdZnS Nanocrystals (λ_{em} = 570, 580 nm)

CdSe NCs overcoated with alloyed CdZnS were prepared using a modified literature method.[40-42] A vial containing cadmium 2,4-pentanedionate (0.317 g, 0.00100 mol), dodecanal (0.5 mL, 0.00225 mol) in trioctylphosphine (6 mL, 0.0135 mol) was degassed at 180 °C for an hour, then cooled to yield a homogenous bright yellow solution. 1.5 M trioctylphosphine selenide (TOPSe, 4 mL, prepared from dissolving 5.92 g Se shot into 50 mL TOP) was subsequently added to the vial being cooled to room temperature. The contents of the vial were subsequently injected rapidly at 360 °C into a three-necked flask (equipped with an air condenser, temperature controller, and a stir bar) containing degassed solvent of trioctylphosphine oxide (6.25 g, 0.0162 mol), hexadecylamine (5.75 g, 0.0238 mol), and trioctylphosphine (3.4 mL, 0.00762mol). The temperature of the growing CdSe NCs was dropped immediately by removing the heating mantle to obtain NCs with first absorption features of 517 nm and 520 nm.

The bare CdSe NCs were precipitated out of the growth solution with butanol and methanol twice and brought up in 4 mL hexanes. The NCs were overcoated by injecting the hexane solution of core CdSe into a degassed solvent of distilled trioctylphosphine oxide (10 g, 0.0259 mol) and n-hexylphosphonic acid (0.4 g, 0.00241 mol). The hexane was removed *in vacuo* at 80 °C, and decylamine (0.5 mL, 0.002 mol) was added. After stirring for 1 hr, the solution temperature was raised to 140 °C. Two separate precursor solutions of bis(trimethylsilyl)sulfide in 5 mL TOP and diethylzinc, and dimethylcadmium (in a 60:40 molar ratio) in 5 mL TOP was slowly added to the core solution over the course of two hours using a syringe pump. Exact amounts were chosen to yield a ~5 monolayer coating of ZnS on the bare CdSe NCs, using the methods of Dabboussi et al.[42] The final emission wavelength was 570 and 580 nm with a FWHM of 32 and 36 nm, respectively. The quantum yield of NCs prepared in this manner was generally on the order of 20-30% against a rhodamine 590 standard which is taken to be Φ = 0.95 in ethanol.[43]

IV.4.d Synthesis of ZnSe/CdSe/CdZnS Nanocrystals (λ_{em} = 550 nm)

ZnSe/CdSe NCs were prepared as previously reported.[44] ZnSe NCs were

synthesized by rapidly injecting a solution consisting of diethylzinc (96 mg, 0.78 mmol) dissolved in TOP (4 mL, 0.009 mol) and 1.0 M TOPSe (1 mL, 1 mmol, prepared from dissolving 3.948 g Se shot into 50 mL TOP) into a 3-necked flask containing degassed hexadecylamine (7 g, 0.0289 mol) at 310 °C. The resulting solution was cooled to 270 °C and the NCs were allowed to grow for an hour until the first absorption feature was λ = 354 nm. The temperature of the ZnSe solution was then lowered to 150 °C. In a separate 4-necked flask equipped with an addition funnel, air condenser, and temperature controller, TOPO (8 g, 0.0207 mol) and HPA (0.4 g, 2.4 mmol) was degassed at 150 °C. The addition funnel was loaded with a solution consisting of dimethylcadmium (78 mg, 0.55 mmol), 1.5 M TOPSe (0.6 mL, 0,9 mmol), and TOP (4.4 mL, 9.9 mmol). Immediately after 4 mL of the ZnSe growth solution prepared above (and maintained at 150 °C) was transferred to the 4-necked flask, the contents of addition funnel was allowed to drip at approximately 1 drip/second. The resulting solution was stirred at 150 °C for 24 hours.

The ZnSe/CdSe NCs were precipitated once with methanol, resulting in a yellow paste. The NCs were extracted with 3 x 5 mL hexanes until the paste turned white. The extracted hexane solution of NCs was re-precipitated with *n*-butanol and methanol twice more and re-dissolved in 4 mL hexanes. The hexane NC solution was then injected into an additional 4-necked flask containing degassed distilled TOPO (10 g, 25.9 mmol) and HPA (0.4 g, 2.4 mmol) that was stirring at 80 °C. The hexanes were removed from the NC solution *in vacuo* at 80 °C, after to which decylamine (0.5 mL, 2.6 mmol) was added under nitrogen and stirred for 3 hours. The temperature of the solution was then raised to 150 °C. Two separate precursor solutions of bis(trimethylsilyl)sulfide in 5 mL TOP, and diethylzinc and dimethylcadmium (in a 70:30 molar ratio) in 5 mL TOP was slowly added to the core solution over the course of two hours using a syringe pump. Exact amounts were chosen to yield a ~5 monolayer coating of ZnS on the bare CdSe NCs, using the methods of Dabboussi et al.[42] The NCs were stirred overnight at 80 °C after the addition of the shell precursors, yielding ZnSe/CdSe/CdZnS NCs with λ_{em} = 550 nm, FWHM of 35 nm, and quantum yield of Φ = 20% against a rhodamine 590 standard which is taken to be Φ = 0.95 in ethanol.[43].

IV.4.e Synthesis of CdSe/CdZnS Nanocrystals (λ_{em} = 525 nm)

CdSe NCs overcoated with alloyed CdZnS were prepared by a modified literature method.[42,45] Briefly, CdO (0.128 g, 1.0 mmol), TDPA (0.418 g, 1.5 mmol) and TOPO (6 g, 15.5 mmol) was loaded into a degassed 3-necked flask and heated to 320 °C. Upon generation of a clear, colorless homogenous solution, the temperature was lowered to 270 °C and 1.5 M TOPSe (5 mL, 7.5 mmol) was rapidly injected into the flask. The resulting solution was heated at 220 °C until the first absorption feature of the core CdSe NCs was 470 nm. The NCs were subsequently overcoated by injecting a hexane solution of the bare CdSe (prepared by size selected precipitation from the original growth solution) into a degassed solvent of TOPO (10 g, 25.9 mmols) and HPA (0.4 g, 2.4 mmols,). The hexane was removed *in vacuo* at 80 °C from the CdSe cores, after to which decylamine (0.25 mL, 1.3 mmols) was added and stirred for 2 hours. Using a syringe pump, two separate solutions of $(TMS)_2S$ in 5 mL TOP and a 90:10 molar ratio of diethylzinc and dimethylcadmium in 5 mL TOP were slowly dripped into the CdSe solution at 130 °C over the course of two hours. Exact amounts were chosen to yield a ~3 monolayer coating of ZnS on the bare CdSe NCs, using the methods of Dabboussi *et al.*[42] NC was found to have a FWHM = 32 nm and a quantum yield of Φ = 58% in hexanes after one precipitation, compared with the reference, rhodamine 590, which was taken to be 0.94 in methanol.[46]

IV.4.f Synthesis of *N*-Octylamine Modified Poly(acrylic acid)

A functionalized polymer was synthesized by coupling a fraction (40%) of the carboxylic acid groups of a 1800 MW poly(acrylic acid) (2 g, 0.0011 mol) with octylamine (1.436 g, 0.011 mol) using 1-ethyl-3-(3-dimethylaminopropyl)carbodiimide (EDC) (2.12g, 0.011mol) in *N,N'*-dimethylformamide according to a previous report.[3] The functionalized polymer was purified by size-exclusion chromatography using Sephadex LH-20 with methanol as the mobile phase. ^{1}H NMR (500MHz, CD_3OD, δ): 3.15 (br s), 2.25 (br, s), 1.98 (s), 1.60 (br s), 1.46 (br s), 1.28 (s), 0.866 (s). IR (KBr, cm^{-1}): 3289 (OH, br), 2930-2853 (CH, aliphatic), 1712 (C=O), 1641 (CO-NH-R), 1564 (CO-NH-R).

IV.4.g Preparation of Polymer Micelle Encapsulated NCs

Water-soluble CdSe/CdZnS NCs were prepared by precipitating 0.5 mL of the NC stock solution. The resulting dried CdSe/ ZnS (5 mgs) was added to *N*-octylamine modified poly(acrylic acid) (30 mgs) in a vial and dissolved in chloroform. The chloroform solution was sonicated and stirred vigorously for 1 hour, after which the solvent was removed *in vacuo.* The resulting solid was then dissolved in 0.2 M NaOH solution, then dialyzed with 50000 MW centrifugal filters until the pH of the filtrate was neutral. The quantum yields of the water soluble NCs prepared in this manner were found to be between Φ = 16 - 30%.

IV.4.h Preparation of NC-NHS Ester

NC-NHS esters were prepared by adding an excess of EDC (100 mg, 0.52 mmol) and NHS (50 mg, 0.43 mmol) to the water-soluble micelle encapsulated NCs as prepared in Secton IV.4.g. Upon addition of both EDC and NHS, flaky precipitate formed, leaving a clear, colorless solution, which was decanted. The solid was washed with water (3 x 5 mL) to remove the excess EDC and NHS, and dried briefly under vacuum. IR (thin film, cm^{-1}) 3281 (OH, br), 2853 (CH, aliphatic), 1731 (C=O), 1715 (C=O), 1643 (CO-NH-R).

IV.4.i Formation of Ethylenediamine-modified SNARF-5F

SNARF-5F (-and -6) carboxylic acid (1 mg, 2.12 μmol) was dissolved in 1 mL DMF. (Benzotriazol-1-yloxy) tris(dimethylamino) phosphonium hexafluorophosphate (BOP, 1.88 mg, 4.24 μmol) and 1-hydroxybenzotriazole (HOBt, 0.57 mg, 4.24 μmol), prepared through serial dilutions in DMF, were added to the SNARF-5F DMF solution and stirred for 10 minutes. Ethylenediamine (0.00141 mL, 42.4 μmol) and *N,N'*-diisopropylethylamine (DIEA, 1 mg, 17 μmol) were subsequently added and stirred overnight. The reaction was monitored through TLC until the SNARF-5F 5-(and-6) carboxylic acid peak disappeared. The DMF and excess ethylenediamine was removed *in vacuo*. The resulting product had a quantitative yield, had a positive ninhydrin stain with a TLC R_f of 0.27. ESI-MS *m/z* 514.0 $[M+H]^+$.

IV.4.j Synthesis of NC-SNARF Sensor with Ethylenediamine Linker

The 580 nm emitting CdSe/CdZnS-NHS ester, and in another instance, a 550 nm emitting ZnSe/CdSe/CdZnS-NHS ester, prepared as described in section IV.4.h, was dissolved in 5 mL DMF. The ethylenediamine modified SNARF-5F, as prepared in section IV.4.i was dissolved in 10 mL DMF. Two drops of DIEA was added to 5 mL of the amine-modified SNARF-5F stock DMF solution, then subsequently mixed to the NC-NHS DMF solution. The reaction was stirred vigorously for 12 hours, and DMF was removed under reduced pressure. To the dried NC-SNARF construct, 10 mL of 0.2 M NaOH was added and stirred for an hour to cleave any unreacted NHS esters. The resulting solution was filtered through a 0.2 μm syringe filter and dialyzed with a 50,000 MWCO centrifugal filters until the filtrate was colorless and clear.

IV.4.k Linkage of Aminated SNARF-5F to Modified Poly(acrylic acid)

Aminated SNARF-5F, as prepared in section IV.4.i, was dissolved in 10 mL DMF. 10 drops of DIEA was added to 5 mL of the aminated SNARF-5F stock solution. *N*-octylamine-modified poly(acrylic acid) (100 mg, 0.86 mmol) was dissolved in 5 mL DMF, to which BOP (1 mg, 2.3 μmol) and HOBt (0.29 mg, 2.1 μmol) was added and stirred for 10 minutes. The aminated SNARF-5F solution was added to the polymer solution and stirred for 24 hours. DMF and excess DIEA was removed *in vacuo*. The polymer was washed with acidic water and dried.

IV.4.l Synthesis of AminoPEGylated NCs

The 570 nm emitting NC-NHS ester, prepared as described in section IV.4.h, was dissolved in an overwhelming excess of neat *O,O'*-bis-(2-aminopropyl)polypropylene glycol-block-polyethylene glycol-block polypropylene glycol 500 (1 mL, 2 mmol). The PEG NC solution was stirred for 1 hour, to which water (5 mL) was added. Slight precipitation formed, which was filtered out with a 0.2 μm syringe filter, and the NC solution was dialyzed with 50,000 MWCO centrifugal filters to remove excess PEG.

IV.4.m Synthesis of NC-SNARF Sensor with AminoPEG Linker

SNARF-5F (-and -6) carboxylic acid (1 mg, 2.12 μmol) was dissolved in 1 mL DMF. Half of the stock SNARF solution (0.5 mg, 1.06 μmol) was mixed with BOP (1 mg, 2.26 μmol) and HOBt (0.29 mg, 2.12 μmol) for 10 minutes. The BOP activated SNARF solution was mixed with 570 nm emitting aminoPEGylated NCs in 5 mL DMF, prepared as described in section IV.4.l, and DIEA (1 mg, 8.5 μmol) for 12 hours. DMF and excess DIEA was removed *in vacuo* and distilled water was added. The NC-SNARF construct was subsequently dialyzed with 50,000 Da MWCO centrifugal filters until all excess dye was removed from the filtrate.

IV.4.n Synthesis of 1,2,7,8-Dibenzofluorescein

The pH sensitive 1,2,7,8-dibenzofluorescein was synthesized according to literature methods.[22] Briefly, 1,3-dihydroxynaphthalene (1.0 g, 6.3 mmol) and phthaloyl dichloride (0.63 g, 3.1 mmol) was mixed in a 250 mL round bottom flask and heated at 130 °C for 10 minutes. An orange solid formed upon heating. The solid was cooled, and 30 mL H_2O and NaOH (1 g, 0.025 mol) was added. Concentrated HCl was added until a precipitate was formed, then subsequently filtered. The filtered solid was refluxed with acetic anhydride (30 mL, 0.317 mol) for 15 minutes. The solution was cooled at 4 °C overnight, then filtered to yield the diacetate product. ^{1}HNMR (500 MHz, $CDCl_3$, δ) 8.19 (d, J = 7.5, 1H), 7.92 (d, J = 8.5, 2H), 7.55 (m, 4H), 7.323 (m, 6H), 7.21 (d, J = 7.5, 1H), 2.50 (s, 6H). In order to obtain the free acid dye, 10 mL H_2O and NaOH (1 g, 0.025 mol) was added to the diacetate product, and the mixture was roto-vapped. Again, the product was dissolved in water and precipitated with concentrated HCl. After filtration, the product was dissolved in benzene and lyophilized to remove all traces of solvent.

IV.4.o Synthesis of Dihydrolipoic Acid-modified Poly(amido amine)

Generation 1 poly(amido amine) [PAMAM] with 8 amine terminus (1.6042 g, 1.1 mmol) was dissolved in DMF. Dihydrolipoic acid (DHLA, 0.467 g, 2.2 mol), prepared by literature methods,[47] was added to a DMF solution containing EDC (1.289 g, 6.7 mmol) and NHS (0.774 g, 6.7 mmol). The DHLA solution was subsequently mixed with the

PAMAM solution and stirred overnight. Removal of DMF *in vacuo* resulted in a pale cream colored oil. The ligand was purified through dialysis with Spectra-por dialysis float-a-lyzer membranes equipped with 500 Da MWCO membranes. ^{1}HNMR (500 MHz, CD_3OD, δ): 3.39 (t, *J*=6.5 Hz, 8H), 3.277 (br t, 16H), 3.08 (m, 2H), 2.94 (br t, ~16H), 2.80 (t, *J*=6.5 Hz, 24H), 2.62-2.5 (m, ~16 H), 2.40 (t, *J*=6.5 Hz, 24 H), 2.16 (t, *J*= 7 Hz, 4H), 1.92-1.19 (m, ~20H).

IV.4.p Cap Exchange of CdSe/CdZnS with DHLA-PAMAM

One mL of the stock CdSe/ZnS solution was precipitated by methanol and re-suspended in 3 mL chloroform. 0.2 g of DHLA-PAMAM was dissolved in 2 mL of methanol, mixed with the chloroform solution of NCs, and stirred vigorously for 5 hours. The solution was then transferred to a 40 mL vial, atop to which 30 mL of H_2O was added and stirred briefly. The resulting mixture was allowed to sit overnight, after which the dendrimer solubilized NCs phase transferred into the aqueous layer. Although most of the excess dendrimer remained in the organic phase, excess ligands were further removed through dialysis of the NC containing aqueous layer, using Millipore centrifuge tubes equipped with 50,000 Da MWCO filters. The isolated aqueous compatible NCs were diluted in distilled water to a final volume of 10 mL. The purified dendrimer-solubilized NCs were found to have a FWHM = 32 nm and a quantum yield of Φ = 26% in water compared with the reference, rhodamine 590, which was taken to be 0.94 in methanol.[46]

IV.4.q Conjugation of SNARF-5F to DHLA-PAMAM Capped NCs

SNARF-5F 5 (-and-6) carboxylic acid (2.5 mg, 0.53 μmol) was activated for amide coupling with EDC (0.50 mg, 2.6 μmol) and NHS (0.31 mg, 2.7 μmol) in pH 6 MES buffer. After vigorous stirring for 20 minutes, the NHS-activated dye was added to 3.3 mL of the DHLA-PAMAM solubilized NCs and stirred overnight. The unreacted dye was removed through dialysis with 50,000 Da MWCO filters.

IV.5 References

1. Jobsis, P. D.; Rothstein, E. C.; Balaban, R. *J. Microsc.-Oxford* **2007**, *226*, 74-81.

2. Somers, R. C. *Unpublished results.*

3. Wu, X.; Liu, H.; Liu, J.; Haley Kari, N.; Treadway Joseph, A.; Larson, J. P.; Ge, N.; Peale, F.; Bruchez Marcel, P. *Nat. Biotechnol.* **2003**, *21*, 41-46.

4. Snee, P. T.; Somers, R. C.; Nair, G.; Zimmer, J. P.; Bawendi, M. G.; Nocera, D. G. *J. Am. Chem. Soc.* **2006**, *128*, 13320-13321.

5. Clapp, A. R.; Goldman, E. R.; Mattoussi, H. *Nat. Protoc.* **2006**, *1*, 1258-1267.

6. Uyeda, H. T.; Medintz, I. L.; Jaiswal, J. K.; Simon, S. M.; Mattoussi, H. *J. Am. Chem. Soc.* **2005**, *127*, 3870-3878.

7. Liu, W.; Choi, H. S.; Zimmer, J. P.; Tanaka, E.; Frangioni, J. V.; Bawendi, M. *J. Am. Chem. Soc.* **2007**, *129*, 14530-14531.

8. Pons, T.; Uyeda, H. T.; Medintz, I. L.; Mattoussi, H. *J. Phys. Chem. B* **2006**, *110*, 20308-20316.

9. Xu, C.; Zipfel, W.; Shear, J. B.; Williams, R. M.; Webb, W. W. *Proc. Natl. Acad. Sci. U.S.A.* **1996**, *93*, 10763-10768.

10. Konig, K. *J. Microsc.-Oxford* **2000**, *200*, 83-104.

11. Denk, W.; Strickler, J. H.; Webb, W. W. *Science* **1990**, *248*, 73-76.

12. Brown, E. B.; Campbell, R. B.; Tsuzuki, Y.; Xu, L.; Carmeliet, P.; Fukumura, D.; Jain, R. K. *Nat. Med.* **2001**, *7*, 864-868.

13. Larson, D. R.; Zipfel, W. R.; Williams, R. M.; Clark, S. W.; Bruchez, M. P.; Wise, F. W.; Webb, W. W. *Science* **2003**, *300*, 1434-1437.

14. Cooper, M. E.; Gregory, S.; Adie, E.; Kalinka, S. *J. Fluoresc.* **2002**, *12*, 425-429.

15. Mujumdar, R.; Smith, J. A.; (Carnegie Mellon University, USA; Amersham Pharmacia Biotech UK Ltd.). Application:WO, 2000, 66 pp.

16. Baeyer, A. *Justus Liebigs Ann. der Chem.* **1876**, 1-74.

17. Rink, T. J.; Tsien, R. Y.; Pozzan, T. *J. Cell Biol.* **1982**, *95*, 189-96.

18. Wolfbeis, O. S.; Rodriguez, N. V.; Werner, T. *Mikrochim. Acta* **1992**, *108*, 133-141.

19. Liu, J.; Diwu, Z.; Leung, W.-Y. *Bioorg. Med. Chem. Lett.* **2001**, *11*, 2903-2905.

20. Valdes-Aguilera, O.; Cincotta, L.; Foley, J.; Kochevar, I. E. *Photochem. Photobiol.* **1987**, *45*, 337-344.

21. Yang, S.; Tian, H.; Xiao, H.; Shang, X.; Gong, X.; Yao, S.; Chen, K. *Dyes Pigments* **2001**, *49*, 93-101.

22. Lee, L. G.; Berry, G. M.; Chen, C. H. *Cytometry* **1989**, *10*, 151-164.

23. Hermanson, G. *Bioconjugate Techniques*; Academic Press: San Diego, 1996.

24. Bruice, P. Y. *Organic Chemistry, second edition*; Prentice-Hall: Upper Saddle River, 1998.

25. Zimmer, J. P.; Kim, S.-W.; Ohnishi, S.; Tanaka, E.; Frangioni, J. V.; Bawendi, M. G. *J. Am. Chem. Soc.* **2006**, *128*, 2526-2527.

26. Susumu, K.; Uyeda, H. T.; Medintz, I. L.; Pons, T.; Delehanty, J. B.; Mattoussi, H. *J. Am. Chem. Soc.* **2007**, *129*, 13987-13996.

27. Wisher, A. C.; Bronstein, I.; Chechik, V. *Chem. Commun.* **2006**, 1637-1639.

28. Aldana, J.; Wang, Y. A.; Peng, X. *J. Am. Chem. Soc.* **2001**, *123*, 8844-8850.

29. Cakara, D.; Kleimann, J.; Borkovec, M. *Macromol.* **2003**, *36*, 4201-4207.

30. Clapp, A. R.; Medintz, I. L.; Mauro, J. M.; Fisher, B. R.; Bawendi, M. G.; Mattoussi, H. *J. Am. Chem. Soc.* **2004**, *126*, 301-310.

31. Quinlan, G. J.; Martin, G. S.; Evans, T. W. *Hepatology* **2005**, *41*, 1211-1219.

32. Gao, X.; Chan, W. C. W.; Nie, S. *J. Biomed. Opt.* **2002**, *7*, 532-537.

33. Derfus, A. M.; Chan, W. C. W.; Bhatia, S. N. *Nano Lett.* **2004**, *4*, 11-18.

34. Fleming, G. R.; Knight, A. W. E.; Morris, J. M.; Morrison, R. J. S.; Robinson, G. W. *J. Am. Chem. Soc.* **1977**, *99*, 4306-4311.

35. Martin, M. M. *Chem. Phys. Lett.* **1975**, *35*, 105-111.

36. Magde, D.; Rojas, G. E.; Seybold, P. G. *Photochem. Photobiol.* **1999**, *70*, 737-744.

37. Taarnhoj, J.; Schlecht, L.; McLaren, J. W.; Brubaker, R. F. *Exper. Eye Res.* **1990**, *51*, 113-118.

38. Buturlakin, M. S. *Fiziologicheskie i Fiziko-Khimicheskie Mekhanizmy Regulyatsii Obmennykh Protsessov Organizma* **1975**, *4*, 47-49.

39. Leunig, M.; Yuan, F.; Menger, M. D.; Boucher, Y.; Goetz, A. E.; Messmer, K.; Jain, R. K. *Cancer Res.* **1992**, *52*, 6553-6560.

40. Murray, C. B.; Norris, D. J.; Bawendi, M. G. *J. Am. Chem. Soc.* **1993**, *115*, 8706-8715.

41. Hines, M. A.; Guyot-Sionnest, P. *J. Phys. Chem.* **1996**, *100*, 468-471.

42. Dabbousi, B. O.; Rodriguez-Viejo, J.; Mikulec, F. V.; Heine, J. R.; Mattoussi, H.; Ober, R.; Jensen, K. F.; Bawendi, M. G. *J. Phys. Chem. B* **1997**, *101*, 9463-9475.

43. Kubin, R. F. F., A. N. *J. Lumin.* **1982**, *27*, 455-462.

44. Ivanov, S. A.; Nanda, J.; Piryatinski, A.; Achermann, M.; Balet, L. P.; Bezel, I. V.; Anikeeva, P. O.; Tretiak, S.; Klimov, V. I. *J. Phys. Chem. B* **2004**, *108*, 10625-10630.

45. Peng, Z. A.; Peng, X. *J. Am. Chem. Soc.* **2001**, *123*, 183-184.

46. Holzer, W.; Gratz, H.; Schmitt, T.; Penzkofer, A.; Costela, A.; Garcia-Moreno, I.; Sastre, R.; Duarte, F. J. *Chem. Phys.* **2000**, *256*, 125-136.

47. Gunsalus, I. C.; Barton, L. S.; Gruber, W. *J. Am. Chem. Soc.* **1956**, *78*, 1763-1766.

Chapter V

Development and Characterization of a Biocompatible Nanocrystal-based pH Sensor

V.1 Introduction

The synthesis and characterization of a bio-compatible NC-SNARF FRET-based pH sensor is the study focus of this Chapter. Chapter IV introduced a number of NC conjugates that sensed pH effectively; however, these constructs were not well-suited towards biological pH sensing, due to either a shift in pKa, large size, or the net charge of the construct. While the dendrimer-coated NC pH sensor showed excellent sensitivity in BSA calibration buffers under two-photon excitation, the net positive charge of the construct resulted in aggregation of the construct when tail-vein injected *in vivo* into a mouse tumor. Therefore, two additional design considerations (along with the previous four discussed in Chapter IV) are required for bio-compatibility.

(1) Sensitive at physiological pH ($pK_a \sim 7.3$)

(2) Robust NC-dye linkages (e.g. amides)

(3) Stability to photobleaching

(4) An acceptor dye that exhibits pH-sensitive absorbance and/or quantum yield for reporting a ratiometric emission spectrum

(5) A compact size, allowing for short NC-dye donor-acceptor distances

(6) A low net charge to mitigate non-specific binding

As discussed in Chapter IV, cap-exchange with dendritic ligands did not diminish the overall size of the NCs compared to those that were encapsulated with amphiphilic polymers. Substitution of the dendrimer for a small molecule-based capping ligands should afford compact NCs suitable for *in vivo* sensing.

A bio-compatible cap recently reported exploits the hydrophilicity and non-interacting nature of poly(ethylene glycol), PEG.[1] NCs prepared with dihydrolipoic acid (DHLA) modified PEG were shown to be stable in intracellular environments.[1] In addition, work by Zimmer *et al.* demonstrated that when incubated with fetal bovine serum (FBS), PEGylated indium arsenide (InAs) NCs did not bind to FBS, while incubation with the smaller, negatively charged DHLA-capped InAs NCs lead to nonspecific binding to FBS.[2] The InAs NCs, sized at 8.7 nm when coated with DHLA-PEG (with 8 repeating units) were shown to extravasate out of blood vessels when injected intravenously into a mouse or a rat, unlike the DHLA-capped NCs. These

results suggest that DHLA-PEGylated NCs exhibit properties 5 and 6 listed above. However, the terminal hydroxyl group of the PEG prevents the construction of robust NC-dye conjugates.

At the time of this work, research was being pursued by collaborators in the Bawendi group to implement standard bioconjugation techniques to PEGylated NCs. By derivatizing amino and carboxylic acid groups onto the PEG terminus, a new class of functional DHLA-PEG ligands was designed as NC coatings.[3] Other work by Mattoussi and co-workers also reported derivatized amino, carboxylic acid, and biotinylated PEG ligands for designing functional NCs.[4] Both groups reported that cap-exchanging a mixture of hydroxy-terminated PEG and a derivatized PEG led to NCs that were both stable in a biological environment and were available for conjugation of dyes and proteins. Liu *et al.* reported that while 100% coated aminoPEG NCs exhibited nonspecific binding to cell surfaces, this could be overcome by employing a 20:80 molar mixture of amino PEG to hydroxyPEG ligands for NC surface modification.

The development of the new derivatized PEG ligands provides a route towards the synthesis of NC-FRET based sensors that exhibit properties 5 and 6, while retaining the sensing properties of 1-4. The use of mixed PEGylated NCs for the development of a NC-SNARF sensor and its photophysical properties are described in this Chapter.

V.2 Results and Discussion

V.2.a Quick Test for Biocompatibility

Encouraged by the extravasation of NCs reported by Zimmer *et al.*,[2] we prepared 10% aminoPEG with 90% hydroxyPEG terminated 556 nm emitting NCs. Under collaboration with the research group of R. Jain at Massachusetts General Hospital, NCs were tail-vein injected into a mouse with a LS174T human colorectal adenocarcinoma dorsal window implant. Cascade blue-dextran, a dye known to image the blood vessels without extravasating, was co-injected along with the NCs. Five points in the tumor, two in the vasculature and three in the interstitium were chosen, and a spectrum was collected at each point using multiphoton laser scanning microscope equipped with a spectrometer. Figure V.1 shows the spectra of the two fluorophores at

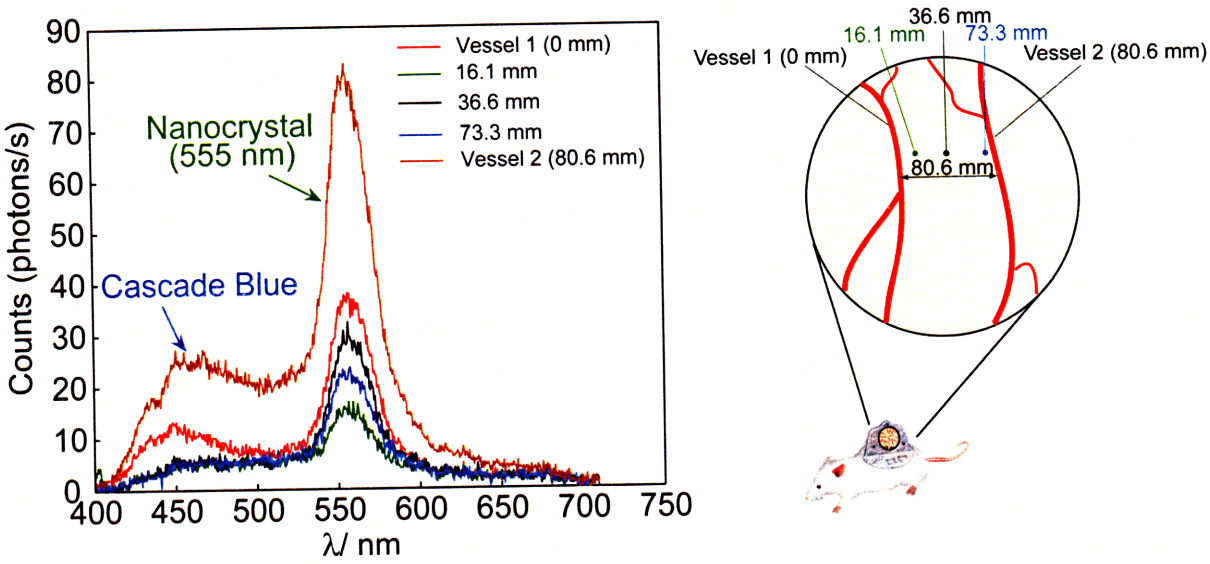

Figure V.1 (Left) Two-photon excited emission spectrum of co-injected cascade blue and PEGylated NCs at five different points in the tumor. (Right) Graphical rendition of location where the emission spectra was collected in the tumor.

the various locations. In the blood vessels, both cascade blue and NC emission are present. In contrast, the three points in the interstitium only exhibit NC emission, indicating that the NCs were able to extravasate out of the blood vessels. The extravasation of the NCs was a positive sign and an impetus for constructing the NC-SNARF sensor using PEGylated ligands.

V.2.b Synthesis

Dihydrolipoic acid-terminated PEGylated and aminoPEGylated ligands were synthesized according to modified literature methods.[1,3-5] Poly(ethylene glycol) 400, containing 8 repeating ethylene glycol units, was chosen as the starting material, because it is long enough to enable water solubilization of NCs, yet short enough to effect efficient energy transfer.[1] In addition to solubility, surface charge was another factor for ligand choice. Chapter IV.2.h discussed an example of a fully amine terminated NC surface that resulted in non-specific binding or aggregation in an *in vivo* environment, underscoring the importance of charge neutrality. Utilization of a mixture of hydroxyl terminated PEG and amine terminated PEG ligands allows for rigorous control of surface charge, as established by Liu et al.[3] We chose a

Scheme V.1 Scheme of NC cap exchange, where the original trioctylphosphine ligands are displaced by the dithiols of the DHLA-modified PEG ligands

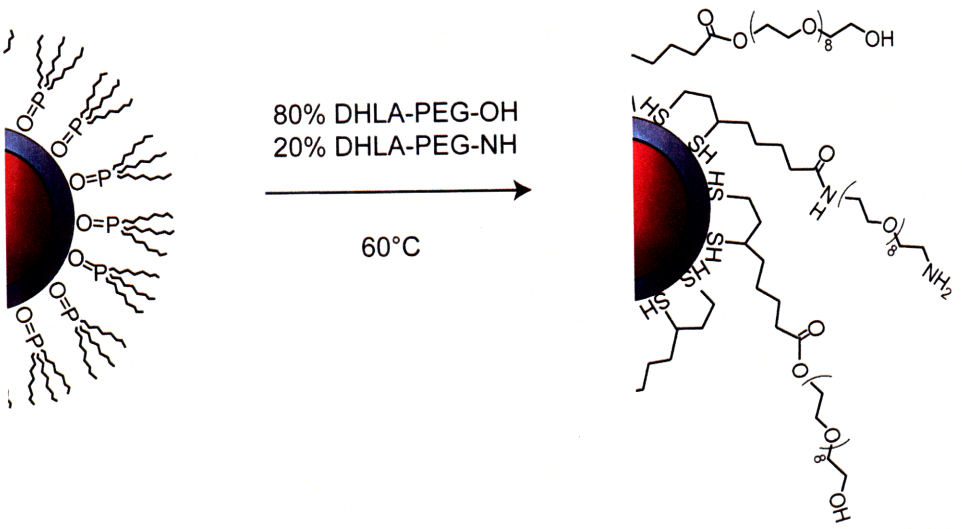

hydroxyPEG:aminoPEG ligand mixture ratio of 80:20, integrating amines for coupling chemistry while maintaining a sufficiently neutral scaffold. 530 nm or 532 nm-emitting NCs were chosen for cap-exchange. The green-emitting NCs were chosen as their emission is far enough from the SNARF-5F emission between 550-750 nm to allow for collection of two discrete emission intensities for ratiometric sensing. In Scheme V.1, the ligand exchange of the native trioctylphosphine ligands with DHLA-PEG mixtures is depicted. The quantum yield of the NCs dropped from 43% in hexanes to 16 - 21% upon water solubilization.

Initial attempts at coupling SNARF-5F 5-(and-6) carboxylic acid to PEGylated NCs with EDC and NHS *in situ* in various buffers (MES, PBS, pH 8.3 bicarbonate) proved to be unsuccessful, as no reaction was observed. Increasing the reaction times and preparing concentrated solutions also resulted in no covalent conjugation. Due to the expensive cost of SNARF-5F, overwhelming the NCs with excess dye to drive the coupling reaction was not a viable option; therefore, a SNARF-5F NHS ester was prepared and isolated in order to promote coupling. Scheme V.2 details the preparation of the SNARF-5F mono-NHS ester, which was characterized with TLC and ESI-MS. Scheme V.3 depicts the coupling of NCs to SNARF-5F as the final step of the reaction. Optimized coupling conditions required the use of pH 8.3 bicarbonate buffer to enhance the nucleophilicity of the amines. Coupling efficiencies ranging from 10 - 20% were

Scheme V.2 Synthesis of SNARF-5F NHS-ester

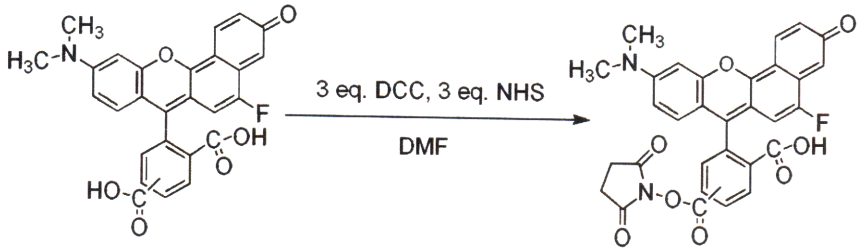

Scheme V.3 The SNARF-5F NHS-ester couples to the amino group of the mixed PEG coated NCs.

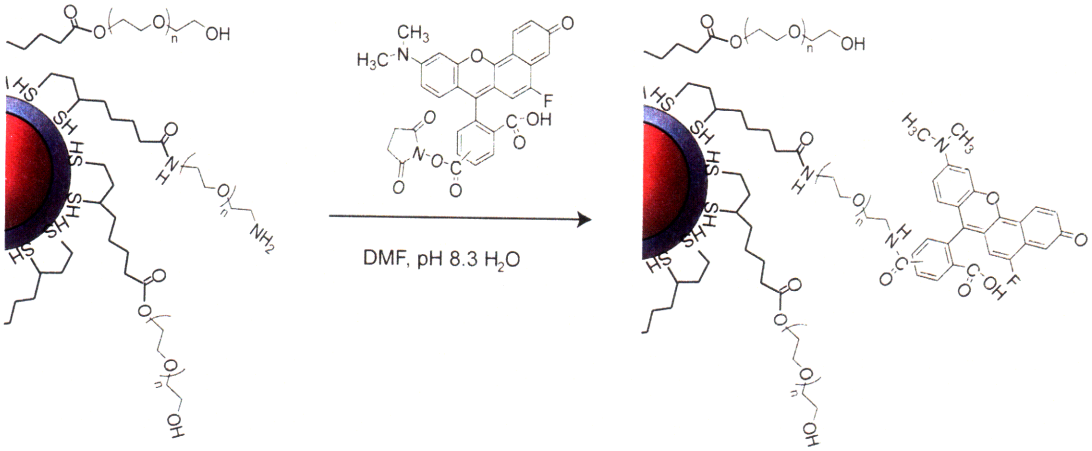

achieved under these conditions. Coupling efficiency is limited, primarily by the low surface coverage of amines (< 20%)[3] on the NC surface.

The size of the construct was measured using gel filtration chromatography. Figure V.2, a gel filtration chromatogram of the NC-SNARF construct, illustrates that the sensor with an average hydrodynamic diameter (H_D) of 10.9 nm was synthesized with minimal aggregation. If aggregation had occurred, the peak shift would be broadly distributed, with a smaller elution volume.

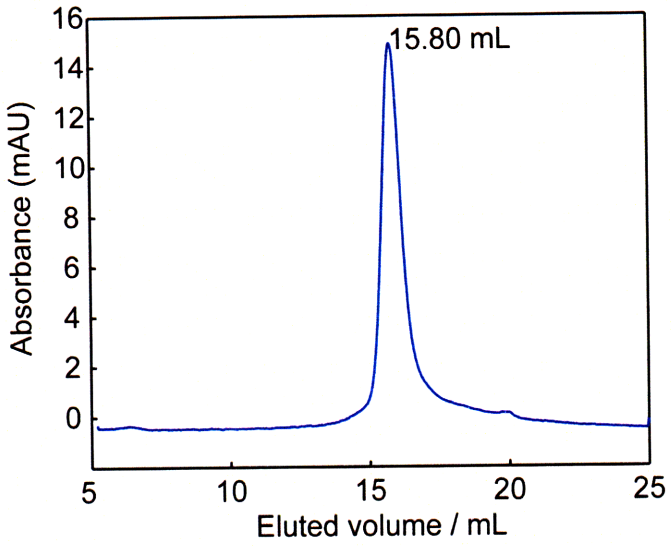

Figure V.2 GRC chromatogram of an NC-SNARF5F construct. The sharp peak indicates minimal to no aggregation, and an elution volume of 15.80 mL corresponds to a size of 10.9 nm hydrodynamic diameter.

V.2.c Photophysical Characterization

Despite the low coupling efficiency, an efficient FRET-based sensor was developed, due to the compact size of the ligands, which shortened the donor-acceptor FRET distance. Figure V.3 shows an example of the UV-vis spectra of SNARF-5F at different pH values. A dye to NC ratio anywhere from 1 to 6 (calculated by separating the dye and NC contributions from the UV-vis spectrum and dividing the concentrations obtained from the respective absorbances) is generally achieved. Figure V.3 depicts a construct with a ratio of approximately 4.5 dyes to NC. The absorption features of the dye red-shifts upon coupling to the NC, presumably due to the proximity of the NC to the dye. In a manner reminiscent of solvochromatism, the NC imparts a local dielectric environment to the dye. The UV-vis spectrum at each 0.5 pH increment between pH 5.5 and pH 8.0 is also distinguishable from each other, rendering the construct sensitive. Figure V.4 shows the normalized emission spectra of the NC-SNARF 5F sensor (dye: NC ratio = 4.5:1) at different pH values, excited at λ_{ex} = 365 nm, where there is minimal SNARF-5F absorption. The 530 nm NC emission is narrow and bright, with a FWHM of 26 nm. Due to the narrow emission profile of the NC and the use of a donor with lower emission wavelength, the acidic and basic forms of SNARF-5F are well-resolved under

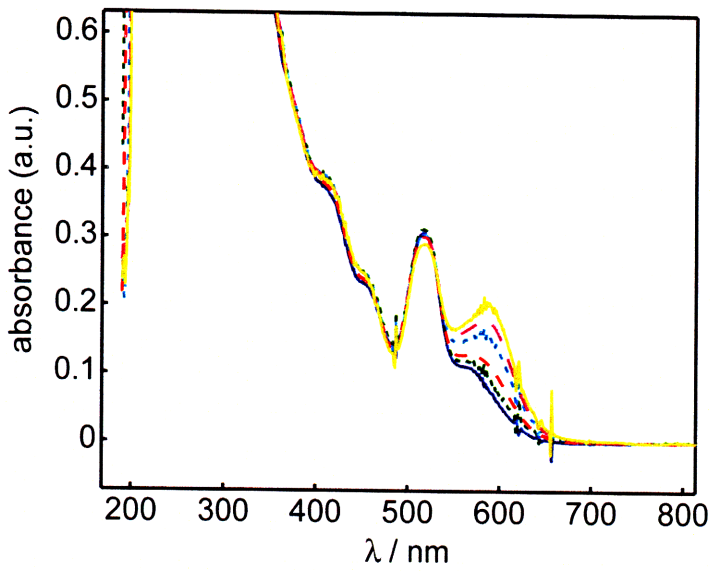

Figure V.3 UV-vis spectra of PEGylated NC-SNARF5F construct at different pH: pH 5.5 (blue solid line —), pH 6.0 (green dashed line - -), pH 6.5 (red dashed line - -), pH 7.0 (cyan dashed line - - -), pH 7.5 (magenta dashed line – – –), and pH 8.0 (yellow solid line —)

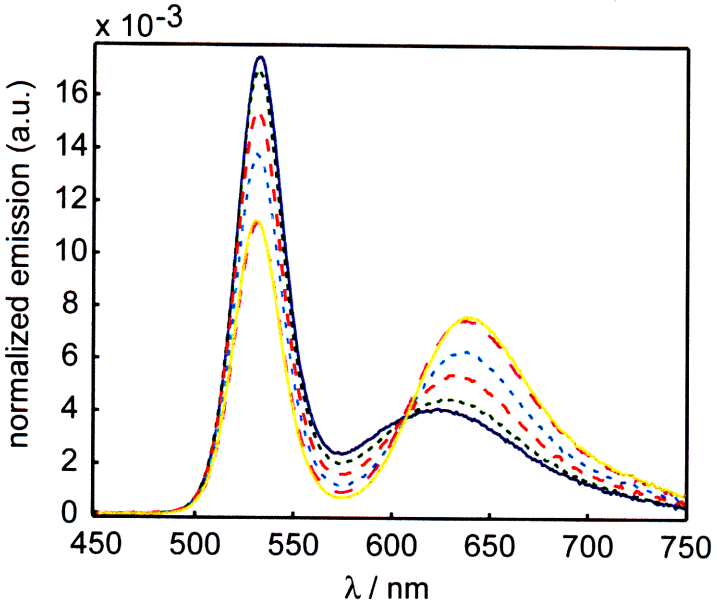

Figure V.4 Emission spectra (λ_{ex}= 365 nm) of PEGylated NC-SNARF5F construct at different pH: pH 5.5 (blue solid line —), pH 6.0 (green dashed line - -), pH 6.5 (red dashed line - -), pH 7.0 (cyan dashed line - - -), pH 7.5 (magenta dashed line – – –), and pH 8.0 (yellow solid line —)

one-photon excitation, and the isosbestic point that is shown in the spectra originates from the two emissive forms of SNARF-5F. As discussed in Chapter I, the isosbestic point will cease to exist under two-photon excitation due to a change in the absorption cross-sections of the two protonated and deprotonated forms of the dye.[6] The presence of the NC is necessary in two ways: 1) as a ratiometric partner and 2) as a FRET antenna. Point 2 is significant under two-photon excitation because very few molecules have a high two-photon absorption cross section as a NC, which may be as high as 10^5 GM. The antenna effect is demonstrated in photoluminescent excitation (PLE) spectra of a sensor with a SNARF to NC ratio of 1.6, shown in Figure V.5. Comparison of the PLE spectra at different pH values between the SNARF-5F and the NC-coupled SNARF-5F reveals a significant difference in the emission intensity at high energy excitation wavelengths, between 300 - 450 nm. The PLE of the NC-coupled SNARF-5F shows that the SNARF emission intensity is actually *higher* when excited at a wavelength where the NC absorbs than when excited at the SNARF absorption maximum, demonstrating an antenna effect. The presence of dye emission when excited at a wavelength when only the NC absorbs is also a very strong evidence of energy transfer, as discussed in previous Chapters.

The NC emission decay rates of the construct (with dye:NC ratio of 1.6:1) and

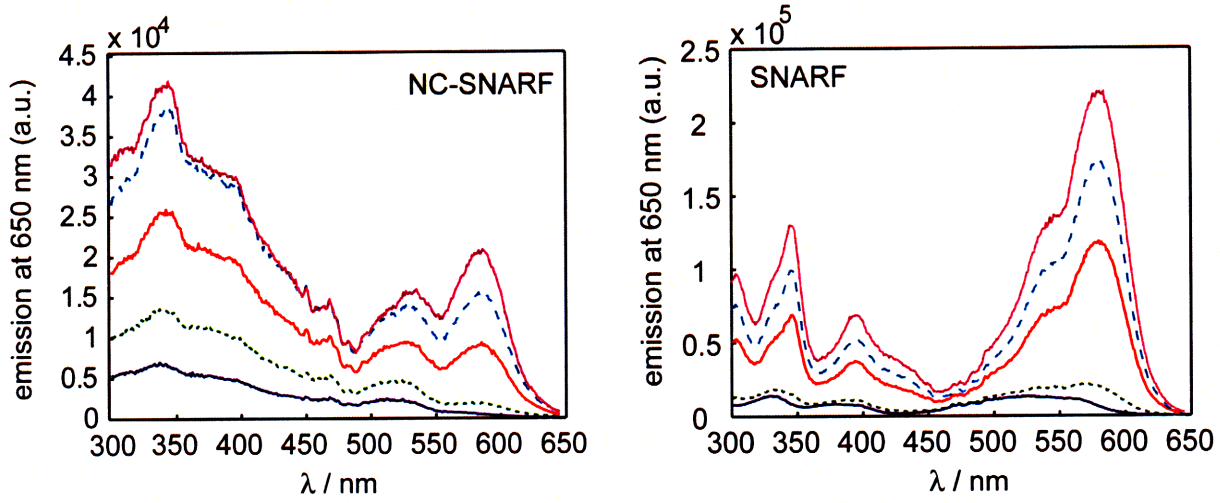

Figure V.5 PLE spectra of (Left) NC-SNARF and (Right) SNARF at λ_{em} = 650 nm at pH 5 (blue solid line —), pH 6 (green dashed line - - -), pH 7 (red solid line —), pH 8 (cyan dashed line – –), and pH 9 (magenta solid line —). The higher intensity in the UV region indicates that the SNARF emission originates from the NC.

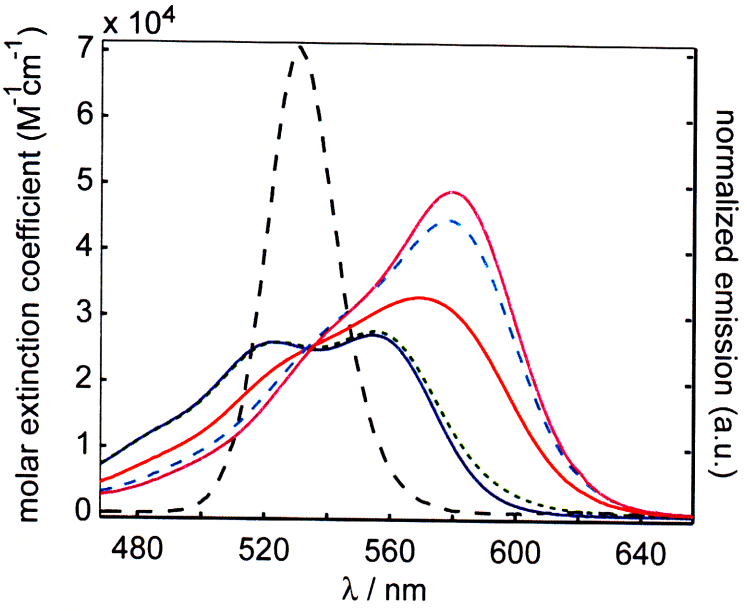

Figure V.6 Overlay of the NC donor emission (black dashed line – –) normalized to unity by area, with the molar absorptivity of the SNARF-5F at pH 5 (blue solid line —), pH 6 (green dashed line - - -), pH 7 (red solid line —), pH 8 (cyan dashed line – –), and pH 9 (magenta solid line —).

unconjugated NC at pH 6 were measured through time-resolved fluorescence spectroscopy. The lifetimes were obtained by fitting the curves as a bi-exponential decay, in accordance with prior literature.[7,8] The longer lifetime component was used for FRET analysis. The lifetime of the uncoupled CdSe/CdZnS NC was τ_D = 15 ns, whereas the lifetime of the NC-SNARF-5F construct was τ_D = 9 ns. From eq. I.9, the efficiency of the NC FRET was calculated to be 40% at pH 6. The critical transfer distance, R_0, was calculated for all pH values and ranged from 44 - 45 Å. Figure V.6 shows the spectral overlap between the donor emission and the acceptor absorbance. The small change in the R_0 distance when using a 532 nm emitting donor with a 21% quantum yield is likely due to the donor emission overlapping in a region where the SNARF-5F isosbestic point occurs. Therefore, the change in the spectral overlap is reduced, and the change in R_0 distance reflects that of the overlap. Using eq. I.10 the average donor-acceptor distance was calculated to be 51 Å, which is consistent with the H_D obtained from the GFC (10.9 nm). The rate of energy transfer for this system was calculated to be 2.8 x 10^7 s^{-1} using eq. I.7.

In order to test the efficacy of the NC-SNARF 5F construct for biological

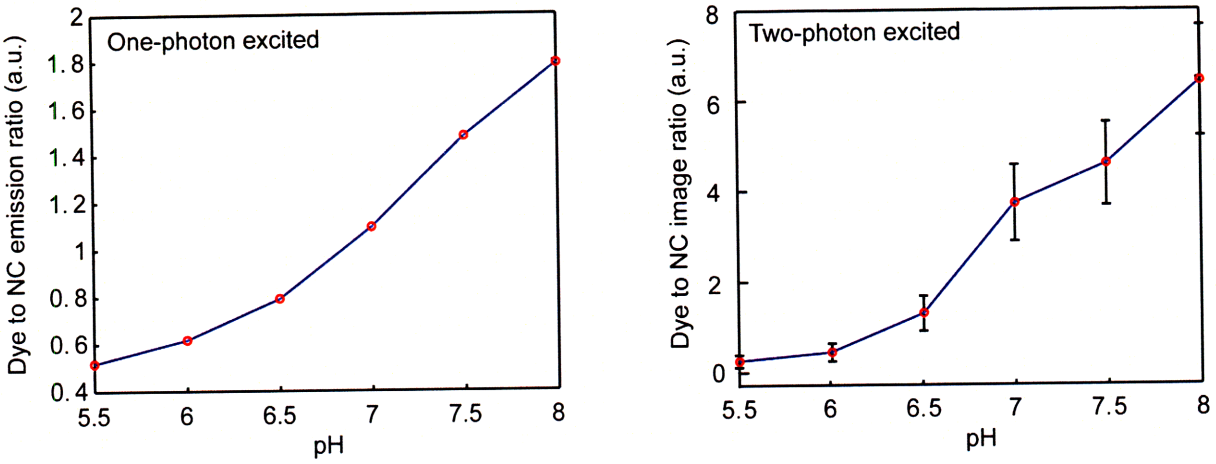

Figure V.7 Comparison of the ratios of dye emission to NC obtained under one-photon excitation (λ_{ex} = 365 nm) versus two-photon excitation (λ_{ex} = 800 nm) of a NC-SNARF construct with a dye to NC ratio of 6.5.

applications, the sensor response was monitored under two-photon excitation. One and two-photon image calibration data in phosphate buffers is shown in Figure V.7. The dye to NC ratio shows a monotonic increase as the pH is increased, consistent with observations from one-photon excitation data. As the pH sensing capability of the NC-SNARF 5F construct was demonstrated successfully in phosphate buffers under two-photon excitation, experiments in biological systems can now be pursued.

V.2.d Stability

The stability of ligand-exchanged NCs is always a concern. Although the use of dithiol as the metal-coordinating moiety afforded extra stability compared to the use of monothiols,[9,10] any type of ligand-exchanged NCs are susceptible towards dissociation.[11] In order to measure the stability of the NC:dye signal over time, the ratios of the NC:dye emissions of the same construct were measured five days apart and compared. Figure V.8 shows the comparison of ratios from pH 6.0 to pH 7.5. In general, the change in ratio of dye to NC emission increased over time, and was enhanced as the pH was lowered. The NC emission is quenched relative to the dye emission, which is consistent with ligand dissociation from the NCs. At pH 7.5, the change in the ratio was 9%, while at pH 6.0, the ratio changed 36%. Given the difficulties of chemically characterizing the exact nature of the ligand association to the surface of the NCs, the

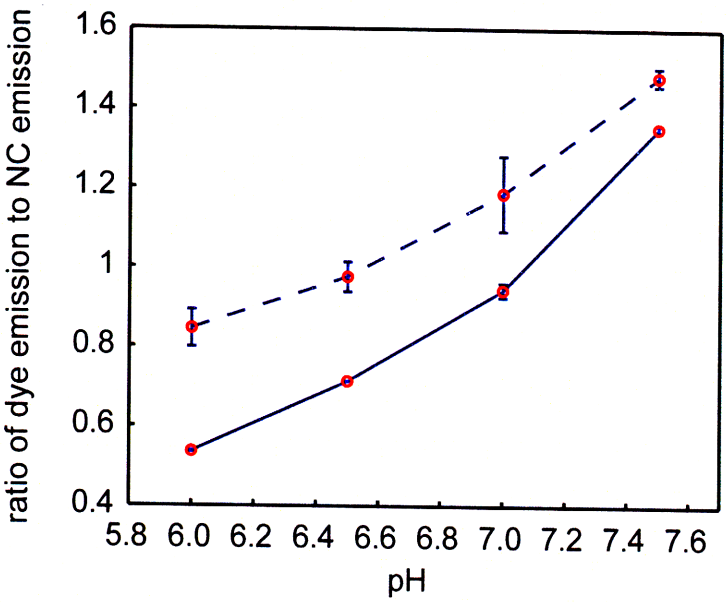

Figure V.8 The ratio of dye to NC area. Measurement made on the day the construct was synthesized (blue solid line —) and five days later (blue dashed line – –). The dye to NC ratio increases over time.

mechanism of dissociation can only be speculated; one hypothesis is that the pH dependence on stability is governed by protonolysis as a pathway for dissociation. It is possible that the coordination of the ligand to the NC surface is through a thiolate datively coordinating to the Zn surface. Protonating the thiolate may enhance dissociation. In addition, the ligand dissociation from the NCs seems to mirror the stability of the dye, as SNARF-5F is more soluble in basic pH. It is possible that the SNARF-5F has an effect on the ligand dissociation of the NCs at different pH. These results suggest that the sensor must be used for measurements within a day of synthesis. Alternatively, the sensor can be calibrated daily or stored in a solution of free DHLA-PEG ligand or dithiothreitol (DTT) to preserve the stability of the sensor, as shown in other systems.[12]

V.3 Concluding Remarks

The first generation bio-compatible sensor was synthesized using a 20:80 molar ratio of DHLA-derivatized amino/hydroxy PEG ligand-coated NCs with covalent SNARF-5F attachment. A dye to NC ratio of 2 to 6 was achieved by preparing and isolating the reactive SNARF-5F NHS-ester. The photoluminescence excitation data illustrated the

NC antenna effect towards enhancing the emission of the dye through the enhanced UV absorption in the conjugate. The pH sensing response also remained active under two-photon excitation, which is critical for biological study. While the stability of the construct is a concern, this first generation design affords sufficient stability for biological study. With a compact, well-characterized NC-SNARF-5F sensor in hand, initial biological experiments can be pursued, the subject which is the focus of Chapter VI.

V.4 Experimental Procedures

V.4.a Materials and Methods

Trioctylphosphine oxide (90%, TOPO), cadmium oxide (CdO), *N*-hydroxysuccinimide (NHS), thioctic acid, thionyl chloride, sodium azide, triphenylphosphine, sodium bicarbonate, dicyclohexylcarbodiimide (DCC), 4,4'-dimethylaminopyridine (DMAP), basic Al_2O_3 (150 mesh), and anhydrous *N,N'*-dimethylformamide (DMF) were purchased from Sigma-Aldrich. 1-Tetradecylphosphonic acid (98%, TDPA), n-hexylphosphonic acid (HPA), dimethylcadmium ($CdMe_2$) and selenium shot were purchased from Alfa Aesar. Trioctylphosphine (TOP) and sodium borohydride ($NaBH_4$) was obtained from Strem Chemicals. Poly(ethylene glycol) 400, bis(trimethylsilyl)sulfide [$(TMS)_2S$] and diethylzinc ($ZnEt_2$) were obtained from Fluka. SNARF-5F (-and -6) carboxylic acid and Cascade Blue 500 kDa dextran was purchased from Molecular Probes, a division of Invitrogen. Silica gel for chromatography (60 Å, 230 - 400 mesh) was obtained through Whatman. All materials were used as purchased, except for TOPO, which was purified through vacuum distillation, and diethylzinc, which was passed through a 0.2 μm syringe filter before use. All air sensitive materials were handled in an Omni-Lab VAC glove box under dry nitrogen atmosphere with oxygen levels <0.2 ppm. Centrifugal filters equipped with a 50,000 Da molecular weight cutoff (MWCO) dialysis membrane were purchased through Millipore Corporation. Glass microslides were obtained from VitroCom. Broadband filters and dichroics were obtained from Chroma Technologies.

V.4.b Spectroscopic Characterization

UV-vis spectroscopy of SNARF coupled CdSe/ZnS were measured on a Hewlett-Packard 8453 UV-vis spectrophotometer. The samples were diluted in appropriate standard pH phosphate buffers for pH 6 - 8 and borate buffer for pH 9. Steady-state fluorescence measurements were obtained in a 1 cm pathlength cuvette from a custom-built Photon Technology Instruments fluorometer installed with a Hamamatsu R928 photomultiplier tube and a 150 W Xe excitation lamp. Gel filtration chromatography (GFC) was performed on an Akta Prime system (GE) with a Superose 6 crosslinked dextran column. The hydrodynamic radii of NCs and conjugates were estimated by comparing the elution volumes to those of protein molecular weight standards (Bio-Rad). Time resolved emission measurements for the NCs, collected at room temperature in a 1 cm path length cuvette, were made with a chirped-pulse amplified Ti:Sapphire laser system using the frequency doubled (400 nm) pump light provided by a Ti:sapphire laser system (100 fs pulsewidth) and collected on a Hamamatsu C4334 Streak Scope streak camera as previously described.[13] Lifetime data was fitted as a bi-exponential decay using Origin 6.0. All NMR spectra were collected at the MIT Department of Chemistry Instrumentation Facility (DCIF) on a Varian Inova 500 MHz NMR Spectrometer at room temperature. Chemical shifts are reported using the standard δ notation in ppm and are referenced to tetramethylsilane (TMS) using the residual ^1H signal of the deuterated solvent, $CDCl_3$, as an internal standard. IR Spectra of samples were collected on a Perkin-Elmer 2000 FTIR Spectrometer.

Two-photon laser scanning microscopy (MPLSM) was performed in collaboration with Rakesh Jain's group in the Edwin L. Steele Laboratories for Tumor Biology, Department of Radiation Oncology at the Massachusetts General Hospital and Harvard Medical School. All spectral measurements were taken on a custom-built multiphoton laser scanning microscope (MPLSM) with the emission output fiber-coupled to a spectrometer. Multiphoton excitation was performed by a Broadband MaiTai diode pumped Ti:Sapphire laser (Spectra-Physics) using 800 nm light at sample powers ranging from 10-60 mW. All measurements were made with the MRC 600 Bio-Rad MPLSM scan-head parked versus scanning on a Zeiss Axioskop20 microscopy using a

Zeiss X20/0.5NA water objective. Fluorescence emission was coupled into a 100-micron core fiber bundle after passing through a 720 nm short-pass filter. Spectra of the fiber-coupled emission were collected on a Shamrock 303 spectrograph with Newton DU-420 CCD detector system (Andor Technology) using a 100 micron slit opening and 1-second detector integration. Emission spectra were analyzed in MATLAB. Imaging was performed on an Olympus Fluoview 300 Laser Scanning Microscope modified with a MaiTai laser (Spectra-Physics). NC-SNARF solutions were prepared in potassium phosphate buffers and placed in 0.1 × 1 mm inner diameter glass microslides attached to a standard microscope slide. All images were taken at 800 nm with excitation powers of 40 mW. Non-descanned fluorescence emission was detected by Hamamatsu HC125-02 PMTs. Descanning the emission to remove out-of-plane fluorescence (essential in most laser scanning microscopies) is unnecessary in MPLSM as all of the emission comes from a focal point. Nanocrystal and dye fluorescence was directed to separate PMTs using a 565 nm-shortpass dichroic. The NC and dye channels were further selected using 660/50 nm and 535/40 nm AR-coated broadband filters, respectively. Image stacks (512 × 512 pixels and 5-micron z-step) were collected throughout the 100 micron pathlength of the microslide for each calibration sample using an Olympus ×20/0.95 NA water objective. Image analysis was performed using NIH ImageJ. Briefly, average intensity projections for each stack were created and converted to 32-bit. The dye channel was divided by the NC channel. The pixel average and standard deviation of the ratiometric image were used to create a pH calibration curve.

A dorsal skinfold window chamber model was prepared on 8-10 week old male SCID mice as previously described.[14] After recovery a small piece of LS174T human colorectal adenocarcinoma tumor (~1 mm diameter) from a serially passaged subcutaneous in vivo source from the same murine background is implanted in the center of the chamber. At 1 - 2 weeks time the tumor in the chamber is of appropriate size for experiments (~ 4 mm diameter). All mice are bred and maintained in a defined-flora animal colony located at the Steele Laboratory. Cascade blue ~500 kDa dextran (10 mg/mL) was tail-vein injected at time 0. After 17 minutes post-injection of the cascade blue dextran, 0.2 mL of 10% aminoPEG/90% hydroxyPEG 555 nm emitting NCs were injected. Five data points in the tumor were taken starting 30 minutes post-

injection, and spectra were integrated for 2.5 seconds.

V.4.c Synthesis of TA-AminoPEG 400

Bis(amino)PEG 400 and thioctic acid-NHS ester (TA-NHS) was prepared through literature methods.[3] TA-AminoPEG 400 was synthesized according to modified literature procedures.[3] A solution of TA-NHS (2.37 g, 7.8 mmol) in 10 mL DMF was added dropwise to a solution of bis(amino)PEG 400 (24.87 g, 62 mmol) and sodium bicarbonate (3.61 g, 43 mmol) in a 1:1 mixture of DMF:H_2O (60 mL) at 4 °C. The reaction was allowed to warm to room temperature after 1 hour and stirred overnight to yield a cloudy yellow solution. The product was filtered to remove byproducts and the solvent from the filtrate was removed to yield a yellow paste, to which 30 mL of H_2O was added. The product was extracted with chloroform (3 x 30 mL), washed with water (3 x 30 mL), dried over sodium sulfate, and filtered. The solvent was removed under reduced pressure to yield a yellow oil. The crude product was purified by chromatography using a basic alumina stationary phase and CH_2Cl_2/MeOH (97:3) as the eluent until the bis-TA PEG 400 was removed. Then CH_2Cl_2/MeOH (92:8) was used as the eluent until the product was collected. Removal of solvent under reduced pressure yielded the product as a yellow oil (1.86 g, 40%). ^{1}H NMR (500 MHz, $CDCl_3$): δ (ppm) 4.22 (m, 2H), 3.72-3.60 (m, 36 H), 3.10 (m, 2H), 2.86 (t, J=5.2 Hz, 2H), 2.40 (m, 1H), 2.35 (t, J=7.5 Hz, 2H), 1.92-1.88 (m, 1H), 1.70-1.65 (m, 4H), 1.51-1.40 (m, 2H).

V.4.d Synthesis of DHLA-AminoPEG 400

DHLA-AminoPEG 400 was synthesized according to modified literature procedures.[3] To a solution of TA-aminoPEG (1.74 g, 3.0 mmol) in a 3:1 ethanol:water mixture (20 mL) at 4 °C, $NaBH_4$ (0.337 g, 9.0 mmol) was added slowly. The solution was stirred for 2 h, warmed to room temperature, acidified with 1.26 M HCl (5 mL), then extracted with chloroform (3 x 20 mL). The combined organic extracts were washed with H_2O (3 x 20 mL), dried over Na_2SO_4, and filtered. The solvent was evaporated to yield a cream colored oil (1.23 g, 70%). ^{1}H NMR (500 MHz, $CDCl_3$): 3.95 (m, 2H), 3.80-3.61 (m, 36 H), 3.48 (m, 4H), 3.21 (m, 2H), 2.92 (m, 2H), 2.71 (m, 2H), 2.29 (m, 2H), 2.04-1.40 (m, 9H).

V.4.e Synthesis of TA-HydroxyPEG 400

The TA-hydroxyPEG 400 ligand was prepared by a modified literature method.[1] PEG 400 (48.47 g, 121 mmol) was degassed at 80 °C for 1 h to remove residual water. After cooling to room temperature, anhydrous CH_2Cl_2 (200 mL) was added along with thioctic acid (2.5 g, 12.1 mmol) and 4,4′-dimethylaminopyridine (DMAP, 0.44g, 3.7 mmol) and stirred vigorously. The yellow solution was cooled on an ice bath, and a solution of DCC (2.75 g, 133 mmol) dissolved in 10 mL CH_2Cl_2 was slowly added dropwise. The reaction was allowed to warm up and stirred overnight. The dicyclohexylurea byproduct was removed by vacuum filtration. The organic layer was washed with H_2O (3 x 50 mL), then washed with brine (3 x 50 mL), dried with Na_2SO_4, and filtered. Removal of organic solvent yielded the crude product as a yellow oil. The product was purified through flash chromatography with silica as the stationary phase and with CH_2Cl_2/MeOH (98:2) until the bis-TA PEG 400 was removed, followed by CH_2Cl_2/MeOH (90:10) as the eluent until the mono-substituted TA-PEG 400 product was collected. Removal of solvent yielded the product as a yellow oil (4.06 g, 57%). ^{1}H 4.10 (t, *J*=4.8 Hz, 2 H), 3.55 (m, 36H), 3.02 (m, 2H), 2.50 (s, 1H), 2.33 (m, 1H), 2.23 (t, *J*=7.4 Hz, 2H), 1.80 (m, 1H), 1.54 (m, 4H), 1.34 (m, 2H).

V.4.f Synthesis of DHLA-HydroxyPEG 400

$NaBH_4$ (0.784 g, 20.7 mmol) was added slowly to a solution of TA-hydroxyPEG (4.06 g, 6.9 mmol) in a 3:1 ethanol:water mixture (20 mL) at 4 °C. The solution was stirred for 2 h, warmed to room temperature, acidified with 1.26 M HCl. The pH was increased to ~7 with addition of 0.2 M NaOH. The product was then extracted with chloroform (3 x 20 mL). The combined organic extracts were washed with H_2O (3 x 20 mL), dried over Na_2SO_4, and filtered. The solvent was evaporated to yield a colorless oil (3.27 g, 80%). ^{1}H NMR (500 MHz, $CDCl_3$): 4.16 (t, *J* = 4.8 Hz, 2H) 3.63 (m, 36H), 3.61 (m, 30 H), 2.92 (m, 1H), 2.73 (m, 3H), 2.36 (t, *J*= 7.5 Hz, 2H), 1.90 (m, 1H), 1.79-1.39 (m, 7H), 1.35 (t, *J*=8 Hz, 1H), 1.30 (d, *J* =7.5 Hz, 1H).

V.4.g Synthesis of CdSe/CdZnS Nanocrystals (λ_{em} = 528 nm)

CdSe NCs overcoated with alloyed CdZnS were prepared by a modified literature method.[15,16] Briefly, CdO (0.128 g, 1.0 mmol), TDPA (0.418 g, 1.5 mmol) and TOPO (6 g, 15.5 mmol) was loaded into a degassed 3-necked flask and heated to 320 °C. Upon generation of a clear, colorless homogenous solution, the temperature was lowered to 270 °C and 1.5 M TOPSe (5 mL, 7.5 mmol) was rapidly injected into the flask. The resulting solution was heated at 220 °C until the first absorption feature of the core CdSe NCs was 494 nm. The NCs were subsequently overcoated by injecting a hexane solution of the bare CdSe (prepared by size selected precipitation from the original growth solution) into a degassed solvent of TOPO (10 g, 25.9 mmols) and HPA (0.4 g, 2.4 mmols,). Hexane was removed *in vacuo* at 80 °C from the CdSe cores, to which decylamine (0.5 mL, 2.6 mmols) was added and stirred for 2 hours. Using a syringe pump, two separate solutions of $(TMS)_2S$ in 5 mL TOP and a 98:2 molar ratio of diethylzinc (109.8 mg, 0.89 mmol) and dimethylcadmium (2.58 mg, 18 μmol) in 5 mL TOP were slowly dripped into the CdSe solution at 130 °C over the course of two hours. Exact amounts were chosen to yield a ~3 monolayer coating of ZnS on the bare CdSe NCs, using the methods of Dabboussi *et al.*[16] NC was found to have a FWHM = 26 nm and a quantum yield of Φ = 43% in hexanes after one precipitation from the growth solution, compared with the reference, rhodamine 560, which was taken to be 0.95 in ethanol. The first absorption feature was found to be 514 nm.

V.4.h Synthesis of Cap-exchanged Water Solubilized NCs

The CdSe/CdZnS synthesized in section V.4.g (0.5 mL) was precipitated from the growth solution once using a mixture of *n*-butanol and methanol. The supernatant was discarded, and the precipitated NCs were re-dispersed in 0.1 mL $CHCl_3$. In a separate vial, DHLA-hydroxyPEG (100 mg) and DHLA-aminoPEG (125 μL, 20% methanolic solution) were stirred and the solvent evaporated. Under N_2, the chloroform NC solution was injected into the ligand mixture and stirred vigorously. The solvent of the NC-ligand mixture was removed, and the reaction was stirred at 60 °C for three hours. Upon removing the reaction from heat, the ethanol (0.5 mL) and chloroform (1

drop) was added, then the NCs were precipitated from solution with hexanes (1 mL). The supernatant was discarded and the NCs were dried briefly to remove residual solvent. The NCs were then re-dispersed in distilled water and dialyzed twice with 50,000 MWCO centrifugal filters to remove excess ligand. The quantum yield was found to be Φ = 16% in water, compared with the reference, rhodamine 560, which was taken to be 0.95 in ethanol. The final emission in water was found to be λ_{em} = 530 nm.

V.4.i Synthesis of SNARF-5F NHS-ester

SNARF-5F 5(-and-6) carboxylic acid (1 mg, 2.12 μmol) was dissolved in DMF (0.5 mL). Dicyclohexylcarbodiimide (DCC, 2.2 mg, 11 μmol) and *N*-hydroxysuccinimide (NHS, 1.2 mg, 10 μmol) were dissolved in DMF (0.5 mL). The DCC and NHS solution was injected into a vigorously stirring SNARF-5F DMF solution, and the reaction mixture was stirred overnight. The DMF was removed *in vacuo* and purification with flash chromatography, with silica as the stationary phase and CH_2Cl_2/MeOH (95:5) as the mobile phase, yielded a purple solid as a product. R_f = 0.61. ESI-MS *m/z* 569.14 $[M+H]^+$.

V.4.j Synthesis of NC-SNARF 5F pH Sensor

CdSe/ CdZnS water-solubilized NCs as prepared from section V.4.h were dialyzed into pH 8.3 sodium bicarbonate buffer (0.1 M) until the final volume was 2 mL. SNARF-5F NHS-ester (from section V.4.i) was dissolved in DMF (100 μL), injected to a vigorously stirring solution of the water-solubilized NCs, and stirred overnight. The reaction mixture was diluted with 10 mL of distilled water, then dialyzed with 50,000 MWCO centrifugal filters until all residual uncoupled dye was removed, as measured from the absorbance of the filtrate. The NC-SNARF pH sensor was characterized by UV-visible and emission spectroscopy in phosphate buffers for pH 6-8 and in borate buffer for pH 9.

V.5 References

1. Uyeda, H. T.; Medintz, I. L.; Jaiswal, J. K.; Simon, S. M.; Mattoussi, H. *J. Am. Chem. Soc.* **2005**, *127*, 3870-3878.

2. Zimmer, J. P.; Kim, S. W.; Ohnishi, S.; Tanaka, E.; Frangioni, J. V.; Bawendi, M. G. *J. Am. Chem. Soc.* **2006**, *128*, 2526-2527.

3. Liu, W.; Howarth, M.; Greytak, A. B.; Zheng, Y.; Nocera, D. G.; Ting, A. Y.; Bawendi, M. G. *J. Am. Chem. Soc.* **2008**, *130*, 1274-1284.

4. Susumu, K.; Uyeda, H. T.; Medintz, I. L.; Pons, T.; Delehanty, J. B.; Mattoussi, H. *J. Am. Chem. Soc.* **2007**, *129*, 13987-13996.

5. Gunsalus, I. C.; Barton, L. S.; Gruber, W. *J. Am. Chem. Soc.* **1956**, *78*, 1763-1766.

6. Baker, G. A.; Munson, C. A.; Bukowski, E. J.; Baker, S. N.; Bright, F. V. *Appl. Spectrosc.* **2002**, *56*, 455-463.

7. Snee, P. T.; Somers, R. C.; Nair, G.; Zimmer, J. P.; Bawendi, M. G.; Nocera, D. G. *J. Am. Chem. Soc.* **2006**, *128*, 13320-13321.

8. Clapp, A. R.; Medintz, I. L.; Mauro, J. M.; Fisher, B. R.; Bawendi, M. G.; Mattoussi, H. *J. Am. Chem. Soc.* **2004**, *126*, 301-310.

9. Aldana, J.; Wang, Y. A.; Peng, X. *J. Am. Chem. Soc.* **2001**, *123*, 8844-8850.

10. Medintz, I. L.; Uyeda, H. T.; Goldman, E. R.; Mattoussi, H. *Nat. Mater.* **2005**, *4*, 435-446.

11. Aldana, J.; Lavelle, N.; Wang, Y.; Peng, X. *J. Am. Chem. Soc.* **2005**, *127*, 2496-504.

12. Liu, W.; Choi, H. S.; Zimmer, J. P.; Tanaka, E.; Frangioni, J. V.; Bawendi, M. *J. Am. Chem. Soc.* **2007**, *129*, 14530-14531.

13. Damrauer, N. H.; Hodgkiss, J. M.; Rosenthal, J.; Nocera, D. G. *J. Phys. Chem. B* **2004**, *108*, 6315-6321.

14. Leunig, M.; Yuan, F.; Menger, M. D.; Boucher, Y.; Goetz, A. E.; Messmer, K.; Jain, R. K. *Cancer Res.* **1992**, *52*, 6553-60.

15. Peng, Z. A.; Peng, X. *J. Am. Chem. Soc.* **2001**, *123*, 183-184.

16. Dabbousi, B. O.; Rodriguez-Viejo, J.; Mikulec, F. V.; Heine, J. R.; Mattoussi, H.; Ober, R.; Jensen, K. F.; Bawendi, M. G. *J. Phys. Chem. B* **1997**, *101*, 9463-9475

Chapter VI

Initial Investigations of NC-based Sensors in an *in vivo* Environment

VI.1 Introduction

A biocompatible NC-based pH sensor was developed and its photophysical properties were characterized in Chapter V. One application for the NC-based sensor is to interrogate the metabolic profile of tumors during the normalization window that was hypothesized by Jain and co-workers, as discussed in Chapter I.[1-3] Obtaining information on pH, O_2, and glucose concentrations is essential to determining the appropriate tumor treatment. Before the NC sensor can be properly applied for *in vivo* study during tumor treatment, the sensor response must be investigated in a biological medium that approximates the tumor microenvironment (i.e. albumin or *ex vivo* tumor tissue samples). This Chapter focuses on the collaborative work among the Nocera, Bawendi and Jain research labs to incorporate the pH sensors described in Chapter V into a biological environment. Comparisons between one- and two-photon excitations, challenges with calibration, and detection of pH changes in biological media are discussed in this Chapter.

VI.2 Results and Discussion

VI.2.a Calibration

The importance of calibration was discussed in Chapter IV.2.g. In order to probe the efficacy of the sensor in a biological environment, the sensor was placed in 4%

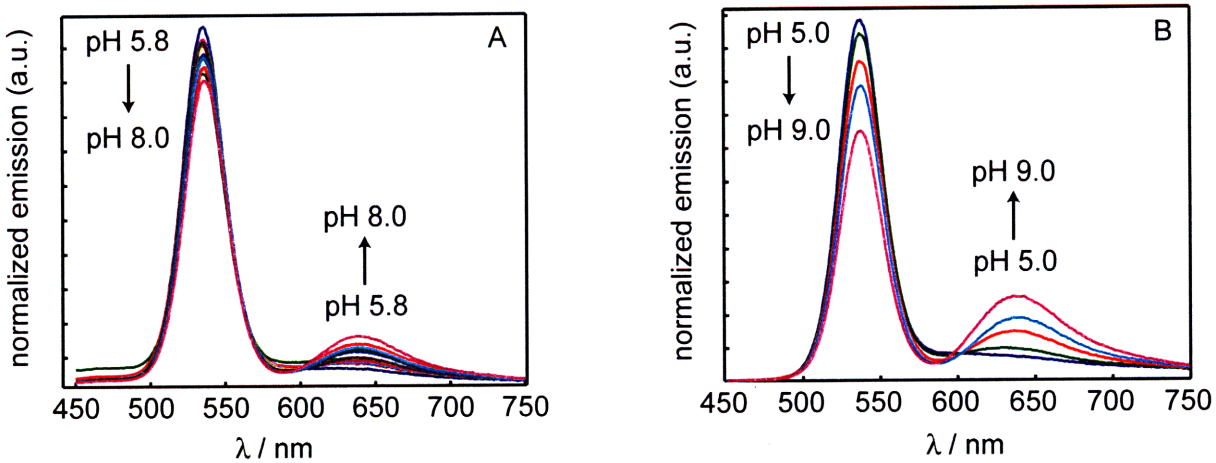

Figure VI.1 Emission profile of the NC-SNARF construct in (A) BSA buffers at 0.2 pH increments and (B) phosphate buffers at 1 pH increments. λ_{ex} = 365 nm.

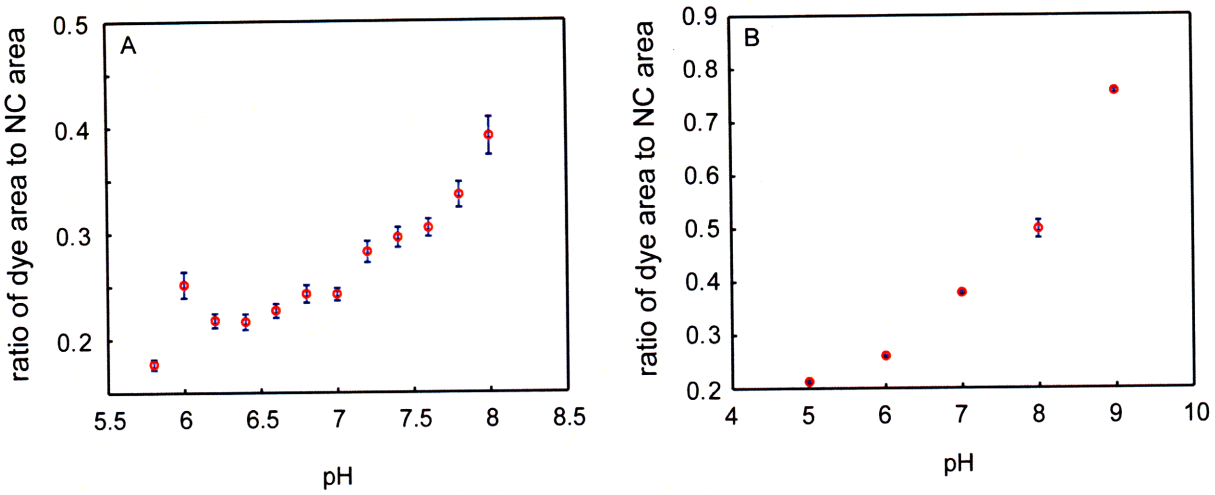

Figure VI.2 Ratio of dye to NC area of NC-SNARF in (A) BSA buffers and (B) phosphate buffers.

bovine serum albumin (BSA) buffers with pH differing in 0.2 pH increments from 5.8 to 8.0. Figure VI.1A shows the emission behavior in BSA buffer of a construct with a typical dye to NC ratio of 1.7. Figure VI.1B is the emission of the same construct in phosphate buffers. Figure VI.2A and VI.B show the calculated ratio of the dye area to the NC area integrated over the same emission wavelengths in BSA and phosphate buffers, respectively. The ratio from pH 6 to 8 ranges from ~0.2 to 0.4 in the case of BSA buffers whereas the ratio changes from approximately 0.25 to 0.5 in phosphate buffer. The comparison of NC to dye ratio in the two buffers demonstrates that the quenching of the SNARF was found not to be as drastic as in the case of the dendritic NC construct described in Chapter IV. The preserved dye emission is most likely due to the PEGylation of NCs, which mitigates nonspecific interactions of the construct in biological environments. The dendritic construct, described in Chapter IV.2.g, may have promoted the interaction of the SNARF-5F with BSA due to the electrostatic attraction of the positively charged NCs to the negatively charged BSA. With a neutral scaffold and the use of poly(ethylene glycol), the emission from the NC-SNARF construct is not as influenced from non-specific binding to its environment.

Figure VI.3 shows the emission of the construct in BSA buffers under two-photon excitation as well as the calibration curve constructed by dividing the integrated NC emission by the integrated SNARF emission. The emission spectral profile is similar,

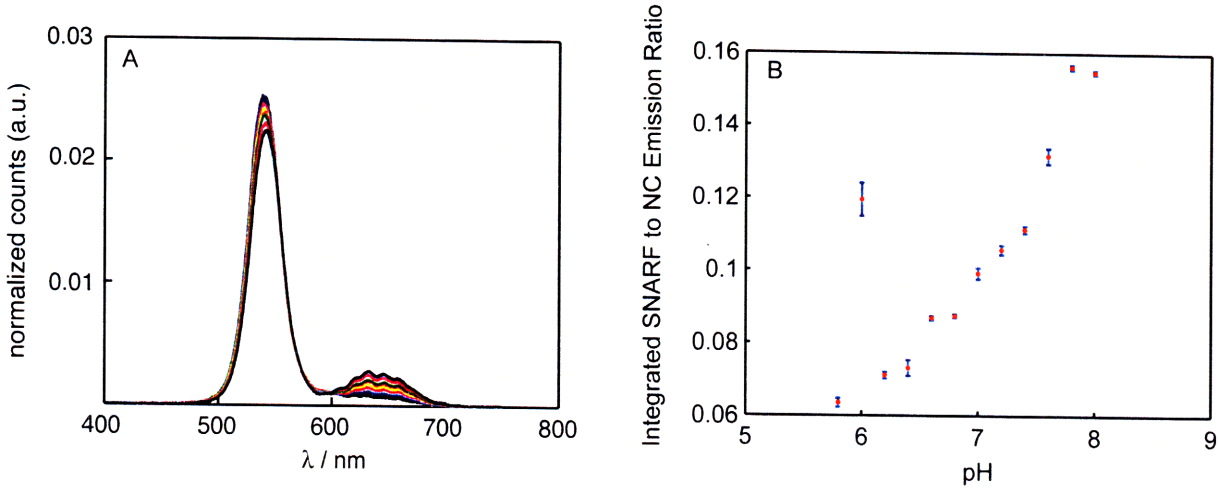

Figure VI.3 (A) Emission profile of NC-SNARF sensor excited at λ_{ex} = 800 nm. (B) Dye to NC area extracted from the emission spectra in (A).

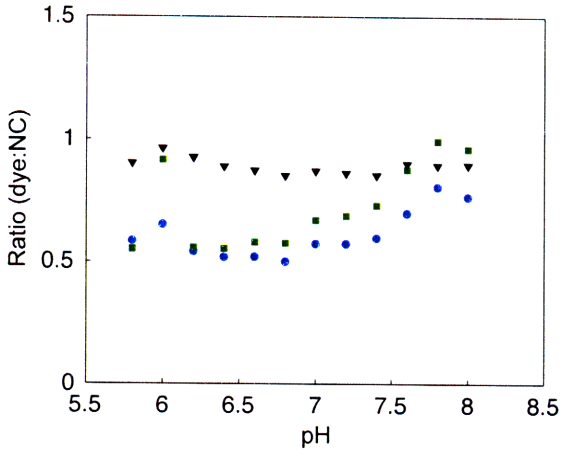

Figure VI.4 Dye to NC ratio obtained through two-photon imaging microscopy. Excitation wavelengths of λ_{ex} = 800 nm (blue circles ●), λ_{ex} = 900 nm (green squares ■), and λ_{ex} = 1000 nm (black triangles ▲).

although a quantitative difference is observed in the ratio under one-photon and two-photon excitation. The difference in ratio is not surprising, as the collection efficiency of the detectors have changed and the variation in relative excitation cross-sections of NC and dye leads to differing direct excitation contribution when moving from one-photon to multi-photon excitation. In both cases, the calibration shows a general monotonic increase in the ratio of dye to NC emission areas (with the exception of pH 6.0, which seemed to have contained an impurity). Finally, a calibration curve was also collected using two-photon laser scanning microscopy imaging. NC and dye fluorescence was directed to two separate PMTs that collected emission at 535 ± 40 nm and 660 ± 50 nm,

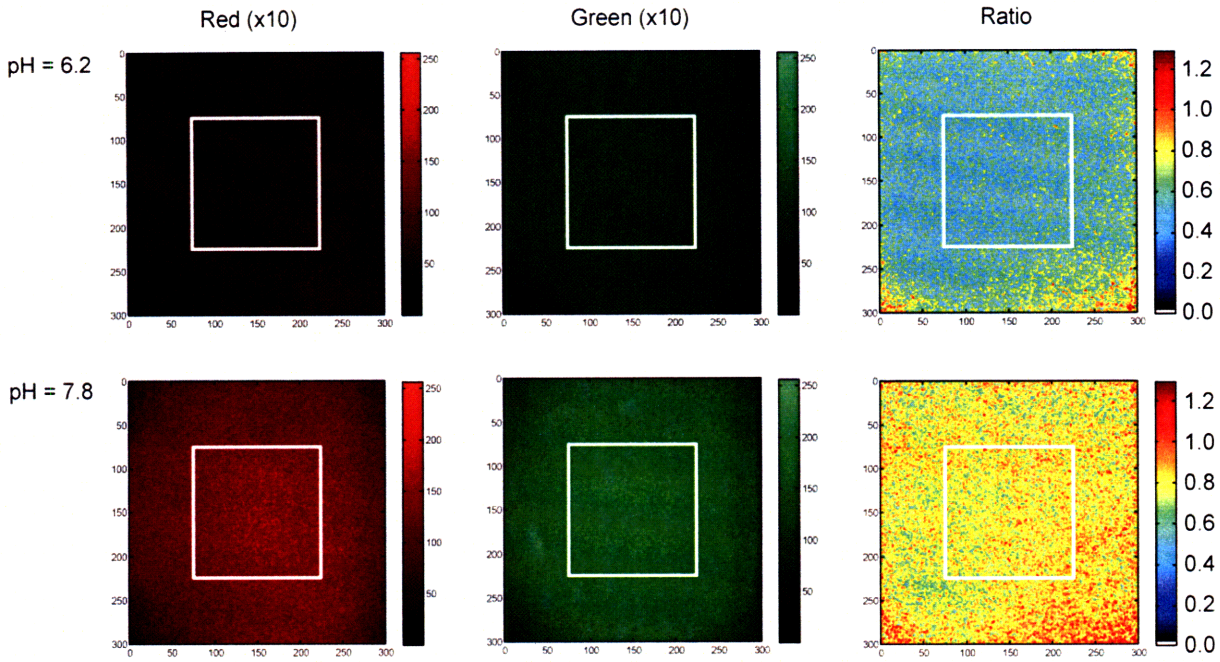

Figure VI.5 Representative images from the image calibration of the NC-SNARF construct at pH 6.2 (Top) and pH 7.8 (Bottom). Separate red (dye) and green (NC) emissions may be collected and the ratio may be taken to yield a calibration image.

and an image of the NC-SNARF 5F construct in BSA buffers were taken at 0.2 pH increments for three different excitation wavelengths (Figure VI.4). When excited at 1000 nm, the signal-to-noise ratio was too low to detect any appreciable change in signal between dye to NC ratio at different pH. Excitation at 800 and 900 nm do show an upward trend with pH as expected, with ratios ranging from approximately 0.5 at pH 5.8 to 0.8 at pH 8. Representative images obtained for pH 6.2 and pH 7.8 are shown in Figure VI.5. The ratio of the images obtained from the channel can be converted into a color map that can be correlated to a specific pH.

With a calibration in hand that describes the behavior of the pH sensor between pH 6 and 8, the sensor was directly microinjected into a LS174T human colon adenocarcinoma tumor intersitium implanted in a mouse outfitted with a dorsal skinfold window chamber model. The sensor was allowed to diffuse in the interstitium over the course of hours, and the NC and SNARF-5F emission from the tumor environment was collected with two different PMTs. Figure VI.6 shows images obtained from the dye channel and the NC channel illustrating that both the dye and the NC are effectively

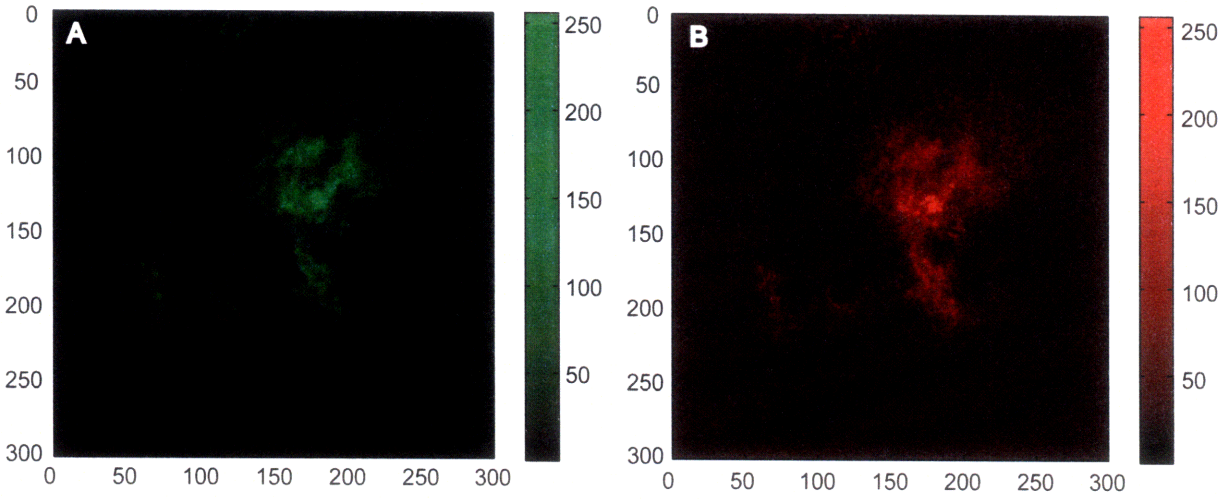

Figure VI.6 (A) Fluorescence image obtained from the green PMT channel. (B) Fluorescence image obtained from the red PMT channel.

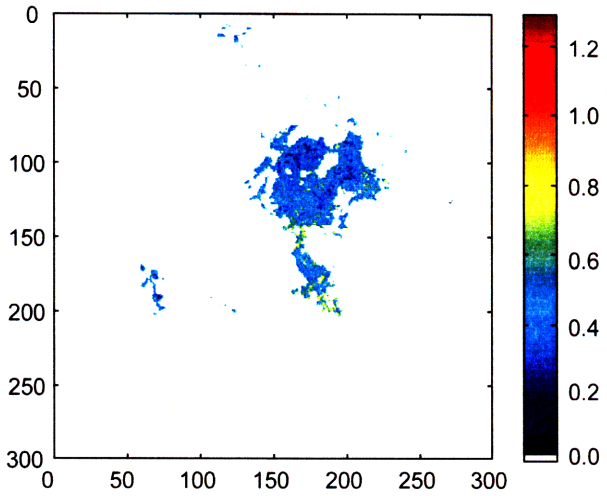

Figure VI.7 Ratio map created from the emissions collected from the two PMT channels.

bright enough to be imaged in the tumor interstitium. The ratio of the two image channels was subsequently taken where only both emission intensities were above background. Figure VI.7 shows a ratio color map of the tumor taken from the two emission intensities. The images can then be calibrated to read a specific pH. The color map indicates a ratio of dye to NC ranging from 0.15 to 0.3. Compared to the ratios obtained from the BSA image calibrations, the ratio of 0.15 ~ 0.3 found in the interstitium is too low, corresponding to a pH of less than 4. Previous reports, using data taken with one-photon microscopy, suggests that the tumor interstitium (without any

external treatment) pH ranges from 6.6 to 7.4 with pH declining as one moves away from the nearest blood vessels.[4,5] One would expect the BSA calibration to span the range of pH found in the tumor environment; however, one report suggests that even under one-photon ratiometric sensing utilizing BCECF, the ratio of two emission intensities varies drastically among PBS buffers, normal tissue environments, and tumor tissue environments.[6] Although the authors only cite intrinsic spectroscopic differences as the cause of the change in ratio between the two different tissue types, an additional confounding factor could be the inhomogeneity of the tumor tissue that could cause scattering or other processes that will skew the ratio between two emission readouts. Therefore, while BSA acts as a sufficient mimic for blood, we find it to be inadequate for use as a calibration environment for tumor tissues.

In order to ensure that a proper ratio signal can be read within tumor tissues, emission from the NC-SNARF construct was probed in a single cell suspension of LS174T tumor tissues. The single cell suspension allows for the sensor to be calibrated in an environment more similar to a live tumor tissue, which includes proteins and possible interfering biomolecules or interfaces, such as cell surface structures. Being chunky, amorphous, and heterogeneous, the tumor suspension provides a highly scattering environment that causes the emission intensity of the same pH to vary

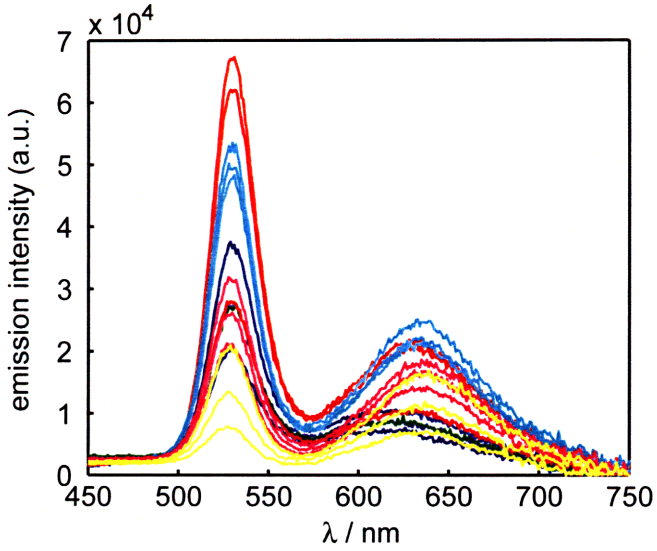

Figure VI.8 Emission of the NC-SNARF construct, excited at λ_{ex} = 365 nm in single-cell tumor suspension. pH 5.5 (blue line —), pH 6.0 (green line —), pH 6.5 (red line —), pH 7.0 (cyan line —), pH 7.5 (magenta line —), and pH 8.0 (yellow line —).

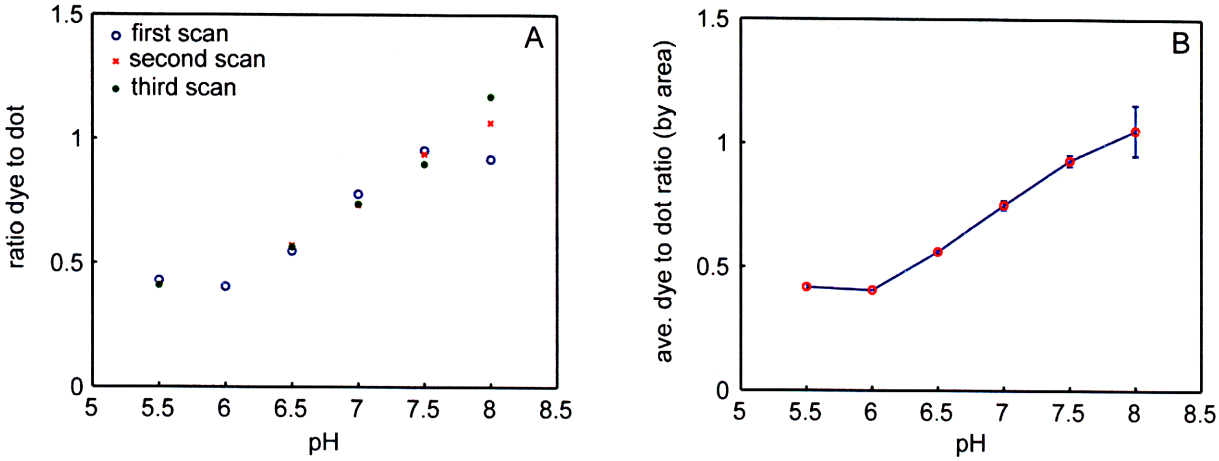

Figure VI.9 (A) Ratio of dye to NC taken from emission spectra shown in Figure VI.8. (B) average of the three different scans of (A) to yield a pH calibration curve.

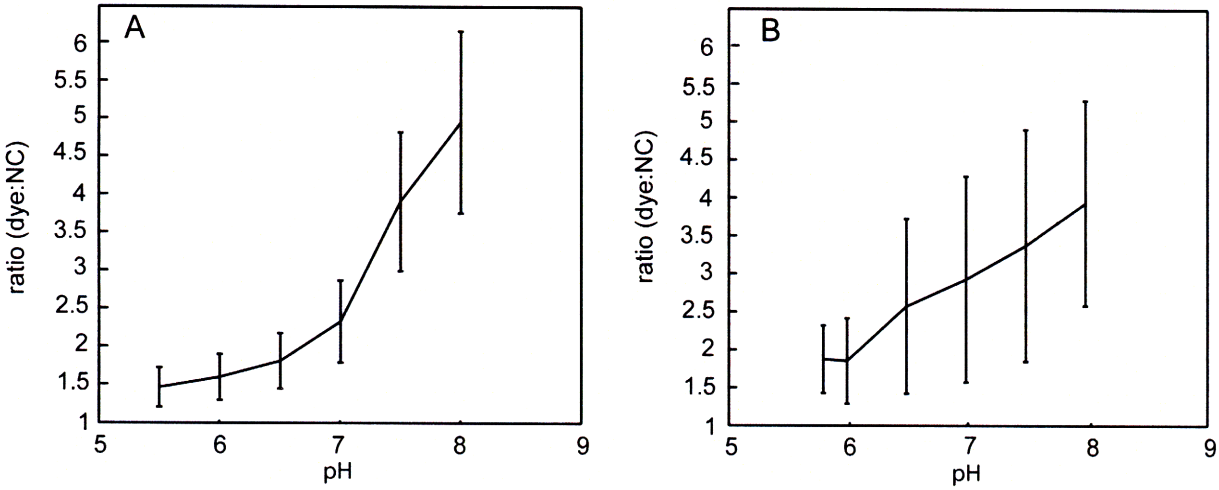

Figure VI.10 Two-photon excited image calibration data in (A) phosphate buffers and (B) *ex vivo* tumor tissues.

significantly, as illustrated in Figure VI.8. Although the intensity fluctuated, the ratio between the dye and NC emissions remained consistent. Figure VI.9 shows the ratio obtained from the emission in Figure VI.8 with three different scans per pH. Averaging the three scans reveal that the pH sensing capability is still conserved in a tumor environment with a monotonic increase of the dye to NC ratio with increasing pH.

A final method of calibration, pursued using *ex vivo* methods, was performed under two-photon excitation. As described by Dellian *et al.,* excised tumor tissue was incubated in phosphate buffers at different pH, then transferred to the same pH buffers mixed in with the NC-SNARF construct. Figure VI.10 shows the comparison of an image based *in vitro* calibration in PBS buffers versus *ex vivo* calibration in tissues. The ratio of

dye:NC varies. This phenomenon is not yet well understood and is most likely due to the heterogeneity of the tumor environment. There is also the possibility that the NC surface is not sufficiently protected, which may lead to nonspecific binding of NCs to tissues altering the emissive properties of the sensor. Stickiness to tissues can be observed in *in vivo* microscopy experiments. It is essential that this first generation NC-SNARF sensor is evaluated in tumor environments before proceeding to designing and refining optimized future generation NC-based sensing constructs.

VI.2.b Monitoring Changes *in vivo*: Initial Experiments

Given that the ultimate goal is the development of the sensors that can monitor changes in the physiological environment during anti-angiogenic therapy, it is essential to measure how effectively the sensor responds to dynamic physiological changes. Hyperglycemia has been shown to increase lactic acid production, as a product of stimulated glycolysis.[7,8] Tail-vein injection of glucose into the bloodstream of a mouse has been shown to lower pH by at least 0.15 pH units[6] and up to 0.3 pH units.[5] Although the sensors developed can distinguish 0.2 pH increments in BSA buffers, we were interested in observing a change in the *ratio* of the pH sensor upon an external stimulant (glucose) in an *in vivo* environment.

An initial experiment probed for the difference in pH in a tumor before and after glucose injection using a single mouse bearing HSTS26T human soft tissue sarcoma.

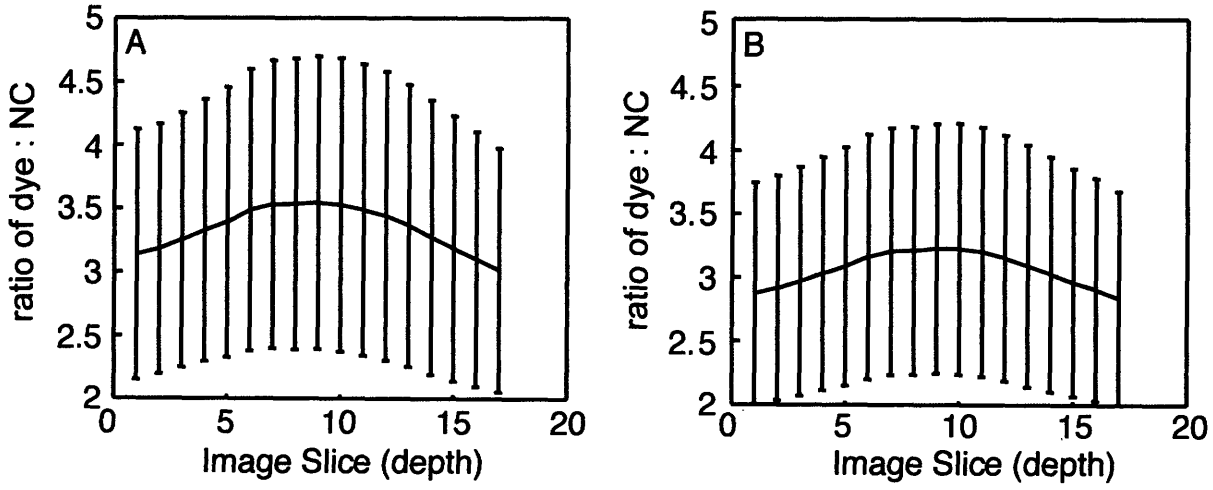

Figure VI.11 Ratio of dye to NC emission (A) pre-glucose injection (B) Five minutes post-glucose injection.

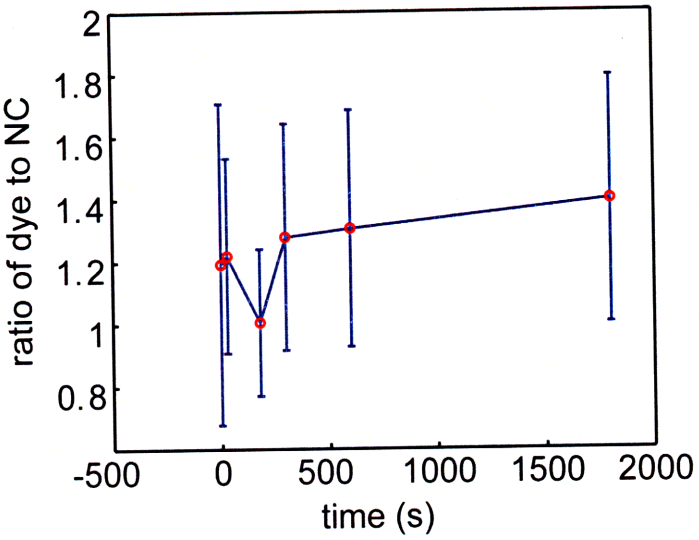

Figure VI.12 Change in the image ratio of the dye to NC PMT channels with respect to time after glucose injection at t = 0 min.

The sensor was microinjected 150 microns below the tumor surface and imaged. Glucose (6g / kg) was tail-vein injected and after waiting for 5 minutes, the tumor with the sensor was imaged again. Figure VI.11 shows the ratio of the image of the two PMT that collected separate dye and NC emissions. While the error bars are high because they represent all of the individual pixel averages, the average ratio of the tumor before glucose injection ranged from 3.0-3.5 and for post-glucose injection, the ratio ranged from 2.8-3.2. Without a proper calibration of the sensor, the actual pH values cannot be extracted; however, the lower dye to NC ratio indicates a more acidic pH. Importantly, the sensor response to external stimulus of a change in pH is exhibited.

The change in the ratio over time after glucose injection was monitored. After tail-vein injecting glucose (6 g/kg) to a mouse bearing a LS174T human colorectal adenocarcinoma, the tumor was imaged in the same location continuously over the course of 30 minutes. Figure VI.12 shows the change in ratio of the NC-dye construct over time. The ratio intensity dropped at approximately three minutes, then returned to normal. The rapid restoration of the pH is somewhat surprising; however, tumor environments are well known to be heterogeneous by nature, and pH response is also widely varied depending on the location of the tumor.[6,8] It is quite possible that a location chosen for the image collection was a spot that responded minimally when a pH change was induced.

In the two initial experiments described above, a dynamic response of the NC-SNARF probe was observed in two different tumor types when hyperglycemia was induced. While the results are encouraging, sensing in a heterogeneous environment *in vivo* requires multiple data points from various location of a single tumor and multiple tumors of the same tissue type to obtain a statistically meaningful average of a tumor pH environment. In addition, a more rigorous indication of success could be obtained through a comparison of pH sensor signal response to injection expected to induce acidosis (glucose) versus benign control (saline). Finally, investigating the differences between tumor tissues and normal tissues is another method to test the efficacy of pH sensor, as normal tissues exhibit average physiological pH (7.2 - 7.3) while tumor tissues are more acidic (pH ~ 6.6 - 6.8).

VI.2.c Monitoring Changes *in vivo*: Glucose versus Saline

VI.2.c.1 Ketamine / Xylazine Anesthetized Mice

Seven mice implanted with LS174T human colorectal adenocarcinoma and one with no tumors (normal mouse tissue) were prepared as dorsal window models. After administration of ketamine / xylazine to render the mice unconscious for study, five of the mice with LS174T tumors were injected with glucose; unfortunately, three of the mice expired during the experiment. The mouse with normal tissue was also injected

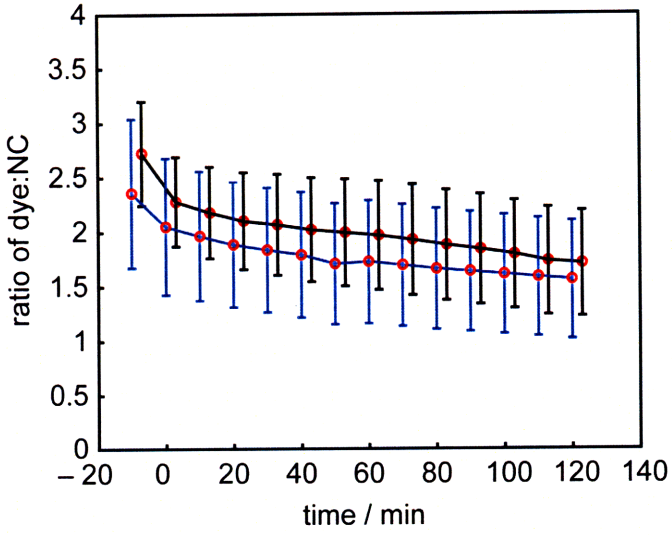

Figure VI.13 Change in dye to NC ratio after glucose injection at t = 0 min in two different locations (blue line — and black line —) of a tumor.

with glucose, and the remaining two mice with LS174T were injected with 6 g/kg of saline solution. All mice were monitored for at least 90 minutes after glucose injection (t = 0 minutes) at 10 minute increments. Figure VI.13 shows a representative plot for the ratio of SNARF to NC emission with respect to time in a glucose injected LS174T tumor in two different locations. Upon injection, the starting ratio drops by approximately 0.5 and continues to drop another 0.3. The drop in the ratio is consistent with a lower metabolic pH. The same experiment was performed on a mouse with normal tissue, and the change of NC:SNARF emission ratio with respect to time in two different tissue locations is exhibited in Figure VI.14. In the normal tissue, the starting ratio is at 5.0, consistent with a higher pH that is exhibited by normal tissues. The ratio drops to 3.0 and slowly starts to rise and return towards the original values after approximately 80 minutes after the glucose administration, which is a behavior that is consistent with prior literature.[6,9] Unfortunately, the mouse expired at 100 minutes after injection.

Figure VI.15 shows the response following saline infusion on the NC-SNARF sensor response in two different locations of the tumor. The ratio continuously dropped from 2.5 to 2.0 over the course of 90 minutes, which is a change similar to that seen following glucose injection. Saline should have no effect on the metabolic pH; therefore, several reasons were postulated for the sensor response.

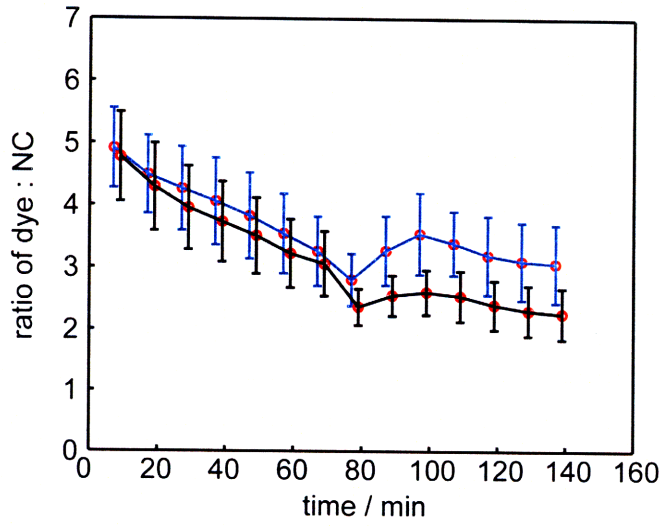

Figure VI.14 Change in dye to NC ratio after glucose injection at t = 0 min in two different locations (blue line — and black line —) in normal tissue.

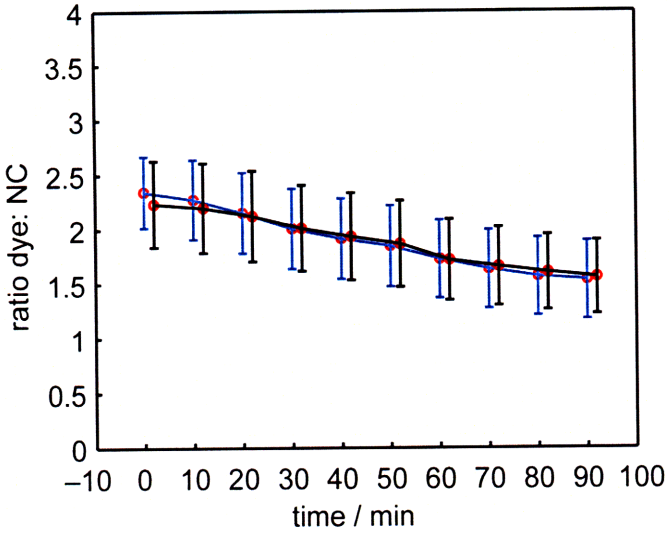

Figure VI.15 Change in dye to NC ratio after saline injection at t = 0 min in two different locations (blue line — and black line —) in tumor tissue.

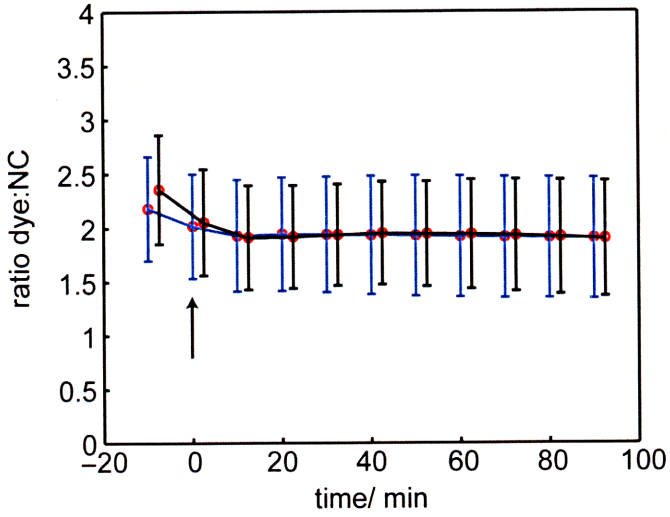

Figure VI.16 Dye to NC ratio after glucose injection at t = 0 min in two different locations (blue line — and black line —) in tumor tissue. The mouse expired at t = 0 min, where the black arrow indicates.

First, photobleaching of the dye would cause the dye to NC emission ratio to go down in all experiments; such photobleaching has been observed under high intensity visible excitation. Second, the ratio of dye to NC would also decrease if the NC-SNARF construct became unstable over time (i.e. dissociation of the dye from the NC due to ligand degradation). Finally, there is a concern that the anesthetic used may affect interstitial pH.

Figure VI.16 shows a 90 minute time trace of a tumor of a mouse that expired immediately upon glucose injection. After the initial drop in the ratio of dye to NC, the ratio remained constant throughout the course of the experiment. This result suggests that the dye is not photobleaching during the 90 minute interval, nor is the construct degrading. We therefore hypothesize that chemical anesthesia may have induced acidosis. Many anesthetics have been reported to lower pH values,[10,11] and ketamine itself has caused acidosis in other animals.[12-14] In order to minimize external pH modification aside from the glucose stimulus, isoflurane gas was chosen for the next set of experiments.[15,16]

VI.2.c.2 Isoflurane Anesthestized Mice

Six mice implanted with LS174T human colorectal adenocarcinoma were prepared, and the NC-SNARF sensor was allowed to superfuse on top of the tumor. Three mice (N = 3) were injected with glucose while the remaining three mice (N=3) were IP injected (into the intraperitoneal cavity) with saline, and the sensor response was monitored at four to five locations of each tumor over the course of 90 minutes. Figure VI.17 shows a representative change after glucose injection in the sensor ratio

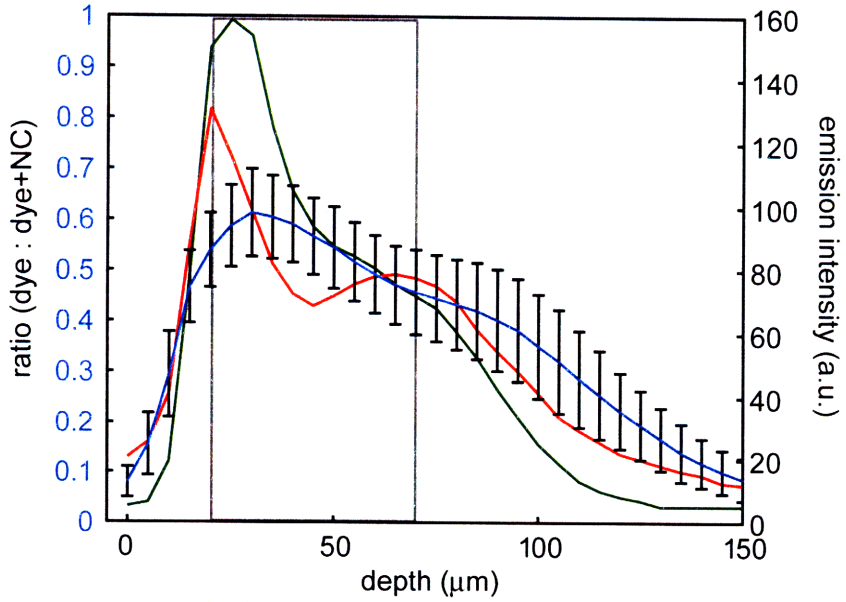

Figure VI.17 Emission intensity of the NC (green solid line —), SNARF-5F (red solid line —), and ratio of SNARF intensity:total intensity (blue solid line —) with respect to depth imaged in a tumor of a glucose injected mouse, at t = 0 min.

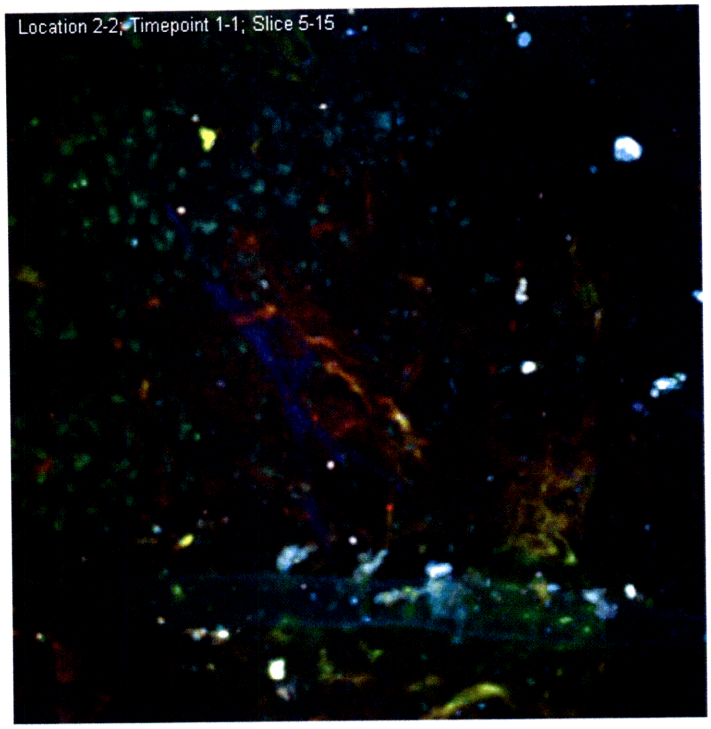

Figure VI.18 Maximum intensity projection image of a tumor superfused with the NC-SNARF sensor at the time of glucose injection. Emissions from all three PMT channels (blue, green, and red) are merged.

with respect to the depth of the tissue imaged, ranging from 0 – 150 microns. Because the signal also depends on the amount of sensor that was actually superfused into the tissue, only sections that exhibited high emission intensity from NC and SNARF were selected for analysis. Images from 20 – 70 micron deep were analyzed, as shown in the grey box in Figure VI.17. An example maximum intensity projected image for one tumor location (20-70 microns deep) of a mouse injected with glucose is shown in Figure VI.18. Emissions collected from all three PMT channels are merged. Cascade blue dextran images the blood vessels with its blue emission. The NC-SNARF construct emission was collected by two different PMTs that selectively detected separate NC and dye emissions, represented by green and red colors in the image. By analyzing the dye and NC emission intensities in the image depth slices of interest, a histogram can be constructed at each time point and the ratio determined, as shown in Figure VI.19. Figure VI.20 is the average ratio and intensities with respect to time, obtained from averaging the values in the histogram at each time point. As shown in Figure VI.20, over the course of 90 minutes after the glucose injection, the average NC emission increases

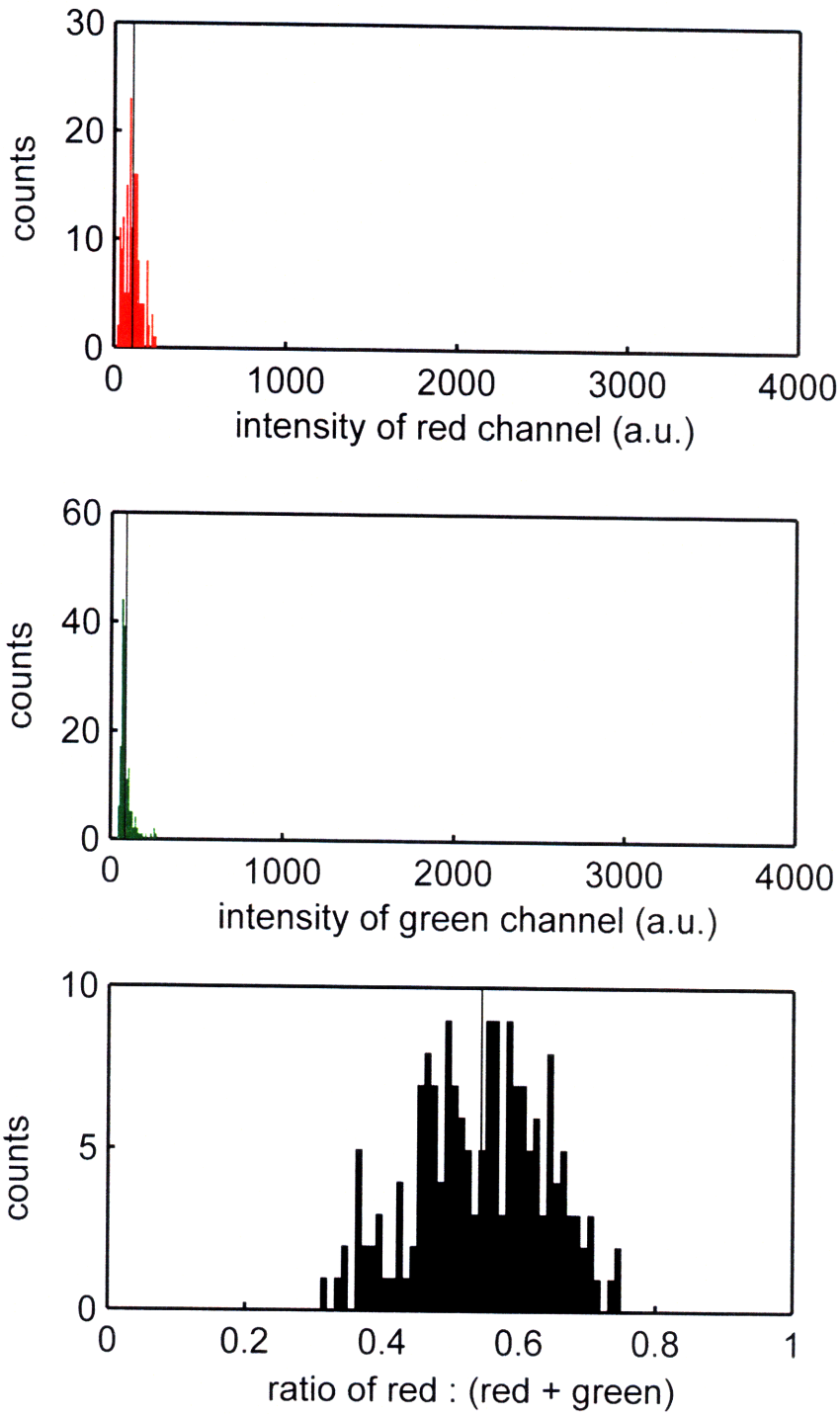

Figure VI.19 A histogram of the emission intensity detected from (Top) red channel, collecting SNARF emission, (Middle) green channel, collecting NC emission. (Bottom) A histogram of the ratios obtained from dividing the red channel intensity with the total intensity.

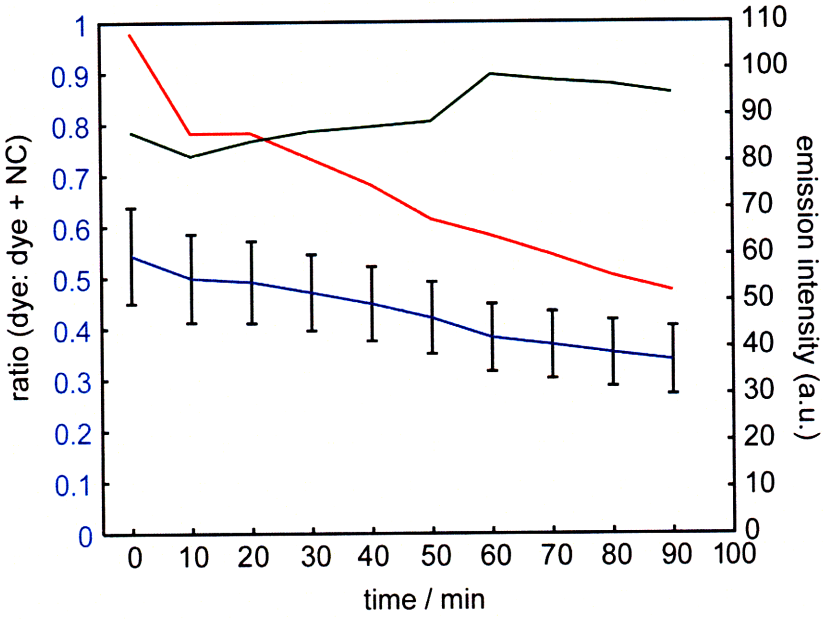

Figure VI.20 Emission intensity of the NC (green solid line —), SNARF-5F (red solid line —), and ratio of SNARF intensity:total intensity (blue solid line —) with respect to time at tissue depth between 20 and 70 microns deep.

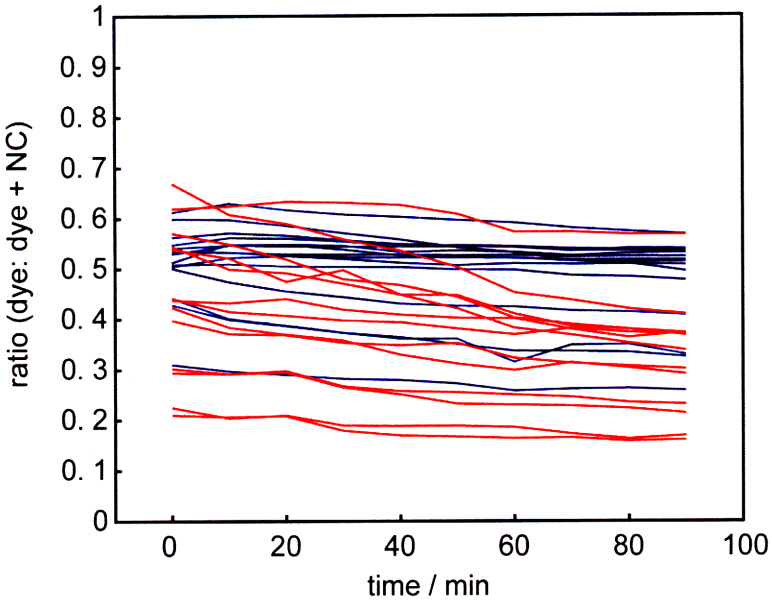

Figure VI.21 Average ratio at all time points in each location of the three tumor mice models for those injected with glucose (red solid line —) and for those injected with saline (blue solid line —).

while the average SNARF-5F emission decreases, consistent with a sensor responding to an increasingly acidic environment. Similar analysis performed over all locations in each of the 3 tumors of the experiment and ratios for each location over time were obtained, as shown in Figure VI.21.

Figure VI.22 shows the sensor response of the glucose vs. saline injection in multiple locations of a tumor averaged over each animal. The traces of the ratio of the sensor response with respect to time are different with each animal, underscoring the heterogeneity of the tumor environment. Figure VI.23 shows the average response of all mice to the glucose and saline injections. At first glance, one can argue that the ratio changed to a lesser extent in the tumors of mice injected with saline than in those injected with glucose. For the saline-injected mice, the averaged ratio changes from 0.511 to 0.470 over the course of 90 minutes, while for the glucose-injected mice, the ratio changes from 0.436 to 0.320. In order to ensure that the changes that were observed in the ratio were statistically significant, the Student's t-test[17,18] was applied to the slopes (or the rate of change) of the sensor response between t = 0 min and t = 90 min. The difference in the change of the sensor response between the saline and glucose samples was found to be statistically significant when each location of the tumors were treated independently, with a p-value of 0.0025, or at a 99% confidence level. When the locations were averaged per animal (as shown in Figure VI.22) and the t-test applied, the p-value was found to be 0.1356, signifying an 86% confidence level. However, a comparison of the initial starting ratio at time t = 0 min between the two injections was also found to be statistically different. The difference in the initial ratio is problematic, as the pH values should be approximately the same. These results indicate that while the sensor is able to detect the *change* in pH induced by the glucose, calibrating the system to read out an exact pH value of the tumor environment is extremely difficult. In addition to probing the tumor environment, the NC-SNARF sensor was also superfused on top of a mouse with a dorsal window exposing normal tissue. No IP injection was performed, and the tissue was imaged for 90 minutes. Figure VI.24 shows the change in the sensor ratio with respect to time. While the figure represents data collected in one mouse (N = 1), the drastic change in ratio seen over the course of 90 minutes is disconcerting. The ratio change from 0.641 to 0.423 is greater than those

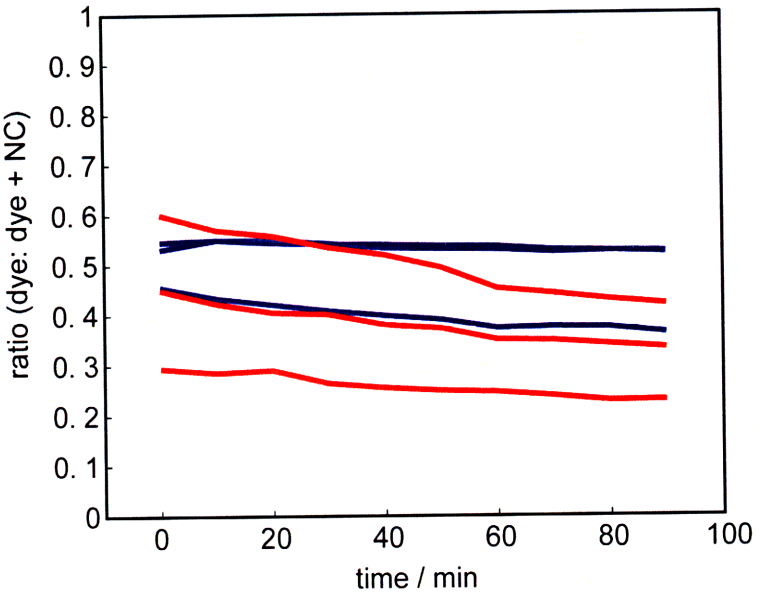

Figure VI.22 Average ratio at all time points averaged per each tumor mice model for those injected with glucose (red solid line —) and for those injected with saline (blue solid line —).

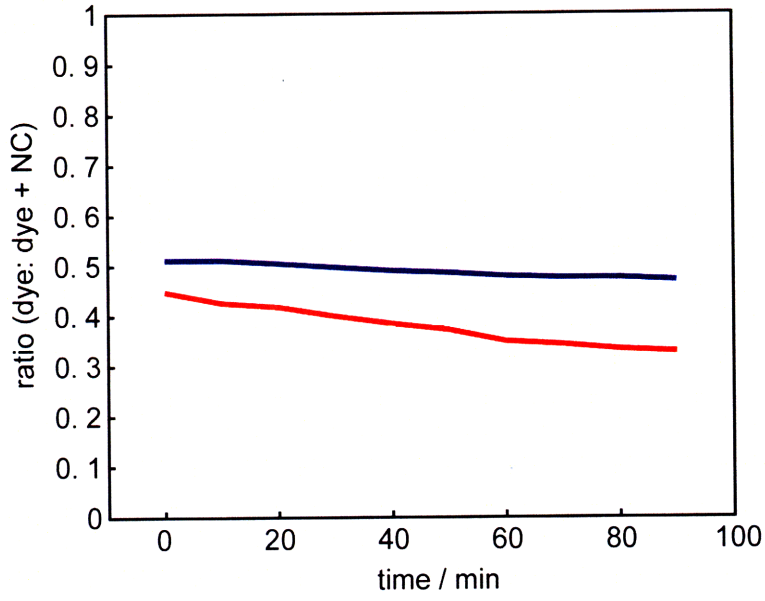

Figure VI.23 Average ratio at all time points averaged over all locations and all tumor mice models injected with glucose (red solid line —) and for those injected with saline (blue solid line —).

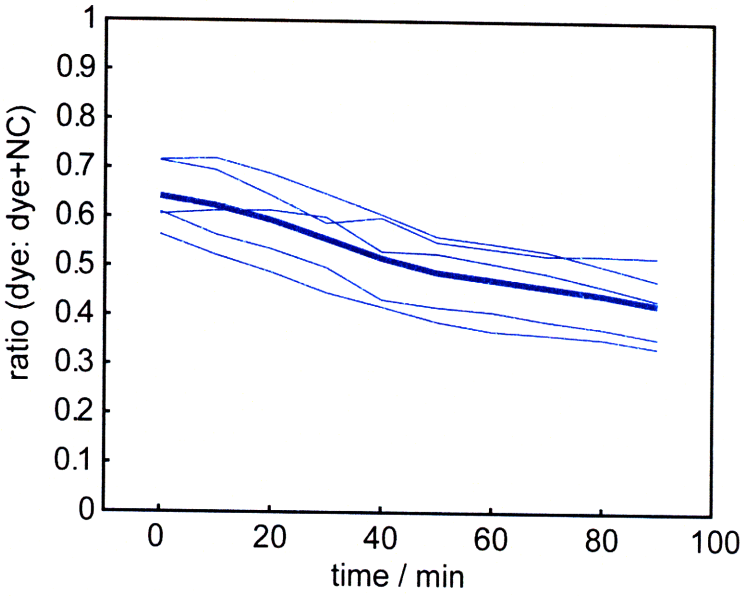

Figure VI.24 Average ratio from the NC sensor at all time points in each location (thin blue line —). The thick blue line represents the average from all location.

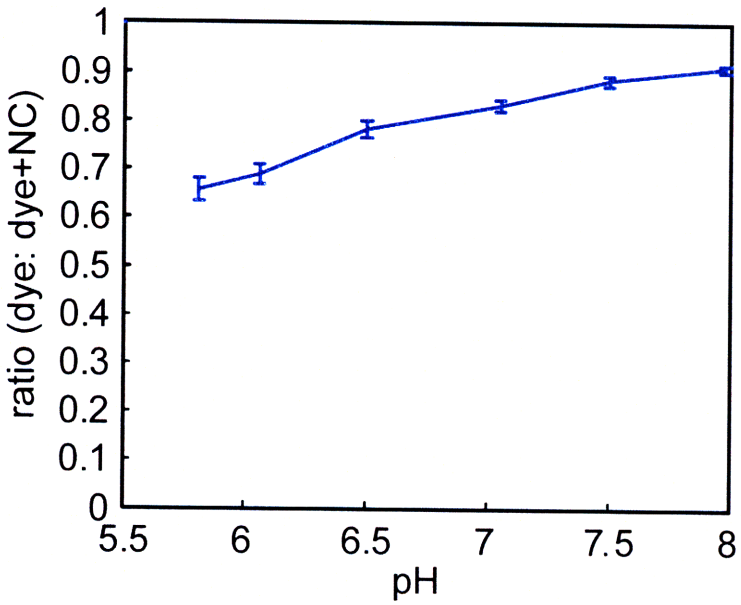

Figure VI.25 Calibration in phosphate buffers of the NC-SNARF construct used in *in vivo* experiments using mice anesthetized with isoflurane gas.

seen for tumor tissues. The construct may be sticking to blood vessels as the NC-construct becomes more diffused into the tissue, or the tissue may have been abnormal, for example, due to damage at time of window insertion. The results shown in Figure VI.22 show that multiple mouse models are necessary in order to make any assessments on the state of the tissue environments, as the *in vivo* environment seem radically different among mouse models.

Figure VI.25 shows the calibration performed in phosphate buffers. The pH range from 5.8 to 8 is bounded by ratios of 0.64 to 0.9. Figures VI.20 to VI.24 exhibit sensor responses that fall outside the range of the phosphate buffered calibration. An appropriate calibration medium is still being investigated, as discussed in Section VI.2.a.

In summary, a significant response of the sensor signal to glucose IP injection (presumed acidic stimulus) was detected in LS174T tumors. The response was significantly greater than that for the sensors in saline, which exhibited a significant but smaller change in ratio over time. Thus, the NC-SNARF sensor appears to be sensitive to a change in pH in a tumor environment.

VI.3 Concluding Remarks

This Chapter describes the progress made towards applying the sensor in a biological context. A robust sensor was made and calibrated in numerous environments, including BSA buffers and single-cell tumor suspensions. Incorporation of the sensor into tumors yielded a ratiometric response. The sensor, when infused into a tumor, was able to detect changes in pH upon introduction of glucose. The heterogeneity of the tissue environment does pose challenges to calibrating the ratiometric readout of the sensor to an absolute pH value. In order to proceed forward towards our goal of utilizing the NC FRET-based sensor for study of pH changes with respect to tumor treatment, a few points should be considered:

1) Calibrations should be performed in a tumor environment with either in *ex vivo* tissues or in single-cell tumor suspensions. In addition, results from Figure VI.22 indicate that calibrations, as well as any *in vivo* experiments, should be performed in several tumors and averaged to minimize error from heterogeneity of the tumor environment.

2) A construct that minimizes non-specific binding to blood vessels or that is "less sticky" is desirable, as it affects *in vivo* delivery of the sensor as well as calibration. The synthesis of the NC-SNARF construct can be redesigned in order to use longer chained PEGs, which may diminish adhesion of biomolecules and/or limit their grip on sensor photophysics. As such, they could make calibration environment less critical. While the longer donor-acceptor distance will lower the efficiency, the efficiency may also be enhanced by using a longer-wavelength emitting NC.

3) A thorough study on the effect of ratio change of the two-photon excited sensor with respect to time and depth of the tumor slice should be done on a non-sensitive NC-dye construct. A better understanding for the effect of the tumor environment on the ratio can be gained.

By considering the above points, a NC-based pH sensor in a tumor environment can be calibrated to read an absolute pH value.

VI.4 Experimental Procedures

VI.4.a Materials and Methods

Cascade Blue Dextran (~500 kDa MW) was purchased from Molecular Probes, a division of Invitrogen. Glucose D-(+) isomer and Bovine Serum Albumin Fraction V (BSA) was purchased from Aldrich. Glass microslides were obtained from VitroCom. Broadband filters and dichroics were obtained through Chroma Technologies. LS174T cell line was obtained through ATCC. A dorsal skinfold window chamber model was prepared on 8 - 10 week old male SCID mice as previously described.[19] After recovery a small piece of LS174T human colorectal adenocarcinoma tumor (~1 mm diameter) from a serially passaged subcutaneous in vivo source from the same murine background is implanted in the center of the chamber. At 1 - 2 weeks time the tumor in the chamber is of appropriate size for experiments (~4 mm diameter). All mice are bred and maintained in a defined-flora animal colony located at the Steele Laboratory. A single-cell suspension of LS174T tumors was obtained from excising the tumors from the dorsal mice models, and trypsinizing the tumors at the Jain laboratory.

VI.4.b Spectroscopic Characterization

Steady-state fluorescence measurements were obtained in a 1 cm pathlength cuvette from a custom-built Photon Technology Instruments fluorometer installed with a Hamamatsu R928 photomultiplier tube and a 150 W Xe excitation. Single-cell suspensions and BSA were prepared in phosphate buffers for all pH.

Multiphoton laser scanning microscopy (MPLSM) was performed in collaboration with Rakesh Jain's group in the Edwin L. Steele Laboratories for Tumor Biology, Department of Radiation Oncology at the Massachusetts General Hospital and Harvard Medical School. All spectral measurements were taken on a custom-built multiphoton laser scanning microscope (MPLSM) with the emission output fiber-coupled to a spectrometer. Multiphoton excitation was performed by a Broadband MaiTai diode pumped Ti:Sapphire laser (Spectra-Physics) using 800 nm, 900 nm or 1000 nm light at sample powers ranging from 10-60 mW. All measurements were made with the MRC 600 Bio-Rad MPLSM scan-head parked versus scanning on a Zeiss Axioskop20 microscopy using a Zeiss X20/0.5NA water objective. Fluorescence emission was coupled into a 100-micron core fiber bundle after passing through a 720 nm short-pass filter. Spectra of the fiber-coupled emission were collected on a Shamrock 303 spectrograph with Newton DU-420 CCD detector system (Andor Technology) using a 100 micron slit opening and 1-second detector integration. Emission spectra were analyzed in MATLAB. Imaging was performed on an Olympus Fluoview 300 Laser Scanning Microscope modified with a MaiTai laser (Spectra-Physics). All images were taken at 800 nm with excitation powers of 40 mW. Non-descanned fluorescence emission was detected by Hamamatsu HC125-02 PMTs. Descanning the emission to remove out-of-plane fluorescence (essential in most laser scanning microscopies) is unnecessary in MPLSM as all of the emission comes from a focal point. Nanocrystal and dye fluorescence was directed to separate PMTs using a 565 nm-shortpass dichroic. The NC and dye channels were further selected using 660/50 nm and 535/40 nm AR-coated broadband filters, respectively. Image stacks (512 × 512 pixels and 5-micron z-step) were collected throughout the 100 micron path-length of the microslide for each calibration sample using an Olympus ×20/0.95 NA water objective. Image

analysis was performed using NIH ImageJ and Matlab. Briefly, average intensity projections for each stack were created and converted to 32-bit. The dye channel was divided by the NC channel. The pixel average and standard deviation of the ratiometric image were used to create a pH calibration curve.

NC-SNARF solutions were prepared in potassium phosphate BSA buffers, and placed in 0.1 × 1 mm^2 inner diameter glass microslides attached to a standard microscope slide for the BSA calibration. NC-SNARF solutions were also incubated in excised tumor tissue and placed onto a microscope slide for other calibrations.

For sensing experiments with ketamine anesthetized mice, the NC sensor was allowed to diffuse for 5 minutes into the tumor prior to replacing the coverslip. After 15 minutes, glucose (6g / kg) or saline (0.3 mL) was intraveneously injected through the tail vein of the mouse. The tumor was imaged every 10 minutes for 90 minutes. For pH sensing experiments using isoflurane anesthetized mice, the NC sensor was allowed to diffuse for 5 minutes into the tumor prior to replacing the coverslip. After 15 minutes, glucose (6 g / kg) or saline (0.3 mL) was intraperitoneally injected and four to five different locations in each tumor were imaged every 10 minutes for 90 minutes.

VI.5 References

1. Jain, R. K. *Science* **2005**, *307*, 58-62.
2. Fukumura, D.; Jain, R. K. *Microvasc. Res.* **2007**, *74*, 72-84.
3. Fukumura, D.; Jain, R. K. *J. Cell. Biochem.* **2007**, *101*, 937-949.
4. Helmlinger, G.; Yuan, F.; Dellian, M.; Jain, R. K. *Nat. Med.* **1997**, *3*, 177-182.
5. Martin, G. R.; Jain, R. K. *Cancer Res.* **1994**, *54*, 5670-5674.
6. Dellian, M.; Helmlinger, G.; Yuan, F.; Jain, R. K. *Br. J. Cancer* **1996**, *74*, 1206-1215.
7. Helmlinger, G.; Sckell, A.; Dellian, M.; Forbes, N. S.; Jain, R. K. *Clin. Cancer Res.* **2002**, *8*, 1284-1291.
8. Jahde, E.; Rajewsky, M. F. *Cancer Res.* **1982**, *42*, 1505-1512.
9. Gerweck, L. E.; Vijayappa, S.; Kozin, S. *Mol. Cancer Ther.* **2006**, *5*, 1275-1279.
10. Cullen, G. E.; Austin, J. H.; Kornblum, K.; Robinson, H. W. *J. Biol. Chem.* **1923**, *56*, 625-661.
11. Stehle, R. L.; Bourne, W. *J. Biol. Chem.* **1924**, *60*, 17-29.
12. Alva, N.; Palomeque, J.; Carbonell, T. *Nitric Oxide* **2006**, *15*, 64-69.
13. Bonath, K.; Hirche, H.; Lange, S. *Berl. Munch. Tieraerztl.* **1980**, *93*, 462-468.
14. Graham, M. S.; Iwama, G. K. *Aquaculture* **1990**, *90*, 323-331.
15. Matsuda, Y.; Ohsaka, K.; Yamamoto, H.; Natsume, K.; Hirabayashi, S.; Kounoike, M.; Inoue, M. *Biol. Pharm. Bull.* **2007**, *30*, 1716-1720.
16. Wen, B.; Urano, M.; O'Donoghue, J. A.; Ling, C. C. *Radiat. Res.* **2006**, *166*, 512-518.
17. Student. *Biometrika* **1908**, *6*, 1-25.
18. Walpole, R.; Myers, R.; Ye, K. *Probability and Statistics for Engineers and Scientists*; 8th ed.; Pearson Prentice Hall: Upper Saddle River, 2007.
19. Leunig, M.; Yuan, F.; Menger, M. D.; Boucher, Y.; Goetz, A. E.; Messmer, K.; Jain, R. K. *Cancer Res.* **1992**, *52*, 6553-6560.

Chapter VII

Development of 'Clickable' NCs and Preliminary Studies on NC-dye Conjugates Formed through the Click Reaction

VII.1 Introduction

Semiconductor nanocrystals (NCs) are useful as biological fluorescent labels and probes in many applications because of their broad absorption, their high luminescence quantum yield, and their narrow, tunable fluorescence emission.[1-15] Chapters II through VI have investigated fluorescence resonance energy transfer (FRET) between covalently linked NCs and dyes. Appending an analyte-sensitive dye allows the NC to be sensitive to its chemical and biological environment. We have shown that the NC-dye FRET based sensors are active under two-photon excitation, making them practical for use as probes for biological microscopy applications.

Thus far, we have successfully employed amide linkages to form robust, biocompatible NC-dye constructs. Other types of linkages probed in Chapters II and III, specifically thiocarbamate and ester linkages, were found to be biologically incompatible due to the instability of the isothiocyanate group and the propensity of the ester bonds toward cleavage.[16] The development of new methodologies for coupling NCs to dyes will expand the library of possible constructs enabling the development of new tools for biological probes sensing.

Click chemistry is a philosophy in coupling chemistry, popularized by K. Barry Sharpless and M. G. Finn, that promotes the synthesis of new compounds by joining small modular units rapidly and reliably through heteroatom linkages, similar to those linkages found in nature.[17-26] Simplicity and biocompatibility are encouraged as the primary criteria for Click chemistry. The most notable "cream of the crop" Click reaction[25] is the 1,3-dipolar cycloaddition between an azide and an alkyne that was first reported by Huisgen.[27,28] The cycloaddition of an azide to an alkyne to produce a 1,2,3-triazole is thermodynamically favorable by approximately 30-35 kcal/mol (Scheme VII.1A).[29] The original synthesis requires high temperatures, long reaction times, and anhydrous media to yield two (1,4- and 1,5-) regioisomers of the triazole. The recent discovery that copper (I) catalyzes the regiospecific formation of the 1,4-triazole under mild conditions in water (Scheme VII.1B) propelled the application of the Click reaction forward in the areas of bioconjugation, materials science, and drug discovery.[21,30,31]

Scheme VII.1 (A) 1,3-dipolar cycloaddition of an alkyne and an azide is activated by heat to give an equimolar mixture of 1,4- and 1,5-stereoisomers of the 1,2,3-triazole. (B) Copper catalyzed alkyne-azide cycloaddition yields exclusively the 1,4-steroisomer.

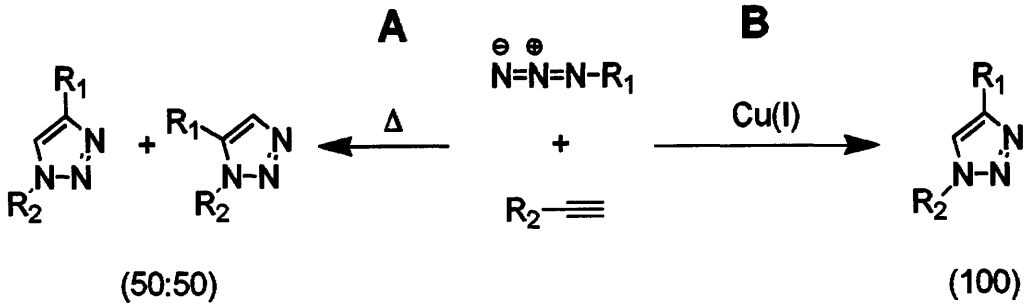

Whereas the copper-catalyzed azide-alkyne cycloaddition has been exploited for nanoparticle conjugation, particularly in gold[32,33] and iron oxide[34] nanoparticles, few reports feature CdSe NCs. Copper ions, which catalyze the cycloaddition, lower the quantum yield of the NCs. In fact, a CdSe based copper dosimeter has been reported where the luminescence quenching mechanism was discussed to be the physical replacement of the cadmium ions by copper ions on the surface of the NC.[35]

Only one example of applying the Click reaction to core CdSe NCs has been reported as a means to functionalize alkyne-terminated NCs to azide coated gold surfaces.[36] While the phosphine oxide-terminated alkyl capping ligands with azide and alkyne functionalities allowed the NCs to access the Click reaction as a coupling strategy, the utility of the NCs in this work was limited due to the low quantum yields (less than 1%). In addition, the reaction occurred in toluene, as the capping ligands incorporated long alkyl chains. Click conjugation was only achieved by heating the reaction to 95 °C, as the copper (I)-mediated route led to complete quenching of the NC emission.

In light of this, other strategies for Click chemistry, that avoid the use of the quenching copper ions, are worth pursuing. Recently, the use of a cyclooctyne moiety to effect a strain-promoted [3+2] azide-alkyne cycloaddition was reported as an alternative to thermal or copper-catalyzed methods, as illustrated in Scheme VII.2.[37,38] The bond angle deformation of the acetylene, at 163°, is responsible for approximately 18 kcal/mol of ring strain relative to the alkene product[39,40] and allows the reaction to proceed readily under mild, ambient conditions.[38] Addition of electron withdrawing

Scheme VII.2 1,2,3-triazoles formed from a strain-promoted azide-alkyne cycloaddition.

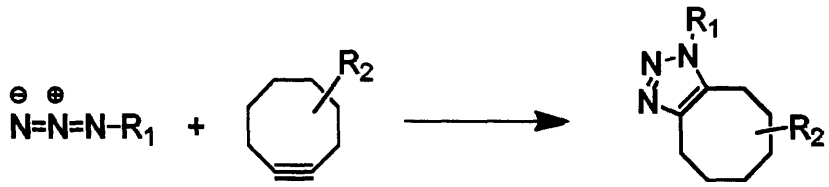

groups, such as fluorine, to the cyclooctyne also promotes the rate of reactivity.[41] The strained-cyclooctyne mediated triazole formation has been used to label live cells and has been found to be biocompatible.[37,41,42]

This Chapter describes the methodologies to synthesize water-soluble CdSe NCs for Click chemistry by modifying the NC surface with azide and alkyne groups. Syntheses for new surface ligands for the NCs are reported. Both micellular encapsulation and cap-exchange methodologies for surface modification of NCs are pursued. Overcoated CdSe/CdZnS NCs are used to preserve a high quantum yield. Cyclooctyne-modified rhodamine was synthesized to pursue the Click reaction without affecting the luminescence of the NCs. Preliminary conjugation studies, as well as future direction with 'clickable' NCs are discussed.

VII.2 Results and Discussion

VII.2.a Synthesis of Rhodamine B-labeled Cyclooctyne

Scheme VII.3 depicts the synthesis of RITC-labeled cyclooctyne. The cyclooctyne reported originally by Bertozzi and co-workers was synthesized according to literature procedures.[37] Since the cyclooctyne compound, **1**, was derivatized with a carboxylic acid, we deemed appropriate that the most facile strategy to couple to a dye was through a diamine linker. Functionalization of the cyclooctyne with an ethylenediamine linker yielded compound **2** that through subsequent coupling using Rhodamine B isothiocyantate afforded the cyclooctyne-modified Rhodamine B, compound **3**, in 50% overall yield. The choice of Rhodamine B was two-fold: 1) the dye allowed for confirmation that the Click reaction occurred, and 2) the dye can potentially be exploited as a FRET acceptor. The RITC-modified cyclooctyne was used to assess the Click reactions with azide-terminated NCs prepared both by micellular encapsulation

Scheme VII.3 Synthetic route to RITC-labeled cyclooctyne, compound **3**.

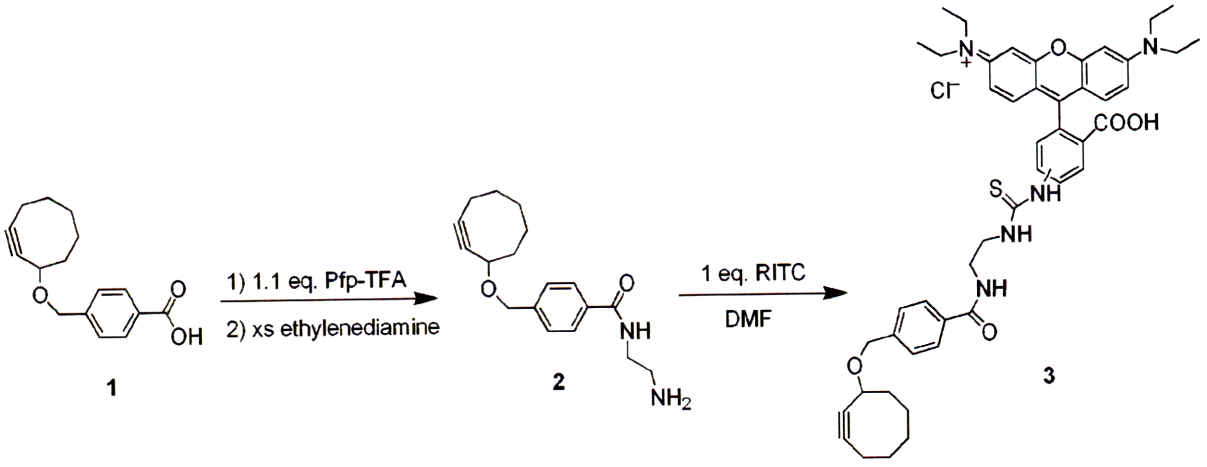

and by cap-exchange.

VII.2.b Click Chemistry with Azide-terminated Micelle Encapsulated NCs

The first method takes advantage of the micelle-encapsulated NC-NHS ester synthon that was developed in Chapter IV.4.h. Scheme VII.4 details the formation of the azide terminated micelle encapsulated NCs. Solvation of the NC-NHS by *O*-(2-aminoethyl)-*O'*-(2-azidoethyl)-heptaethylene glycol yielded a bright clear reaction solution that was stirred for 4 hours. Addition of water to the azide NCs resulted in slight precipitation and lowered the quantum yield of the NCs from 53% to 2.1%. Purification by filtration and centrifugal dialysis resulted in water-soluble azide terminated NCs.

With the azide terminated NCs in hand, the Click reaction was attempted using the dye-labeled cyclooctyne that was developed as shown in Scheme VII.3. The two

Scheme VII.4 Synthesis of azide-terminated micelle encapsulated NCs.

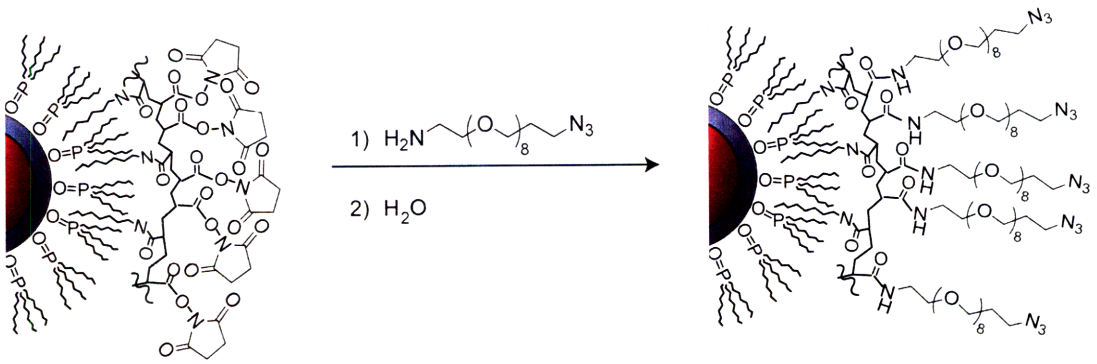

reacting species were mixed in PBS at room temperature and stirred overnight. Purification by dialysis with distilled water yielded the NC-dye conjugate that was coupled with 1,2,3-triazole formation. The construct was characterized using photophysical methods. By determining the concentrations of the reacting dye and the filtrate wash, the coupling efficiency was found to be low, at approximately 3%.

Figure VII.1 shows the UV-vis absorption profile of the NC-RITC conjugate. The first absorption peak of both NCs and RITC are clearly visible. Decomposing the spectrum into the respective NC and dye components reveals that the dye to NC ratio was 2.2. Figure VII.2 shows the steady-state emission spectrum of the NC-dye conjugate, when excited at λ_{ex} = 350 nm. The emission of the conjugate exhibits both NC and dye features. Figure VII.3 compares the photoluminescence excitation spectrum between the conjugate and the RITC-cyclooctyne. The results suggest a small degree of energy transfer from the NC. When monitoring the emission at λ_{em} = 625 nm, the emission intensity at higher-energy excitation wavelengths (between 300 - 450 nm) is greater for the NC-RITC construct compared to the RITC-cyclooctyne molecule. Lifetimes of the NC were also measured through time-resolved emission spectroscopy. Donor lifetime quenching was minimal, changing from 3.5 ns for the uncoupled azide-terminated NCs to 2.9 ns when the RITC was conjugated onto the NC. The overall efficiency of energy transfer for this system is 17%, due to the long distance between

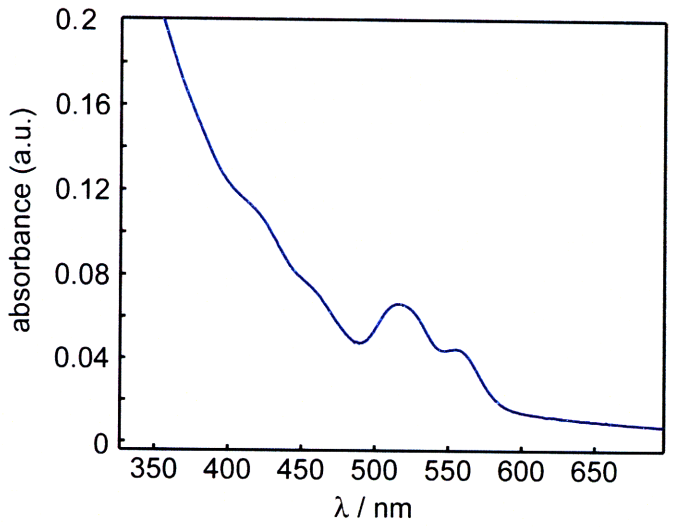

Figure VII.1 UV-visible absorption spectrum of the clicked NC-RITC conjugate (blue line —) clearly exhibits both NC and dye first absorption features.

the donor and acceptor, which is imposed by the PEG linker, as well as the low dye to NC ratio of 2.2.

These results describe the *first* example of a system where a Click reaction was achieved in water using CdSe NCs. Although the overall objective was achieved, the system can be further improved by preparing azide-terminated NCs that exhibit less aggregation. A smaller donor-acceptor distance will also be useful for FRET

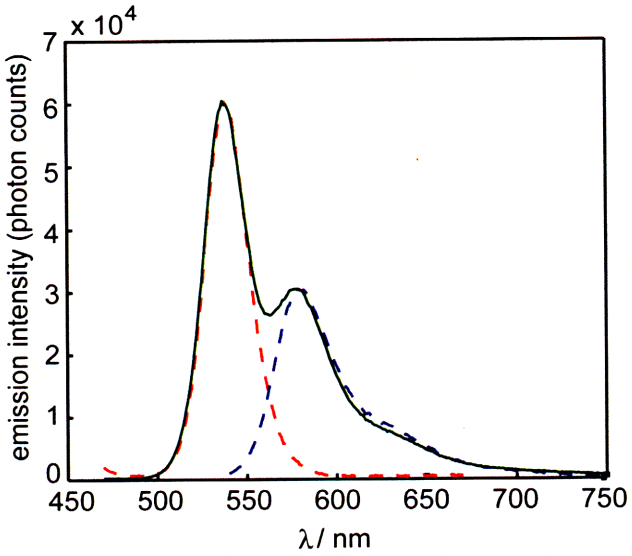

Figure VII.2 The emission of the clicked NC-RITC conjugate (λ_{ex} = 365 nm, green solid line —) can be deconstructed to the NC only (red dashed line - -) and the RITC only (blue dashed line - -) components.

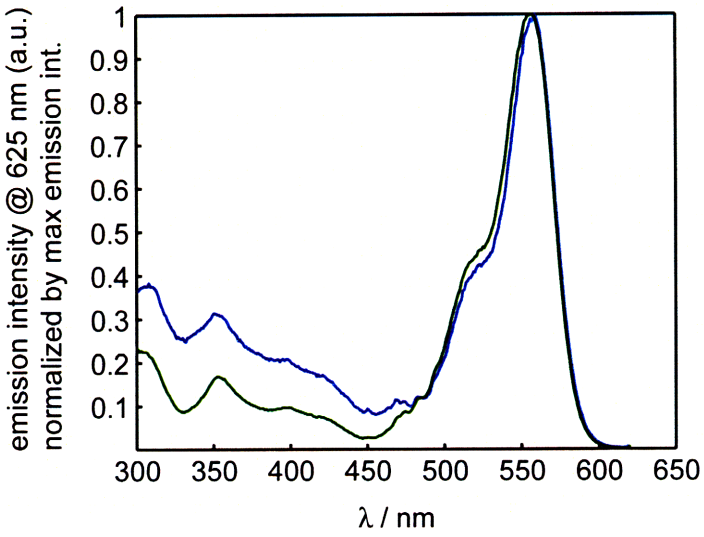

Figure VII.3 The photoluminescence excitation spectrum (λ_{em} = 625 nm) of the clicked NC-RITC (blue solid line —) show a slight enhancement in the emission intensity in the UV-region compared to the spectrum of the RITC alone (green solid line —).

demonstration. The above two points provided the impetus to move towards cap-exchanged water-soluble NCs that incorporate azide or alkyne functionalities.

VII.2.c Synthesis of Azide-terminated NCs

Based on the work from Chapter V, the use of a dihydrolipoic acid (DHLA)-modified azide-terminated PEG was a natural initial target as a cap-exchanging ligand. Scheme VII.5 illustrates the attempted synthesis of DHLA-azidePEG. While the synthesis of thioctic acid (TA)-modified azide-terminated PEG proceeds expeditiously, reduction of the TA to DHLA without reducing the azide group proved to be challenging. The use of a mild reducing agent, dithiothreitol (DTT) still reduced the azide to an amine. Directly coupling DHLA to *O*-(2-aminoethyl)-*O'*-(2-azidoethyl)-heptaethylene glycol results in a mixture of products that yields TA-aminoPEG upon purification. While the DHLA functionality is beneficial for stable chelation onto the NC surface, it also results in the reduction of the azide on the ligand; a number of different structures of dithiols have been shown to reduce azides.[43,44] Due to the incompatibility of the two functional groups, monothiols instead of dithiols were incorporated in the azide terminated capping ligand design. While enhanced stability was sacrificed, we were interested in demonstrating the feasibility and the efficiency of coupling using Click chemistry methods.

Scheme VII.6 describes the synthesis of the capping ligands. The capping ligand was synthesized by coupling 3-mercaptopropionic ester, **4**, with *O*-(2-aminoethyl)-*O'*-(2-azidoethyl)-heptaethylene glycol. The ligand was purified by flash chromatography and characterized by ^{1}H NMR and IR. The IR spectrum is shown in Figure VII.4. The sharp feature at 2108 cm^{-1} indicates that the azide is preserved upon ligand isolation. TOPO-

Scheme VII.5 Synthesis of DHLA modified azidePEG reveals that DHLA and azide are two incompatible functional groups.

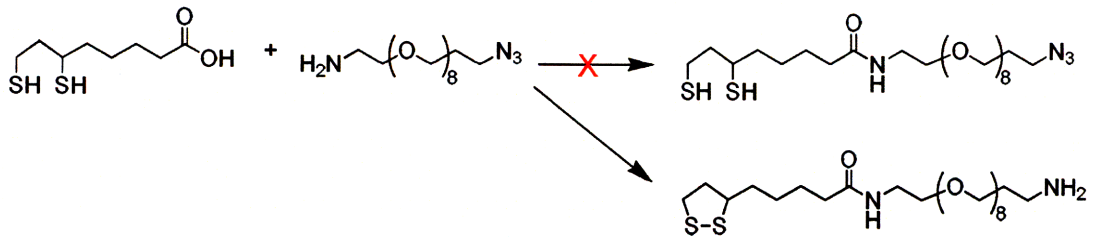

Scheme VII.6 Synthesis of azide terminated NC capping ligand.

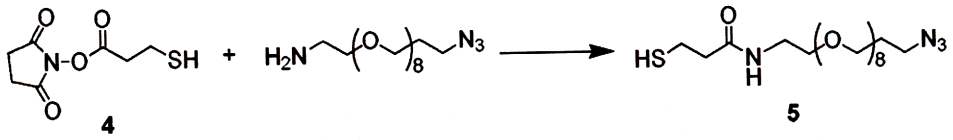

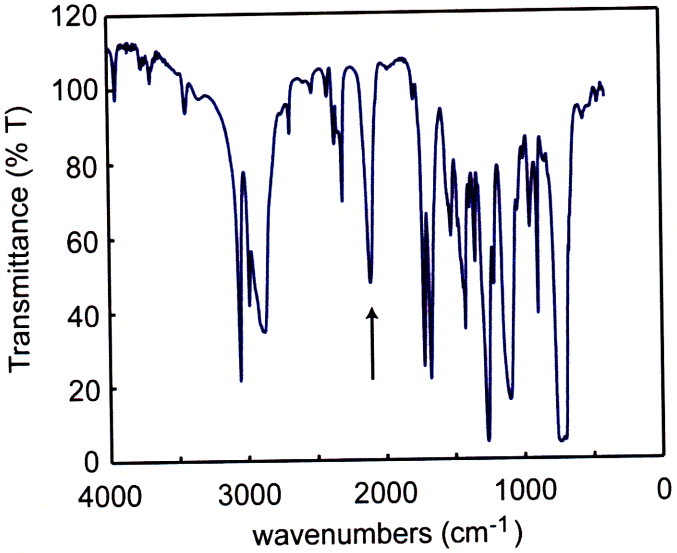

Figure VII.4 IR spectrum of the ligand, compound **5**, confirms the presence of an azide feature at 2108 cm^{-1} as indicated by the black arrow.

coated 542 nm emitting NCs were subsequently cap-exchanged at 60°C.

Due to concerns of water-solubility, three different sets of ligands were used for the cap-exchange. Table II.1 lists the solubility properties of NCs cap-exchanged with A) 100% azide-PEG-SH. B) 1:1 molar mixture of azide-PEG-SH and 3-mercaptopropionic acid, and C) 100% 3-mercaptopropionic acid. 3-Mercaptopropionic acid is a well-known

Table VII.1 Solubility properties imparted to the NCs by capping ligand mixtures used to synthesize azide-terminated NCs.

NC sample cap-exchanged with:	Soluble in EtOH	Soluble in H_2O
A) 100% azide-PEG-SH, compound **5**	yes	no
B) 50% compound **5**, 50% mercaptopropionic acid	yes	yes
C)100% mercaptopropionic acid	yes	yes

ligand to impart water solubility to CdSe NCs and is used as a comparative control for the cap-exchange process. While all NCs are well-dispersed in ethanol, the NCs exchanged with 100% azide-terminated ligand did not solubilize in water. The use of a longer-chained PEG, *O*-(2-aminoethyl)-*O'*-(2-azidoethyl)-nonaaethylene glycol, did not impart any further water solubility to the NCs. NCs prepared from a mixture of azide-terminated ligand with 3-mercaptopropionic acid did disperse in water; however, the presence of the azide ligand had to be verified to dismiss the possibility that only the 3-mercaptopropionic acid coordinated to the NC surface.

The presence of the azide functionality on the NCs was confirmed through infrared spectroscopy. The NC samples were purified by multiple precipitation and redispersion in solvent to ensure that all excess ligands were removed. Figure VII.5 shows the IR spectra for all three types of NCs. The sharp stretch at 2106 - 2107 cm^{-1} was observed for samples A and B, indicative of azides. Sample B exhibits a prominent broad –OH stretch at 3335 cm^{-1} that is missing in sample A, indicating a mixture with mercaptopropionic acid. Finally, NCs coated exclusively with 3-mercaptopropionic acid exhibits no azide stretch and a broad —OH peak at 3435 cm^{-1}. IR spectroscopy of the cap-exchanged NCs establishes that a mixture of 3-mercaptopropionic acid and azidePEG ligands sufficiently coats the NC with azides for click coupling purposes.

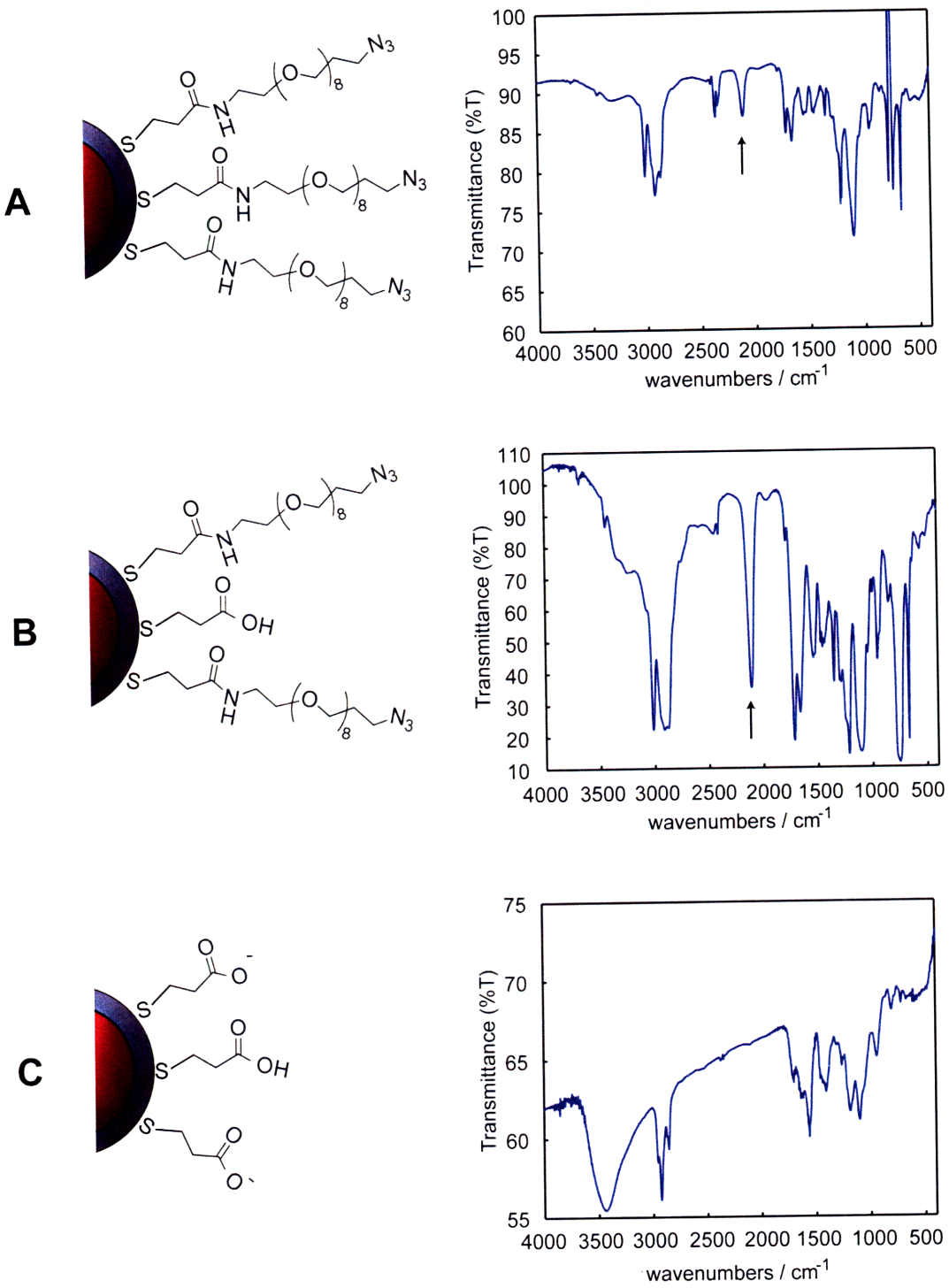

Figure VII.5 (Left) graphical rendition and (Right) IR spectra of the three different ligand exchanged NCs for ligand mixtures A, B, and C that are listed in Table VII.1. The arrow points to the azide stretch.

Scheme VII.7 Synthesis of N-propargyl-dihydrolipoamide for preparation of alkyne terminated NCs.

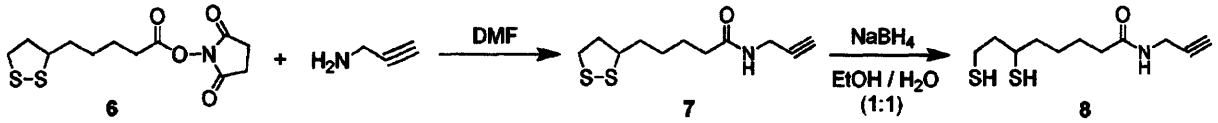

VII.2.d Synthesis of Alkyne-terminated NCs

Synthesis of alkyne-terminated NCs was pursued as a target to add to the toolbox of functionalized NCs. Scheme VII.7 shows the synthesis of propargylamine modified thioctic acid, with subsequent reduction of the dithiolane ring to dithiol. The TOPO-coated 542 nm emitting NCs were cap-exchanged at 60°C. As in the case with azide NCs, concerns of water-solubility when cap-exchanged with 100% alkyne terminated ligands were present; therefore, three ligand batches were prepared and their solubility properties are listed in Table VII.2: A) 100% alkyne-modified dihydrolipoic acid, B) 1:1 molar mixture of alkyne-modified DHLA and free DHLA, and C) 100% DHLA. Similar to the azide modified NCs, the alkyne-modified dihydrolipoic acid ligand can only impart water solubility when mixed with its free acid form. Attempts to characterize the alkyne group on the NC surface were inconclusive. The terminal alkyne stretch expected between 2100 to 2200 cm^{-1} is typically a very weak band, and a clear (high signal to noise) IR spectrum of the NCs could not be obtained.

Table VII.2 Solubility properties imparted to the NCs by capping ligand mixtures used to synthesize alkyne-terminated NCs.

NC sample cap-exchanged with:	Soluble in EtOH	Soluble in H_2O
A) 100% DHLA-alkyne, compound **8**	yes	no
B) 50% compound **8**, 50% DHLA	yes	yes
C)100% DHLA	yes	yes

VII.2.e Click Reactions with Azide-terminated Cap-exchanged NCs

The Click reaction was performed using the cyclooctyne-modified RITC with water-soluble NCs exhibiting azide functionality and a quantum yield of 43%. The azide terminated NCs were dialyzed into PBS until the final concentration was 16 μM. The cyclooctyne-RITC was dissolved in DMF to yield a final concentration of 0.3 mM. Upon preparing a 10:1 dye to NC molar mixture, the NC emission was found to quench, and the NCs themselves started to precipitate. In order to probe whether the mechanism of quenching was due to the reagents used to prepare the cyclooctyne or to the actual coupling of the dye to the NCs, a series of NCs and reagents were mixed as listed in Table VII.3. Only the addition of the compound 3-modified RITC and pentafluorophenyl trifluoroacetate (pfp-TFA) to azide-terminated NCs seem to quench the NCs. Because pfp-TFA was removed by chromatography, it is unlikely to be the cause of the quenching during the Click reaction. Different molar ratios prepared between the azide NCs and the cyclooctyne dye exhibited different quenching rates, although attempted purification of these NC conjugates resulted in precipitation. UV-vis and steady-state emission spectroscopies verified the presence of both dye and NC for NC conjugates

Table VII.3 Reaction conditions used to probe the cause of quenching of azide-capped NC luminescence during the Click reaction

Reaction Mixtures	Degree of NC luminescence quenching
RITC-cyclooctyne and azide-NCs (10:1)	Immediate quenching
RITC-cyclooctyne and azide-NCs (5:1)	Immediate quenching
RITC-cyclooctyne and azide-NCs (2:1)	Delayed (2h) quenching
RITC-cyclooctyne and azide-NCs (1:1)	No quenching, but precipitated
Compound **1** and azide-NCs (20:1)	No quenching
Ethylenediamine and azide-NCs	No quenching
TFA-pfp (in DMF) and azide-NCs	Immediate quenching
RITC and azide-NCs (10:1)	No quenching
Compound **2** and azide-NCs	No quenching
Alkyne-modified RITC and azide NCs	No quenching
RITC-cyclooctyne and carboxyPEG NCs	No quenching

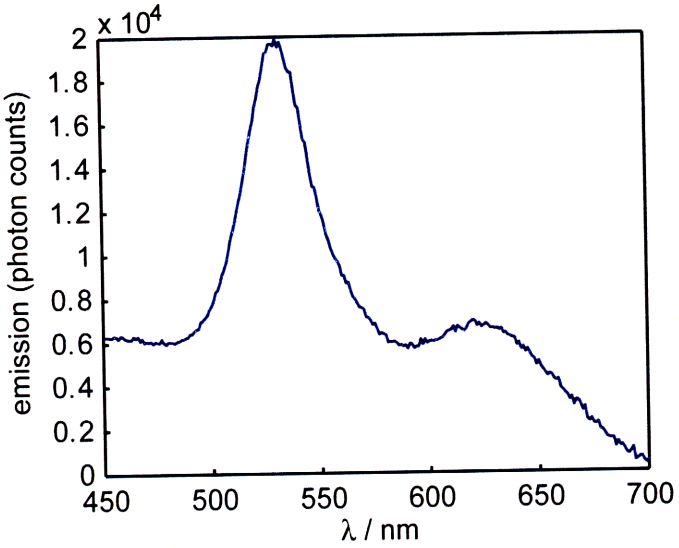

Figure VII.6 Emission spectrum (λ_{ex} = 350 nm) of the clicked NC-RITC (blue solid line —) that remained in solution.

from the dialyzed fraction that did not precipitate. As the NC-RITC construct precipitated, a blue emission began to appear when exposed to UV-light. The emission spectrum is shown in Figure VII.6, and both dye and NC features are present.

Addition of the RITC-modified cyclooctyne dye to carboxylic acid terminated PEGylated NCs did not quench the NC luminescence. The addition of the RITC dye itself, propargylamine-modified RITC or the compound 3 itself also did not quench luminescence. Given these results, a reaction most likely did occur between the azide terminated NCs and the RITC-cyclooctyne; however, the monothiolated ligands of the NCs were unstable to allow the construct to remain in solution. Degradation of the construct putatively results in the blue observed emission.

VII.2.f Concluding Remarks and Future Direction

A Click reaction in water between azide terminated NCs and RITC-labeled cyclooctyne was demonstrated with micellular encapsulated NCs. Because of low quantum yields and the NC's propensity to aggregate, a cap-exchange strategy for Click chemistry was also pursued. Both azide and alkyne terminated NCs were synthesized, and they were found to be well-dispersed in aqueous environments. Unfortunately, the use of monothiols as capping ligands of NCs proved to be detrimental for the Click reaction.

Scheme VII.8 Synthesis of the proposed ligand for NCs undergoing the Click reaction.

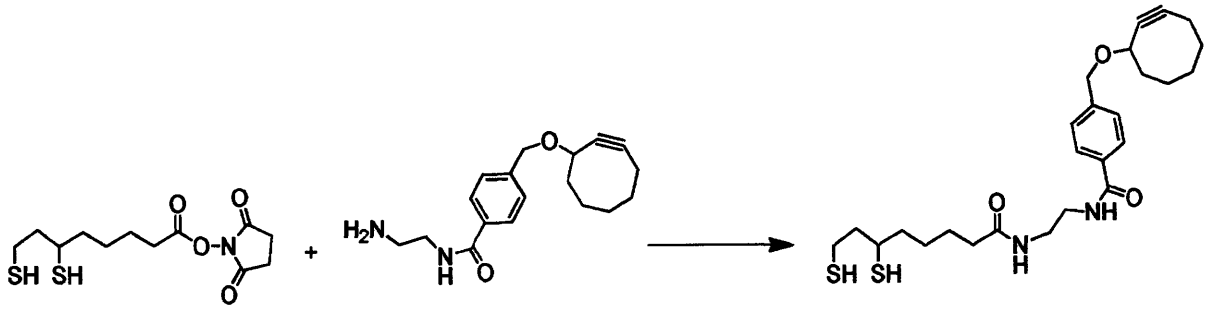

6 2 9

Nevertheless, the Click reaction for NCs is worth pursuing. An alternative ligand for NCs to undergo the Click reaction is proposed in Scheme VII.8. Given the stability of alkynes in the presence of thiols, the cyclooctyne moiety may be coupled to DHLA or a DHLA-modified PEG for the placement on the NC surface. An azide terminated dye, such as 7-methoxycoumarin-3-carbonyl azide, may be used to monitor the Click reaction.

VII.3 Experimental Procedures

VII.3.a Materials and Methods

Trioctylphosphine oxide (90%, TOPO), cadmium 2,4-pentanedionate, *N*-hydroxysuccinimide (NHS), propargylamine, rhodamine B isothiocyanate (RITC), *N,N'*-dimethylformamide (DMF), anhydrous pyridine, pentafluorophenyl trifluoroacetate (Pfp-TFA), cycloheptene, sodium methoxide, silver perchlorate, methyl 4-hydroxymethylbenzoate, 1800 MW poly(acrylic acid), Sephadex LH-20, and *N*-octylamine were purchased from Sigma-Aldrich. 1-Tetradecylphosphonic acid (98%, TDPA), n-hexylphosphonic acid (HPA), dimethylcadmium ($CdMe_2$) and selenium shot were purchased from Alfa Aesar. Trioctylphosphine (TOP) and tributylphosphine (TBP) were obtained from Strem Chemicals. 1-Ethyl-3,3'-dimethylaminopropylcarbodiimide (EDC), 3-mercaptopropionic acid, *O*-(2-Aminoethyl)-*O'*-(2-azidoethyl)-heptaethylene glycol, *O*-(2-aminoethyl)-*O'*-(2-azidoethyl)-nonaethylene glycol, bis(trimethylsilyl)sulfide [$(TMS)_2S$] and diethylzinc ($ZnEt_2$) were obtained from Fluka. NCs cap-exchanged with 25% DHLA-carboxyPEG and 75% DHLA-hydroxyPEG ligands were provided by W. Liu

in the Bawendi group. All materials were used as purchased, except for TOPO, which was purified through vacuum distillation, and diethylzinc, which was passed through a 0.2 μm syringe filter before use. All air sensitive materials were handled in an Omni-Lab VAC glove box under dry nitrogen atmosphere with oxygen levels <0.2 ppm. Centrifugal filters equipped with a 50,000 Da molecular weight cutoff (MWCO) dialysis membrane were purchased through Millipore Corporation.

VII.3.b Spectroscopic Characterization

UV-visible spectroscopy of RITC coupled CdSe/CdZnS were measured on a Hewlett-Packard 8453 UV-vis spectrophotometer with the Chemstation software. Steady-state fluorescence measurements were obtained in a 1 cm path-length cuvette from a custom-built Photon Technology Instruments fluorometer installed with a Hamamatsu R928 photomultiplier tube and a 150 W Xe excitation lamp. Time resolved emission measurements for the NCs, collected at room temperature in a 1 cm path length cuvette, were made with a chirped-pulse amplified Ti:Sapphire laser system using the frequency doubled (400 nm) pump light provided by a Ti:Sapphire laser system (100 fs pulsewidth) and collected on a Hamamatsu C4334 Streak Scope streak camera as previously described.[45] Lifetime data was fitted as a bi-exponential decay using Origin 6.0. All NMR spectra were collected at the MIT Department of Chemistry Instrumentation Facility (DCIF) on a Varian Mercury 300 MHz or a Varian Inova 500 MHz NMR Spectrometer at room temperature. Chemical shifts are reported using the standard δ notation in ppm and are referenced to tetramethylsilane (TMS) using the residual ^1H signal of the deuterated solvent, $CDCl_3$, CD_3OD, or D_2O, as an internal standard. IR Spectra of samples were collected on a Perkin-Elmer 2000 FTIR Spectrometer.

VII.3.c Synthesis of Ethylenediamine-modified Cyclooctyne

4-[(2-Cyclooctyn-1-yloxy)methyl]benzoic acid (118 mg, 0.460 mmol) was synthesized according to literature methods[37] and dissolved in anhydrous pyridine (1 mL), to which Pfp-TFA (81 μL, 0.47 mmol) was added and stirred for 4 hours. The reaction mixture was diluted with CH_2Cl_2 (30 mL), washed with 1 M HCl (3 x 20 mL) and

saturated $NaHCO_3$ (3 x 20 mL), and washed with H_2O (3 x 20 mL). The organic layer was dried with anhydrous $MgSO_4$. The solvent was reduced *in vacuo*, and excess ethylenediamine (138 mg, 2.30 mmol) was added and stirred overnight. Excess ethylenediamine was removed *in vacuo*, and the ethylenediamine modified 4-[{2-cyclooctyn-1-yloxy)methyl]benzoic acid, compound **2**, was purified by chromatography, with silica as the stationary phase and EtOAc:MeOH:H_2O (70:15:15) as the mobile phase. Product yield: 69%. ^{1}H NMR (300MHz, D_2O, δ): 7.63 (d, *J* = 8.1 Hz, 1H), 7.34 (d, *J* = 8.1 Hz, 1H), 4.52 (d, *J* = 12, 1H), 4.37 (d, *J* = 11.4, 1H), 4.21 (m, 1H), 3.54 (t, *J* = 5.7, 2H), 3.09 (t, *J* = 5.7 Hz, 2H), 2.18-1.90 (m, 3H), 1.82-1.20 (m, 8H), 1.16 (m, 1H). ESI-MS: m/z 301.1 $[M+H]^+$.

VII.3.d Synthesis of RITC-modified Cyclooctyne

Compound **2** (63 mg, 0.21 mmol) was allowed to react with RITC (111 mg, 0.210 mmol) in DMF (3 mL) and stirred overnight. DMF was removed *in vacuo*, and the crude product was purified by chromatography, with silica as the stationary phase and EtOAc:MeOH:H_2O (70:15:15) as the mobile phase. RITC-labeled cyclooctyne product, compound **3**, was isolated in 74% yield as a red solid. ^{1}H NMR (500MHz, $CDCl_3$, δ): 8.76 (br s, 1H), 8.12 (br s, 1H), 7.97 (d, *J* = 8.5 Hz 1H), 7.92 (d, *J* = 8.5 Hz, 1H), 7.30 (d, *J* = 8 Hz, 1H), 7.08 (br s, 1H), 7.04 (d, *J* = 7 Hz, 1H), 6.79 (br s, 1H), 6.66 (br s, 1H), 6.58 (br s, 2H), 6.52 – 6.43 (m, 3H), 6.17 (dd, *J* = 11.5 and 4 Hz, 1H), 4.61 (d, *J* = 12, 1H), 4.28 (d, *J* = 12.5, 1H), 4.05 (m, 1H), 3.56 (t, *J* = 4.5 Hz, 2H), 3.46-3.30 (m, 10 H), 2.30-2.27 (m, 2H), 2.04-1.84 (m, 4H), 1.72-1.66 (m, 2H), 1.52-1.43 (m, 1H), 1.32-1.04 (m, 14H).

VII.3.e Synthesis of RITC-modified Propargylamine

Rhodamine B Isothiocyanate (RITC, 100 mg, 0.190 mmol) was dissolved in DMF (6 mL) and stirred vigorously, to which propargylamine (128 μL, 1.90 mmol) was added. The reaction mixture was stirred overnight, and the solvent was removed *in vacuo*. The crude product was purified by chromatography, with silica as the stationary phase and CH_2Cl_2:EtOH (85:15) as the mobile phase. Removal of solvent under reduced pressure yields the product as a purple solid (49 mg, 44%). ^{1}H NMR (500MHz, $CDCl_3$, δ): 7.79 (d,

J = 8.5 Hz, 1H), 7.05 (m, 1H), 6.89 (m, 1H), 6.57 (m, 2H), 6.39 (m, 2H), 5.98 (m, 2H), 3.97 (q, J = 2.5, 8 H), 3.14 (t, J = 6.5, 2 H), 2.26 (t, J = 2.5 Hz, 1H). ^{13}C NMR (500MHz, $CDCl_3$, δ): 79.24, 71.93.

VII.3.f Synthesis of CdSe/CdZnS Nanocrystals (542 nm)

CdSe NCs overcoated with alloyed CdZnS were prepared using a modified literature method.[1,46,47] In a three-necked flask, vacuum distilled trioctylphosphine oxide (TOPO, 6.0 g, 16 mmol), trioctylphosphine (TOP, 6.0 mL, 14 mmol), cadmium 2,4-pentanedionate (0.306 g, 0.980 mmol) and 1-tetradecylphosphonic acid (0.549 g, 1.97 mmol) were added and degassed at 180 °C for three hours. The reaction vessel was backfilled with N_2, and the temperature was heated to 260 °C. A venting needle was inserted into the septa of the flask, and N_2 was allowed to flow for 20 minutes. After the removal of the venting needle, the temperature was raised to 360 °C and 1.5M solution of TBP (1.5 mL, prepared from dissolving 5.92 g of Se shot into 50 mL TBP) was rapidly injected. The reaction was cooled immediately, and stirred overnight at 80 °C to obtain core CdSe NCs with a first absorption feature at 501 nm.

The bare CdSe NCs were precipitated twice out of the growth solution with butanol and methanol and redissolved in 4 mL hexanes. The NCs were overcoated by injecting the hexane solution of core CdSe into a degassed solvent of distilled trioctylphosphine oxide (10.0 g, 0.0259 mol) and n-hexylphosphonic acid (0.40 g, 0.0024 mol). The hexane was removed *in vacuo* at 80 °C and the solution temperature was raised to 140 °C. Two separate precursor solutions of bis(trimethylsilyl)sulfide in 5 mL TOP, and diethylzinc and dimethylcadmium (in a 90: 10 molar ratio) in 5 mL TOP was slowly added to the core solution over the course of two hours using a syringe pump. Exact amounts were chosen (134 mg, 1.10 mmol $ZnEt_2$: 17 mg, 0.12 mmol $CdMe_2$) to yield a ~4 monolayer coating of ZnS on the bare CdSe NCs, using the methods of Dabboussi et al.[47] The final emission wavelength was 542 nm with a FWHM of 26 nm. The quantum yield of NCs prepared was 53% after one size-selected precipitation against a rhodamine 560 standard which is taken to be Φ = 0.95 in ethanol.

VII.3.g Synthesis of *N*-Octylamine-modified Poly(acrylic acid)

A functionalized polymer was synthesized by coupling a fraction (40%) of the carboxylic acid groups of a 1800 MW poly(acrylic acid) (2.0 g, 0.0011 mol) with octylamine (1.44 g, 0.0110 mol) using 1-ethyl-3-(3-dimethylaminopropyl)carbodiimide (EDC) (2.12g, 0.0110 mol) in *N,N'*-dimethylformamide according to a previous report.[48] The functionalized polymer was purified by size-exclusion chromatography using Sephadex LH-20 with methanol as the mobile phase. ^{1}H NMR (500MHz, CD_3OD, δ): 3.15 (br s), 2.25 (br, s), 1.98 (s), 1.60 (br s), 1.46 (br s), 1.28 (s), 0.866 (s). IR (KBr, cm^{-1}): 3289 (OH, br), 2930-2853 (CH, aliphatic), 1712 (C=O), 1641 (CO-NH-R), 1564 (CO-NH-R).

VII.3.h Preparation of Azide-terminated Micelle Encapsulated NCs

Water-soluble CdSe/CdZnS NCs were prepared by precipitating 0.5 mL of the NC stock solution. The resulting dried CdSe/ZnS (5 mgs) was added to *N*-octylamine modified poly(acrylic acid) (30 mgs) in a vial and dissolved in chloroform. The chloroform solution was sonicated and stirred vigorously for 1 hour, after which the solvent was removed *in vacuo.* The resulting solid was then dissolved in 0.2 M NaOH solution, then dialyzed with 50000 MW centrifugal filters until the pH of the filtrate was neutral. NC-NHS esters were subsequently prepared by adding an excess of EDC (100 mg, 0.520 mmol) and NHS (50 mg, 0.43 mmol) to the water-soluble micelle encapsulated NCs as prepared in Section IV.4.g. Upon addition of both EDC and NHS, flaky precipitate formed, leaving a clear, colorless solution, which was decanted. The solid was washed with water (3 x 5 mL) to remove the excess EDC and NHS. The 542 nm emitting NC NHS-ester was dissolved in an overwhelming excess of neat *O*-(2-aminoethyl)-*O'*-(2-azidoethyl)-heptaethylene glycol (500 mg, 1.10 mmol). The azidePEG-NC solution was stirred for 1 hour, to which water (5 mL) was added. Slight precipitation formed, which was filtered with a 0.2 μm syringe filter, and the NC solution was dialyzed with 50,000 Da MWCO centrifugal filters to remove excess starting material azidePEG. After purification, the quantum yield of the NCs was found to be 2.1% against a rhodamine 560 as a reference standard, which was taken to be 95% in

ethanol.

VII.3.i Click Reaction of Azide-terminated Micelle Encapsulated NCs with RITC-labeled Cyclooctyne

RITC-cyclooctyne was dissolved in PBS buffer (pH ~ 7.4) to make an 18 μM stock solution. 1.5 mL of the RITC solution was mixed with 2 mL of 0.5 μM azidePEG NC solution in PBS, and the reaction mixture was stirred for 20 hours. Purification was achieved through multiple dialysis through 50000 MWCO centrifugal filters until the filtrate was free from any residual dye, as confirmed by UV-vis spectroscopy. The final dialyzed construct was filtered through a 0.2 μm filter. The coupling efficiency was calculated to be 3% by comparing the dye component of the UV-vis spectrum between the reaction mixture and the final NC-dye conjugate.

VII.3.j Synthesis of *N-(*2-Azidoethyl)heptaethylene Glycol Mercaptoacetamide [AzidePEG]

3-Mercaptopropionic acid NHS-ester, **4**, was synthesized using literature methods.[49] *O*-(2-Aminoethyl)-*O'*-(2-azidoethyl)-heptaethylene glycol (500 mg, 1.10 mmol) was allowed to react with 3-mercaptopropionic acid NHS-ester (0.278 g, 1.40 mmol) in 5 mL DMF and stirred overnight. Solvent was removed *in vacuo* and the product, compound **5**, was purified using flash chromatography with silica as a stationary phase and CH_2Cl_2: MeOH (93:7) as the mobile phase. The product yield was 47%. ^{1}H NMR (500 MHz, $CDCl_3$): 3.65 (m, 30H), 3.56 (m, 2 H), 3.47 (m, 2H), 3.39 (t, J = 5 Hz, 2H), 2.81 (q, J = 7.5 Hz, 2H), 2.51 (t, J = 7,2H), 1.64 (t, J = 8.5 Hz, 1H). IR (neat, cm^{-1}): 2986-2878 (CH, aliphatic), 2686 (-SH), 2108 (N_3), 1720 (C=O), 1673(CO-NH-R).

VII.3.k Synthesis of *N-(*2-Azidoethyl)nonaethylene Glycol Mercaptoacetamide

Same procedure was applied for the synthesis of *N*-(2-azidoethyl)nonaethylene glycol mercaptoacetamide as described in section VII.3.j. ^{1}H NMR (500 MHz, $CDCl_3$): 3.63 (m, 32H), 3.53 (m, 2 H), 3.45 (m, 2H), 3.37 (t, J = 5 Hz, 2H), 2.81 (m, 2H), 2.49 (t, J = 7, 2H), 1.64 (t, J = 8.5 Hz, 1H).

VII.3.l Cap-exchange of NCs with AzidePEG

Three separate vials with stirbars containing ligands A) azidePEG (50 mg, 0.095 mmol) B) azidePEG:3-mercaptopropionic acid mixture (50 mg, 0.095 mmol : 10 mg, 0.094 mmol), and C) 3-mercaptopropionic acid (20 mg, 0.19 mmol) were prepared. Three separate 0.2 mL aliquots of CdSe/CdZnS solution were precipitated by methanol and resuspended in 0.1 mL chloroform. The NC chloroform solution was injected into the vial containing the vigorously stirred ligand, and the chloroform was removed under reduced pressure. The vials were placed in a 60 °C oil bath for 6 hours, then cooled to room temperature. Ethanol was added to the cap-exchanged NCs. After addition of 1 drop of chloroform and 5 mL of hexanes, the NCs precipitated and the supernatant was decanted. Addition of pH 6.0 buffer to NCs capped with ligand set A failed to dissolve the NCs; however, addition of pH 9.0 borate buffer resulted in water solubilized NCs for ligand sets B and C. The water solubilized NCs were dialyzed with distilled water to remove excess ligand and to neutralize the pH. The NCs were filtered using 0.2 μm filter. The NCs coated with ligand set B was further dialyzed in PBS to a final concentration of 16 μM. The purified azidePEG-solubilized NCs (with ligand set B) were found to exhibit a quantum yield of Φ = 45% in water compared with the reference, rhodamine 590, which was taken to be 95% in ethanol.[50] NC-ligand set A, IR (CH_2Cl_2, cm^{-1}): 2925 (CH, aliphatic), 2106 (N_3), 1714 (C=O), 1661 (CO-NH-R). NC-ligand set B, IR (CH_2Cl_2, cm^{-1}): 3335 (OH, br), 2912 (CH, aliphatic), 2107 (N_3), 1717 (C=O), 1662 (CO-NH-R). NC-ligand set C, IR (KBr, cm^{-1}): 3435 (OH, br), 2926 (CH, aliphatic), 1701 (C=O).

VII.3.m Synthesis of *N*-Propargyl Lipoamide (Alkyne-TA)

The alkyne-modified dihydrolipoic acid (DHLA) was prepared as follows. Thioctic acid NHS-ester, **6**, was prepared according to literature methods.[51] TA-NHS (3.0 g, 9.9 mmol) and propargylamine (0.68 mL, 9.9 mmol) were allowed to react in 20 mL DMF overnight. The solvent was removed *in vacuo,* then the crude product was purified by flash chromatography, with silica as the stationery phase and CH_2Cl_2:MeOH (97:3) as the mobile phase. Removal of solvent under reduced pressure gave *N*-propargyl

lipoamide, compound **7**. ^{1}H NMR (500 MHz, $CDCl_3$): 5.61 (br s, 1H), 4.05 (m, 2H), 3.56 (m, 1H), 3.14 (m, 2H), 2.45 (m, 1H), 2.21 (m, 2H), 1.72 (m, 1H), 1.69 (m, 4H), 1.46 (m, 2H).

VII.3.n Synthesis of *N*-Propargyl Dihydrolipoamide (Alkyne-DHLA)

N-Propargyl lipoamide, **7**, (1.42 g, 5.60 mmol) was dissolved in a ethanol:water mixture (1:1) and cooled to 4 °C. Excess sodium borohydride (3 equiv.) was slowly added and the reaction was allowed to warm up to room temperature and stirred 10 hours. The product was extracted with CH_2Cl_2 (3 x 75 mL), washed with water (3 x 75 mL), dried with Na_2SO_4, and filtered. Removal of solvent under reduced pressure yielded a white amorphous solid, compound **8**, at 60% yield. ^{1}H NMR (500 MHz, $CDCl_3$): 5.63 (br s, 1H), 4.05 (m, 2H), 3.65 (m, 1H), 2.81 (m, 1H), 2.63 (m, 3H), 2.23 (m, 3H), 2.02-1.10 (m, 10H).

VII.3.o Cap-exchange of NCs with Alkyne-terminated Ligands

Three separate vials with stirbars containing ligands A) alkyne-DHLA (100 mg, 0.20 mmol) B) alkyne-DHLA: free DHLA mixture (50 mg, 0.20 mmol : 50 mg, 0.24 mmol), and C) free DHLA (100 mg, 0.48 mmol) were prepared. Three separate 0.2 mL aliquots of CdSe/CdZnS solution were precipitated by methanol and resuspended in 0.1 mL chloroform. The NC chloroform solution was injected into the vial containing the vigorously stirred ligand, and the chloroform was removed under reduced pressure. The vials were placed in a 60 °C oil bath for 2 hours, then cooled to room temperature. Ethanol was added to the cap-exchanged NCs. After addition of 1 drop of chloroform and 5 mL of hexanes, the NCs precipitated and the supernatant was decanted. Addition of distilled water to the NCs exchanged with ligand set A failed to dissolve the NCs; however, addition of distilled water resulted in solubilized NCs for ligand sets B and C. The water solubilized NCs were dialyzed with distilled water to remove excess ligand and to neutralize the pH. The NCs were filtered using 0.2 μm filter.

VII.3.p Click Reaction with Azide-terminated NCs and RITC-labeled Cyclooctyne

A spatula-tip of RITC-labeled cyclooctyne dye was dissolved in 100 μL of DMF to give a final concentration of 0.3 mM, as measured by UV-vis absorbance, with the approximation that the extinction coefficient, ε at 556 nm of RITC in ethanol is given to be 100,000 M^{-1} cm^{-1}. 20 μL of 16 μM azide-NC PBS solution was added to 4 separate 2 mL Eppendorf tubes. In each of the 4 vials different molar ratios of dye to NCs were added: 5.3 μL (5:1), 2.12 μL (2:1), and 1.06 μL (1:1) of the RITC-cyclooctyne DMF solution and 0.54 μL (5:1) of RITC-modified propargylamine (control) were added, respectively and stirred for 2 hours. A second control construct with DHLA-carboxyPEG:DHLA-hydroxyPEG (25:75) terminated NCs (5 μL) with RITC-cyclooctyne DMF (1 μL) was also mixed and stirred for 2 hours. A quenching of the NC luminescence and precipitation was observed immediately for the azide NC:RITC-cyclooctyne (5:1) mixture and after 1 hour for the (2:1) mixture. The sample with the least amount of RITC-cyclooctyne (1:1 solution) remained luminescent, but purification of the compound by dialysis resulted in the majority of the products being precipitated. After dialysis, the NC-RITC construct that remained in solution was characterized by UV-vis and steady-state emission spectroscopies. Both control constructs were shown to retain their NC luminescence properties.

VII.4 References

1. Murray, C. B.; Norris, D. J.; Bawendi, M. G. *J. Am. Chem. Soc.* **1993**, *115*, 8706-8715.

2. Bawendi, M. C.; Steigerwald, M. L.; Brus, L. E. *Annu. Rev. Phys. Chem.* **1990**, *41*, 477-496.

3. Kastner, M. A. *Phys. Today* **1993**, *46*, 24-31.

4. Anscombe, N. *Nat. Photon.* **2007**, *1*, 360-361.

5. Azzazy, H. M. E.; Mansour, M. M. H.; Kazmierczak, S. C. *Clin. Biochem.* **2007**, *40*, 917-927.

6. Hammer, N. I.; Emrick, T.; Barnes, M. D. *Nanosc. Res. Lett.* **2007**, *2*, 282-290.

7. Coe-Sullivan, S. *Mater. Matters* **2007**, *2*, 13-14.

8. Corbin, J. G.; Haydar, T. F. *Nanomedicine* **2007**, *2*, 579-581.

9. Guyot-Sionnest, P. *Mater. Matters* **2007**, *2*, 10-12.

10. Pinaud, F.; Michalet, X.; Bentolila, L. A.; Tsay, J. M.; Doose, S.; Li, J. J.; Iyer, G.; Weiss, S. *Biomaterials* **2006**, *27*, 1679-1687.

11. Reithmaier, J. P.; Somers, A.; Kaiser, W.; Deubert, S.; Gerschuetz, F.; Forchel, A.; Parillaud, O.; Krakowski, M.; Alizon, R.; Hadass, D.; Bilenca, A.; Dery, H.; Mikhelashvili, V.; Eisenstein, G.; Gioannini, M.; Montrosset, I.; Berg, T. W.; van der Poel, M.; Mork, J.; Tromborg, B. *Phys. Status Solidi B* **2006**, *243*, 3981-3987.

12. Samia, A. C. S.; Dayal, S.; Burda, C. *Photochem. Photobiol.* **2006**, *82*, 617-625.

13. Scholz, M.; Aichele, T.; Benson, O. *Adv. Solid State Phys.* **2008**, *46*, 3-14.

14. Wu, M. H.; Ueda, A.; Mu, R. *Opt. Sci. Eng.* **2005**, *99*, 331-350.

15. Somers, R. C.; Bawendi, M. G.; Nocera, D. G. *Chem. Soc. Rev.* **2007**, *36*, 579-591.

16. Jobsis, P. D.; Rothstein, E. C.; Balaban, R. *J. Microscoc.-Oxford* **2007**, *226*, 74-81.

17. Fokin, V. V. *ACS Chem. Biol.* **2007**, *2*, 775-778.

18. Gil, M. V.; Arevalo, M. J.; Lopez, O. *Synthesis* **2007**, 1589-1620.

19. Lutz, J.-F. *Angew. Chem., Int. Ed. Engl.* **2007**, *46*, 1018-1025.

20. Lutz, J.-F. *Angew. Chem., Int. Ed. Engl.* **2008**, *47*, 2182-2184.

21. Moses, J. E.; Moorhouse, A. D. *Chem. Soc. Rev.* **2007**, *36*, 1249-1262.

22. Nandivada, H.; Jiang, X.; Lahann, J. *Adv. Mater.* **2007**, *19*, 2197-2208.

23. Hawker, C. J.; Fokin, V. V.; Finn, M. G.; Sharpless, K. B. *Aust. J. Chem.* **2007**, *60*, 381-383.

24. Kolb Hartmuth, C.; Sharpless, K. B. *Drug Discov. Today* **2003**, *8*, 1128-37.

25. Kolb, H. C.; Finn, M. G.; Sharpless, K. B. *Angew. Chem., Int. Ed. Engl.* **2001**, *40*, 2004-2021.

26. Sharpless, K. B.; Manetsch, R. *Expert Opin. Drug Disc.* **2006**, *1*, 525-538.

27. Huisgen, R. *Angew. Chem.* **1963**, *75*, 742-54.

28. Huisgen, R. *Angew. Chem.* **1963**, *75*, 604-37.

29. Prescher, J. A.; Bertozzi, C. R. *Nat. Chem. Biol.* **2005**, *1*, 13-21.

30. Tornoe, C. W.; Christensen, C.; Meldal, M. *J. Org. Chem.* **2002**, *67*, 3057-3064.

31. Rostovtsev, V. V.; Green, L. G.; Fokin, V. V.; Sharpless, K. B. *Angew. Chem., Int. Ed. Engl.* **2002**, *41*, 2596-2599.

32. Brennan, J. L.; Hatzakis, N. S.; Tshikhudo, T. R.; Dirvianskyte, N.; Razumas, V.; Patkar, S.; Vind, J.; Svendsen, A.; Nolte, R. J. M.; Rowan, A. E.; Brust, M. *Bioconj. Chem.* **2006**, *17*, 1373-1375.

33. Fleming, D. A.; Thode, C. J.; Williams, M. E. *Chem. Mater.* **2006**, *18*, 2327-2334.

34. Sun Eric, Y.; Josephson, L.; Weissleder, R. *Mol. Imaging* **2006**, *5*, 122-128.

35. Xie, H.-Y.; Liang, J.-G.; Zhang, Z.-L.; Liu, Y.; He, Z.-K.; Pang, D.-W. *Spectrochim. Acta, Part A* **2004**, *60A*, 2527-2530.

36. Binder, W. H.; Sachsenhofer, R.; Straif, C. J.; Zirbs, R. *J. Mater. Chem.* **2007**, *17*, 2125-2132.

37. Agard, N. J.; Prescher, J. A.; Bertozzi, C. R. *J. Am. Chem. Soc.* **2004**, *126*, 15046-15047.

38. Agard, N. J.; Prescher, J. A.; Bertozzi, C. R. *J. Am. Chem. Soc.* **2005**, *127*, 11196.

39. Mieier, H.; Petersen, H.; Kolshorn, H. *Chem. Ber.* **1980**, *133*, 2398-2409.

40. Turner, R.; Jarret, A. D.; Goebel, P.; Mallon, B. J. *J. Am. Chem. Soc.* **1972**, *95*, 790-792.

41. Agard, N. J.; Baskin, J. M.; Prescher, J. A.; Lo, A.; Bertozzi, C. R. *ACS Chem. Biol.* **2006**, *1*, 644-648.

42. Baskin, J. M.; Prescher, J. A.; Laughlin, S. T.; Agard, N. J.; Chang, P. V.; Miller, I. A.; Lo, A.; Codelli, J. A.; Bertozzi, C. R. *Proc. Natl. Acad. Sci. U.S.A.* **2007**, *104*, 16793-16797.

43. Bertozzi, C. R.; Bednarski, M. D. *J. Org. Chem.* **1991**, *56*, 4326-4329.

44. Staros, J. V.; Bayley, H.; Standring, D. N.; Knowles, J. R. *Biochem. Biophys. Res. Commun.* **1978**, *80*, 568-572.

45. Damrauer, N. H.; Hodgkiss, J. M.; Rosenthal, J.; Nocera, D. G. *J. Phys. Chem. B* **2004**, *108*, 6315-6321.

46. Hines, M. A.; Guyot-Sionnest, P. *J. Phys. Chem.* **1996**, *100*, 468-471.

47. Dabbousi, B. O.; RodriguezViejo, J.; Mikulec, F. V.; Heine, J. R.; Mattoussi, H.; Ober, R.; Jensen, K. F.; Bawendi, M. G. *J. Phys. Chem. B* **1997**, *101*, 9463-9475.

48. Wu, X.; Liu, H.; Liu, J.; Haley Kari, N.; Treadway Joseph, A.; Larson, J. P.; Ge, N.; Peale, F.; Bruchez Marcel, P. *Nat. Biotechnol.* **2003**, *21*, 41-46.

49. Connolly, S.; Rao, S. N.; Fitzmaurice, D. *J. Phys. Chem. B* **2000**, *104*, 4765-4776.

50. Kubin, R. F. F., A. N. *J. Lumin.* **1982**, *27*, 455-462.

51. Liu, W.; Howarth, M.; Greytak, A. B.; Zheng, Y.; Nocera, D. G.; Ting, A. Y.; Bawendi, M. G. *J. Am. Chem. Soc.* **2008**, *130*, 1274-1284.

Chapter VIII

Conclusions and Future Outlook

VIII.1 Introduction

Through the manipulation of the CdSe NC surface and through the modulation of FRET, Chapters II-VII have demonstrated various approaches of conjugating NCs to energy acceptor molecules, as well as imparting to the NCs chemical and biological sensitivity to their environment. The scope of this thesis has been limited to primarily one type of quantum dot and sensing one analyte, hydronium ions. NC-based pH sensors were constructed, initially as a proof-of-concept, and several years of work have culminated into optimizing a NC-based pH sensor into a tool for sensing using multi-photon microscopy methods. With a better understanding of the surface chemistry of NCs and the sensing mechanism that underpins the sensitivity that NCs possess, new opportunities for NC sensing arise. This Chapter attempts to put into perspective the future possibilities that may appear from the work described in this Thesis. Proof-of-concept ideas for new analytes, as well as new applications of pH, are outlined and discussed in this section.

VIII.2 New Applications for pH Sensing

Chapters IV and V focused on the synthesis and development of biocompatible pH sensors specifically for incorporation into an *in vivo* tumor environment. However, a need exists in other areas for pH reporting, especially inside live cells.[1-3] Intracellular pH affects a wide range of cellular processes, such as cell proliferation, apoptosis, and mitochondrial dysfunction.[2] These processes are often regulated by transport proteins that transfer ions across cell membranes.[3,4] Despite established effects of pH on the cellular functions, understanding and knowledge of how pH changes affect specific proteins and assemblies that drive the processes are limited.[2] Endocytosis is an additional cellular process that exhibits a great pH change from pH 7.3 to less than 5.0.[5] Studies of endocytotic processes often entail monitoring pH concurrently.[6,7] NCs have been used for cell studies such as single particle tracking of receptor endocytotic trafficking[8] and labeling cell surface proteins.[9,10] A NC-based pH sensor would have great potential for studying intracellular processes.

In the Nocera and Bawendi groups, we have begun a program to investigate pH sensing and imaging in cells using NC-based sensors. Because SNARF-5F, the pH dye

Scheme VIII.1 Structure of CypHer 5E, a pH sensitive dye that fluoresces in acidic environments.

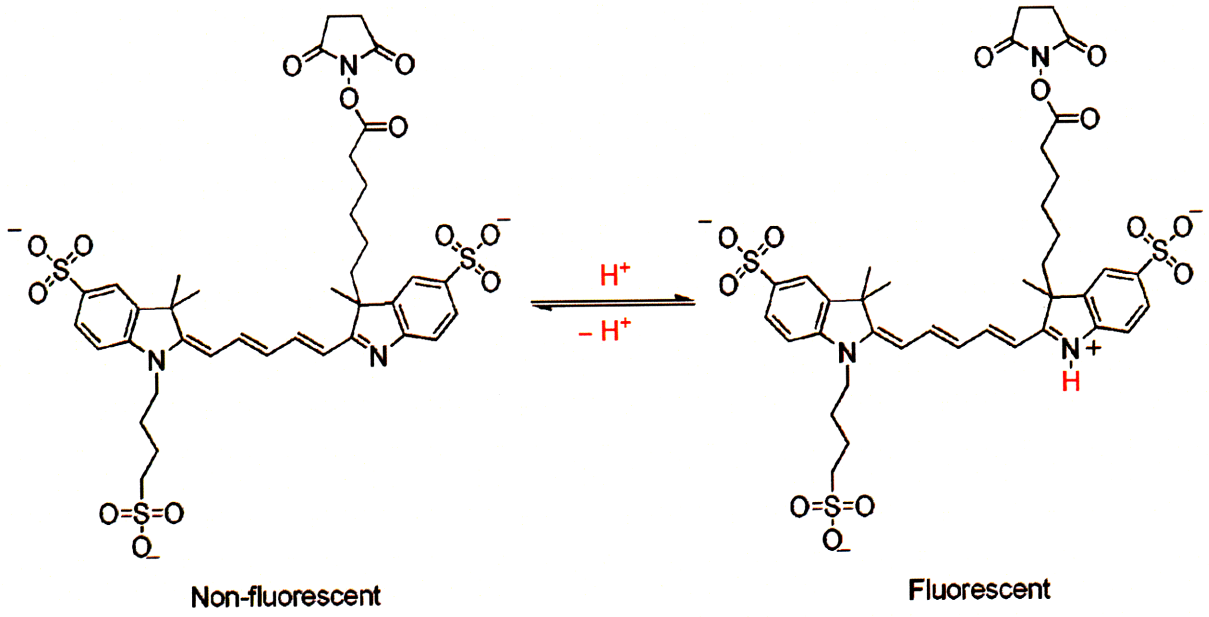

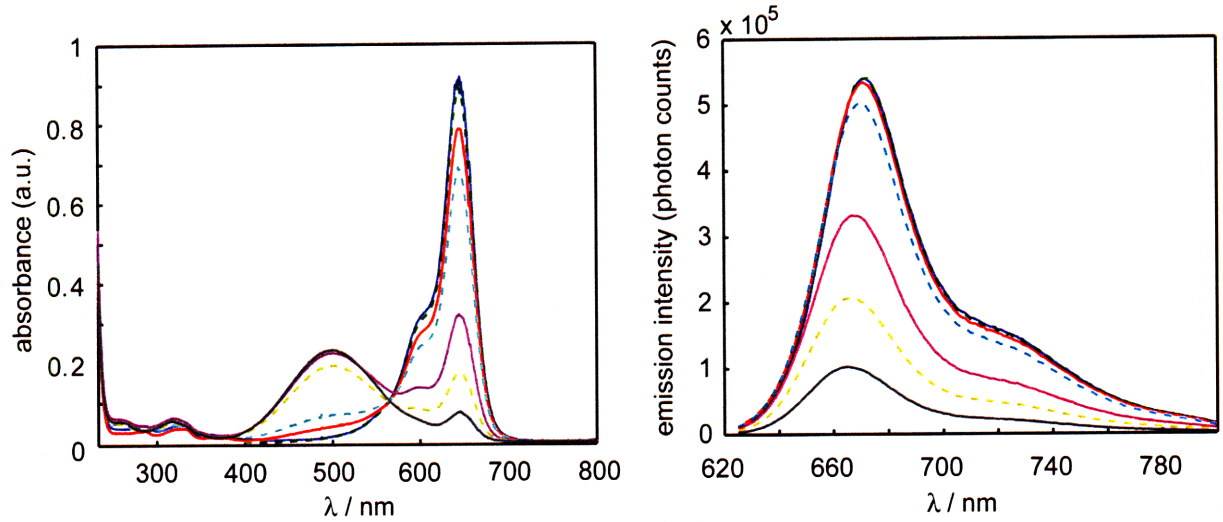

Figure VIII.1 (Left) UV-vis absorbance spectra of CypHer 5E at different pH. (Right) Relative emission intensity of CypHer 5E at different pH (λ_{ex} = 620 nm). pH 4.0 (blue solid line —), pH 5.0 (green dashed line - -), pH 6.0 (red solid line —), pH 6.5 (cyan dashed line - -), pH 7.0 (magenta solid line —), pH 7.5 (yellow dashed line - -), and pH 8.0 (black solid line —).

used in Chapters IV through VI exhibited enhanced emission intensity as the pH increased, a new dye that was more sensitive over acidic regions was desired in order to probe the cellular environment. Scheme VIII.1 and Figure VIII.1 show the structure and the photophysical properties of CypHer 5E NHS-ester, a popular choice among cellular biologists as a FRET acceptor dye. CypHer 5E is a cyanine-based pH sensor that exhibits distinct pH-dependent acid and base forms in its absorbance spectrum but only one emissive form when excited at the maximum absorbance wavelength of λ_{max} = 620 nm. The acceptor dye may be paired with a 620 nm emitting donor NC to construct a FRET-based pH sensor, similar to the sensor discussed in Chapter III.

Figure VIII.2 shows the photophysical properties of the NC-CypHer construct. The dye to NC ratio is estimated to be 1:1. In this preliminary construct, the emission of the dye was minimal, compared to that of the NC, due to the low coupling of the dye. Nevertheless, we were interested in observing whether the construct itself may undergo endocytosis into cells. The NC-CypHer and casein (which was used to help block nonspecific binding) was co-incubated with bovine aeortal endothelial cells (BAOEC), washed, and imaged, using two bandpass filters at 605 nm and 655 nm to collect the NC and dye emissions. Figure VIII.3 shows the merged image of the fluorescence of the sample with the differential interference contrast (DIC) image that outlines the cell features. The fluorescence seems to be localized within the cells, which indicated that they were successfully endocytosed, and both the dye and the NC emissions are visible, which is promising for developing NC based tools for intracellular imaging and pH sensing.

Much work remains to be done. A proper calibration in cellular media, the study of photobleaching of the CypHer 5E, and an improved, optimized coupling efficiency of the CypHer 5E to the NC are all necessary in order to effectively utilize the sensor. Once a change in the pH sensor emission is shown through endocytosis as a proof-of-concept, the NC-CypHer construct may be used as a tool for studying various endocytotic processes.

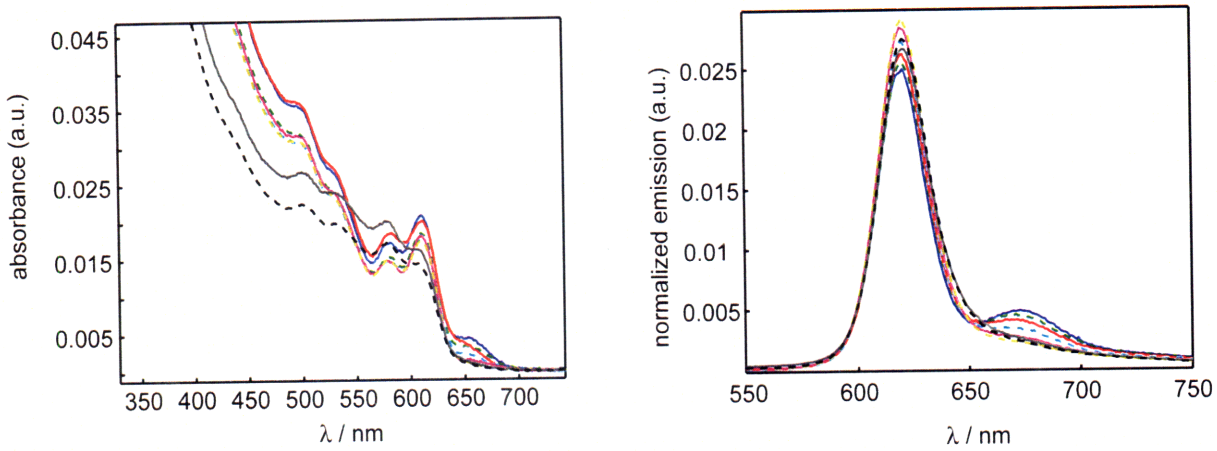

Figure VIII.2 (Left) UV-vis absorption of NC-CypHer 5E construct at different pH values. (Right) Normalized emission intensity (λ_{ex} = 420 nm) of NC-CypHer 5E at different pH values. pH 4.0 (blue solid line —), pH 5.0 (green dashed line - -), pH 5.5 (red solid line —), pH 6.0 (cyan dashed line - -), pH 6.5 (magenta solid line —), pH 7.0 (yellow dashed line - -), pH 7.5 (black solid line —), pH 8.0 (black dashed line - -).

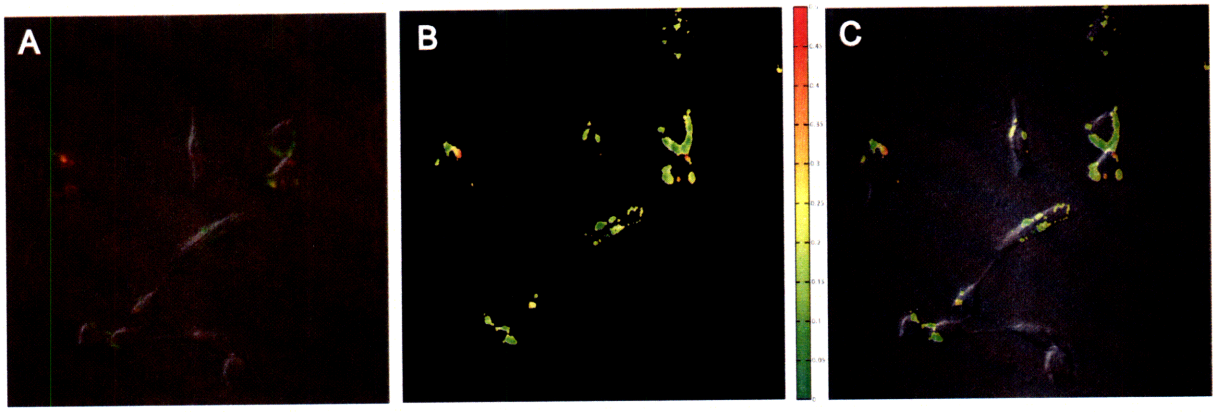

Figure VIII.3 (A) Merged image of the DIC and the fluorescence collected from the 605 filter (green) and the 655 filter (red). (B) Ratio map constructed from the emissions of the two filters. (C) Ratio map overlaid with the DIC image of the cells.

VIII.3 New Analytes to Sense

The NC FRET-based mechanism of sensing analytes is general and can easily be applied to other targets. As mentioned in Chapter I, oxygen tension is also another metabolic functional parameter in a tumor environment that would be informative for cancer treatment. Chapter I.1.b describes the collisional quenching mechanism used in phosphorescent oxygen sensors. One such sensor is a palladium meso-tetra-(4-carboxyphenyl)porphyrin (Oxyphor R_0).[11,12] The Q band absorption of the porphyrin at

524 nm is readily accessible to NC FRET donors. Figure VIII.4 A shows UV-vis absorption spectra of the Oxyphor R_0 by itself and when conjugated to the NC. The broad NC absorption feature is apparent at the wavelengths of higher energy. Figure VIII.4 B shows the emission spectra of the NC-oxyphor conjugate when the sensor is saturated with nitrogen, then later saturated with oxygen. Scheme VIII.2 depicts the mechanism of the NC-oxyphor sensor. The oxyphor emission, ranging from 650 to 800 nm, is clearly enhanced in the absence of oxygen. However, the absorbance of the sensor is oxygen independent; therefore, NC FRET-based ratiometric sensing is achieved by utilizing the NC emission as an internal standard that remains insensitive to

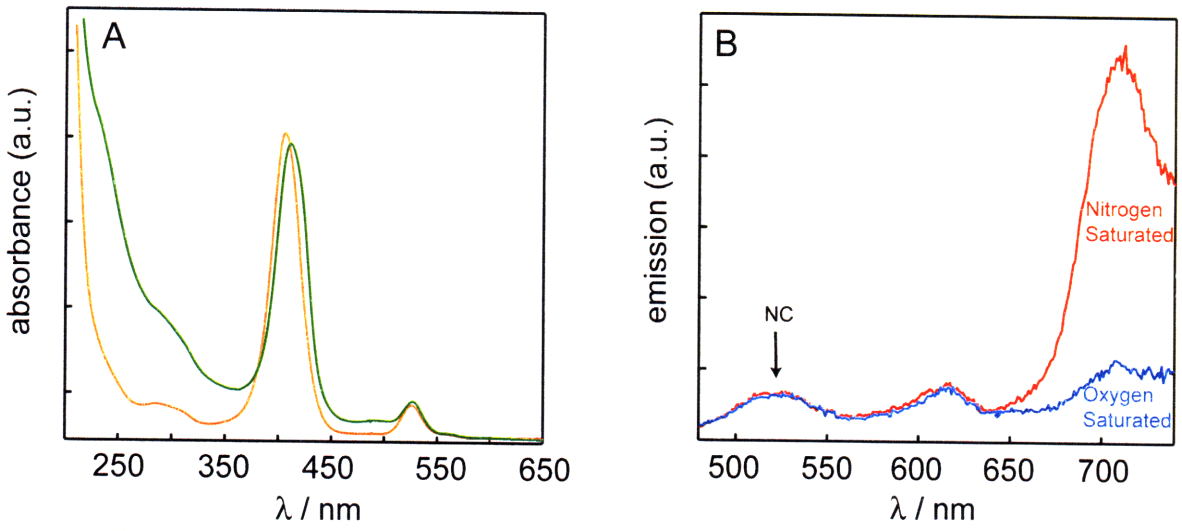

Figure VIII.4 (A) absorption spectra of Oxyphor R_0 (yellow solid line —) and NC-Oxyphor R_0 conjugate (light green solid line —). (B) Emission intensity (λ_{ex} = 350 nm) of the NC-Oxyphor R_0 conjugate saturated with oxygen (blue solid line —) and nitrogen (red solid line —).

Scheme VIII.2 The signal transduction mechanism for the oxygen sensor is different from that of the NC-based pH sensors. The oxygen sensor relies on the NC as a two photon antenna and as an internal standard.

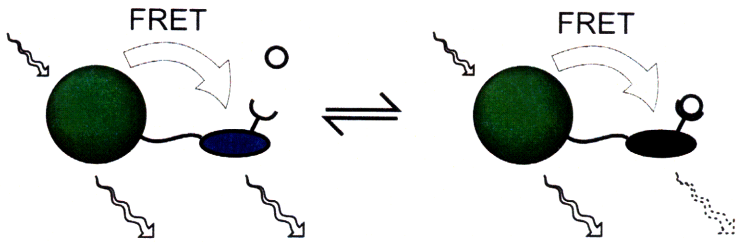

oxygen concentration. The photophysical characterization of the NC-oxyphor construct was sufficient as a proof-of-concept for a new type of NC FRET-based sensor, and more sophisticated NC-based oxygen sensors are currently being pursued in our laboratory.[13]

VIII.4 Moving beyond CdSe Nanocrystals

The scope of this Thesis has been limited to CdSe/CdZnS, CdSe/ZnS, or in one case, ZnSe/CdSe/ZnS, with emission ranges of approximately 500-660 nm.[14-17] Although the use of the CdSe system has been advantageous due to the well-developed synthesis, high quantum yields in water, and visible nature of their photoluminescence, the choice of acceptor dyes for the FRET system becomes restricted to those that only absorb between 500-660 nm. Many chemically-sensitive molecular fluorophores have absorption at shorter wavelengths than is easily accessed with cadmium based NC emission, rendering them unsuitable for FRET pairing with CdSe NCs.[1,18-23] The use of NCs composed of different materials would allow us to access more wavelengths for the creation of donor-acceptor FRET pairs. CdS,[14] ZnSe,[24] and ZnSeTe[25] would access NC donor wavelengths that are higher in energy, between 400-550 nm. In fact, CdS/ZnS has already been used to construct a fluorescein-based pH sensor using the sensing mechanism described in Chapter III.[26] Other materials, such as InAs,[27] CdTe,[14,28-30] Cu-In-Se, and Ag-In-Se[31] NCs would access NC donor wavelengths that are lower in energy, between 600-1000 nm. The NCs emitting in the red or NIR are better suited towards biological applications due to the existing 'biological window' that would minimize autofluorescence by other absorbing biomolecules.[32] As InAs and CdTe have been used for biological applications,[27,30] they may be a natural choice as NIR-emitting FRET donors for new sensing constructs.

VIII.5 New Mechanism of Sensing Incorporating NCs

In order to expand our sensing repertoire for NCs, new mechanisms for signal transduction should be considered. Recently, NCs have been shown to undergo electron transfer as both donors[33-35] and acceptors, resulting in a quenching of the NC

luminescence.[36-39] Modulation of the charge transfer processes through analyte interactions have resulted in maltose[38,39] and glucose[34,40] sensors. However, these sensors usually relied on the conformational change of the maltose binding protein for maltose sensors,[38,39] or a mixture of reagents for glucose sensors.[34,40] No small molecule, covalently tethered NC donor-acceptor electron transfer pair has been used for sensing. A good starting point for sensor design is an understanding of the parameters that affect electron transfer using NCs. In fact, a thorough investigation of NC electron transfer (both as donor and acceptor) that examines the rate of electron transfer through modulation of distance, solvent reorganization energy, or driving force has not been performed. The NC surface chemistry discussed in this thesis may aid in modulating the distance between the donor-acceptor pair. Surface chemistry of the NCs must also be considered for solubility, if electron transfer rates with respect to solvent reorganization energy are to be studied. Variation of redox potentials of the charge transfer partner will aid in the study of driving force dependence. An electron transfer partner to the NC that has a clear charge separated state that can be easily distinguished, such as the rhenium complex reported by Huang *et al.*[33] would be ideal for characterization of charge transfer through ultrafast techniques. Additional considerations for the study of charge transfer include the effect of the overcoating layer of the NCs, the size of the NCs, and the materials of the NCs. All the aspects discussed above must be considered before a reliable, well-understood, well-characterized, and robust sensor using a charge transfer mechanism can be created.

VIII.6 Concluding Remarks

This Thesis has focused on NC surface chemistry, conjugation techniques of NCs to small molecules, and characterization of NCs as FRET donors for the purpose of constructing NC-based chemical and biological sensors. Applications for *in vivo* sensing of the tumor metabolic environment have been pursued. Many avenues of NC sensing still remain unexplored, some of which are described in this Chapter. The development of the NC constructs will supplement and complement existing sensing technologies for new applications and techniques. Further research on NC-acceptor molecule conjugates will bring forth new and exciting opportunities to contribute to the

field of optical sensing.

VIII.7 Experimental Procedures

VIII.7.a Materials and Methods

CypHer 5E was purchased from GE Healthcare. Oxyphor R_0 was purchased from Oxygen Enterprises. Decylamine, anhydrous *N,N'*-dimethylformamide (DMF), trioctylphosphine oxide (90%, TOPO), cadmium 2,4-pentanedionate, dodecanal, 1800 MW poly(acrylic acid), 5-amino-1-pentanol, *N*-octylamine, 0.1 M tetrabutylammonium hydroxide in methanol, *N*-hydroxysuccinimide (NHS), thioctic acid, thionyl chloride, sodium azide, triphenylphosphine, sodium bicarbonate, dicyclohexylcarbodiimide (DCC), 4,4'-dimethylaminopyridine (DMAP), basic Al_2O_3 (150 mesh), and Sephadex LH-20 were purchased from Sigma-Aldrich. 1-Ethyl-3,3′-dimethylaminopropylcarbodiimide (EDC), hexadecylamine (HDA), poly(ethylene glycol) 400, bis(trimethylsilyl)sulfide [$(TMS)_2S$], and diethylzinc ($ZnEt_2$) were purchased from Fluka. Selenium shot and hexylphosphonic acid (HPA) were obtained from Alfa Aesar. Trioctylphosphine (TOP) and sodium borohydride ($NaBH_4$) were purchased from Strem Chemicals. Bovine *N,N'*-dimethylcasein was ordered from Calbiochem. Bovine aeortal endothelial cells were ordered from Genlantis. All air sensitive materials were handled in an Omni-Lab VAC glove box under dry nitrogen atmosphere with oxygen levels <0.2 ppm. All materials were used as purchased, except for TOPO and 5-amino-1-pentanol, which were purified through vacuum distillation, and diethylzinc which was passed through a 0.2 μm syringe filter before use. Centrifugal filters equipped with a 50,000 Da molecular weight cutoff (MWCO) dialysis membrane were purchased through Millipore Corporation.

VIII.7.b Spectroscopic Characterization

UV-vis spectroscopy of SNARF coupled CdSe/CdZnS were measured on a Hewlett-Packard 8453 UV-vis spectrophotometer with the Chemstation software. Steady-state fluorescence measurements were obtained in a 1 cm pathlength cuvette from a custom-built Photon Technology Instruments fluorometer installed with a Hamamatsu R928 photomultiplier tube and a 150 W Xe excitation lamp.

All NMR spectra were collected at the MIT Department of Chemistry Instrumentation Facility (DCIF) on a Varian Mercury 300 MHz or a Varian Inova 500 MHz NMR spectrometer at room temperature. Chemical shifts are reported using the standard δ notation in ppm and are referenced to tetramethylsilane (TMS) using the residual ^1H signal of the deuterated solvent, $CDCl_3$, as an internal standard. IR Spectra of samples were collected on a Perkin-Elmer 2000 FTIR spectrometer. Differential interference contrast imaging and fluorescence imaging of cells were performed on a Nikon Eclipse TEU 2000 microscope equipped with 488 nm excitation source and emission filters at 605 ± 55 and 655 ± 15 nm.

VIII.7.c Synthesis of CdSe/CdZnS (λ_{em} = 620 nm)

CdSe NCs overcoated with alloyed CdZnS were prepared using a modified literature method.[14-16] A vial containing cadmium 2,4-pentanedionate (0.317 g, 0.00100 mol), dodecanal (0.50 mL, 0.0023 mol) in trioctylphosphine (6.0 mL, 0.0135 mol) was degassed at 180 °C for an hour, then cooled to yield a homogenous bright yellow solution. 1.5 M trioctylphosphine selenide (TOPSe, 4 mL, prepared from dissolving 5.92 g Se shot into 50 mL TOP) was subsequently added to the vial being cooled to room temperature. The contents of the vial were subsequently injected rapidly at 360 °C into a three-necked flask (equipped with an air condenser, temperature controller, and a stir bar) containing degassed solvent of trioctylphosphine oxide (6.25 g, 0.0162 mol), hexadecylamine (5.75 g, 0.0238 mol), and trioctylphosphine (3.4 mL, 0.0076 mol). The temperature of the growing CdSe NCs was cooled immediately by removing the heating mantle to obtain NCs with a first absorption feature of 596 nm.

The bare CdSe NCs were precipitated out of the growth solution with butanol and methanol twice and brought up in 4 mL hexanes. The NCs were overcoated by injecting the hexane solution of core CdSe into a degassed solvent of distilled trioctylphosphine oxide (10.0 g, 0.0259 mol) and n-hexylphosphonic acid (0.40 g, 0.0024 mol). The hexane was removed *in vacuo* at 80 °C, and decylamine (0.50 mL, 0.0020 mol) was added. After stirring for 1 hr, the solution temperature was raised to 140 °C. Two separate precursor solutions of bis(trimethylsilyl)sulfide in 5 mL TOP, and diethylzinc and dimethylcadmium (in a 80: 20 molar ratio) in 5 mL TOP was slowly added to the

core solution over the course of two hours using a syringe pump. Exact amounts were chosen to yield a ~2.5 monolayer coating of ZnS on the bare CdSe NCs, using the methods of Dabboussi et al.[16] The final emission wavelength was 620 nm with a FWHM of 26 nm.

VIII.7.d Synthesis of Cap-exchanged Water-soluble NCs

The CdSe/CdZnS synthesized in section VIII.7.c (0.5 mL) was precipitated from the growth solution once using a mixture of n-butanol and methanol. DHLA-hydroxyPEG and DHLA-aminoPEG were prepared as described in Chapter V.4, and the cap-exchange proceeded as described in Chapter V.4.h.

VIII.7.e Synthesis of NC-CypHer Construct

CdSe/CdZnS water-solubilized NCs as prepared from Section VIII.7.d was dialyzed into pH 8.3 sodium bicarbonate buffer (0.1 M) until the final volume was 0.6 mL, which was estimated to be 3 μM. CypHer 5E mono-NHS ester (1 mg) was dissolved in DMSO (100 μL), 9 μL of which was injected to a vigorously stirring solution of the water-solubilized NCs, and stirred overnight. The reaction mixture was diluted with 10 mL of distilled water, then dialyzed with 50,000 MWCO centrifugal filters until all residual uncoupled dye was removed, as measured from the absorbance of the filtrate. The NC-CypHer pH sensor was characterized by UV-vis and emission spectroscopy in acetate buffer for pH 4 and in phosphate buffers for pH 5-8.

VIII.7.f Incorporation of NC-CypHer Construct into Cells

Bovine aeortal endothelial cells (BAOEC) in a Petri dish were washed with PBS buffer (3 x 100 μL) and incubated with 100 μL of 1% casein solution in PBS for 2 minutes. NC-CypHer construct mixed with 0.5% casein was added to the cells (100μL total volume, ~200 nM) and incubated at 37 °C and 5% CO_2 for 30 minutes. Afterwards, the cells were washed with PBS (7 x 100 μL). Cells were place on microscope slides and imaged under the microscope at 488 nm excitation at an acquisition time of 5 seconds. Fluorescence images were collected using emission filters centered at 605 ±

55 and 655 ± 15 nm.

VIII.7.g Synthesis of ZnSe/CdSe/ZnS Nanocrystals (λ_{em} = 533 nm)

ZnSe/CdSe NCs were prepared as previously reported.[17] ZnSe NCs were synthesized by rapidly injecting a solution consisting of diethylzinc (96 mg, 0.78 mmol) dissolved in TOP (4.0 mL, 0.0090 mol) and 1.0 M TOPSe (1 mL, 1 mmol, prepared from dissolving 3.948 g Se shot into 50 mL TOP) into a 3-necked flask containing degassed hexadecylamine (7.0 g, 0.029 mol) at 310 °C. The resulting solution was cooled to 270°C and the NCs were allowed to grow for an hour. The temperature of the ZnSe solution was then lowered to 150 °C. In a separate 4-necked flask equipped with an addition funnel, air condenser, and temperature controller, TOPO (8.0 g, 0.0207 mol) and HPA (0.40 g, 2.4 mmol) was degassed at 150°C. The addition funnel was loaded with a solution consisting of dimethylcadmium (78 mg, 0.55 mmol), 1.5M TOPSe (0.60 mL, 0.90 mmol), and TOP (4.4 mL, 9.9 mmol). Immediately after 4 mL of the ZnSe growth solution prepared above (and maintained at 150 °C) was transferred to the 4 necked flask, the contents of addition funnel was allowed to drip at approximately 1 drip/second. The resulting solution was stirred at 150 °C for 24 hours and was found to have a first absorption feature at λ_{abs} = 472 nm.

The ZnSe/CdSe NCs were precipitated once with methanol, resulting in a yellow paste. The NCs were extracted with 3 x 5 mL hexanes until the paste turned white. The extracted hexane solution of NCs were re-precipitated with n-butanol and methanol twice more and re-dissolved in 4 mL hexanes. The hexane NC solution was then injected into an additional 4-necked flask containing degassed distilled TOPO (10.0 g, 25.9 mmol) and HPA (0.40 g, 2.4 mmol) that was stirring at 80°C. The hexanes were removed from the NC solution *in vacuo* at 80°C. The temperature of the solution was then raised to 150 °C. Two separate precursor solutions of bis(trimethylsilyl)sulfide in 5.0 mL TOP, and diethylzinc and dimethylcadmium (in a 80: 20 molar ratio) in 5.0 mL TOP was slowly added to the core solution over the course of two hours using a syringe pump. Exact amounts were chosen to yield a ~5 monolayer coating of ZnS on the bare CdSe nanocrystals, using the methods of Dabboussi et al.[16] The NCs were stirred

overnight at 80°C after the addition of the shell precursors, yielding ZnSe/ CdSe/ CdZnS NCs with a first absorption feature of λ_{abs} = 505 nm and an emission centered at λ_{em} = 533 nm.

VIII.7.h Preparation of Polymer Micelle Encapsulated NCs

Water-soluble CdSe/CdZnS nanocrystals were prepared by precipitating 1 mL of the NC stock solution. The resulting dried CdSe/ ZnS (10 mgs) was added to octylamine and 5-amino-1-pentanol modified poly(acrylic acid) (60 mgs) in a vial and dissolved in chloroform. The chloroform solution was sonicated and stirred vigorously for 1 hour, after which the solvent was removed *in vacuo.*

VIII.7.i Preparation of NC-Oxyphor Construct

A sample of the polymer coated NCs was dissolved in 2 mL DMF, to which Oxyphor R_0 (2.0 mg, 2.2 μmol) and EDC (2.0 mg, 10 μmol) was added and stirred overnight. . Evaporation of DMF and addition of H_2O and 0.1 mL 0.1 M tetrabuytlammonium hydroxide in methanol yielded water-solubilized ZnSe/CdSe/ZnS NCs conjugated to Oxyphor R_0. The conjugates were purified by dialysis through Millipore centrifuge tubes equipped with 50000 Da MWCO filters. After multiple washings, the free dye was completely removed from the NC-dye construct as verified by the absence of the parent dye absorption features in the UV-vis absorption spectrum of the filtrate.

VIII.8 References

1. Haugland, R. P. *The Handbook-A Guide to Fluorescent Probes and Labeling Technologies* 10th edition ed.; Molecular Probes: Eugene, OR, 2005.

2. Srivastava, J.; Barber, D. L.; Jacobson, M. P. *Physiology* **2007**, *22*, 30-39.

3. Roos, A.; Boron, W. F. *Physiol. Rev.* **1981**, *61*, 296-434.

4. Bradley, M.; Alexander, L.; Duncan, K.; Chennaoui, M.; Jones, A. C.; Sanchez-Martin, R. M. *Bioorg. Med. Chem. Lett.* **2008**, *18*, 313-317.

5. Pillay, C. S.; Elliott, E.; Dennison, C. *Biochem. J.* **2002**, *363*, 417-429.

6. Lakadamyali, M.; Rust, M. J.; Zhuang, X. *Cell* **2006**, *124*, 997-1009.

7. Rust, M. J.; Lakadamyali, M.; Zhang, F.; Zhuang, X. *Nat. Struct. Mol. Biol.* **2004**, *11*, 567-573.

8. Rajan, S. S.; Liu, H. Y.; Vu, T. Q. *ACS Nano, in press* **2008**.

9. Howarth, M.; Liu, W.; Puthenveetil, S.; Zheng, Y.; Marshall, L. F.; Schmidt, M. M.; Wittrup, K. D.; Bawendi, M. G.; Ting, A. Y. *Nat. Methods* **2008**, *5*, 397-399.

10. Howarth, M.; Takao, K.; Hayashi, Y.; Ting, A. Y. *Proc. Natl. Acad. Sci. U.S.A.* **2005**, *102*, 7583-7588.

11. Dunphy, I.; Vinogradov, S. A.; Wilson, D. F. *Anal. Biochem.* **2002**, *310*, 191-198.

12. Vinogradov, S. A.; Wilson, D. F. *J. Chem. Soc., Perkin Trans. 2* **1995**, 103-11.

13. McLaurin, E.; Greytak, A. B.; Bawendi, M. G.; Nocera, D. G. *Unpublished results.*

14. Murray, C. B.; Norris, D. J.; Bawendi, M. G. *J. Am. Chem. Soc.* **1993**, *115*, 8706-8715.

15. Hines, M. A.; Guyot-Sionnest, P. *J. Phys. Chem.* **1996**, *100*, 468-471.

16. Dabbousi, B. O.; Rodriguez-Viejo, J.; Mikulec, F. V.; Heine, J. R.; Mattoussi, H.; Ober, R.; Jensen, K. F.; Bawendi, M. G. *J. Phys. Chem. B* **1997**, *101*, 9463-9475.

17. Ivanov, S. A.; Nanda, J.; Piryatinski, A.; Achermann, M.; Balet, L. P.; Bezel, I. V.; Anikeeva, P. O.; Tretiak, S.; Klimov, V. I. *J. Phys. Chem. B* **2004**, *108*, 10625-10630.

18. Kikuchi, K.; Takakusa, H.; Nagano, T. *Trends Anal. Chem.* **2004**, *23*, 407-415.

19. Woodroofe, C. C.; Won, A. C.; Lippard, S. J. *Inorg. Chem.* **2005**, *44*, 3112-3120.

20. Tsien, R. Y. *Trends Neurosci.* **1988**, *11*, 419-424.

21. Tsien, R. Y. *Method Cell Biol.* **1989**, *30*, 127-156.

22. Domaille, D. W.; Que, E. L.; Chang, C. J. *Nat. Chem. Biol.* **2008**, *4*, 168-175.

23. Martinez-Manez, R.; Sancenon, F. *Chem. Rev.* **2003**, *103*, 4419-4476.

24. Hines, M. A.; Guyot-Sionnest, P. *J. Phys.Chem. B* **1998**, *102*, 3655-3657.

25. Guan, J.; Nair, G.; Bawendi, M. G. *J. Am. Chem. Soc.* **2008**, *in press.*

26. Chen, Y.; Thakar, R.; Snee, P. T. *J. Am. Chem. Soc.* **2008**, *130*, 3744-3745.

27. Zimmer, J. P.; Kim, S.-W.; Ohnishi, S.; Tanaka, E.; Frangioni, J. V.; Bawendi, M. G. *J. Am. Chem. Soc.* **2006**, *128*, 2526-2527.

28. Wang, S.; Mamedova, N.; Kotov, N. A.; Chen, W.; Studer, J. *Nano Lett.* **2002**, *2*, 817-822.

29. Mamedova, N. N.; Kotov, N. A.; Rogach, A. L.; Studer, J. *Nano Lett.* **2001**, *1*, 281-286.

30. Kim, S.; Lim, Y. T.; Soltesz, E. G.; De Grand, A. M.; Lee, J.; Nakayama, A.; Parker, J. A.; Mihaljevic, T.; Laurence, R. G.; Dor, D. M.; Cohn, L. H.; Bawendi, M. G.; Frangioni, J. V. *Nat. Biotechnol.* **2004**, *22*, 93-97.

31. Allen, P.; Bawendi, M. G. *Submitted.* **2008**.

32. Konig, K. *J. Microsc- Oxford* **2000**, *200*, 83-104.

33. Huang, J.; Stockwell, D.; Huang, Z.; Mohler, D. L.; Lian, T. *J. Am. Chem. Soc.* **2008**, *130*, 5632-5633.

34. Cordes, D. B.; Gamsey, S.; Singaram, B. *Angew. Chem., Int. Ed. Engl.* **2006**, *45*, 3829-3832.

35. Liu, Q.; Lu, X.; Li, J.; Yao, X.; Li, J. *Biosens. Bioelectron.* **2007**, *22*, 3203-3209.

36. Sykora, M.; Petruska, M. A.; Alstrum-Acevedo, J.; Bezel, I.; Meyer, T. J.; Klimov, V. I. *J. Am. Chem. Soc.* **2006**, *128*, 9984-9985.

37. Aryal, B. P.; Benson, D. E. *J. Am. Chem. Soc.* **2006**, *128*, 15986-15987.

38. Sandros, M. G.; Gao, D.; Benson, D. E. *J. Am. Chem. Soc.* **2005**, *127*, 12198-12199.

39. Sandros, M. G.; Shete, V.; Benson, D. E. *Analyst* **2006**, *131*, 229-235.

40. Yuan, J.; Guo, W.; Wang, E. *Biosens. Bioelectron.* **2008**, *23*, 1567-1571.

Acknowledgements

There are so many people that I would like to thank, as over the past five years, I've had the pleasure of working with great collaborators and colleagues. It's very difficult to put into words how grateful I am to be surrounded by such amazing people, but here goes.

I'd like to first thank my family for their love and encouragement. My parents, David and Kiyomi, never wavered in their support during my studies at MIT. Holly, always upbeat and cheerful, gave me pep talks and tough love when needed. Although I've only known him for a short period of time, I've also enjoyed getting to know and interacting with my brother-in-law Steve. I am so lucky to have a very supportive and close-knit family.

I've been fortunate to work directly with two amazing post-docs in my research. Preston Snee (a.k.a. Dr. Chicken) took me under his wing and taught me everything he knows about the world of nanocrystals. Preston patiently answered a barrage of questions that I had on my project and constantly challenged how I thought about a scientific problem. Awesome friend who also deserves credit for introducing me to the world of Halo and... terrorizing people online through Halo. Fortunately, that phase of my life ended as soon as Preston left, but not the scientific training. Preston's enthusiasm for everything from a new reaction to a weird cat was definitely contagious, and I had a lot of fun working alongside him the first few years of my graduate years, when most of the work described in Chapters II and III were accomplished. Andrew Greytak, who took over as the post-doc on the chemosensing project, brought calm, logical efficiency to our subgroup. Andrew was also the primary editor of my thesis chapters (thank you!) and contributed to Chapters V and VI. I am also in awe of his matlabbing skills, which is something that I benefited and learned from during the course of research. Looking forward to seeing more pictures of baby Alex, and I will miss our morning coffee outings.

Little Emily brought style and trendiness into our subgroup when she decided to tackle oxygen sensing using dots. I admire her prowess with the nanosecond laser, as well as skill with her turntables. She's also a very considerate person that also throws great parties. Ryan Lanning, an intelligent and laid-back multiphoton microscopy graduate student in Rakesh Jain's lab, bravely injected all my sensing concoctions into innocent mice. He fielded my questions about biology and tumors with ease and all the biology experiments described in Ch. VI were done in collaboration with him.

Labmates outside of my subgroup also contributed to the fun times and interesting discussions found in the Nocera group. Liz Young helped me out whenever I needed a set up for lifetime measurements, and she was always a pleasure to chat with about research (hers or mine). I'm also deeply grateful for her friendship throughout our time here at MIT (she bravely agreed to be my Muddy Buddy!) and especially during the dark parts of the thesis writing time. The sauna breaks were rejuvenating and definitely kept me going towards the end. Justin Hodgkiss and Julien Bachmann were always receptive towards chemistry discussions and helped me critique ideas that I had, and we also shared the same passion for traveling. I found Jenny Yang to be very helpful, whether it was lab advice or hockey tips. Joel Rosenthal contributed more than his share in the Nocera lab fun, especially with the latest acquisition of the lab chin-up bar. Streece and Arthur can always be counted on to dispense scientific advice and be at the center of lab social events. Aetna, Bart, and Manke ruled the lab when I first joined,

and their three completely different personalities combined made the lab festive. Glen, I am amazed at how you are able to work for two different advisors and still get work done. Montana, I admire your strength and determination as you explore metal oxide colloids. Changhoon, where did Japanese girls fall on your scale again??? -- J/K. Good luck with your cobalt chemistry, and if you need someone to gang up against Dino, give me a call. I have to acknowledge the very exclusive cult called the Cornucopia for some fun company: Tim- thanks for being a good sport when I decided that you were going to be the primary victim of my rare and occasional teasing. It is well known that every inorganic thesis should include a crystal structure. Thanks to the mad crystallographic skills of Tim, my thesis is now a true inorganic thesis, complete with a *bona fide* crystal structure (see Figure Ack.1) and a table of parameters (see Table Ack.1). Yogi can engage anyone into a scientific debate with ease, and I am fascinated by his fascination of all things magnetic. Finally, Tom, the youngest of the Cornucopians, is an inspiring softball captain that is always ready to bring his A game. He should also be the new Poland Springs waterboy, as the lab hasn't had one since Jake Soper. I'm very happy to have briefly worked next to Jay Yang to get a sense of his sarcastic humor and wish him the best maneuvering the intricacies of the picosecond laser. Marshak-where do I begin? Thanks for tolerating my increasing presence in the Vortex of Unproductivity. It was very fun just chatting and looking at various YouTube footages with you. I also expect you to keep your promise regarding a particular karaoke video. Too bad we only

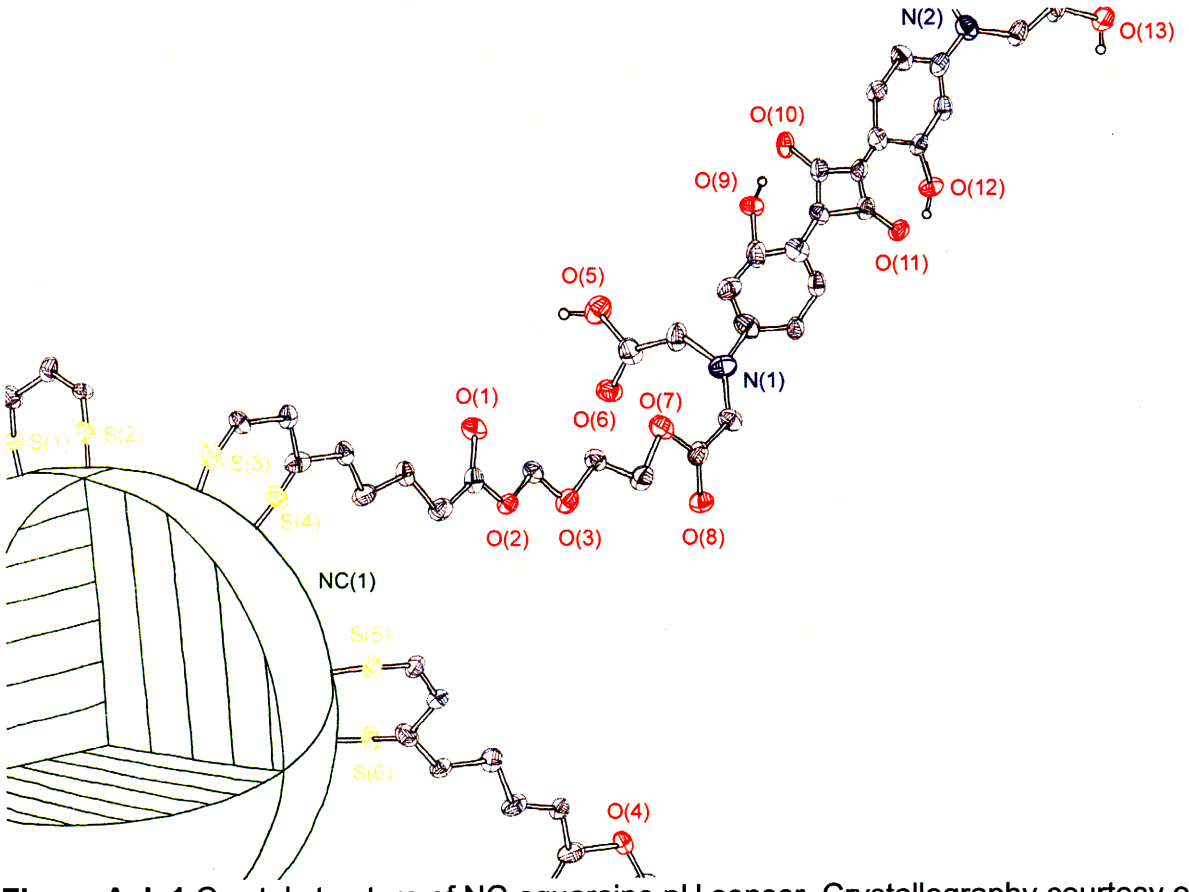

Figure Ack.1 Crystal structure of NC-squaraine pH sensor. Crystallography courtesy of Tim Cook.

Table Ack.1. Crystal data and structure refinement for NC-squaraine crystal

Empirical formula	$NC_1C_{95}H_{117}O_{39}N_6S_6$
Formula weight	100,000
Temperature	298 K
Wavelength	0.71073 Å
Crystal system	Triclinic
Space group	$P\bar{1}$
Z	2
Crystal size	100 × 100 × 100 nm^3
Θ range for data collection	1.65 to 30.0°
Reflections collected	1000
Independent reflections	1000 [R_{int} = 0.01]
Completeness to Θ =30.0°	100%
Absorption correction	Empirical Ginger Ale
Refinement method	TRC Least-squares on F^2
Goodness–of–fit on F^2	1.0000000(0)
Final R indices [I>2σ(I)]	R_1 = 0.00001, wR_2 = 0.00002
R indices (all data)	R_1 = 0.000015, wR_2 = 0.000023
Largest diff. peak and hole	1.07 and –1.03 e/$Å^{-3}$

[a] GOF = $(\Sigma\, w(F_o^2 - F_c^2)^2/(n-p))^{1/2}$ where n is the number of data and p is the number of parameters refined. [b] $R1 = \Sigma||F_o| - |F_c||/\Sigma|F_o|$. [c] $wR2 = (\Sigma(w(F_o^2 - F_c^2)^2)/\Sigma(w(F_o^2)^2))^{1/2}$.

had a chance to go once. I hope you keep on organizing fun lab social events. Chambers (a.k.a. Dorothy for reasons that hopefully will eventually be explained to me) – I wish I had the chance to score at least once while you were the hockey goalie. Also, I want to thank Arturo, the two-time Nocera lab hotdog eating champ, who reminded me of the positive attitude I had as a first year when he cheerfully claimed that he would be making friends with a column after some unknown pink crap invaded his reaction flask. I was sad to overlap only briefly with Kate and Hannah, but I wish them all the best. Last but not least, I'd like to thank my fellow inorganic classmate and good friend, Emily Nytko. Her husband John and she allowed me to join their morning runs on the Charles, which definitely mitigated some of the thesis stress. ☺ Emily and I studied, commiserated, partied, and played as we jumped through all the hurdles of the inorganic degree program together. I'm looking forward to finding a good place where we can all hang out together in the DC area.

In addition to grad students, Dan has the ability to pick out extraordinary postdocs. I'd like to acknowledge Matt Shores, Adam Viege, and Jake Soper for all the laughs they provided at the Muddy. Daniel Grohol's birthday singing is still remembered by the lab. Thomas Gray gave me an insight into being a professor when he gave me his itemized budget for his Case Western start-up, and I'm glad to see him so

successful at Case. I felt privileged to have taken rumba, jive and salsa lessons from Shih-Yuan Liu, great organic chemist as well as ballroom dance champ. Deqiang An and Alex Krivokapic were efficient porphyrin chemists that were happy to give me tips on organic chemistry. Poul was helpful with IR advice, and he also has an amazingly green thumb! I'd like to thank Ted Betley for his professionalism and for giving me insight into proposal writing. Matt Kanan will be remembered for his deadpan humor that constantly keeps me on my toes and also for letting me defend on his 30th birthday. Dino Villagrán's friendship and encouragement has helped me get through some tough times. Thank you for the chair where there was a lot of laughter shared, for the three minute Instructions, and for re-iterating that life is simple. I'm ready to wager another ten dollars for the next OU – Texas A&M game. Be ready to pay up for the third year in a row. Sitting in between Sebastian and Rick inevitably led to some fun interesting conversations on the second floor. I had fun working with you guys in the second floor labs. I admire Danny Lutterman and Jon Melnick's ability to not get sucked into the Vortex upstairs. Thank you Alex R. for always having a beer on hand when I needed it. Good luck to Matthias as he expands the Nocera lab into new, uncharted territory.

The Nocera lab has had some key undergraduates to make some events memorable. Kris Tantillo, future medical doctor, worked with me synthesizing cyclooctyne derivatives described in Chapter VII. Queen Jillian is a good friend who is intelligent, compassionate, and funny. I wish the best for all past and present undergrads who passed through our lab, including T.D., Barchi, Kate, Steven, Noah, and Froylan.

I've had the pleasure of interacting with several visiting scientists that have passed through our labs. Thank you to Mike Sailor, Silvio Decurtins and Jeff Zaleski for insightful scientific discussions, Cassandra Fraser for general career advice, and Dai Ooyama for letting me practice my Japanese and for teaching me the difference between 我慢 and 忍耐.

I was very fortunate to have had the opportunity to collaborate with the Bawendi lab. The members of the Bawendi lab have been very welcoming and have allowed me to use their hood space, equipment, and supplies. Yinthai Chan gave me some good advice early on and is a good friend. Thank you Hee-Sun for sharing your space with me and for teaching me how to cook bulgogi. Wen is an amazingly productive chemist with whom I collaborated on work described in Ch. VII. Gautham was my second go-to person for lifetime setup. I'd like to thank every Bawendi member really, for letting me in on their 4 pm coffee breaks with their cappuccino machine, play with the nanoballers and tag on their ski trip.

Grad school would have been tough without friends outside the lab. Thanks to Leah, Mary, Chiao, Chia, Andy, Roje, Galen, and Catharine for being there for a quick escape as lunch or coffee buddies. I'd like to thank Lance for his friendship through the majority of my time at MIT. Tuesday nights were always great because of my dance friends. Kate Rich was a great duet partner, Najmat's classes makes me look forward to all the amazing moves that I'll hopefully master in the future, and Loni, I can't thank you enough for the belly dance cool-down mantra that I looked forward to at the end of your classes and for all the gigging opportunities around town.

There are many key members that keep the department running smoothly. Thank you to Gretchen, Allison, Francis and Janet for all the administrative affairs that I didn't

have to worry about. Susan Brighton was a valuable resource to graduate students. I also enjoyed working with Liz McGrath organizing events in conjunction with WIC. Members of the DCIF (Dave, Bob, Jeff, Anne, and LiLi) kept the spectroscopic instruments running for students. Debby Pheasant at BIF was always helpful when I was using the light scattering instrument.

I'd like to thank members of the inorganic faculty, Professors Cummins, Sadighi, Schrock and Lippard for solid training in inorganic chemistry concepts. Professor Lippard has been particularly helpful as my thesis chair giving me feedback on my research, and I hope finds a "true" baroque violinist.

Professor Bawendi is like a second advisor to me. His door was always open whenever I had questions regarding my research, and he was also helpful when I was considering various career options. Thank you for allowing me to collaborate and interact with your wonderful research group.

Finally, my thanks go out to Dan Nocera, Professor of Energy. Thank you for accepting me into your group, continuing to believe in me even at times when I didn't, granting me the freedom to pursue my own research interests, teaching me to think scientifically, training me in proposal writing, and assembling a team of very talented people. Your passion for science is very inspiring and motivating, not to mention contagious. Thanks for introducing me to fine wines and dining and making us laugh with all your funny stories and occasional ranting. I am a stronger (and smarter?) person after being trained by you. Thank you.

Biographical Note

Becky was born in Kawasaki, Japan to her parents David and Kiyomi Somers, six minutes after her twin sister Holly. She attended Japanese public school until the age of 10, when she and her family moved to the United States. Her love of travel was born when they took the long way to travel to the States, taking four months to backpack across China, Russia, and Europe before settling in Tulsa, OK. Her adolescent years were spent in Tulsa, where she graduated from Booker T. Washington High School in 1999 at the top of her class. At Northwestern University, she dabbled in organic synthesis with Professor Sonbinh Nguyen before switching to solid-state chemistry under the direction of Professor Jim Ibers, where she made metal chalcogenide-containing compounds that were potentially applicable for thermoelectrics. A short hiatus in Nantes, France in the spring of 2002 could not separate her from concepts in chemistry, where she learned about different crystallinities of chocolate and their application towards cooking. After earning a B.A. in chemistry and a minor in French in June of 2003, Becky moved to Cambridge, MA to pursue a doctoral degree in inorganic chemistry at the Massachusetts Institute of Technology. She joined the laboratory of Professor Daniel G. Nocera where she developed methods of making inorganic semiconductor nanocrystals into chemical sensors, a project that allowed her to collaborate with Professor Moungi G. Bawendi. After obtaining her Ph.D. in July 2008, Becky will disappear for a few months before starting as an associate at McKinsey and Company at their Washington D.C. office.

Rebecca C. Somers

82 Pleasant St.
Cambridge, MA 02139

Phone: 617-233-4370
Email: rsomers@mit.edu

EDUCATION

Massachusetts Institute of Technology — **Cambridge, MA**
Ph.D., Inorganic Chemistry — July 2008
Thesis title: "Nanocrystal-Molecule Energy Transfer Conjugates for Chemical and Biological Sensing"

Northwestern University — **Evanston, IL**
B.A., Chemistry, minor: French, GPA: 3.71/ 4.00 — June 2003

Institute for the International Education of Students (IES) — **Nantes, France**
Université de Nantes — Spring 2002
Semester study abroad, all classes conducted in French.

SKILLS

Languages: Fluent in English and Japanese. Highly proficient in French. Basic knowledge of Mandarin Chinese
Computers: Matlab, Adobe Illustrator, Adobe Photoshop, MS Office
Technical: NMR, IR, UV-vis, Steady-state and time-resolved emission, DLS, GFC, Zeta-Potential

RESEARCH EXPERIENCE

Massachusetts Institute of Technology, Dept. of Chemistry — **Cambridge, MA**
Research Assistant. Advisor: Daniel G. Nocera — Nov. '03- July '08
- Investigated energy transfer with nanocrystals (NC) as donors and acceptors.
- Developed a novel sensing mechanism applying energy transfer from NCs to an analyte receptor to synthesize the first NC reversible and ratiometric sensor.
- Collaborated with researchers from Mass General Hospital to study the metabolic profile of tumors using NC sensors.
- Mentored an undergraduate student on a research project.

Northwestern University, Dept. of Chemistry — **Evanston, IL**
Research Assistant. Advisor: James A. Ibers — June '02 – May '03
- Utilized high-temperature solid state synthetic techniques to synthesize and characterize inorganic compounds applicable for thermoelectrics. — Apr. '01-Dec. '01

Northwestern University, Dept. of Chemistry — **Evanston, IL**
Research Assistant. Advisor: Sonbinh T. Nguyen — Sept. '00 – Mar '01
- Synthesized salens and utilized organic lab techniques in the field of organometallic catalysis.

LEADERSHIP EXPERIENCE

Resources for Easing Friction and Stress (REFS), MIT — Jan '05-Jun '08
Peer mediator among the students of the MIT chemistry department

Women in Chemistry (WIC), MIT — Jun. '04-May '08
Co-Chair (Jun. '06- Aug. '07) and Committee Member

TEACHING EXPERIENCE

Massachusetts Institute of Technology, — **Cambridge, MA**
Teaching Assistant. — Sept '03- Jan '04
- Courses taught: Intro to Laboratory Chemistry and Intro to Experimental Chemistry
- Given an "Outstanding Teaching Award."
- Supervised lab work of 80 students, graded lab reports, prepared and delivered pre-lab lectures, held office hours and led study sessions.

Northwestern University Searle Center for Teaching Excellence — **Evanston, IL**
Teaching Partner for international graduate students; Supervisor — Aug. '02 -June '03
- Critiqued teaching performance of international graduate students.

- Developed creative teaching methods to enhance communication skills of international T.A.s.

Northwestern School of Continuing Studies **Evanston, IL**
Teaching Assistant. June'01-Dec.'01 & Sept. '02-Dec. '02

- Courses taught: Organic Chemistry Laboratory
- Supervised lab work of 15-20 pre-medical students, graded lab reports, prepared and delivered pre-lab lectures, held office hours and led study sessions

Languagestars Ltd. **Chicago, IL**
Japanese Language Instructor Mar. '01- Sept. '01

- Taught a class of 4-8 year olds in an interactive manner through song and play, emphasizing repetition and responsiveness.
- Incorporated ideas in the teaching curriculum and translated curriculum-related materials in Japanese to enhance foreign vocabulary in young children.

AWARDS & HONORS

Eli Lily American Chemical Society Women Chemists' Committee Travel Award ('07), Award in Outstanding Teaching ('03-'04), Corning Fellowship ('03-'04), Northwestern University Chemistry Departmental Award ('03), Undergraduate Research Grant ('03), Undergraduate Summer Research Grant ('02), Dean's List, Northwestern University.

PUBLICATIONS

1) **Somers R. C.**; Bawendi, M. G.; Nocera, D. G. "CdSe Nanocrystal Based Chem- / Bio- Sensors." *Chem. Soc. Rev.* **2007**, *36*, 579.

2) Snee, P. T.; **Somers, R. C.**; Nair, G.; Zimmer, J. P.; Bawendi, M. G.; Nocera, D. G. "A Ratiometric CdSe/ZnS Nanocrystal pH Sensor." *J. Am. Chem. Soc.* **2006**, *128*, 13320.

3) Mitchell, K.; Huang, F. Q.; Caspi, E. N.; McFarland, A. D; Haynes, C. L.; **Somers, R.C.**; Jorgensen, J. D.; Van Duyne, R. P.; Ibers, J. A. "Syntheses, Structure, and Selected Physical Properties of $CsLnMnSe_3$ (Ln = Sm, Gd, Tb, Dy, Ho, Er, Tm, Yb, Y) and $AybZnQ_3$ (A = Rb, Cs; Q = S, Se, Te)." *Inorg. Chem.* **2004**, *43*, 1082-1089.

4) Mitchell K.; **Somers R. C.**; Huang F. Q.; Ibers J. A. "Syntheses, Structure and Magnetic Properties of Several $LnYbQ_3$ Chalcogenides, Q= S, Se." *J. Solid State Chem.*, **2004**, *177*, 709-713.

5) Mitchell K.; Huang F. Q.; McFarland A. D.; Haynes C. L.; **Somers R. C.**; Van Duyne R. P.; Ibers J. A. "The $CsLnMSe_3$ Semiconductors (Ln= Rare-Earth Element, Y; M =Zn, Cd, Hg)." *Inorg. Chem.* **2003**, *42*, 4109-4116.

6) Huang F. Q.; **Somers R. C.**; McFarland A. D.; Van Duyne R. P.; Ibers, J. A. "Syntheses, Structures, Optical Properties, and Theoretical Calculations of $Cs_2Bi_2ZnS_5$, $Cs_2Bi_2CdS_5$, and $Cs_2Bi_2MnS_5$." *J. Solid State Chem.*, **2003**, *174*, 334-341.

PRESENTATIONS

1) Oral Presentation: National American Chemical Society Conference, Spring 2007. Chicago, IL. "Ratiometric Quantum Dot Chemosensors Based on Fluorescent Resonant Energy Transfer."

2) Poster Presentation: National American Chemical Society Conference, Eli Lilly Travel Award Poster Session, Spring 2007. Chicago, IL. "Ratiometric Quantum Dot Chemosensors Based on Fluorescent Resonant Energy Transfer."

3) Oral Presentation: National Materials Research Society Conference, Fall 2006. Boston, MA. "Ratiometric Nanocrystal Sensors Based on Resonant Energy Transfer."

4) Poster Presentation: National American Chemical Society Conference, Spring 2003. New Orleans, LA. "The $CsLnMSe_3$ Semiconductors."

PATENTS

1) Snee, P. T.; **Somers, R. C.**; Nocera, D. G.; Bawendi, M. G. "Fluorescent sensors and methods based on semiconductor nanocrystals." PCT Int. Appl. (2007), 34pp.

REFERENCES

Professor Daniel G. Nocera
Dept. of Chemistry
77 Massachusetts Ave.
Rm 6-335
Cambridge, MA 02139
617-253-5537
nocera@mit.edu

Professor Stephen J. Lippard
Dept. of Chemistry
77 Massachusetts Ave.
Rm 18-498
Cambridge, MA 02139
617-253-1892
lippard@mit.edu

Professor Moungi G. Bawendi
Dept. of Chemistry
77 Massachusetts Ave.
Rm 6-221
Cambridge, MA 02139
617-253-9796
mgb@mit.edu